

Bifurcation analysis of Bogdanov-Takens bifurcations in delay differential equations*

M.M. Bosschaert[†] Yu.A. Kuznetsov[‡]

October 7, 2022

Abstract: In this paper, we will perform the parameter-dependent center manifold reduction near the generic and transcritical codimension two Bogdanov–Takens bifurcation in classical delay differential equations (DDEs). Using a generalization of the Lindstedt-Poincaré method to approximate the homoclinic solution allows us to initialize the continuation of the homoclinic bifurcation curves emanating from these points. The normal form transformation is derived in the functional analytic perturbation framework for dual semigroups (sun-star calculus) using a normalization technique based on the Fredholm alternative. The obtained expressions give explicit formulas, which have been implemented in the freely available bifurcation software package `DDE-BifTool`. The effectiveness is demonstrated on various models.

Keywords: generic Bogdanov–Takens bifurcation, transcritical Bogdanov–Takens bifurcation, homoclinic solutions, delay differential equations, sun-star calculus, strongly continuous semi-groups, Center Manifold Theorem, `DDE-BifTool`

2020 MSC: 37G05, 37G10, 65P30, 34K16, 34K18, 34K19

1 Introduction

The *Bogdanov–Takens bifurcation* caused by the presence of an equilibrium with a double zero eigenvalue is a well-studied singularity in dynamical systems. It implies existence of saddle homoclinic orbits nearby, which is a global phenomenon. In particular, the codimension two Bogdanov–Takens bifurcation in finite-dimensional ordinary differential equations (ODEs) has been studied theoretically and applied in numerous reserach publications. The same is true for the infinite-dimensional dynamical systems generated by delay differential equations (DDEs). In the simplest case, often encountered in applications, such DDEs have the form

$$\dot{x}(t) = f(x(t), x(t - \tau_1), \dots, x(t - \tau_m), \alpha), \quad t \geq 0, \quad (1)$$

where $x(t) \in \mathbb{R}^n$, $\alpha \in \mathbb{R}^p$, while $0 < \tau_1 < \tau_2 < \dots < \tau_m$ are constant delays, and $f : \mathbb{R}^{n \times (m+1)} \times \mathbb{R}^p \rightarrow \mathbb{R}^n$ is a smooth mapping. These are known as *discrete* DDEs.

Up to date, the standard available parameter-dependent center manifold theorem for DDEs in [13] assumed that the equilibrium persists for all nearby parameter values. This was a serious limitation, since in generic unfoldings of the codimension two Bogdanov–Takens singularity it is not the case.

*Submitted to the editors DATE.

[†]Department of Mathematics, Hasselt University, Diepenbeek Campus, Agoralaan Gebouw D, 3590 Diepenbeek, Belgium (maikel.bosschaert@uhasselt.be).

[‡]Department of Mathematics, Utrecht University, Budapestlaan 6, 3508 TA Utrecht, The Netherlands and Department of Applied Mathematics, University of Twente, Zilverling Building, 7500AE Enschede, The Netherlands (I.A.Kouznetsov@uu.nl).

However, recently, in [2], this obstruction has been removed and the existence of finite-dimensional smooth parameter-dependent local center manifolds has been rigorously established in the functional analytic perturbation framework for dual semigroups (sun-star calculus) developed in [5, 6, 7, 8]. Once the existence of these invariant manifolds is proved, the normalization technique for local bifurcations of ODEs developed in [27] can be lifted rather easily to the infinite dimensional setting of DDEs. The advantages of this normalization technique are that the center manifold reduction and the calculation of the normal form coefficients are performed simultaneously by solving the so-called *homological equation*. This method gives explicit expressions for the coefficients rather than a procedure as developed in [17, 18]. The explicit expressions make them particularly suitable for both symbolic and numerical evaluation.

Indeed, utilizing the normalization method, the authors in [2] obtained asymptotics to initialize the continuation of codimension one bifurcation curves of nonhyperbolic equilibria and cycles emanating from the codimension two *generalized Hopf*, *fold-Hopf*, *Hopf-Hopf* and *transcritical-Hopf* bifurcation points in DDEs of the form (1). These asymptotics have been implemented into the fully GNU Octave compatible MATLAB package DDE-BifTool [16, 35].

Another recent development is the rigorous derivation of higher-order asymptotics for the codimension one homoclinic bifurcation curve emanating from the generic codimension two Bogdanov–Takens bifurcation point in two-parameter ODEs [3]. Thus, by combining the results of the parameter-dependent center manifolds in DDEs from [2] and the homoclinic asymptotics in ODEs from [3], we are in the position to perform the parameter-dependent center manifold reduction and normalization for the *generic* and *transcritical codimension two Bogdanov–Takens* bifurcations. This will allow us to initialize the continuation of codimension one bifurcation curves of nonhyperbolic equilibria and homoclinic solutions emanating from these codimension two points. Hopefully, our results and their software implementation will make the numerical analysis of Bogdanov–Takens bifurcations in DDEs from applications rather routine.

This paper is organized as follows. We begin in Section 2 with a short summary from [2] on parameter-dependent center manifolds for classical DDEs and we state various results needed for the normalization technique. In Section 3 we describe the general technique that we use to derive the transformation from the orbital normal form on the parameter-dependent center manifold in the infinite-dimensional setting of DDEs. In Section 4 the method is then applied to the generic and transcritical codimension two Bogdanov–Takens bifurcations. We provide explicit transformations necessary for the predictors of codimension one bifurcation curves. We do this in a form suitable for classical DDEs, covering cases that are more general than (1). It is here where we see the true benefit of allowing for orbital normal forms on the center manifold. Indeed, we do not need to derive homoclinic asymptotics for the transcritical codimension two Bogdanov–Takens bifurcation separately. Instead, we only need to derive the center manifold transformation for the transcritical codimension two Bogdanov–Takens bifurcation. Then, using the blow-up transformations (82), we obtain the same perturbed Hamiltonian system (up to order three) as in the generic Bogdanov–Takens bifurcation.

We employ our implementation in DDE-BifTool to illustrate the accuracy of the codimension one bifurcation curve predictors through various example models, displaying the generic and transcritical codimension two Bogdanov–Takens bifurcations in Section 5. An in-depth treatment of the examples, including the MATLAB and Julia source code to reproduce the obtained results, as well as a more in-depth analysis of the examples, are provided in the Supplement.

2 Parameter-dependent center manifolds for DDEs

Here we summarize those results from [2] on parameter-dependent center manifold for classical DDEs, which are required for the normalization technique in Section 4. For a general introduction on perturbation theory for dual semigroups (also known as sun-star calculus) we refer to [13].

Consider the classical parameter-dependent DDE

$$\dot{x}(t) = F(x_t, \alpha), \quad t \geq 0, \quad (\text{DDE})$$

where $F : X \times \mathbb{R}^p \rightarrow \mathbb{R}^n$ is C^k -smooth for some $k \geq 1$ with $F(0, 0) = 0$ and $X := C([-h, 0], \mathbb{R}^n)$. Here for each $t \geq 0$, the *history function* $x_t : [-h, 0] \rightarrow \mathbb{R}^n$ defined by

$$x_t(\theta) := x(t + \theta), \quad \forall \theta \in [-h, 0].$$

It is convenient to split the right hand-side into its linear and nonlinear parts and write

$$F(\phi, \alpha) = \langle \zeta, \phi \rangle + D_2 F(0, 0)\alpha + G(x_t, \alpha). \quad (2)$$

Here $\zeta : [0, h] \rightarrow \mathbb{R}^{n \times n}$ is a matrix-valued function of bounded variation, normalized by the requirement that $\zeta(0) = 0$ and is right-continuous on the open interval $(0, h)$, and $G : X \rightarrow \mathbb{R}^n$ is a C^k -smooth nonlinear operator with $G(0, 0) = G_1(0, 0) = G_2(0, 0) = 0$. The pairing is defined by

$$\langle \zeta, \phi \rangle := \int_0^h d\zeta(\theta)\phi(-\theta), \quad (3)$$

where the integral is of the Riemann–Stieltjes type.

Let T be the \mathcal{C}_0 -semigroup on X corresponding to the linearization of (DDE) at $0 \in X$ for the critical parameter value $\alpha = 0$. Suppose that the generator

$$\mathcal{D}(A) = \{\phi \mid \dot{\phi} \in X, \dot{\phi}(0) = \langle \zeta, \phi \rangle\}, \quad A\phi = \dot{\phi},$$

of T has $1 \leq n_0 < \infty$ purely imaginary eigenvalues with corresponding n_0 -dimensional real center eigenspace X_0 . Then by [2, Corollary 20] there exists a C^k -smooth map $\mathcal{C} : U \times U_p \rightarrow X$ defined in a neighborhood of the origin in $X_0 \times \mathbb{R}^p$ and such that for every sufficiently small $\alpha \in \mathbb{R}^p$ the manifold $\mathcal{W}_{\text{loc}}^c(\alpha) := \mathcal{C}(U, \alpha)$ is locally positively invariant for the semiflow generated by (DDE) at parameter value α .

Since X is not reflexive, i.e. does not isomorphic to its dual space X^* , the adjoint semigroup T^* is only weak* continuous on X^* and A^* generates T^* only in the weak* sense. The maximal subspace of strong continuity

$$X^\odot := \{x^* \in X^* : t \mapsto T^*(t)x^* \text{ is norm-continuous on } \mathbb{R}_+\}$$

is invariant under T^* , and we have the representation

$$X^\odot = \mathbb{R}^{n^*} \times L^1([0, h], \mathbb{R}^{n^*}). \quad (4)$$

The duality pairing between $\phi^\odot = (c, g) \in X^\odot$ and $\phi \in X$ is

$$\langle \phi^\odot, \phi \rangle = c\phi(0) + \int_0^h g(\theta)\phi(-\theta) d\theta. \quad (5)$$

At this stage, we again have a \mathcal{C}_0 -semigroup T^\odot with generator A^\odot on a Banach space X^\odot so we can iterate the above construction once more. On the dual space

$$X^{\odot*} = \mathbb{R}^n \times L^\infty([-h, 0], \mathbb{R}^n),$$

we obtain the adjoint semigroup $T^{\odot*}$ with the weak* generator

$$\mathcal{D}(A^{\odot*}) = \{(\alpha, \phi) \in X^{\odot*} \mid \phi \in \text{Lip}(\alpha)\}, \quad A^{\odot*}(\alpha, \phi) = (\langle \zeta, \phi \rangle, \dot{\phi}). \quad (6)$$

The duality pairing between $\phi^{\odot\star} = (a, \psi) \in X^{\odot\star}$ and $\phi^{\odot} = (c, g) \in X^{\odot}$ is

$$\langle \phi^{\odot\star}, \phi^{\odot} \rangle = ca + \int_0^h g(\theta) \psi(-\theta) d\theta. \quad (7)$$

By restriction to the maximal subspace of strong continuity $X^{\odot\odot} = \overline{\mathcal{D}(A^{\odot\star})}$, we end up with the \mathcal{C} -semigroup $T^{\odot\odot}$. Its generator $A^{\odot\odot}$ is the part of $A^{\odot\star}$ in $X^{\odot\odot}$. The canonical injection $j : X \rightarrow X^{\odot\star}$ is given by

$$j(\phi) = (\phi(0), \phi), \quad (8)$$

mapping X onto $X^{\odot\odot}$. Therefore, X is sun-reflexive with respect to the shift semigroup T .

We are now in the position to state the second part of [2, Corollary 20]. That is, if the history x_t associated with a solution of (DDE) exists on some nondegenerate interval I and $x_t \in \mathcal{W}_{\text{loc}}^c(\alpha)$ for all $t \in I$, then $u : I \rightarrow X$ defined by $u(t) := x_t$ is differentiable and satisfies

$$j\dot{u}(t) = A^{\odot\star}ju(t) + (D_2F(0, 0)\alpha)r^{\odot\star} + G(u(t), \alpha)r^{\odot\star}, \quad \forall t \in I.$$

Here, for $i = 1, \dots, n$, we denote $r_i^{\odot\star} := (e_i, 0)$, where e_i is the i th standard basis vector of \mathbb{R}^n and

$$wr^{\odot\star} := \sum_{i=1}^n w_i r_i^{\odot\star}, \quad \forall w = (w_1, \dots, w_n) \in \mathbb{R}^n.$$

2.1 Spectral computations for classical DDEs in case of multiple eigenvalues

It is well known that for classical DDEs all spectral information about the generator A is contained in a holomorphic *characteristic matrix function* $\Delta : \mathbb{C} \rightarrow \mathbb{C}^{n \times n}$ defined by

$$\Delta(z) := zI - \hat{\zeta}(z) \quad \text{with} \quad \hat{\zeta}(z) := \int_0^h e^{-z\theta} d\zeta(\theta), \quad (9)$$

where ζ is the real kernel from (3), see [13, Sections IV.4 and IV.5]. In particular, the eigenvalues of A are the roots of the *characteristic equation*

$$\det \Delta(z) = 0, \quad (10)$$

and the algebraic multiplicity of an eigenvalue equals its order as a root of (10).

For the normalization technique in Section 4, we will need normalized representations for the (generalized) eigenfunctions and adjoint (generalized) eigenfunctions of the generator A and A^* , respectively. In this section, we will consider the more general case where λ is an eigenvalue of algebraic multiplicity $k \in \mathbb{N}$ and geometric multiplicity 1. Although in Section 4 we will only need the special case where $\lambda = 0$ is a double eigenvalue of A , the expressions are useful when considering for example the 1:1 resonant Hopf bifurcation and the triple zero bifurcation.

Proposition 1. *Let λ be an eigenvalue of the generator A with algebraic multiplicity $k \in \mathbb{N}$ and geometric multiplicity one, then there are (generalized) eigenfunctions ϕ_i such that*

$$A\phi_0 = \lambda\phi_0, \quad A\phi_i = \lambda\phi_i + \phi_{i-1}, \quad i \in \{1, \dots, k-1\}, \quad (11)$$

and adjoint (generalized) eigenfunctions ψ_i such that

$$A^*\psi_{k-1} = \lambda\psi_{k-1}, \quad A^*\psi_{k-i} = \lambda\psi_{k-i} + \psi_{k-i+1}, \quad i \in \{2, \dots, k\}. \quad (12)$$

Let the ordered set (q_0, \dots, q_{k-1}) of vectors be a Jordan chain for $\Delta(\lambda)$, i.e. $q_0 \neq 0$ and

$$\Delta(z)[q_0 + (z - \lambda)q_1 + \dots + (z - \lambda)^k q_{k-1}] = \mathcal{O}((z - \lambda)^k).$$

Similarly, let (p_{k-1}, \dots, p_0) be a Jordan chain for $\Delta^T(\lambda)$. Then the (generalized) eigenfunctions and adjoint (generalized) eigenfunctions are given by

$$\begin{aligned}\phi_i: [-h, 0] \rightarrow \mathbb{R}^n: \theta &\mapsto e^{\lambda\theta} \sum_{l=0}^i q_{i-l} \frac{\theta^l}{l!}, \\ \psi_i: [0, h] \rightarrow \mathbb{R}^n: \theta &\mapsto p_i + \sum_{l=0}^{k-1-i} p_{i+l} \int_0^\theta \int_\sigma^h e^{\lambda(\sigma-s)} \frac{(\sigma-s)^l}{l!} d\zeta(s) d\sigma,\end{aligned}\tag{13}$$

for $i \in \{0, \dots, k-1\}$, respectively. Furthermore, the following identities hold

$$\begin{aligned}\langle \psi_i, \phi_j \rangle &= \langle \psi_{i+1}, \phi_{j+1} \rangle, & i, j \in \{0, \dots, k-2\}, \\ \langle \psi_{k-1}, \phi_{k-1} \rangle &= p_{k-1} \sum_{l=0}^{k-1} \frac{\Delta^{(l+1)}(\lambda)}{(l+1)!} q_{k-1-l}, \\ \langle \psi_i, \phi_j \rangle &= 0, & i > j, \\ \langle \psi_0, \phi_j \rangle &= \sum_{l=0}^{k-1} \sum_{m=0}^j p_l \frac{\Delta^{(l+m+1)}(\lambda)}{(l+m+1)!} q_{j-m}, & j > 0,\end{aligned}\tag{14}$$

which can be normalized to satisfy

$$\langle \psi_i, \phi_j \rangle = \delta_{ij}.\tag{15}$$

Proof. The (generalized) eigenspace at an eigenvalue λ of A of algebraic multiplicity k and geometric multiplicity 1 is given by

$$\mathcal{N}((A - \lambda)^k),$$

which leads to the expressions in (11) and similarly for (12). The representations of the (generalized) eigenfunctions and adjoint (generalized) eigenfunctions can be found in Theorem IV.5.5 and IV.5.9 in [13], respectively.

The first identity in (14) follows directly from

$$\langle \psi_{i+1}, \phi_{j+1} \rangle = \langle (\lambda - A^*)\psi_i, \phi_{j+1} \rangle = \langle \psi_i, (\lambda - A)\phi_{j+1} \rangle = \langle \psi_i, \phi_j \rangle,$$

where $i, j \in \{0, \dots, k-2\}$. For the second identity in (14) we notice that

$$\begin{aligned}\langle \psi_{k-1}, \phi_{k-1} \rangle &= \int_0^h d\psi_{k-1}(\theta) \phi_{k-1}(-\theta) = p_{k-1} q_0 + \int_0^h \psi'_{k-1}(\theta) \phi_{k-1}(-\theta) d\theta \\ &= p_{k-1} q_0 + \int_0^h p_{k-i} \int_\theta^h e^{\lambda(\theta-s)} d\zeta(s) e^{-\lambda\theta} \sum_{l=0}^{k-1} q_{i-l} \frac{(-1)^l \theta^l}{l!} d\theta \\ &= p_{k-1} q_0 + p_{k-i} \sum_{l=0}^{k-1} \int_0^h \int_\theta^h e^{-\lambda s} \frac{(-1)^l \theta^l}{l!} d\zeta(s) d\theta q_{i-l} \\ &= p_{k-1} q_0 + p_{k-i} \sum_{l=0}^{k-1} \int_0^h \int_0^s e^{-\lambda s} \frac{(-1)^l \theta^l}{l!} d\theta d\zeta(s) q_{i-l} \\ &= p_{k-1} q_0 + p_{k-i} \sum_{l=0}^{k-1} \int_0^h e^{-\lambda s} \frac{(-1)^l s^{l+1}}{(l+1)!} d\zeta(s) q_{i-l} = p_{k-1} \sum_{l=0}^{k-1} \frac{\Delta^{(l)}(\lambda)}{(l+1)!} q_{i-l},\end{aligned}$$

where we used Fubini's theorem to change the order of integration. The last equality holds since

$$\Delta'(z) = zI + \int_0^h \theta e^{-z\theta} d\zeta(\theta)$$

and

$$\Delta^{(n)}(z) = (-1)^{n+1} \int_0^h \theta^n e^{-z\theta} d\zeta(\theta), \quad n > 1.$$

Using the first identity in (14) and that for $j > 0$ we have

$$\langle \psi_j, \phi_0 \rangle = \langle (\lambda - A^*)\psi_{j-1}, \phi_0 \rangle = \langle \psi_{j-1}, (\lambda - A)\phi_0 \rangle = 0,$$

the third identity in (14) follows.

For the last identity in (14), we have that

$$\begin{aligned} \langle \psi_0, \phi_j \rangle &= \int_0^h d\psi_0(\theta) \phi_j(-\theta) = p_0 q_j + \int_0^h \psi'_0(\theta) \phi_j(-\theta) d\theta \\ &= p_0 q_j + \int_0^h \left(\sum_{l=0}^{k-1} p_l \int_\theta^h e^{\lambda(\theta-s)} \frac{(\theta-s)^l}{l!} d\zeta(s) e^{-\lambda\theta} \sum_{m=0}^j q_{j-m} (-1)^m \frac{\theta^m}{m!} \right) d\theta \\ &= p_0 q_j + \sum_{l=0}^{k-1} \sum_{m=0}^j p_l \int_0^h \int_\theta^h e^{-s\lambda} \frac{(\theta-s)^l}{l!} d\zeta(s) (-1)^m \frac{\theta^m}{m!} d\theta q_{j-m} \\ &= p_0 q_j + \sum_{l=0}^{k-1} \sum_{m=0}^j p_l \int_0^h \int_0^s e^{-s\lambda} \frac{(\theta-s)^l}{l!} (-1)^m \frac{\theta^m}{m!} d\theta d\zeta(s) q_{j-m} \\ &= p_0 q_j + \sum_{l=0}^{k-1} \sum_{m=0}^j p_l \int_0^h e^{-s\lambda} \frac{(-1)^{l+m} s^{l+m+1}}{(l+m+1)!} d\zeta(s) q_{j-m} = \sum_{l=0}^{k-1} \sum_{m=0}^j p_l \frac{\Delta^{(l+m+1)}(\lambda)}{(l+m+1)!} q_{j-m}. \end{aligned}$$

Here we again used Fubini's theorem to reverse the order of integration and the beta function of Euler to integrate the term

$$\int_0^s (\theta-s)^l \theta^m d\theta.$$

To prove the normalization condition $\langle \psi_0, \phi_0 \rangle = 1$, we start by showing that $\langle \psi_0, \phi_0 \rangle$ is non-vanishing. Consider the direct sum decomposition

$$X = \mathcal{N}((\lambda - A)^k) \oplus \overline{\mathcal{R}((\lambda - A)^k)} = \mathcal{N}((\lambda - A)^k) \oplus {}^\perp \mathcal{N}((\lambda - A^*)^k),$$

see Theorem IV.2.5 in [13]. Since $\phi_0 \in \mathcal{N}((\lambda - A)^k)$ and $\mathcal{N}((\lambda - A^*)^k)$ is spanned by $\{\psi_0, \dots, \psi_k\}$ it follows that $\langle \psi_0, \phi_0 \rangle \neq 0$.

In order to achieve the normalization in (15), we observe that the eigenfunctions ϕ_j ($j \in \{0, \dots, k-1\}$), are invariant under the transformations

$$\phi_0 \rightarrow \alpha \phi_0, \tag{16}$$

$$\phi_j \rightarrow \alpha(\phi_j + \delta_j \phi_0), \quad j \in \{1, \dots, n\}, \tag{17}$$

where $\alpha, \delta_j \in \mathbb{R}$ for $j \in \{0, \dots, k-1\}$ and $\alpha \neq 0$. Using the first identity in (14), we see that it is sufficient to normalize $\langle \psi_0, \phi_0 \rangle$ to 1 and $\langle \psi_0, \phi_j \rangle$ to 0. Thus, using the invariance of the eigenfunctions, we obtain the solutions

$$\alpha = \frac{1}{\langle \psi_0, \phi_0 \rangle}, \quad \delta_j = -\langle \psi_0, \phi_j \rangle, \quad j \in \{1, \dots, n\}.$$

We finish with the remark that the invariance of the eigenfunctions is equivalent to the invariance for the Jordan chains $(q_0, q_1, \dots, q_{k-1}) \rightarrow \alpha(q_0, q_1 + \delta_1 q_0, \dots, q_{k-1} + \delta_{k-1} q_0)$. \square

Remark 2. The Jordan chains for (q_0, \dots, q_{k-1}) and (p_{k-1}, \dots, p_0) in the previous [Proposition 1](#) can be computed as follows. Set for $j \in \mathbb{N}$

$$P_j = P_j(z) = \frac{\Delta^{(j-1)}(z)}{(j-1)!},$$

and define $A_k = A_k(z)$ to be the $(nk) \times (nk)$ -matrix

$$A_k = \begin{pmatrix} P_1 & 0 & \cdots & 0 \\ P_1 & P_2 & \cdots & 0 \\ \cdots & & \ddots & \vdots \\ P_k & P_{k-1} & \cdots & P_1 \end{pmatrix} \quad k \in \mathbb{N}.$$

Then the Jordan chains for (q_0, \dots, q_{k-1}) and (p_{k-1}, \dots, p_0) can be constructed via

$$A_k(\lambda) \begin{pmatrix} q_0 \\ q_1 \\ \vdots \\ q_{k-1} \end{pmatrix} = 0, \quad (p_0 \ p_1 \ \cdots \ p_{k-1}) A_k(\lambda) = 0,$$

see [\[13, Chapter IV Exercise 5.11\]](#).

2.2 Solvability of linear operator equations with double eigenvalues

When computing the normal form coefficients for the Bogdanov–Takens bifurcation in [Section 4](#), using the normalization technique described in [Section 3](#), we will encounter linear operator equations of the following form

$$(\lambda - A^{\odot*}) jv = (w_0, w), \quad (18)$$

where λ is a double eigenvalue, while no other eigenvalues are present on the imaginary axis, $(w_0, w) \in X^{\odot*}$ is given and $v \in D(A)$ is the unknown. Note that in general $w_0 \neq w(0)$. Although we will in [Section 4](#) only need the special case where $\lambda = 0$, the results below hold for non-zero (complex) eigenvalues as well.

Firstly, since $\lambda = 0$ is an eigenvalue, we need to assure that [\(18\)](#) is solvable. Therefore, let ψ_1 , as given in [Proposition 1](#) with $k = 2$ and $\lambda = 0$, be the adjoint eigenfunction of A^* . Then [\(18\)](#) has a solution $(\phi_0, \phi) \in \mathcal{D}(A^{\odot*})$ if and only if (w_0, w) annihilates the null space $\mathcal{N}(\lambda I - A^*)$, i.e., if and only if

$$\langle (w_0, w), \psi_1 \rangle = 0. \quad (\text{FSC})$$

A proof can be found in [\[22, Lemma 3.2\]](#). This condition is often referred to as the *Fredholm solvability condition*.

Proposition 3. *Suppose λ is a double eigenvalue of A and assume that [\(18\)](#) is consistent for a given $(w_0, w) \in X^{\odot*}$. Let (q_0, q_1) and (p_1, p_0) be the Jordan chains for $\Delta(0)$ and $\Delta^T(0)$, respectively. Let ϕ_0 be an eigenfunction of A as in [Proposition 1](#). Then the solution to [\(18\)](#) is given by*

$$v(\theta) = e^{\lambda\theta} \xi + \int_{\theta}^0 e^{\lambda(\theta-s)} w(s) ds + \gamma \phi_0(\theta), \quad \theta \in [-h, 0],$$

with

$$\xi = \Delta(\lambda)^{\text{INV}} \left[w_0 + \int_0^h d\zeta(\theta) \int_{-\theta}^0 e^{-\lambda(\theta+s)} w(s) ds \right].$$

and γ some constant.

Proof. From formula (6) we see that (18) is nothing more than solving the first order ordinary differential equation

$$\lambda v - \dot{v} = w, \quad (19)$$

which must satisfy

$$\lambda v(0) - \int_0^h d\zeta(\theta)v(-\theta) = w_0. \quad (20)$$

Solving (19) for $v \in \mathcal{D}(A)$ we obtain

$$v(\theta) = e^{\lambda\theta}v(0) + \int_{\theta}^0 e^{\lambda(\theta-s)}w(s) ds \quad (\theta \in [-h, 0]).$$

It then follows from (20) that

$$\Delta(\lambda)v(0) = w_0 + \int_0^h d\zeta(\theta) \int_{-\theta}^0 e^{-\lambda(\theta+s)}w(s) ds,$$

where we used the definition of the characteristic matrix in (9). Solving for $v(0)$ yields

$$v(0) = \Delta(\lambda)^{\text{INV}} \left\{ w_0 + \int_0^h d\zeta(\theta) \int_{-\theta}^0 e^{-\lambda(\theta+s)}w(s) ds \right\} + \gamma q_0,$$

where γ is some constant. Now define

$$\tilde{v}(\theta) = e^{\lambda\theta}\xi + \int_{\theta}^0 e^{\lambda(\theta-s)}w(s) ds,$$

so that

$$v(\theta) = \tilde{v}(\theta) + \gamma\phi_0(\theta).$$

□

Remark 4. We observe that the expression for $v(0)$ itself involves a bordered *matrix* inverse,

$$\Delta^{\text{INV}}(\lambda) : \mathcal{R}(\Delta(\lambda)) \rightarrow \mathbb{C}^n,$$

which assigns the unique solution of the extended linear system

$$\Delta(\lambda)x = y, \quad q_0 \cdot x = 0,$$

to every $y \in \mathbb{C}^n$ for which the system $\Delta(\lambda)x = y$ is consistent. In practice, $x = \Delta^{\text{INV}}(\lambda)y$ can be obtained by solving the nonsingular bordered *matrix* system

$$\begin{pmatrix} \Delta(\lambda) & p_1^T \\ q_0^T & 0 \end{pmatrix} \begin{pmatrix} x \\ s \end{pmatrix} = \begin{pmatrix} y \\ 0 \end{pmatrix}$$

for the unknown $(x, s) \in \mathbb{C}^{n+1}$ that, by Cramer's rule, necessarily satisfies $s = 0$. The properties of (finite dimensional) bordered linear systems and their role in numerical bifurcation analysis are discussed more extensively in [26] and [20, Chapter 3].

In Section 4, we will encounter solely systems in which $\lambda = 0$ and w is of polynomial type. For this situation, we have the following results.

Corollary 5. *Suppose that in addition to the assumptions in Proposition 3 that $\lambda = 0$ and the right-hand side in (18) is given by*

$$\begin{pmatrix} w_0 \\ w \end{pmatrix} = \kappa r^{\odot \star} - j(\theta \mapsto c_0 + c_1\theta + \cdots + c_n\theta^n),$$

then

$$v(\theta) = \xi + c_0\theta + \frac{c_1}{2}\theta^2 + \cdots + \frac{c_n}{n+1}\theta^{n+1} + \gamma\phi_0(\theta), \quad (\theta \in [-h, 0]),$$

with

$$\xi = \Delta^{\text{INV}}(0) \left[\kappa - \Delta'(0)c_0 - \frac{\Delta''(0)}{2}c_1 - \cdots - \frac{\Delta^{(n+1)}(0)}{n+1}c_n \right],$$

is the solution to the system

$$-A^{\odot \star}jv = \begin{pmatrix} w_0 \\ w \end{pmatrix}.$$

Remark 6. In Section 4 we will use the shorthand notation

$$v = B_0^{\text{INV}}(\kappa - w)$$

for the solutions in Corollary 5.

Lemma 7. *Suppose that in addition to the assumptions in Proposition 3 that $\lambda = 0$ and let $w \in X$ be given by*

$$w: [-h, 0] \rightarrow \mathbb{R}^n: \theta \mapsto c_0 + c_1\theta + \cdots + c_n\theta^n.$$

Then the pairing with the adjoint (generalized) eigenfunctions ψ_0 and ψ_1 in Proposition 1 with $k = 0$ and $\lambda = 0$ are given by

$$\begin{aligned} \langle \psi_0, w \rangle &= p_0 \left(\Delta'(0)c_0 + \frac{\Delta''(0)}{2}c_1 + \cdots + \frac{\Delta^{(n+1)}(0)}{n+1}c_n \right) \\ &\quad + p_1 \left(\frac{\Delta''(0)}{2}c_0 + \frac{\Delta'''(0)}{3 \times 2}c_1 + \cdots + \frac{\Delta^{(n+2)}(0)}{(n+2)(n+1)}c_n \right) \end{aligned}$$

and

$$\langle \psi_1, w \rangle = p_1 \left(\Delta'(0)c_0 + \frac{\Delta''(0)}{2}c_1 + \cdots + \frac{\Delta^{(n+1)}(0)}{n+1}c_n \right),$$

respectively.

3 Parameter-dependent center manifold reduction combined with normalization and time-reparametrization

In this section, we combine the results from [3] and [2]. That is, we lift the normalization technique for local bifurcations of ODEs to the infinite dimensional settings of DDEs [2], while simultaneously incorporating a time-reparametrization to allow for a further simplification of the normal form [3]. Thus, suppose that $0 \in X$ is a stationary state of (DDE) at the critical parameter value $0 \in \mathbb{R}^p$ and assume there are $n_0 \geq 1$ eigenvalues on the imaginary axis, counting algebraic multiplicities. Let P_0 be the corresponding *real* spectral projector on X , so the range X_0 of P_0 is the *real* n_0 -dimensional center eigenspace. [2, Corollary 20] applies to give a parameter-dependent local center manifold $\mathcal{W}_{\text{loc}}^c(\alpha)$ for (DDE).

We allow for the introduction of a new parameter β defined in a neighborhood of $0 \in \mathbb{R}^p$ such that $\alpha = K(\beta)$ for some locally defined C^k -diffeomorphism $K : \mathbb{R}^p \rightarrow \mathbb{R}^p$ that is to be determined below. If $u : I \rightarrow X$ with $u(t) := x_t \in \mathcal{W}_{\text{loc}}^c(\alpha)$ is as in [2, Corollary 20], then u is differentiable on I and satisfies

$$j\dot{u}(t) = A^{\odot*}ju(t) + (D_2F(0,0)K(\beta))r^{\odot*} + R(u(t), K(\beta)), \quad \forall t \in I, \quad (21)$$

where R encodes the nonlinear part of F as given by $G(u(t), K(\beta))r^{\odot*}$. Choose a basis Φ of X_0 and let $\mathcal{H} : \mathbb{R}^{n_0} \times \mathbb{R}^p \rightarrow X$ be a locally defined C^k -smooth parametrization of $\mathcal{W}_{\text{loc}}^c(\alpha)$ with respect to Φ and in terms of the new parameter β . For every $t \in I$ we define $v(t) \in \mathbb{R}^{n_0}$ as the coordinate vector of $P_0u(t)$ with respect to Φ . Then $v : I \rightarrow \mathbb{R}^{n_0}$ satisfies a parameter-dependent ordinary differential equation of the form

$$\dot{v}(\eta) = \sum_{|\nu|+|\mu| \geq 1} \frac{1}{\nu! \mu!} g_{\nu\mu} v^\nu(\eta) \beta^\mu. \quad (22)$$

The multi-indices ν and μ have lengths n_0 and p , respectively. We assume that (22) is known. Since \mathcal{H} parametrizes $\mathcal{W}_{\text{loc}}^c(\alpha)$,

$$u(t(\eta)) = \mathcal{H}(v(\eta), \beta), \quad t \in I, \quad (23)$$

with both u and v depending on the parameter, although this is left implicit in the notation. Next, let the time t in (21) and the time η in the normal form (22) be related through the parameter-dependent time-rescaling

$$\frac{dt}{d\eta} = \vartheta(v, \beta), \quad \vartheta : \mathbb{R}^{n_0} \times \mathbb{R}^p \rightarrow \mathbb{R}. \quad (24)$$

Substituting the above relation (23) into (21) and taking into account (24) produces the *homological equation*

$$(A^{\odot*}j\mathcal{H}(v, \beta) + (D_2F(0,0)K(\beta))r^{\odot*} + R(\mathcal{H}(v, \beta), K(\beta))) \vartheta(v, \beta) = jD_1\mathcal{H}(v, \beta)\dot{v}, \quad (\text{HOM})$$

with \dot{v} given by the parameter-dependent normal form (22). The unknowns in (HOM) are \mathcal{H} , K , ϑ , and the coefficients $g_{\nu\mu}$ from (22). For $r, s \geq 0$ with $r+s \geq 1$ we denote by $D_1^r D_2^s F(0,0) : X^r \times [\mathbb{R}^p]^s \rightarrow \mathbb{R}^n$ the mixed Fréchet derivative of order $r+s$, evaluated at $(0,0) \in X \times \mathbb{R}^p$, with the understanding that at most one of the factor spaces X^r or $[\mathbb{R}^p]^s$ is absent if either $r=0$ or $s=0$. We expand the nonlinearity R as

$$R(\phi, \alpha) = \sum_{r+s > 1} \frac{1}{r! s!} D_1^r D_2^s F(0,0)(\phi^{(r)}, \alpha^{(s)}) r^{\odot*}, \quad (25)$$

where $\phi^{(r)} := (\phi, \dots, \phi) \in X^r$ and $\alpha^{(s)} := (\alpha, \dots, \alpha) \in [\mathbb{R}^p]^s$. The mappings \mathcal{H} , K , and θ can be expanded as

$$\begin{aligned} \mathcal{H}(v, \beta) &= \sum_{|\nu|+|\mu| \geq 1} \frac{1}{\nu! \mu!} h_{\nu\mu} v^\nu \beta^\mu, \\ K(\beta) &= \sum_{|\mu| \geq 1} \frac{1}{\mu!} K_\mu \beta^\mu, \\ \vartheta(w, \beta) &= \sum_{|\nu|+|\mu| \geq 0} \frac{1}{\nu! \mu!} \theta_{\nu\mu} w^\nu \beta^\mu. \end{aligned} \quad (26)$$

Substituting (22), (25), and (26) into (HOM), collecting coefficients of terms $v^\nu \beta^\mu$ from lower to higher order and solving the resulting linear systems, one can solve recursively for the unknown coefficients $g_{\nu\mu}$, $h_{\nu\mu}$, and K_μ by applying the Fredholm alternative and taking bordered inverses, as explained in Section 2.2.

Remark 8. To determine the coefficients $g_{\nu\mu}$, $h_{\nu\mu}$, K_μ and $\theta_{\nu\mu}$ that are needed to include in order to translate asymptotics to solutions in the normal form (22) in such a way that the approximation order to the asymptotics are also obtained in the original system under consideration, is a non-trivial task. Indeed, one needs to understand precisely which coefficients $g_{\nu\mu}$ in (22) affect the obtained asymptotic up to a certain order. Then, using [3, Proposition 1], we can derive which coefficients $h_{\nu\mu}$, K_μ and $\theta_{\nu\mu}$ are sufficient to include into the transformations.

4 Parameter-dependent center manifold reduction near Bogdanov–Takens points

Using the method as outlined in Section 3, we derive here the coefficients needed to translate the homoclinic third-order asymptotics emanating from generic and transcritical codimension two Bogdanov–Takens bifurcations to the parameter-dependent center manifold. Additionally, we derive asymptotics for the codimension one equilibria bifurcations emanating from these Bogdanov–Takens bifurcation points.

Thus, suppose that (DDE) has an equilibrium $x_0 \equiv 0$ at the critical parameter value $\alpha_0 = (0, 0) \in \mathbb{R}^2$ with a double (but not semisimple) zero eigenvalue

$$\lambda_{1,2} = 0, \tag{27}$$

which are the only eigenvalues on the imaginary axis. Furthermore, we assume that the critical normal coefficients a and b , to be defined below, are non-zero. We then consider two different cases, depending on whether the equilibrium remains fixed under parameter variation or not. For both cases there are additional transversality conditions which need to be met, guaranteeing the local invertibility of the parameter mapping K , see (31).

4.1 Generic Bogdanov–Takens bifurcation

The C^∞ -equivalent normal form on the parameter-dependent center manifold is

$$\begin{cases} \dot{w}_0 = w_1, \\ \dot{w}_1 = \beta_1 + \beta_2 w_1 + a w_0^2 + b w_0 w_1 + w_0^2 w_1 h(w_0, \beta) + w_1^2 Q(w_0, w_1, \beta), \end{cases} \tag{28}$$

where h is C^∞ and Q is N -flat for an a priori given N , see [4]. Here, the dot represents the derivative with respect to the new time η of $w_i(\eta)$ ($i = 0, 1$). Furthermore, it is shown in [3] that we can assume $h(0, 0) = 0$. By [3, Proposition 1], it is both necessary and sufficient in order to translate the third-order homoclinic predictor to the system (DDE) to expand the functions $R: X \times \mathbb{R}^2 \rightarrow X^{\odot\star}$, $\mathcal{H}: \mathbb{R}^2 \times \mathbb{R}^2 \rightarrow X$,

$K: \mathbb{R}^2 \rightarrow \mathbb{R}^2$, and $\vartheta: \mathbb{R}^2 \rightarrow \mathbb{R}$ defined in [Section 3](#) as follows

$$R(u, \alpha) = \left(\frac{1}{2}B(u, u) + A_1(u, \alpha) + \frac{1}{2}J_2(\alpha, \alpha) + \frac{1}{6}C(u, u, u) + \frac{1}{2}B_1(u, u, \alpha) \right. \\ \left. + \frac{1}{2}A_2(u, \alpha, \alpha) + \frac{1}{6}J_3(\alpha, \alpha, \alpha) + \mathcal{O}(\|(u, \alpha)\|^4) \right) r^{\odot \star}, \quad (29)$$

$$\mathcal{H}(w, \beta) = h_{0010}\beta_1 + h_{0001}\beta_2 + \frac{1}{2}h_{2000}w_0^2 + h_{1100}w_0w_1 + \frac{1}{2}h_{0200}w_1^2 \quad (30)$$

$$+ h_{1010}w_0\beta_1 + h_{1001}w_0\beta_2 + h_{0110}w_1\beta_1 + h_{0101}w_1\beta_2 + \frac{1}{2}h_{0002}\beta_2^2 \\ + h_{0011}\beta_1\beta_2 + \frac{1}{6}h_{3000}w_0^3 + \frac{1}{2}h_{2100}w_0^2w_1 + h_{1101}w_0w_1\beta_2 + \frac{1}{2}h_{2001}w_0^2\beta_2 \\ + \frac{1}{6}h_{0003}\beta_2^3 + \frac{1}{2}h_{1002}w_0\beta_2^2 + \frac{1}{2}h_{0102}w_1\beta_2^2 \\ + \mathcal{O}(|w_1|^3 + |w_0w_1^2| + |\beta_2w_1^2| + |\beta_1||w|^2 + |\beta_1^2||w| + |\beta_1^2| + \|(w, \beta)\|^4),$$

$$K(\beta) = K_{10}\beta_1 + K_{01}\beta_2 + \frac{1}{2}K_{02}\beta_2^2 + K_{11}\beta_1\beta_2 + \frac{1}{6}K_{03}\beta_2^3 \quad (31)$$

$$+ \mathcal{O}(|\beta_1|^2 + |\beta_1||\beta_2|^2 + |\beta_1|^2|\beta_2| + \|\beta\|^4),$$

$$\vartheta(w, \beta) = 1 + \vartheta_{1000}w_0 + \vartheta_{0001}\beta_2 + \mathcal{O}(|w_1| + |\beta_2| + \|(w, \beta)\|^2). \quad (32)$$

Here B , A_1 , J_2 , C , B_1 , A_2 , and J_3 are the standard multilinear forms arising from the expansion of $F(u, \alpha)$. For example,

$$B(u, u) = D_1^2 F(0, 0)(u, u), \quad J_2(\alpha, \alpha) = D_2^2 F(0, 0)(\alpha, \alpha), \quad B_1(u, u, \alpha) = D_2^1 D_1^2 F(0, 0)(u, u, \alpha),$$

etc. Explicit formulas for the multilinear forms for the simplest DDE [\(1\)](#) are given in [\[2, Section 6\]](#).

We insert the expansions [\(29\)](#)–[\(32\)](#) into the homological equation [\(HOM\)](#).

4.1.1 (Generalized) eigenfunctions

By collecting the coefficients of the linear terms in w in the homological equation, we obtain precisely the systems defining the (generalized) eigenfunctions. By [Proposition 1](#) with $k = 2$ and $\lambda = 0$ we obtain

$$\begin{aligned} \phi_0 &= \vartheta \mapsto q_0, \\ \phi_1 &= \vartheta \mapsto \vartheta q_0 + q_1, \\ \psi_1 &= \left(p_1, \vartheta \mapsto p_1 \int_{\vartheta}^h d\zeta(s) \right), \\ \psi_0 &= \left(p_0, \vartheta \mapsto p_0 \int_{\vartheta}^h d\zeta(s) + p_1 \int_{\vartheta}^h (\vartheta - s) d\zeta(s) \right), \end{aligned}$$

where (q_0, q_1) and (p_1, p_0) are the Jordan chain for $\Delta(0)$ and $\Delta^T(0)$, respectively. Furthermore, we assume the eigenfunctions to be normalized such that

$$\langle \psi_i, \phi_j \rangle = \delta_{ij}, \quad 0 \leq i, j \leq 1. \quad (33)$$

Remark 9. Note that the normalization condition above does not uniquely define the eigenfunction. Indeed, the transformation

$$\psi_1 \mapsto \frac{1}{c}\psi_1, \quad \psi_0 \mapsto \frac{1}{c}\psi_0, \quad \phi_0 \mapsto c\phi_0, \quad \phi_1 \mapsto c\phi_1, \quad (34)$$

for some non-zero constant c , leaves (33) invariant. The same holds true for the transformation

$$\psi_0 \mapsto \psi_0 + \tilde{c}\psi_1, \quad \phi_1 \mapsto \phi_1 - \tilde{c}\phi_0, \quad (35)$$

for some constant \tilde{c} . In [28], the condition

$$q_0^T q_0 = 1, \quad q_1^T q_0 = 0, \quad (36)$$

is imposed to uniquely define the vectors $\{q_0, q_1, p_1, p_0\}$ up to a plus or minus sign. However, since the non-uniqueness in the eigenfunctions does not alter the order of accuracy of the homoclinic predictors, we will not explicitly impose (36).

4.1.2 Critical coefficients

Collecting the w_0^2 , $w_0 w_1$ and w_1^2 terms in the homological equation (HOM), lead to the systems

$$-A^{\odot*} j h_{2000} = B(\phi_0, \phi_0) r^{\odot*} - 2aj\phi_1, \quad (37)$$

$$-A^{\odot*} j h_{1100} = B(\phi_0, \phi_1) r^{\odot*} - j(b\phi_1 - \vartheta_{1000}\phi_0 + h_{2000}), \quad (38)$$

$$-A^{\odot*} j h_{0200} = B(\phi_1, \phi_1) r^{\odot*} - 2jh_{1100}. \quad (39)$$

Pairing equations (37) and (38) with the adjoint eigenfunctions ψ_1 and ψ_0 yields critical normal form coefficients

$$a = \frac{1}{2} p_1 B(\phi_0, \phi_0),$$

$$b = p_0 B(\phi_0, \phi_0) + p_1 B(\phi_0, \phi_1).$$

Now that (37) and (38) are solvable, we use Corollary 5 to define the functions

$$\hat{h}_{2000} = B_0^{\text{INV}} (B(\phi_0, \phi_0) - 2aj\phi_1),$$

$$\hat{h}_{1100} = B_0^{\text{INV}} \left(B(\phi_0, \phi_1) - (b\phi_1 + \hat{h}_{2000}) \right).$$

It follows that the general solutions of the systems (37) and (38) are given by

$$h_{2000} = \hat{h}_{2000} + \gamma_1 \phi_0,$$

$$h_{1100} = \hat{h}_{1100} + \gamma_1 \phi_1 - \vartheta_{1000} \phi_1 + \gamma_2 \phi_0.$$

The constant γ_1 is determined by the solvability condition from (39), which gives

$$\gamma_1 = p_0 B(q_0, q_1) - \langle \psi_0, \hat{h}_{2000} \rangle + \frac{1}{2} p_1 B(q_1, q_1) + \vartheta_{1000},$$

where $\langle \psi_0, \hat{h}_{2000} \rangle$ is given through Lemma 7.

To determine the constant γ_2 and the coefficient ϑ_{1000} we consider the w_0^3 and $w_0^2 w_1$ terms in the homological equation (HOM). After some simplification, we obtain the systems

$$-A^{\odot*} j h_{3000} = [3B(h_{2000}, \phi_0) + C(\phi_0, \phi_0, \phi_0)] r^{\odot*} - 6aj(h_{1100} - \vartheta_{1000}\phi_1), \quad (40)$$

$$-A^{\odot*} j h_{2100} = [2B(h_{1100}, \phi_0) + B(h_{2000}, \phi_1) + C(\phi_0, \phi_0, \phi_1)] r^{\odot*} \quad (41)$$

$$- j(2ah_{0200} + 2bh_{1100} + h_{3000} - 2\vartheta_{1000}(b\phi_1 - \vartheta_{1000}\phi_0 + h_{2000})). \quad (42)$$

The solvability condition of the first equation determines ϑ_{1000} as

$$\vartheta_{1000} = -\frac{1}{12a} p_1 \left\{ 3B(\hat{h}_{2000}, \phi_0) + C(\phi_0, \phi_0, \phi_0) \right\} + \frac{1}{2} \langle \psi_1, \hat{h}_{1100} \rangle. \quad (43)$$

The solvability condition for the system in (41) yields, after a rather lengthy calculation, that γ_2 is determined by

$$\begin{aligned} \gamma_2 = \frac{1}{6a} \left[p_1 \left\{ 2B(\hat{h}_{1100}, q_0) + B(\hat{h}_{2000}, q_1) + C(q_0, q_0, q_1) \right\} + 2ap_0 B(q_1, q_1) \right. \\ \left. - bp_1 B(\phi_1, \phi_1) + p_0 \left(3B(\hat{h}_{2000}, q_0) + C(q_0, q_0, q_0) \right) + 3\gamma_1 b - 10a \langle \hat{h}_{1100}, \psi_0 \rangle \right]. \end{aligned}$$

Since the systems in (39)–(41) are now all consistent, we are allowed to take the bordered inverses to obtain

$$\begin{aligned} h_{0200} &= B_0^{\text{INV}} (B(\phi_1, \phi_1) - h_{1100}), \\ h_{3000} &= B_0^{\text{INV}} (3B(h_{2000}, \phi_0) + C(\phi_0, \phi_0, \phi_0) - 6a(h_{1100} - \vartheta_{1000}\phi_1)) \\ h_{2100} &= B_0^{\text{INV}} (2B(h_{1100}, \phi_0) + B(h_{2000}, \phi_1) + C(\phi_0, \phi_0, \phi_1) \\ &\quad - (2ah_{0200} + 2bh_{1100} + h_{3000} - 2\vartheta_{1000}(b\phi_1 - \vartheta_{1000}\phi_0 + h_{2000}))). \end{aligned}$$

4.1.3 Parameter-dependent linear coefficients

The coefficients of the linear terms in β give the systems

$$\begin{aligned} -A^{\odot*} j h_{0001} &= J_1 K_{01}, \\ -A^{\odot*} j h_{0010} &= J_1 K_{10} - \phi_1. \end{aligned} \tag{44}$$

Since p_1 and J_1 are known, we can calculate

$$\nu := (p_1 J_1)^T.$$

By the transversality condition, the vector ν is nonzero. It then follows from the Fredholm alternative that

$$\begin{aligned} K_{01} &= \delta_1 \hat{K}_{01}, \\ h_{0001} &= \delta_1 (\hat{h}_{0001} + \gamma_3 \phi_0), \\ K_{10} &= \hat{K}_{10} + \delta_2 K_{01}, \\ h_{0010} &= \hat{h}_{0010} + \delta_2 h_{0001} + \gamma_4 \phi_0, \end{aligned}$$

where

$$\begin{aligned} \hat{K}_{10} &= \frac{1}{\|\nu\|^2} \nu, \\ \hat{h}_{0010} &= B_0^{\text{INV}} (J_1 K_{10} - \phi_1) \\ \hat{K}_{01} &= \begin{pmatrix} 0 & -1 \\ 1 & 0 \end{pmatrix} \hat{K}_{10}, \\ \hat{h}_{0001} &= B_0^{\text{INV}} (J_1 \hat{K}_{01}), \end{aligned}$$

and $\delta_{1,2}, \gamma_{3,4}$ are real constants determined by the solvability condition of the $w\beta$ terms in the homological equation. Collecting the corresponding systems in the homological equation yields

$$-A^{\odot*} j h_{1001} = (B(h_{0001}, \phi_0) + A_1(\phi_0, K_{01})) r^{\odot*}, \tag{45}$$

$$-A^{\odot*} j h_{0101} = (B(h_{0001}, \phi_1) + A_1(\phi_1, K_{01})) r^{\odot*} - j(h_{1001} + \phi_1 - \vartheta_{0001}\phi_0), \tag{46}$$

$$-A^{\odot*} j h_{1010} = (B(h_{0010}, \phi_0) + A_1(\phi_0, K_{10})) r^{\odot*} - j(h_{1100} - \vartheta_{1000}\phi_1),$$

$$-A^{\odot*} j h_{0110} = (B(h_{0010}, \phi_1) + A_1(\phi_1, K_{10})) r^{\odot*} - j(h_{0200} + h_{1010}).$$

The solvability condition for the first two systems yields

$$\gamma_3 = -\frac{p_1 \left(B(\hat{h}_{0001}, \phi_0) + A_1(\phi_0, \hat{K}_{01}) \right)}{2a},$$

$$\delta_1 = \frac{1}{p_1 \left(B(\hat{h}_{0001}, \phi_1) + A_1(\phi_1, \hat{K}_{01}) \right) + p_0 \left(B(\hat{h}_{0001}, \phi_0) + A_1(\phi_0, \hat{K}_{01}) \right) + \gamma_3 b},$$

while the solvability condition for the latter two systems yields

$$\gamma_4 = \frac{\langle \psi_1, h_{1100} \rangle - \vartheta_{1000} - p_1 \left(B(\hat{h}_{0010}, \phi_0) + A_1(\phi_0, \hat{K}_{10}) \right)}{2a},$$

$$\delta_2 = -p_1 \left(B(\hat{h}_{0010}, \phi_1) + A_1(\phi_1, \hat{K}_{10}) \right) - \gamma_4 b + \langle \psi_1, h_{0200} \rangle$$

$$- p_0 \left(B(\hat{h}_{0010}, \phi_0) + A_1(\phi_0, \hat{K}_{10}) \right) + \langle \psi_1, h_{1100} \rangle.$$

Note that the denominator in δ_1 is nonzero by the transversality condition.

4.1.4 Coefficients h_{1010} and h_{0110}

Since we do not need to use the non-uniqueness in the systems for the coefficients h_{1010} and h_{0110} to simplify higher-order systems, it is sufficient to let

$$h_{1010} = B_0^{\text{INV}} \left(B(h_{0010}, \phi_0) + A_1(\phi_0, K_{10}) - (h_{1100} - \vartheta_{1000}\phi_1) \right),$$

$$h_{0110} = B_0^{\text{INV}} \left(B(h_{0010}, \phi_1) + A_1(\phi_1, K_{10}) - (h_{0200} + h_{1010}) \right).$$

4.1.5 Coefficients $(\vartheta_{0001}, \gamma_5), h_{1001}, h_{0101}, h_{2001}, h_{1101}$

Define

$$\hat{h}_{1001} = B_0^{\text{INV}} \left(B(h_{0001}, \phi_0) + A_1(\phi_0, K_{01}) \right),$$

$$\hat{h}_{0101} = B_0^{\text{INV}} \left(\left(B(h_{0001}, \phi_1) + A_1(\phi_1, K_{01}) \right) - \left(\hat{h}_{1001} + \phi_1 \right) \right).$$

Then the general solutions to the systems in (45) and (46) are given by

$$h_{1001} = \hat{h}_{1001} + \gamma_5 \phi_0,$$

$$h_{0101} = \hat{h}_{0101} + \gamma_5 \phi_1 - \vartheta_{0001} \phi_1.$$

In order to determine γ_5 and ϑ_{0001} , we consider the systems corresponding to the $w_0^2\beta_2$ and $w_0w_1\beta_2$ terms in the homological equation. These are given by

$$\begin{aligned} -A^{\odot*}jh_{2001} &= A_1(h_{2000}, K_{01}) + B(h_{0001}, h_{2000}) + 2B(h_{1001}, \phi_0) \\ &\quad + B_1(\phi_0, \phi_0, K_{01}) + C(h_{0001}, \phi_0, \phi_0) - 2aj(h_{0101} - \vartheta_{0001}\phi_1), \\ -A^{\odot*}jh_{1101} &= A_1(h_{1100}, K_{01}) + B(h_{0001}, h_{1100}) + B(h_{0101}, \phi_0) + B(h_{1001}, \phi_1) \\ &\quad + B_1(\phi_0, \phi_1, K_{01}) + C(h_{0001}, \phi_0, \phi_1) - j[bh_{0101} + h_{1100} + h_{2001} \\ &\quad - \vartheta_{1000}(h_{1001} + \phi_1 - \vartheta_{0001}\phi_0) - \vartheta_{0001}(h_{2000} + b\phi_1 - \vartheta_{1000}\phi_0)]. \end{aligned} \tag{47}$$

The Fredholm solvability condition leads to the following system to be solved

$$\begin{pmatrix} 2a & 4a \\ b & b \end{pmatrix} \begin{pmatrix} \gamma_5 \\ \vartheta_{0001} \end{pmatrix} = \begin{pmatrix} \zeta_1 \\ \zeta_2 \end{pmatrix}. \tag{48}$$

Here the right-hand side is given by

$$\begin{aligned}
\zeta_1 &= 2a\langle\psi_1, \hat{h}_{0101}\rangle - p_1 [A_1(h_{2000}, K_{01}) + B(h_{0001}, h_{2000}) \\
&\quad + 2B(\hat{h}_{1001}, \phi_0) + B_1(\phi_0, \phi_0, K_{01}) + C(h_{0001}, \phi_0, \phi_0)], \\
\zeta_2 &= \langle\psi_1, b\hat{h}_{0101} + h_{1100} - \vartheta_{1000}\hat{h}_{1001}\rangle - \vartheta_{1000} \\
&\quad - p_1 \left[A_1(h_{1100}, K_{01}) + B(h_{0001}, h_{1100}) + B(\hat{h}_{0101}, \phi_0) \right. \\
&\quad \left. + B(\hat{h}_{1001}, \phi_1) + B_1(\phi_0, \phi_1, K_{01}) + C(h_{0001}, \phi_0, \phi_1) \right] \\
&\quad + 2a\langle\psi_0, \hat{h}_{0101}\rangle - p_0 [A_1(h_{2000}, K_{01}) + B(h_{0001}, h_{2000}) \\
&\quad + 2B(\hat{h}_{1001}, \phi_0) + B_1(\phi_0, \phi_0, K_{01}) + C(h_{0001}, \phi_0, \phi_0)].
\end{aligned} \tag{49}$$

Notice that the matrix in (48) is invertible by the non-degeneracy condition.

Now that the systems in (47) are solvable, we obtain

$$\begin{aligned}
h_{2001} &= B_0^{\text{INV}} ((A_1(h_{2000}, K_{01}) + B(h_{0001}, h_{2000}) + 2B(h_{1001}, \phi_0) \\
&\quad + B_1(\phi_0, \phi_0, K_{01}) + C(h_{0001}, \phi_0, \phi_0)) - 2a(h_{0101} - \vartheta_{0001}\phi_1)), \\
h_{1101} &= B_0^{\text{INV}} ((A_1(h_{1100}, K_{01}) + B(h_{0001}, h_{1100}) + B(h_{0101}, \phi_0) + B(h_{1001}, \phi_1) \\
&\quad + B_1(\phi_0, \phi_1, K_{01}) + C(h_{0001}, \phi_0, \phi_1)) - [bh_{0101} + h_{1100} + h_{2001} \\
&\quad - \vartheta_{1000}(h_{1001} + \phi_1 - \vartheta_{0001}\phi_0) - \vartheta_{0001}(h_{2000} + b\phi_1 - \vartheta_{1000}\phi_0)]).
\end{aligned} \tag{50}$$

4.1.6 Coefficients K_{11} and h_{0011}

Collecting the systems corresponding to the $\beta_1\beta_2$ term in the homological equation yields

$$\begin{aligned}
-A^{\odot*}jh_{0011} &= (J_1K_{11} + A_1(h_{0001}, K_{10}) + A_1(h_{0010}, K_{01}) \\
&\quad + B(h_{0001}, h_{0010}) + J_2(K_{01}, K_{10}))r^{\odot*} - j(h_{0101} - \vartheta_{0001}\phi_1).
\end{aligned} \tag{51}$$

Using the identity

$$p_1J_1K_{10} = 1$$

from the second system in (44), combined with the solvability condition, yields

$$\begin{aligned}
K_{11} &= \left[\langle\psi_1, \hat{h}_{0101}\rangle + \gamma_5 - 2\vartheta_{0001} - p_1 (A_1(h_{0001}, K_{10}) + A_1(h_{0010}, K_{01}) \right. \\
&\quad \left. + B(h_{0010}, h_{0001}) + J_2(K_{10}, K_{01})) \right] K_{10}.
\end{aligned}$$

It follows that

$$\begin{aligned}
h_{0011}(\vartheta) &= B_0^{\text{INV}} (J_1K_{11} + A_1(h_{0001}, K_{10}) + A_1(h_{0010}, K_{01}) \\
&\quad + B(h_{0001}, h_{0010}) + J_2(K_{01}, K_{10}) - (h_{0101} - \vartheta_{0001}\phi_1)).
\end{aligned} \tag{52}$$

4.1.7 Coefficients $K_{02}, h_{0002}, h_{1002}, h_{0102}$

The systems corresponding to the $\beta_2^2, w_0\beta_2^2,$ and $w_1\beta_2^2,$ terms in the homological equation yields

$$\begin{aligned}
-A^{\odot\star} j h_{0002} &= (J_1 K_{02} + 2A_1(h_{0001}, K_{01}) + B(h_{0001}, h_{0001}) + J_2(K_{01}, K_{01})) r^{\odot\star}, \\
-A^{\odot\star} j h_{1002} &= (2A_1(h_{1001}, K_{01}) + A_1(\phi_0, K_{02}) + A_2(\phi_0, K_{01}, K_{01}) \\
&\quad + B(\phi_0, h_{0002}) + 2B(h_{0001}, h_{1001}) + 2B_1(\phi_0, h_{0001}, K_{01}) \\
&\quad + C(\phi_0, h_{0001}, h_{0001})) r^{\odot\star}, \\
-A^{\odot\star} j h_{0102} &= (2A_1(h_{0101}, K_{01}) + A_1(\phi_1, K_{02}) + A_2(\phi_1, K_{01}, K_{01}) \\
&\quad + B(\phi_1, h_{0002}) + 2B(h_{0001}, h_{0101}) + 2B_1(\phi_1, h_{0001}, K_{01}) \\
&\quad + C(\phi_1, h_{0001}, h_{0001})) r^{\odot\star} - j [2h_{0101} + h_{1002} \\
&\quad - 2\vartheta_{0001}(h_{1001} + \phi_1 - \vartheta_{0001}\phi_0)].
\end{aligned} \tag{53}$$

The first system is solved similarly as (51). In order to make the second and third systems consistent, define

$$\begin{aligned}
\hat{K}_{02} &= -p_1 [2A_1(h_{0001}, K_{01}) + B(h_{0001}, h_{0001}) + J_2(K_{01}, K_{01})] K_{10}, \\
\hat{h}_{0002} &= B_0^{\text{INV}} \left(J_1 \hat{K}_{02} + 2A_1(h_{0001}, K_{01}) + B(h_{0001}, h_{0001}) + J_2(K_{01}, K_{01}) \right).
\end{aligned}$$

Then the general solutions to the first system in (53) can be written as

$$\begin{aligned}
K_{02} &= \hat{K}_{02} + \delta_3 K_{01}, \\
h_{0002} &= \hat{h}_{0002} + \delta_3 h_{0001} + \gamma_6 \phi_0.
\end{aligned}$$

Substituting these two expressions into the last two systems of (53) and using the solvability condition yields

$$\begin{aligned}
\gamma_6 &= -\frac{1}{2a} p_1 \left[2A_1(h_{1001}, K_{01}) + A_1(\phi_0, \hat{K}_{02}) + A_2(\phi_0, K_{01}, K_{01}) \right. \\
&\quad + B(\phi_0, \hat{h}_{0002}) + 2B(h_{0001}, h_{1001}) + 2B_1(\phi_0, h_{0001}, K_{01}) \\
&\quad \left. + C(\phi_0, h_{0001}, h_{0001}) \right], \\
\delta_3 &= 2\langle \psi_1, \hat{h}_{0101} \rangle + 2\gamma_5 - 2\vartheta_{0001} \langle \psi_1, \hat{h}_{1001} \rangle - 4\vartheta_{0001} - p_1 [2A_1(h_{0101}, K_{01}) \\
&\quad + A_1(\phi_1, \hat{K}_{02}) + A_2(\phi_1, K_{01}, K_{01}) + B(\phi_1, \hat{h}_{0002}) \\
&\quad + 2B(h_{0001}, h_{0101}) + 2B_1(\phi_1, h_{0001}, K_{01}) + C(\phi_1, h_{0001}, h_{0001})] \\
&\quad - p_0 \left[2A_1(h_{1001}, K_{01}) + A_1(\phi_0, \hat{K}_{02}) + A_2(\phi_0, K_{01}, K_{01}) \right. \\
&\quad + B(\phi_0, \hat{h}_{0002}) + 2B(h_{0001}, h_{1001}) + 2B_1(\phi_0, h_{0001}, K_{01}) \\
&\quad \left. + C(\phi_0, h_{0001}, h_{0001}) \right] - \gamma_6 b,
\end{aligned}$$

where $\langle \psi_1, \hat{h}_{1001} \rangle = p_0 (B(h_{0001}, \phi_0) + A_1(\phi_0, K_{01}))$.

Now that the last two systems in (53) are consistent, we obtain

$$\begin{aligned}
h_{1002} &= B_0^{\text{INV}} (2A_1(h_{1001}, K_{01}) + A_1(\phi_0, K_{02}) + A_2(\phi_0, K_{01}, K_{01}) \\
&\quad + B(\phi_0, h_{0002}) + 2B(h_{0001}, h_{1001}) + 2B_1(\phi_0, h_{0001}, K_{01}) \\
&\quad + C(\phi_0, h_{0001}, h_{0001})), \\
h_{0102} &= B_0^{\text{INV}} ((2A_1(h_{0101}, K_{01}) + A_1(\phi_1, K_{02}) + A_2(\phi_1, K_{01}, K_{01}) \\
&\quad + B(\phi_1, h_{0002}) + 2B(h_{0001}, h_{0101}) + 2B_1(\phi_1, h_{0001}, K_{01}) \\
&\quad + C(\phi_1, h_{0001}, h_{0001})) - [2h_{0101} + h_{1002} \\
&\quad - 2\vartheta_{0001}(h_{1001} + \phi_1 - \vartheta_{0001}\phi_0)]).
\end{aligned}$$

4.1.8 Coefficients K_{03} and h_{0003}

Collecting the systems corresponding to the β_2^3 term in the homological equation yields

$$\begin{aligned} -A^{\odot\star} j h_{0003} = & (J_1 K_{03} + A_1(h_{0001}, K_{02}) + A_1(h_{0002}, K_{01}) + 2(A_1(h_{0001}, K_{02}) \\ & + A_1(h_{0002}, K_{01}) + 3B(h_{0001}, h_{0002}) + 3J_2(K_{01}, K_{02}) \\ & + 3A_2(h_{0001}, K_{01}, K_{01}) + 3B_1(h_{0001}, h_{0001}, K_{01}) \\ & + C(h_{0001}, h_{0001}, h_{0001}) + J_3(K_{01}, K_{01}, K_{01})) r^{\odot\star}. \end{aligned}$$

This equation is solved similarly as equation (51). We obtain

$$\begin{aligned} K_{03} = & -p_1 [A_1(h_{0001}, K_{02}) + A_1(h_{0002}, K_{01}) + 2A_1(h_{0001}, K_{02}) \\ & + 2A_1(h_{0002}, K_{01}) + 3B(h_{0001}, h_{0002}) + 3J_2(K_{01}, K_{02}) \\ & + 3A_2(h_{0001}, K_{01}, K_{01}) + 3B_1(h_{0001}, h_{0001}, K_{01}) \\ & + C(h_{0001}, h_{0001}, h_{0001}) + J_3(K_{01}, K_{01}, K_{01})] K_{10}, \\ h_{0003} = & B_0^{\text{INV}} (J_1 K_{03} + A_1(h_{0001}, K_{02}) + A_1(h_{0002}, K_{01}) + 2A_1(h_{0001}, K_{02}) \\ & + 2A_1(h_{0002}, K_{01}) + 3B(h_{0001}, h_{0002}) + 3J_2(K_{01}, K_{02}) \\ & + 3A_2(h_{0001}, K_{01}, K_{01}) + 3B_1(h_{0001}, h_{0001}, K_{01}) \\ & + C(h_{0001}, h_{0001}, h_{0001}) + J_3(K_{01}, K_{01}, K_{01})). \end{aligned}$$

4.1.9 Homoclinic asymptotics

The third-order homoclinic asymptotics for the homoclinic orbits emanating from (28) have been derived in [3] and are given by

$$\begin{cases} w_0(\eta) = \frac{a}{b^2} \tilde{u} \left(\tanh \left(\xi \left(\frac{a}{b} \epsilon \eta \right) \right) \right) \epsilon^2, \\ w_1(\eta) = \frac{a^2}{b^3} \tilde{v} \left(\tanh \left(\xi \left(\frac{a}{b} \epsilon \eta \right) \right) \right) \epsilon^3, \\ \beta_1 = -4 \frac{a^3}{b^4} \epsilon^4, \\ \beta_2 = \frac{a}{b} \epsilon^2 \tau, \end{cases} \quad (54)$$

where

$$\begin{aligned} \tau = & \frac{10}{7} + \frac{288}{2401} \epsilon^2 + \mathcal{O}(\epsilon^4), \\ \tilde{u}(\zeta) = & 2 - (1 - \zeta^2) \left(6 + \frac{18}{49} \epsilon^2 \right) + \mathcal{O}(\epsilon^4), \\ \tilde{v}(\zeta) = & - \left[-12 + \frac{72}{7} \zeta \epsilon - \left(\frac{90}{49} + \frac{162}{49} \zeta^2 \right) \epsilon^2 + \left(\frac{3888}{2401} \zeta - \frac{216}{343} \zeta^3 \right) \epsilon^3 \right] (1 - \zeta^2) \zeta + \mathcal{O}(\epsilon^4), \\ \xi(s) = & s - \frac{6}{7} \log(\cosh(s)) \epsilon + \left(-\frac{18s}{49} + \frac{45 \tanh(s)}{98} + \frac{36}{49} \tanh(s) \log(\cosh(s)) \right) \epsilon^2 \\ & + \left(-\frac{117}{343} + \frac{3 \operatorname{sech}^2(s)}{4802} (-504 \log^2(\cosh(s)) - 276 \cosh(2s) \log(\cosh(s)) \right. \\ & \left. + 102 \log(\cosh(s)) + 252s \sinh(2s)) \right) \epsilon^3 + \mathcal{O}(\epsilon^4). \end{aligned} \quad (55)$$

To translate the asymptotics to a generic codimension two Bogdanov–Takens point in (DDE), one should substitute the expressions in (54) into (30) and (31). Furthermore, to accurately approximate

the profiles of the homoclinic orbit, one needs to numerically solve the equation

$$t(\eta) - t = 0,$$

for η , where

$$\begin{aligned} t(\eta) = & \eta \left(1 + \vartheta_{0001} \frac{a}{b} \epsilon^2 \left(\frac{10}{7} + \frac{288}{2401} \epsilon^2 + \mathcal{O}(\epsilon^4) \right) \right) + \vartheta_{1000} \frac{1}{b} \epsilon \left(\xi \left(\frac{a}{b} \eta \epsilon \right) - 6 \tanh \left(\xi \left(\frac{a}{b} \eta \epsilon \right) \right) + \right. \\ & \left. \left(\frac{18 \operatorname{sech}^2 \left(\xi \left(\frac{a}{b} \eta \epsilon \right) \right)}{7} + \frac{12}{7} \log \left(\cosh \left(\xi \left(\frac{a}{b} \eta \epsilon \right) \right) \right) \right) \epsilon \right. \\ & + \frac{9}{49} \left(4 \xi \left(\frac{a}{b} \eta \epsilon \right) - 9 \tanh \left(\xi \left(\frac{a}{b} \eta \epsilon \right) \right) + 5 \tanh \left(\xi \left(\frac{a}{b} \eta \epsilon \right) \right) \operatorname{sech}^2 \left(\xi \left(\frac{a}{b} \eta \epsilon \right) \right) \right) \epsilon^2 \\ & \left. + \frac{18 \left(-21 \operatorname{sech}^4 \left(\xi \left(\frac{a}{b} \eta \epsilon \right) \right) + 47 \operatorname{sech}^2 \left(\xi \left(\frac{a}{b} \eta \epsilon \right) \right) + 8 \log \left(\cosh \left(\xi \left(\frac{a}{b} \eta \epsilon \right) \right) \right) \right)}{2401} \epsilon^3 \right) + \mathcal{O}(\epsilon^4). \end{aligned}$$

4.1.10 Codimension-one equilibria bifurcations

To approximate the fold and Hopf curves and their corresponding equilibria in (28), one should substitute the expressions for β and the equilibrium coordinates into the expansions (30) and (31). It follows that the fold curve is approximated by

$$\begin{cases} x = \mathcal{H}(0, 0, 0, 0), \\ \alpha = K(0, \epsilon), \end{cases}$$

for $|\epsilon|$ small, and the Hopf curve by

$$\begin{cases} \omega = \epsilon, \\ x = \mathcal{H} \left(-\frac{\epsilon^2}{2a}, 0, -\frac{\epsilon^4}{4a}, \frac{b\epsilon^2}{2a} \right), \\ \alpha = K \left(-\frac{\epsilon^4}{4a}, \frac{b\epsilon^2}{2a} \right), \end{cases}$$

for $\epsilon > 0$ small.

4.2 Transcritical Bogdanov–Takens bifurcation

In this section, we consider the situation in which the origin remains an equilibrium under variation of the parameters.

Following [4], it is not difficult to show that the C^∞ -equivalent normal form on the parameter-dependent center manifold takes the form

$$\begin{cases} \dot{w}_0 = w_1, \\ \dot{w}_1 = \beta_1 w_0 + \beta_2 w_1 + a w_0^2 + b w_0 w_1 + w_0^2 w_1 h(w_0, \beta) + w_1^2 Q(w_0, w_1, \beta), \end{cases} \quad (56)$$

where h is C^∞ and Q is N -flat for an a priori given N . Here, the dot represents the derivative with respect to the new time η of $w_i(\eta)$ ($i = 0, 1$).

In Table 1, we have listed the terms in the parameter-dependent orbital normal form (56) affecting the third-order homoclinic asymptotics in (83). Therefore, by [3, Theorem 1], it is both necessary and sufficient in order to translate the third-order homoclinic predictor to the system (DDE) to expand the

order in ϵ	affected terms
ϵ^{-2}	w_0
ϵ^{-1}	w_1
ϵ^0	$w_0^2, w_0\beta_1, w_0\beta_2$
ϵ^1	$w_1\beta_1, w_1\beta_2, w_0w_1$
ϵ^2	$w_0\beta_1^2, w_0\beta_1\beta_2, w_0\beta_2^2, w_0^2\beta_1, w_0^2\beta_2, w_0^3, w_1^2$
ϵ^3	$w_1\beta_1^2, w_1\beta_1\beta_2, w_1\beta_2^2, w_0w_1\beta_1, w_0w_1\beta_2, w_0^2w_1$

Table 1: Terms in the reduced system restricted to the parameter-dependent center manifold of the codimension two Bogdanov–Takens point in (1) that affect the third-order homoclinic predictor.

functions $R: X \times \mathbb{R}^2 \rightarrow X^{\odot\star}$, $\mathcal{H}: \mathbb{R}^2 \times \mathbb{R}^2 \rightarrow X$, $K: \mathbb{R}^2 \rightarrow \mathbb{R}^2$, and $\vartheta: \mathbb{R}^2 \rightarrow \mathbb{R}$ defined in Section 3 as follows

$$R(u, \alpha) = \left(\frac{1}{2}B(u, u) + A_1(u, \alpha) + \frac{1}{6}C(u, u, u) + \frac{1}{2}B_1(u, u, \alpha) + \frac{1}{2}A_2(u, \alpha, \alpha) + \mathcal{O}(\|(u, \alpha)\|^4) \right) r^{\odot\star}, \quad (57)$$

$$\begin{aligned} \mathcal{H}(w, \beta) = & \phi_0 w_0 + \phi_1 w_1 + \frac{1}{2}h_{2000}w_0^2 + h_{1100}w_0w_1 + \frac{1}{2}h_{0200}w_1^2 + h_{1010}w_0\beta_1 \\ & + h_{1001}w_0\beta_2 + h_{0110}w_1\beta_1 + h_{0101}w_1\beta_2 + \frac{1}{2}h_{0102}w_1\beta_2^2 \\ & + h_{0111}w_1\beta_1\beta_2 + \frac{1}{2}h_{0120}w_1\beta_1^2 + \frac{1}{2}h_{1002}w_0\beta_2^2 + h_{1011}w_0\beta_1\beta_2 \\ & + \frac{1}{2}h_{1020}w_0\beta_1^2 + h_{1101}w_0w_1\beta_2 + h_{1110}w_0w_1\beta_1 \\ & + \frac{1}{2}h_{2001}w_0^2\beta_2 + \frac{1}{2}h_{2010}w_0^2\beta_1 + \frac{1}{2}h_{2100}w_0^2w_1 + \frac{1}{6}h_{3000}w_0^3 \\ & + \mathcal{O}(|\beta_2w_1^2| + |\beta_1w_1^2| + |w_1^3| + |w_0w_1^2|) + \mathcal{O}(\|(w, \beta)\|^4), \end{aligned} \quad (58)$$

$$K(\beta) = K_{10}\beta_1 + K_{01}\beta_2 + \frac{1}{2}K_{20}\beta_1^2 + K_{11}\beta_1\beta_2 + \frac{1}{2}K_{02}\beta_2^2 + \mathcal{O}(\|\beta\|^3). \quad (59)$$

$$\vartheta(w, \beta) = 1 + \vartheta_{1000}w_0 + \vartheta_{0010}\beta_1 + \vartheta_{0001}\beta_2 + \mathcal{O}(|w_1| + \|(w, \beta)\|^2). \quad (60)$$

The coefficients of the time-reparametrization ϑ have been determined such that the linear systems resulting from the homological equations are solvable, see [3, Remark 2.2]. Note that, since the steady-state remains fixed under variations of parameters, we leave out all coefficients in the expansion of \mathcal{H} which solely depend on the parameters.

Also note that the critical coefficients, i.e. coefficients not depending on any parameters, have already been derived in Section 4.1.2. Therefore, we will start directly with the parameter-dependent systems.

4.2.1 Quadratic terms

Collecting the coefficients of the linear and quadratic terms in the homological equation lead to the systems

$$\begin{aligned}
-A^{\odot*}jh_{1010} &= A_1(\phi_0, K_{10}) - j\phi_1, \\
-A^{\odot*}jh_{1001} &= A_1(\phi_0, K_{01}), \\
-A^{\odot*}jh_{0110} &= A_1(\phi_1, K_{10}) - j(h_{1010} - \vartheta_{0010}\phi_0), \\
-A^{\odot*}jh_{0101} &= A_1(\phi_1, K_{01}) - j(h_{1001} - \vartheta_{0001}\phi_0) - \phi_1.
\end{aligned} \tag{61}$$

The solvability condition implies that

$$\begin{aligned}
0 &= 1 - p_1A_1(\phi_0, K_{10}), \\
0 &= -p_1A_1(\phi_0, K_{01}), \\
0 &= -p_1A_1(\phi_1, K_{10}) + \langle \psi_1, h_{1010} \rangle, \\
0 &= -p_1A_1(\phi_1, K_{01}) + \langle \psi_1, h_{1001} \rangle + 1.
\end{aligned} \tag{62}$$

Pairing the first two systems in (61) with ψ_0 yields

$$\begin{aligned}
\langle \psi_1, h_{1010} \rangle &= -p_0A_1(\phi_0, K_{10}), \\
\langle \psi_1, h_{1001} \rangle &= -p_0A_1(\phi_0, K_{01}).
\end{aligned}$$

Using these identities in the last two equations of (62) yields

$$\begin{cases} 0 &= -p_1A_1(\phi_1, K_{10}) - p_0A_1(\phi_0, K_{10}), \\ 0 &= -p_1A_1(\phi_1, K_{01}) - p_0A_1(\phi_0, K_{01}) + 1. \end{cases} \tag{63}$$

Now, let

$$\begin{aligned}
K_{10} &= \delta_1e_1 + \delta_2e_2, \\
K_{01} &= \delta_3e_1 + \delta_4e_2,
\end{aligned}$$

where e_1 and e_2 are the standard basis vectors in \mathbb{R}^2 and $\delta_i (i = 1 \dots 4)$ are constants to be determined. Substituting the above expressions for K_{10} and K_{01} into equations (63), and the first two equations of (62), we obtain, by using the linearity of the multilinear forms, that

$$\begin{cases} 0 &= \delta_1(p_1A_1(\phi_1, e_1) + p_0A_1(\phi_0, e_1)) + \delta_2(p_0A_1(\phi_0, e_2) + p_1A_1(\phi_1, e_2)), \\ 1 &= \delta_3(p_1A_1(\phi_1, e_1) + p_0A_1(\phi_0, e_1)) + \delta_4(p_0A_1(\phi_1, e_2) + p_1A_1(\phi_0, e_2)). \end{cases} \tag{64}$$

and

$$\begin{cases} 1 &= \delta_1p_1A_1(\phi_0, e_1) + \delta_2p_1A_1(\phi_0, e_2), \\ 0 &= \delta_3p_1(A_1(\phi_0, e_1) + A_1(\phi_1, e_2)) + \delta_4p_1(A_1(\phi_0, e_2) + A_1(\phi_1, e_1)), \end{cases} \tag{65}$$

respectively. Thus, the constants $\delta_i (i = 1 \dots 4)$ are obtained by solving the system

$$\begin{pmatrix} p_1A_1(\phi_0, e_1) & p_1A_1(\phi_0, e_2) \\ p_1A_1(\phi_1, e_1) + p_0A_1(\phi_0, e_1) & p_0A_1(\phi_0, e_2) + p_1A_1(\phi_1, e_2) \end{pmatrix} \begin{bmatrix} \delta_1 & \delta_2 \\ \delta_3 & \delta_4 \end{bmatrix} = \begin{pmatrix} 1 & 0 \\ 0 & 1 \end{pmatrix}.$$

Using [Corollary 5](#) we now define the coefficients

$$\hat{h}_{1010} = B_0^{\text{INV}}(A_1(\phi_0, K_{10}), \phi_1) \quad (66)$$

$$\hat{h}_{1001} = B_0^{\text{INV}}(A_1(\phi_0, K_{01}), \phi_1), \quad (67)$$

$$\hat{h}_{0110} = B_0^{\text{INV}}(A_1(\phi_1, K_{10}), h_{1010}), \quad (68)$$

$$\hat{h}_{0101} = B_0^{\text{INV}}(A_1(\phi_1, K_{01}), h_{1001} + \phi_1). \quad (69)$$

Then it follows that solutions to [\(61\)](#) are given by

$$\begin{aligned} h_{1010} &= \hat{h}_{1010} + \gamma_3 \phi_0, \\ h_{1001} &= \hat{h}_{1001} + \gamma_4 \phi_0, \\ h_{0110} &= \hat{h}_{0110} + \gamma_3 \phi_1 - \vartheta_{0010} \phi_1, \\ h_{0101} &= \hat{h}_{0101} + \gamma_4 \phi_1 - \vartheta_{0001} \phi_1, \end{aligned} \quad (70)$$

where γ_3 and γ_4 are constants to be determined. Note that we still have freedom in the coefficients h_{0110} and h_{0101} by an addition of a multiple of the eigenfunction ϕ_0 . However, for our purposes, we will not need to include it here.

4.2.2 Cubic terms

By collecting the cubic terms in the homological equation, we obtain the following systems

$$\begin{aligned} -A^{\odot\star} j h_{2010} &= [A_1(h_{2000}, K_{10}) + 2B(h_{1010}, \phi_0) + B_1(\phi_0, \phi_0, K_{10})] r^{\odot\star} \\ &\quad - 2j (ah_{0110} + h_{1100} - \vartheta_{1000} \phi_1 - a\vartheta_{0010} \phi_1), \\ -A^{\odot\star} j h_{1110} &= [A_1(h_{1100}, K_{10}) + B(h_{0110}, \phi_0) + B(h_{1010}, \phi_1) + B_1(\phi_0, \phi_1, K_{10})] r^{\odot\star} \\ &\quad - j (bh_{0110} + h_{0200} + h_{2010} - \vartheta_{1000}(h_{1010} - \vartheta_{0010} \phi_0) \\ &\quad - \vartheta_{0010}(b\phi_1 - \vartheta_{1000} \phi_0 + h_{2000})), \\ -A^{\odot\star} j h_{2001} &= [A_1(h_{2000}, K_{01}) + 2B(h_{1001}, \phi_0) + B_1(\phi_0, \phi_0, K_{01})] r^{\odot\star} \\ &\quad - 2aj(h_{0101} - \vartheta_{0001} \phi_1), \\ -A^{\odot\star} j h_{1101} &= [A_1(h_{1100}, K_{01}) + B(h_{0101}, \phi_0) + B(h_{1001}, \phi_1) + B_1(\phi_0, \phi_1, K_{01})] r^{\odot\star} \\ &\quad - j (bh_{0101} + h_{1100} + h_{2001} - \vartheta_{1000}(h_{1001} + \phi_1 - \vartheta_{0001} \phi_0) \\ &\quad - \vartheta_{0001}(b\phi_1 - \vartheta_{1000} \phi_0 + h_{2000})), \\ -A^{\odot\star} j h_{1002} &= [2A_1(h_{1001}, K_{01}) + A_1(\phi_0, K_{02}) + A_2(\phi_0, K_{01}, K_{01})] r^{\odot\star}, \\ -A^{\odot\star} j h_{0102} &= [2A_1(h_{0101}, K_{01}) + A_1(\phi_1, K_{02}) + A_2(\phi_1, K_{01}, K_{01})] r^{\odot\star} \\ &\quad - j (2h_{0101} + h_{1002} - 2\vartheta_{0001}(h_{1001} + \phi_1 - \vartheta_{0001} \phi_0)), \\ -A^{\odot\star} j h_{1011} &= [A_1(h_{1001}, K_{10}) + A_1(h_{1010}, K_{01}) + A_1(\phi_0, K_{11}) + A_2(\phi_0, K_{01}, K_{10})] r^{\odot\star} \\ &\quad - j (h_{0101} - \vartheta_{0001} \phi_1), \\ -A^{\odot\star} j h_{0111} &= [A_1(h_{0101}, K_{10}) + A_1(h_{0110}, K_{01}) + A_1(\phi_1, K_{11}) + A_2(\phi_1, K_{01}, K_{10})] r^{\odot\star}, \\ &\quad - j (h_{0110} + h_{1011} - \vartheta_{0010}(h_{1001} + \phi_1 - \vartheta_{0001} \phi_0) - \vartheta_{0001}(h_{1010} - \vartheta_{0010} \phi_0)), \\ -A^{\odot\star} j h_{1020} &= [2A_1(h_{1010}, K_{10}) + A_1(\phi_0, K_{20}) + A_2(\phi_0, K_{10}, K_{10})] r^{\odot\star} \\ &\quad - 2j (h_{0110} - \vartheta_{0010} \phi_1), \\ -A^{\odot\star} j h_{0120} &= [2A_1(h_{0110}, K_{10}) + A_1(\phi_1, K_{20}) + A_2(\phi_1, K_{10}, K_{10})] r^{\odot\star} \\ &\quad - j (h_{1020} - 2\vartheta_{0010}(h_{1010} - \vartheta_{0010} \phi_0)). \end{aligned} \quad (71)$$

To solve the above systems, we write the second order parameter coefficients in K with respect to a basis in K_{10} and K_{01} as follows

$$\begin{aligned} K_{02} &= \gamma_5 K_{10} + \gamma_6 K_{01}, \\ K_{11} &= \gamma_7 K_{10} + \gamma_8 K_{01}, \\ K_{20} &= \gamma_9 K_{10} + \gamma_{10} K_{01}. \end{aligned} \tag{72}$$

By applying the Fredholm alternative to the systems in (71), we obtain ten equations to be solved for (also the ten) variables $\vartheta_{0010}, \vartheta_{0001}, \gamma_3, \gamma_4, \gamma_5, \gamma_6, \gamma_7, \gamma_8, \gamma_9, \gamma_{10}$.

Pairing the first two equations in (71) with ψ_1 and using (70) yields

$$\begin{aligned} 0 &= p_1 \left[A_1(h_{2000}, K_{10}) + 2B(\hat{h}_{1010}, \phi_0) + B_1(\phi_0, \phi_0, K_{10}) \right] \\ &\quad - 2\langle \psi_1, a\hat{h}_{0110} + h_{1100} \rangle + 2\vartheta_{1000} + 2a\gamma_3 + 4a\vartheta_{0010}, \\ 0 &= p_1 \left[A_1(h_{1100}, K_{10}) + B(h_{0110}, \phi_0) + B(h_{1010}, \phi_1) + B_1(\phi_0, \phi_1, K_{10}) \right] \\ &\quad - \langle \psi_1, ah_{0110} + h_{0200} + h_{2010} - \vartheta_{1000}(bh_{1010} - \vartheta_{0010}\phi_0) \\ &\quad - \vartheta_{0010}(b\phi_1 - \vartheta_{1000}\phi_0 + h_{2000}) \rangle. \end{aligned} \tag{73}$$

Since h_{2010} is still to be determined we use that

$$\langle \psi_1, h_{2010} \rangle = \langle jh_{2010}, A^\odot \psi_0 \rangle = \langle A^{\odot*} jh_{2010}, \psi_0 \rangle,$$

Furthermore, from (38) we obtain that

$$\langle \psi_1, b\phi_1 - \vartheta_{1000}\phi_0 + h_{2000} \rangle = p_1 B(\phi_0, \phi_1). \tag{74}$$

Thus, the second equation in (73) becomes

$$\begin{aligned} 0 &= p_1 \left[A_1(h_{1100}, K_{10}) + B(h_{0110}, \phi_0) + B(h_{1010}, \phi_1) + B_1(\phi_0, \phi_1, K_{10}) \right] \\ &\quad + p_0 \left[A_1(h_{2000}, K_{10}) + 2B(h_{1010}, \phi_0) + B_1(\phi_0, \phi_0, K_{10}) \right] \\ &\quad - 2\langle \psi_0, ah_{0110} + h_{1100} \rangle - \langle \psi_1, bh_{0110} + h_{0200} - \vartheta_{1000}(h_{1010} - \vartheta_{0010}\phi_0) \rangle \\ &\quad + \vartheta_{0010} p_1 B(\phi_0, \phi_1). \end{aligned}$$

Substituting (72) into the above expression, and using the linearity of the multilinear forms yields

$$\begin{aligned} 0 &= p_1 \left[A_1(h_{1100}, K_{10}) + B(\hat{h}_{0110}, \phi_0) + B(\hat{h}_{1010}, \phi_1) + B_1(\phi_0, \phi_1, K_{10}) \right] \\ &\quad + p_0 \left[A_1(h_{2000}, K_{10}) + 2B(\hat{h}_{1010}, \phi_0) + B_1(\phi_0, \phi_0, K_{10}) \right] \\ &\quad - 2\langle \psi_0, a\hat{h}_{0110} + h_{1100} \rangle - \langle \psi_1, b\hat{h}_{0110} + h_{0200} - \vartheta_{1000}\hat{h}_{1010} \rangle \\ &\quad + b\gamma_3 + b\vartheta_{0010}. \end{aligned}$$

It follows that the constants γ_3 and ϑ_{0010} are give by

$$\begin{pmatrix} 2a & 4a \\ b & b \end{pmatrix} \begin{pmatrix} \gamma_3 \\ \vartheta_{0010} \end{pmatrix} = \begin{pmatrix} \zeta_1 \\ \zeta_2 \end{pmatrix}, \tag{75}$$

where the right-hand side is given by

$$\begin{aligned} \zeta_1 &= -p_1 \left[A_1(h_{2000}, K_{10}) + 2B(\hat{h}_{1010}, \phi_0) + B_1(\phi_0, \phi_0, K_{10}) \right] \\ &\quad + 2\langle \psi_1, a\hat{h}_{0110} + h_{1100} \rangle - 2\vartheta_{1000}, \\ \zeta_2 &= -p_1 \left[A_1(h_{1100}, K_{10}) + B(\hat{h}_{0110}, \phi_0) + B(\hat{h}_{1010}, \phi_1) + B_1(\phi_0, \phi_1, K_{10}) \right] \\ &\quad - p_0 \left[A_1(h_{2000}, K_{10}) + 2B(\hat{h}_{1010}, \phi_0) + B_1(\phi_0, \phi_0, K_{10}) \right] \\ &\quad + 2\langle \psi_0, a\hat{h}_{0110} + h_{1100} \rangle + \langle \psi_1, b\hat{h}_{0110} + h_{0200} - \vartheta_{1000}\hat{h}_{1010} \rangle. \end{aligned} \tag{76}$$

Notice here that the matrix given in the left-hand side in (75) is equivalent to the matrix in (48) when performing the center manifold reduction near the generic Bogdanov–Takens bifurcation.

The third and fourth systems in (71) lead to a similar system. Indeed, by pairing these systems with the adjoint eigenfunction ψ_1 and using (70) leads to the equations

$$\begin{aligned} 0 &= p_1 \left[A_1(h_{2000}, K_{01}) + 2B(\hat{h}_{1001}, \phi_0) + B_1(\phi_0, \phi_0, K_{01}) \right] - 2a\langle \psi_1, \hat{h}_{0101} \rangle + 2a\gamma_4 + 4a\vartheta_{0001}, \\ 0 &= p_1 \left[A_1(h_{1100}, K_{01}) + B(h_{0101}, \phi_0) + B(h_{1001}, \phi_1) + B_1(\phi_0, \phi_1, K_{01}) \right] \\ &\quad - \langle \psi_1, bh_{0101} + h_{1100} + h_{2001} - \vartheta_{1000}(h_{1001} + \phi_1 - \vartheta_{0001}\phi_0) \\ &\quad - \vartheta_{0001}(b\phi_1 - \vartheta_{1000}\phi_0 + h_{2000}) \rangle. \end{aligned} \quad (77)$$

By using (70) and (74) the second equation becomes

$$\begin{aligned} 0 &= p_1 \left[A_1(h_{1100}, K_{01}) + B(\hat{h}_{0101}, \phi_0) + B(\hat{h}_{1001}, \phi_1) + B_1(\phi_0, \phi_1, K_{01}) \right] + \\ &\quad p_0 \left[A_1(h_{2000}, K_{01}) + 2B(\hat{h}_{1001}, \phi_0) + B_1(\phi_0, \phi_0, K_{01}) \right] - 2a\langle \psi_0, \hat{h}_{0101} \rangle \\ &\quad - \langle \psi_1, b\hat{h}_{0101} + h_{1100} - \vartheta_{1000}\hat{h}_{1001} \rangle + \vartheta_{1000} + b\gamma_4 + b\vartheta_{0001}. \end{aligned}$$

It follows that the constants γ_4 and ϑ_{0001} are give by

$$\begin{pmatrix} 2a & 4a \\ b & b \end{pmatrix} \begin{pmatrix} \gamma_4 \\ \vartheta_{0001} \end{pmatrix} = \begin{pmatrix} \zeta_3 \\ \zeta_4 \end{pmatrix}, \quad (78)$$

where the right-hand side is given by

$$\begin{aligned} \zeta_3 &= -p_1 \left[A_1(h_{2000}, K_{01}) + 2B(\hat{h}_{1001}, \phi_0) + B_1(\phi_0, \phi_0, K_{01}) \right] + 2a\langle \psi_1, \hat{h}_{0101} \rangle \\ \zeta_4 &= -p_1 \left[A_1(h_{1100}, K_{01}) + B(\hat{h}_{0101}, \phi_0) + B(\hat{h}_{1001}, \phi_1) + B_1(\phi_0, \phi_1, K_{01}) \right] + \\ &\quad - p_0 \left[A_1(h_{2000}, K_{01}) + 2B(\hat{h}_{1001}, \phi_0) + B_1(\phi_0, \phi_0, K_{01}) \right] + 2a\langle \psi_0, \hat{h}_{0101} \rangle \\ &\quad + \langle \psi_1, b\hat{h}_{0101} + h_{1100} - \vartheta_{1000}\hat{h}_{1001} \rangle + \vartheta_{1000}. \end{aligned} \quad (79)$$

Now that ϑ_{0010} , ϑ_{0001} , γ_3 , and γ_4 are known, we can apply the Fredholm alternative to the remaining six systems in (71). This yields equations which can be solved separately, i.e. without a matrix as in (76) and (79). To keep the derivation readable, we divide six equations into three groups. We start by pairing the fifth and sixth equations in (71) with ψ_1 . We obtain that

$$\begin{aligned} \gamma_5 &= -p_1 \left[2A_1(\hat{h}_{1001}, K_{01}) + A_2(\phi_0, K_{01}, K_{01}) \right]. \\ 0 &= p_1 \left[2A_1(h_{0101}, K_{01}) + A_1(\phi_1, K_{02}) + A_2(\phi_1, K_{01}, K_{01}) \right] \\ &\quad - \langle \psi_1, 2h_{0101} + h_{1002} - 2\vartheta_{0001}(h_{1001} + \phi_1 - \vartheta_{0001}\phi_0) \rangle, \\ &= p_1 \left[2A_1(\hat{h}_{0101}, K_{01}) + A_2(\phi_1, K_{01}, K_{01}) \right] + p_0 \left[2A_1(\hat{h}_{1001}, K_{01}) + A_2(\phi_0, K_{01}, K_{01}) \right] \\ &\quad - 2\langle \psi_1, \hat{h}_{0101} \rangle + \gamma_6 + 2\vartheta_{0001} \end{aligned}$$

Here we used (70) and (72), and the (by now) equalities given (62) and (63). It follows that

$$\begin{aligned} \gamma_6 &= -p_1 \left[2A_1(\hat{h}_{0101}, K_{01}) + A_2(\phi_1, K_{01}, K_{01}) \right] - p_0 \left[2A_1(\hat{h}_{1001}, K_{01}) + A_2(\phi_0, K_{01}, K_{01}) \right] \\ &\quad + 2\langle \psi_1, \hat{h}_{0101} \rangle - 2\vartheta_{0001}. \end{aligned}$$

By applying the Fredholm alternative to the last four systems in (71), we obtain equations which can be solved similarly as the last two equations. We obtain that

$$\begin{aligned}
\gamma_7 &= -p_1 \left[A_1(\hat{h}_{1001}, K_{10}) + A_1(\hat{h}_{1010}, K_{01}) + A_2(\phi_0, K_{01}, K_{10}) \right] + \langle \psi_1, \hat{h}_{0101} \rangle - 2\vartheta_{0001}, \\
\gamma_8 &= -p_1 \left[A_1(\hat{h}_{0101}, K_{10}) + A_1(\hat{h}_{0110}, K_{01}) + A_2(\phi_1, K_{01}, K_{10}) \right] + \langle \psi_1, \hat{h}_{0110} \rangle \\
&\quad - p_0 \left[A_1(\hat{h}_{1001}, K_{10}) + A_1(\hat{h}_{1010}, K_{01}) + A_2(\phi_0, K_{01}, K_{10}) \right] + \langle \psi_0, \hat{h}_{0101} \rangle - \vartheta_{0010}, \\
\gamma_9 &= -p_1 \left[2A_1(\hat{h}_{1010}, K_{10}) + A_2(\phi_0, K_{10}, K_{10}) \right] + 2\langle \psi_1, \hat{h}_{0110} \rangle - 4\vartheta_{0010}, \\
\gamma_{10} &= -p_1 \left[2A_1(\hat{h}_{0110}, K_{10}) + A_2(\phi_1, K_{10}, K_{10}) \right] \\
&\quad - p_0 \left[2A_1(\hat{h}_{1010}, K_{10}) + A_2(\phi_0, K_{10}, K_{10}) \right] + 2\langle \psi_0, \hat{h}_{0110} \rangle.
\end{aligned} \tag{80}$$

Now when all systems in (71) are consistent, we use Corollary 5 to obtain the solutions

$$\begin{aligned}
h_{2010} &= B_0^{\text{INV}} (A_1(h_{2000}, K_{10}) + 2B(h_{1010}, \phi_0) + B_1(\phi_0, \phi_0, K_{10}), \\
&\quad 2(a h_{0110} + h_{1100} - \vartheta_{1000}\phi_1 - a\vartheta_{0010}\phi_1)), \\
h_{1110} &= B_0^{\text{INV}} (A_1(h_{1100}, K_{10}) + B(h_{0110}, \phi_0) + B(h_{1010}, \phi_1) + B_1(\phi_0, \phi_1, K_{10}), \\
&\quad b h_{0110} + h_{0200} + h_{2010} - \vartheta_{1000}(h_{1010} - \vartheta_{0010}\phi_0) \\
&\quad - \vartheta_{0010}(b\phi_1 - \vartheta_{1000}\phi_0 + h_{2000})), \\
h_{2001} &= B_0^{\text{INV}} (A_1(h_{2000}, K_{01}) + 2B(h_{1001}, \phi_0) + B_1(\phi_0, \phi_0, K_{01}), 2a(h_{0101} - \vartheta_{0001}\phi_1)), \\
h_{1101} &= B_0^{\text{INV}} (A_1(h_{1100}, K_{01}) + B(h_{0101}, \phi_0) + B(h_{1001}, \phi_1) + B_1(\phi_0, \phi_1, K_{01}), \\
&\quad b h_{0101} + h_{1100} + h_{2001} - \vartheta_{1000}(h_{1001} + \phi_1 - \vartheta_{0001}\phi_0) \\
&\quad - \vartheta_{0001}(b\phi_1 - \vartheta_{1000}\phi_0 + h_{2000})), \\
h_{1002} &= B_0^{\text{INV}} (2A_1(h_{1001}, K_{01}) + A_1(\phi_0, K_{02}) + A_2(\phi_0, K_{01}, K_{01})), \\
h_{0102} &= B_0^{\text{INV}} (2A_1(h_{0101}, K_{01}) + A_1(\phi_1, K_{02}) + A_2(\phi_1, K_{01}, K_{01}), \\
&\quad 2h_{0101} + h_{1002} - 2\vartheta_{0001}(h_{1001} + \phi_1 - \vartheta_{0001}\phi_0)), \\
h_{1011} &= B_0^{\text{INV}} (A_1(h_{1001}, K_{10}) + A_1(h_{1010}, K_{01}) + A_1(\phi_0, K_{11}) + A_2(\phi_0, K_{01}, K_{10}), \\
&\quad h_{0101} - \vartheta_{0001}\phi_1), \\
h_{0111} &= B_0^{\text{INV}} (A_1(h_{0101}, K_{10}) + A_1(h_{0110}, K_{01}) + A_1(\phi_1, K_{11}) + A_2(\phi_1, K_{01}, K_{10}), \\
&\quad h_{0110} + h_{1011} - \vartheta_{0010}(h_{1001} + \phi_1 - \vartheta_{0001}\phi_0) - \vartheta_{0001}(h_{1010} - \vartheta_{0010}\phi_0)), \\
h_{1020} &= B_0^{\text{INV}} (2A_1(h_{1010}, K_{10}) + A_1(\phi_0, K_{20}) + A_2(\phi_0, K_{10}, K_{10}), 2(h_{0110} - \vartheta_{0010}\phi_1)), \\
h_{0120} &= B_0^{\text{INV}} (2A_1(h_{0110}, K_{10}) + A_1(\phi_1, K_{20}) + A_2(\phi_1, K_{10}, K_{10}), \\
&\quad h_{1020} - 2\vartheta_{0010}(h_{1010} - \vartheta_{0010}\phi_0)).
\end{aligned} \tag{81}$$

4.2.3 Homolinc asymptotics

To approximate the homoclinic solutions emanating from the transcritical Bogdanov–Takens point, we apply the singular rescaling

$$\beta_1 = \pm 4 \frac{a^2}{b^2} \epsilon^2, \quad \beta_2 = \frac{a}{b} (\tau \pm 2) \epsilon^2, \quad w_0 = \frac{a}{b^2} (u \mp 2) \epsilon^2, \quad w_1 = \frac{a^2}{b^3} v \epsilon^3, \quad s = \frac{a}{b} \epsilon \eta, \quad (\epsilon \neq 0), \tag{82}$$

to (56) with $h(0, 0) = 0$ to obtain the second-order nonlinear oscillator

$$\ddot{u} = -4 + u^2 + \dot{u}(u + \tau)\epsilon + \mathcal{O}(\epsilon^4). \quad (83)$$

Note that this is precisely the second-order nonlinear oscillator obtained in [3] when deriving asymptotics for the homoclinic solutions emanating from the generic Bogdanov–Takens bifurcation. Therefore, the third-order homoclinic asymptotics for the homoclinic orbits emanating from (56) are given by

$$\begin{cases} w_0(\eta) = \frac{a}{b^2} \left[\tilde{u} \left(\tanh \left(\xi \left(\frac{a}{b} \epsilon \eta \right) \right) \mp 2 \right) \right] \epsilon^2, \\ w_1(\eta) = \frac{a^2}{b^3} \tilde{v} \left(\tanh \left(\xi \left(\frac{a}{b} \epsilon \eta \right) \right) \right) \epsilon^3, \\ \beta_1 = \pm 4 \frac{a^2}{b^2} \epsilon^2, \\ \beta_2 = \frac{a}{b} (\tau \pm 2) \epsilon^2, \end{cases} \quad (84)$$

where $\tau, \tilde{u}, \tilde{v}$, and ξ are again given by (55). Next, we need to obtain $\eta(t)$ to approximate the profiles of the homoclinic solution. For this we integrate (60) to obtain

$$t(\eta) = (1 + \vartheta_{0010}\beta_1 + \vartheta_{0001}\beta_2)\eta + \vartheta_{1000} \frac{a}{b^2} \int \left[\tilde{u} \left(\tanh \left(\xi \left(\frac{a}{b} \epsilon \eta \right) \right) \mp 2 \right) \right] \epsilon^2 d\eta.$$

Here, β_1 and β_2 are given by (84) and from [3] we obtain that

$$\begin{aligned} \epsilon \frac{a}{b} \int \tilde{u} \left(\tanh \left(\xi \left(\frac{a}{b} \epsilon \eta \right) \right) \right) d\eta &= 2\tilde{\xi} - 6 \tanh(\tilde{\xi}) + \left(\frac{18 \operatorname{sech}^2(\tilde{\xi})}{7} + \frac{12}{7} \log(\cosh(\tilde{\xi})) \right) \epsilon \\ &+ \frac{9}{49} \left(4\tilde{\xi} - 9 \tanh(\tilde{\xi}) + 5 \tanh(\tilde{\xi}) \operatorname{sech}^2(\tilde{\xi}) \right) \epsilon^2 \\ &+ \frac{18 \left(-21 \operatorname{sech}^4(\tilde{\xi}) + 47 \operatorname{sech}^2(\tilde{\xi}) + 8 \log(\cosh(\tilde{\xi})) \right)}{2401} \epsilon^3 \\ &+ \mathcal{O}(\epsilon^4), \end{aligned} \quad (85)$$

where $\tilde{\xi} = \xi \left(\frac{a}{b} \eta \epsilon \right)$.

It remains to numerically solve the equation

$$t(\eta) - t = 0,$$

for η .

4.2.4 Codimension-one equilibrium bifurcations

To approximate the transcritical and Hopf curves and their corresponding equilibria in (56), one should substitute the expressions for β and the equilibrium coordinates into the expansions (58) and (59). It follows that the transcritical curve is approximated by

$$\begin{cases} x = \mathcal{H}(0, 0, 0, 0), \\ \alpha = K(0, \epsilon), \end{cases}$$

for $|\epsilon|$ small. The Hopf curves are approximated by

$$\begin{cases} \omega = \epsilon, \\ x = \mathcal{H}(0, 0, -\epsilon^2, 0), \\ \alpha = K(-\epsilon^2, 0), \end{cases}$$

and

$$\begin{cases} \omega = \epsilon, \\ x = \mathcal{H} \left(-\frac{\epsilon^2}{a}, 0, \epsilon^2, \frac{b}{a}\epsilon^2 \right), \\ \alpha = K \left(\epsilon^2, \frac{b}{a}\epsilon^2 \right), \end{cases}$$

for $\epsilon > 0$ small.

5 Examples

In this section, we will demonstrate the correctness of the center manifold reduction and the homoclinic asymptotics from [Section 4](#) on four different models from [\[15, 19, 24, 25\]](#) in which Bogdanov–Takens bifurcation points are present. Using our implementation in `DDE-BifTool`, we will compute the local unfolding of the Bogdanov–Takens singularities and compare the emanating codimension one curves with the derived asymptotics. We will show a clear improvement to the homoclinic solutions by using the third-order instead of the first order asymptotics.

Additionally, following [\[3\]](#), we will also show that the approximation order of the homoclinic asymptotic lifts correctly to the parameter-dependent center manifold, see in particular [Figures 3 and 4](#).

Lastly, we will perform numerical simulations near the bifurcation point under consideration. The reason for this extra step is twofold. Firstly, it will provide additional verification of the given results. Secondly, it seems to be a standard part in papers studying Bogdanov–Takens bifurcation points in DDEs. We will integrate the DDE directly, not the reduced system on the center manifold, which is often the case in literature. The simulation is performed using the Julia package `DifferentialEquations.jl` [\[30\]](#). However, since in this section only the main results are given, we provide full details (including simulation results) in the [Supplement](#). Furthermore, the source code of the examples has been included into the `DDE-BifTool` software package. Altogether, this will hopefully provide a good starting point when considering other models.

5.1 Bogdanov–Takens bifurcation in a predator-prey system with double Allee effect

In [\[25\]](#) the following predator-prey model with double Allee effect and delay is considered

$$\begin{cases} \dot{x}(t) = \frac{rx}{x+n_0} \left(1 - \frac{1}{K} \right) (x - m_0) - \frac{cxy}{x + \varrho y}, \\ \dot{y}(t) = -dy + \frac{c_1 x(t-\tau)y}{x(t-\tau) + \varrho y(t-\tau)}. \end{cases} \quad (86)$$

Here, the time delay $\tau \geq 0$ is introduced due to the fact that the reproduction of predator after consuming the prey is not instantaneous, but is mediated by some time lag required for gestation. The variables and parameters occurring in [\(86\)](#) have the following meaning:

- $x, y: \mathbb{R} \rightarrow \mathbb{R}$ denote the prey and predator population densities, respectively.
- r denotes the maximum prey population growth in absence of the Allee effect.
- K is the carrying capacity of the environment.
- m_0 is the Allee threshold.
- n_0 is the auxiliary parameter in order to quantify the strength of the Allee effect.

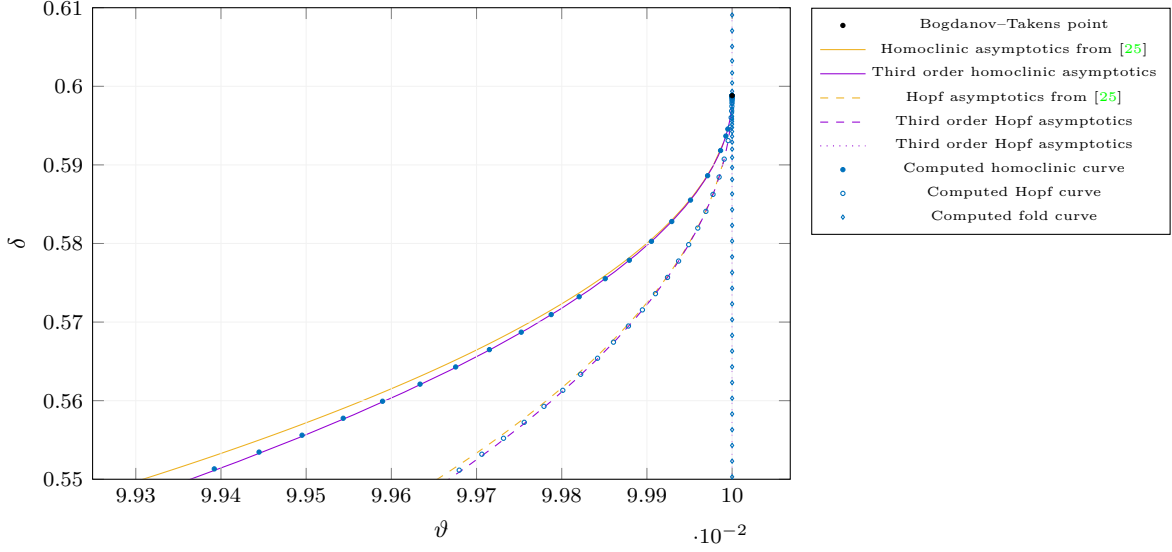


Figure 1: Bifurcation diagram near the derived generic Bogdanov-Takens point in (87) comparing computed codimension one using DDE-BifTool with the asymptotics obtained in this paper and in [25].

- c denotes the capturing rate of the predator.
- ϱ is the half capturing saturation constant.
- c_1 is the conversion rate of prey into predators biomass.
- d is the per capita predator mortality rate.

Following [25], let $(x, y, t) = \left(K\bar{x}, \frac{K}{\varrho}\bar{y}, \frac{\bar{t}}{r}\right)$, and immediately dropping the bars again for readability, then (86) becomes

$$\begin{cases} \dot{x}(t) = x \left(\frac{(1-x)(x-\gamma)}{x+\vartheta} - \frac{\alpha y}{x+y} \right), \\ \dot{y}(t) = \delta y \left(-1 + \frac{mx(t-\tau)}{x(t-\tau) + y(t-\tau)} \right), \end{cases} \quad (87)$$

where $\vartheta = \frac{n_0}{K}$, $\alpha = \frac{c}{r\varrho}$, $\gamma = \frac{m_0}{K}$, $\delta = \frac{d}{r}$ and $m = \frac{c_1}{d}$. In [25] the phase-space is (although possible) unnecessarily enlarged to include a parameter. The resulting extended system is used to derive conditions for a Bogdanov-Takens bifurcation to occur and obtain the normal form on the center manifold. In our opinion, one should only use the extended system to prove the existence of a parameter-dependent center manifold, from which it then follows that we can perform the normalization as described in Section 3. Thus, solving (87) for a double equilibrium with respect to (x, y) and ϑ yields

$$\begin{cases} x_0 = \frac{m + \alpha - m\alpha + m\gamma}{2m}, \\ y_0 = (m-1)x_0, \\ \vartheta_0 = \frac{(\alpha + m(1 - \alpha + \gamma))^2 - 4m^2\gamma}{4(m-1)m\alpha}, \end{cases} \quad (88)$$

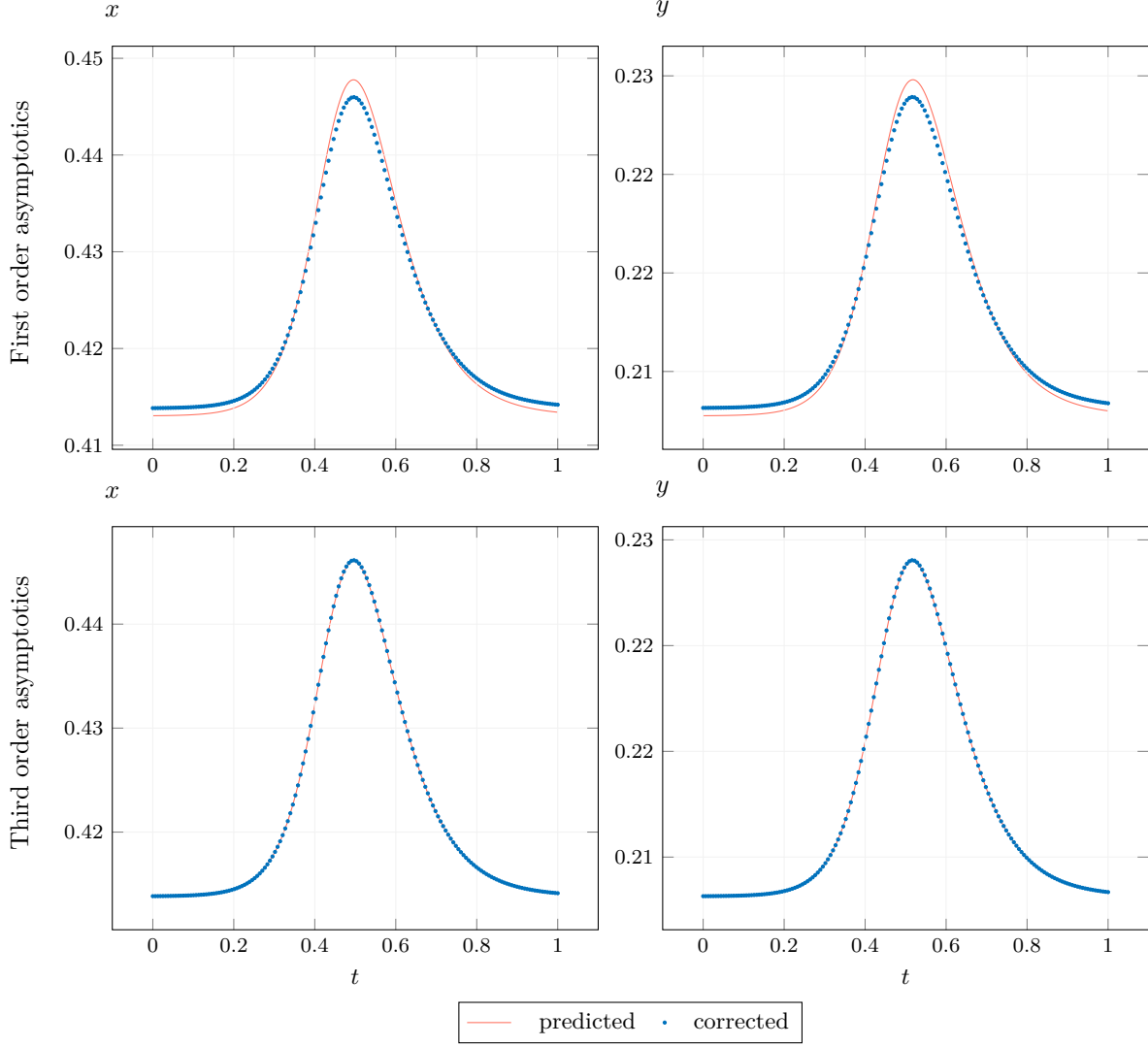


Figure 2: Comparison between the profiles of the first and third-order asymptotics from Section 4.1.9 with the Newton correct solutions near the generic Bogdanov–Takens bifurcation in (87) with the perturbation parameter set to $\epsilon = 0.3$.

for $m \neq 1$. The parameters should of course be chosen such that x and y are non-negative. The characteristic matrix at $(x, y, \vartheta) = (x_0, y_0, \vartheta_0)$ becomes

$$\Delta(z) = \begin{pmatrix} z + \frac{1-m}{m^2}\alpha & \frac{\alpha}{m^2} \\ -\frac{(m-1)^2\delta}{m}e^{-z\tau} & z + \frac{(m-1)\delta}{m}e^{-z\tau} \end{pmatrix}$$

for $m \neq 0$. A simple calculation confirms indeed that $\det \Delta(0) = 0$. Furthermore, $\det \Delta'(0) = \frac{(m-1)(m\delta-\alpha)}{m^2}$ and $\det \Delta''(0) = 2 - \frac{2(m-1)\delta\tau}{m}$. Thus, for $(x, y, \vartheta, \delta) = (x_0, y_0, \vartheta_0, \delta_0)$, with $\delta_0 = \frac{\alpha}{m}$, we have a double zero eigenvalue, provided that $\det \Delta''(0) \neq 0$. To confirm their analytical findings in [25]

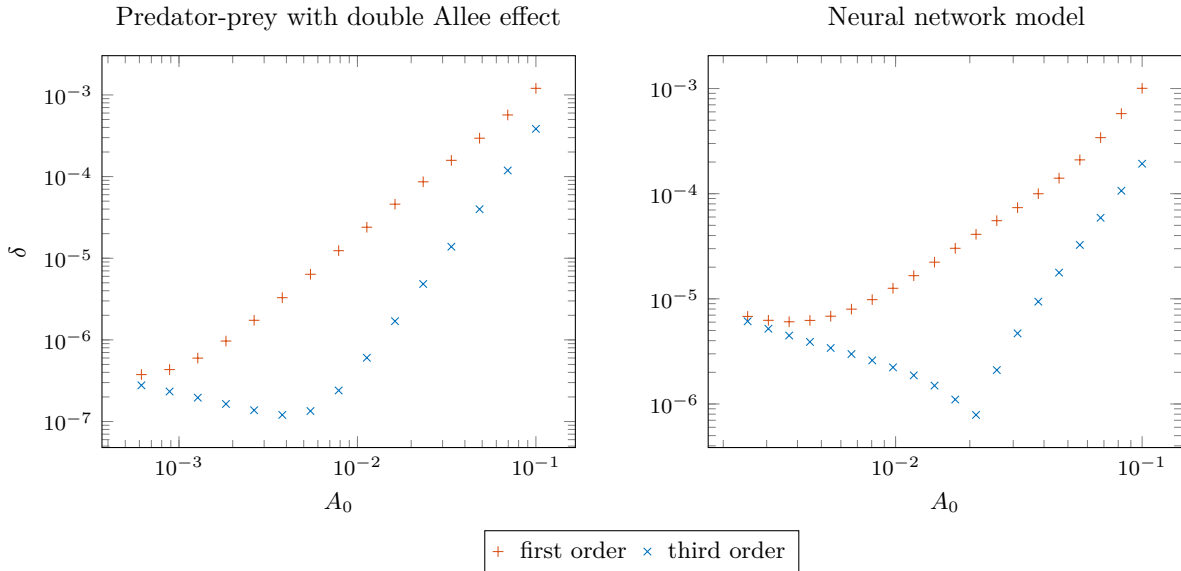


Figure 3: On the abscissa is the approximation to the amplitude A_0 and on the ordinate the relative error δ between the constructed solution to the defining system [32] for the homoclinic orbit and the Newton corrected solution.

numerically, the parameters $\gamma = 0.15$, $\alpha = 0.9$ and $m = 1.50298303$ are fixed and (ϑ, δ) are taken as unfolding parameters. For these parameters, we indeed have that $\det \Delta''(0) \neq 0$. Calculating the normal form coefficients a and b reveal that,

$$a \approx 0.1479, \quad b \approx 1.4457.$$

Thus, the codimension two Bogdanov–Takens bifurcation is non-degenerate. Furthermore, since the equilibrium (x_0, y_0) depends on the unfolding parameters, we are in the generic case. Using our implementation of the homoclinic predictor Section 4.1.9 in DDE-BifTool, we start the continuation of the homoclinic branch emanating from the Bogdanov–Takens point.

In Figure 1, we compare the parameters of the computed homoclinic branch with our third-order parameter asymptotics and the parameters for the homoclinic branch given in [25]. We observe that although the derivation of the asymptotics for the parameters is non-rigorous, it provides a good predictor. Nonetheless, our third-order asymptotics for the parameter values provides clearly a better approximation to the parameter values of the computed homoclinic branch.

Of course, most work lies in the derivation of the asymptotics for the homoclinic solutions in phase-space itself, which is not available in [25]. In Figure 2 we compare the first and third-order asymptotics for the profiles of the homoclinic solution. Here, we set the perturbation parameter to $\epsilon = 0.3$ such that both approximations converge, and we observe a visual difference.

However, a better way to compare the first and third-order asymptotics for the homoclinic solution numerically is through the convergence plots, similarly as in [3]. In Figure 3 we clearly see an improvement of using the third-order asymptotics over the first order asymptotics. We furthermore observe the standard V-shaped graphs due to round-off error.

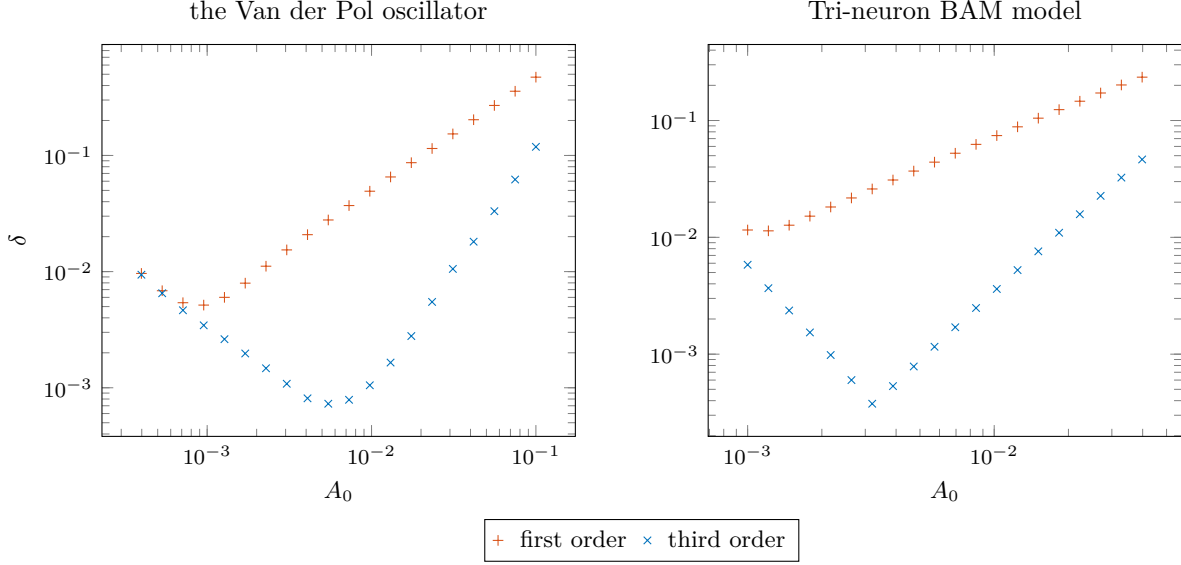


Figure 4: On the abscissa is the approximation to the amplitude A_0 and on the ordinate the relative error δ between the constructed solution to the defining system for the homoclinic orbit and the Newton corrected solution.

5.2 Generic Bogdanov–Takens bifurcation in a neural network model

In this example, we will consider the model

$$\begin{cases} \mu \dot{u}_1(t) = -u_1(t) + q_{11}\alpha(u_1(t-T)) - q_{12}u_2(t-T) + e_1, \\ \mu \dot{u}_2(t) = -u_2(t) + q_{21}\alpha(u_1(t-T)) - q_{22}u_2(t-T) + e_2, \end{cases} \quad (89)$$

which describes the dynamics of a neural network consisting of an excitatory and inhibitory neuron [19]. The variables and parameters occurring in (89) have the following neurophysiological meaning:

- $u_1, u_2 : \mathbb{R} \rightarrow \mathbb{R}$ denote the total post-synaptic potentials of the excitatory and inhibitory neurons, respectively.
- $\mu > 0$ is a time constant characterizing the dynamical properties of cell membrane.
- $q_{ik} \geq 0$ represent the strength of the connection line from the k th neuron to the i th neuron.
- $\alpha : \mathbb{R} \rightarrow \mathbb{R}$ is the transfer function which describes the activity generation of the excitatory neuron as a function of its total potential u_1 . The function α is smooth, increasing and has a unique turning point at $u_1 = \theta$. The transfer function corresponding to the inhibitory neuron is assumed to be the identity.
- $T \geq 0$ is a time delay reflecting synaptic delay, axonal and dendritic propagation time.
- e_1 and e_2 are external stimuli acting on the excitatory and inhibitory neuron, respectively.

Following [19] we consider the equation (89) with

$$\begin{aligned} \alpha(u_1) &= \frac{1}{1 + e^{-4u_1}} - \frac{1}{2}, & q_{11} &= 2.6, & q_{21} &= 1.0, & q_{22} &= 0.0, \\ \mu &= 1.0, & T &= 1.0, & e_2 &= 0.0, \end{aligned}$$

and $Q := q_{12}$, $E := e_1$ as bifurcation parameters. Substituting into (89) yields

$$\begin{cases} \dot{u}_1(t) = -u_1(t) + 2.6\alpha(u_1(t-1)) - Qu_2(t-1) + E, \\ \dot{u}_2(t) = -u_2(t) + \alpha(u_1(t-1)). \end{cases} \quad (90)$$

Notice that for any steady-state we have the symmetry $(u_1, u_2, E) \rightarrow (-u_1, -u_2, -E)$. It is easy to explicitly derive that the system has a double eigenvalue zero for

$$\begin{cases} u_1(t) = \frac{1}{4} \log\left(\frac{8 - \sqrt{39}}{5}\right) \approx -0.2617, \\ u_2(t) = -\frac{1}{2} \sqrt{\frac{3}{13}} \approx -0.2402, \\ Q = \frac{13}{10}, \\ E = \frac{\sqrt{39} - 10 \operatorname{atanh}\sqrt{\frac{3}{13}}}{20} \approx 0.0505. \end{cases} \quad (91)$$

The dependence of the equilibria on the parameters (Q, E) yields a generic Bogdanov–Takens bifurcation, see [19]. Notice that the normal form reduction in [19] is incorrect, which leads to the normal form for a transcritical Bogdanov–Takens bifurcation.

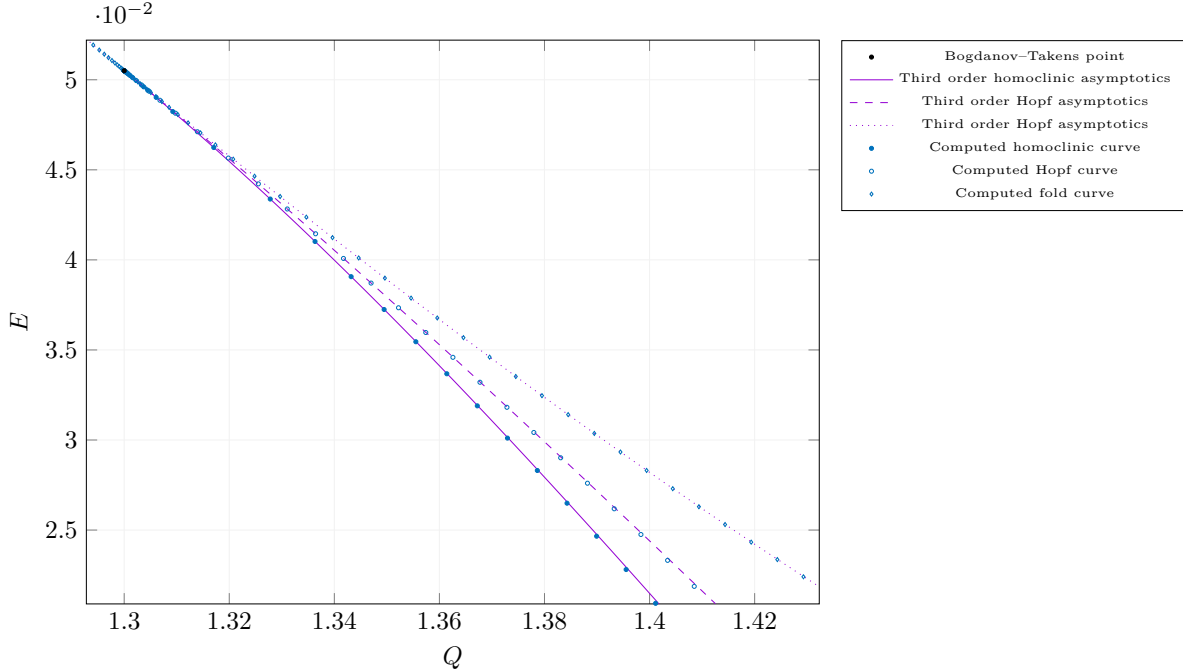


Figure 5: Bifurcation diagram near the derived generic Bogdanov-Takens point in (90) comparing computed codimension one curves using DDE-BifTool with the third-order homoclinic parameter asymptotics obtained in Section 4.1.9.

In Figure 5 we compared the computed codimension one curves emanating from a generic Bogdanov–Takens point in (90) using our implementation in DDE-BifTool with the third-order homoclinic parameter asymptotics obtained in Section 4.1.9. We see that the predicted and computed curves are almost

indistinguishable. Furthermore, in [Figure 3](#), we see that using the third-order homoclinic asymptotics over the first order is clearly superior.

5.3 Transcritical Bogdanov–Takens bifurcation in the Van der Pol oscillator with delay feedback

We consider the Van der Pol oscillator with delay feedback [\[24\]](#) given by

$$\ddot{x}(t) + \epsilon(x^2(t) - 1)\dot{x}(t) + x(t) = \epsilon g(x(t - \tau)), \quad (92)$$

where $\epsilon > 0$ is a parameter, $\tau > 0$ is a delay and $g : \mathbb{R} \rightarrow \mathbb{R}$ is a smooth function with $g(0) = 0$ and $g'(0) \neq 0$. We rewrite the Van der Pol equation [\(92\)](#) as

$$\begin{cases} \dot{x}_1 = x_2, \\ \dot{x}_2 = \epsilon g(x_1(t - \tau)) - \epsilon(x_1^2 - 1)x_2 - x_1. \end{cases} \quad (93)$$

Rescaling time with $t \rightarrow \frac{t}{\tau}$ to normalize the delay yields

$$\begin{cases} \dot{x}_1 = \tau x_2, \\ \dot{x}_2 = \tau (\epsilon g(x_1(t - 1)) - \epsilon(x_1^2 - 1)x_2 - x_1). \end{cases} \quad (94)$$

This allows us to treat τ as a bifurcation parameter.

Following [\[24\]](#), we consider [\(92\)](#) with

$$g(x) = \frac{e^x - 1}{c_1 e^x + c_2},$$

where $c_1 = \frac{1}{4}$ and $c_2 = \frac{1}{2}$. Then the trivial equilibrium undergoes a transcritical Bogdanov–Takens bifurcation at parameter values $(\epsilon, \tau) = (0.75, 0.75)$, see [\[24\]](#) and the supplement.

In [Figure 6](#) we compared the computed codimension one curves emanating from a transcritical Bogdanov–Takens point in [\(94\)](#) using our implementation in `DDE-BifTool` with the third-order homoclinic parameter asymptotics obtained in [Section 4.2.3](#). We see that the predicted and computed curves are almost indistinguishable. Furthermore, in [Figure 4](#) we see that using the third-order homoclinic asymptotics over the first order is clearly superior.

5.4 Transcritical Bogdanov–Takens bifurcation in a tri-neuron BAM neural network model

We consider a three-component system of a tri-neuron bidirectional associative memory (BAM) neural network model with multiple delays [\[15\]](#). The architecture of this BAM model is illustrated in [Figure 7](#).

In this model, there is only one neuron with the activation function f_1 on the I -layer and there are two neurons with respective activation functions f_2 and f_3 on the J -layer. It is assumed that the time delay from the I -layer to the J -layer is τ_1 , while the time delay from the J -layer to the I -layer is τ_2 . Then the network can be described by the following delay differential equation

$$\begin{cases} \dot{x}_1(t) &= -\mu_1 x_1(t) + c_{21} f_1(x_2(t - \tau_2)) + c_{31} f_1(x_3(t - \tau_2)), \\ \dot{x}_2(t) &= -\mu_2 x_2(t) + c_{12} f_2(x_1(t - \tau_1)), \\ \dot{x}_3(t) &= -\mu_3 x_3(t) + c_{13} f_3(x_1(t - \tau_1)). \end{cases} \quad (95)$$

Here

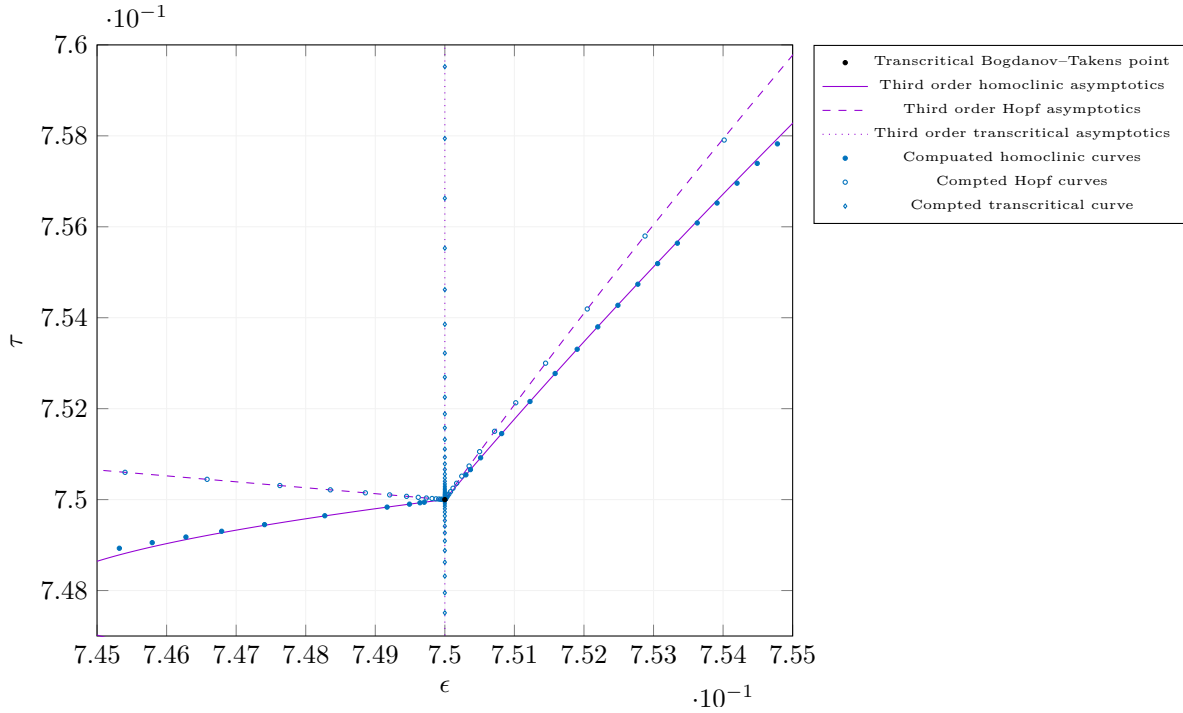


Figure 6: Bifurcation diagram near the derived generic Bogdanov-Takens point in (94) comparing computed codimension one curves using DDE-BifTool with the third-order homoclinic parameter asymptotics obtained in Section 4.2.3.

- $x_i(t)$ ($i = 1, 2, 3$) denote the state of the neuron at time t ;
- μ_i ($i = 1, 2, 3$) describe the attenuation rate of internal neurons processing on the I -layer and the J -layer and $\mu_i > 0$;
- the real constants c_{i1} and c_{1i} ($2, 3$) denote the neurons in two layers: the I -layer and the J -layer.

Letting $u_1(t) = x_1(t - \tau_1)$, $u_2(t) = x_2(t)$, $u_3(t) = x_3(t)$ and $\tau = \tau_1 + \tau_2$, then system (95) is equivalent to the following system

$$\begin{cases} \dot{u}_1(t) &= -\mu_1 u_1(t) + c_{21} f_1(u_2(t - \tau)) + c_{31} f_1(u_3(t - \tau)), \\ \dot{u}_2(t) &= -\mu_2 u_2(t) + c_{12} f_2(u_1(t)), \\ \dot{u}_3(t) &= -\mu_3 u_3(t) + c_{13} f_3(u_1(t)). \end{cases} \quad (96)$$

In [15] conditions for (96) are derived for the origin to have a double zero eigenvalue, while all other eigenvalues have negative real parts. Since the provided expression did not give the correct results, we corrected the given expression from [15]. We postpone the proof of the next two lemma's to the Supplement.

Lemma 10. Assume that $f_i(0) = 0$ ($i = 1, 2, 3$), $f'_i(0) \neq 0$ ($i = 1, 2, 3$) and $\mu_2 \neq \mu_3$, then the steady-

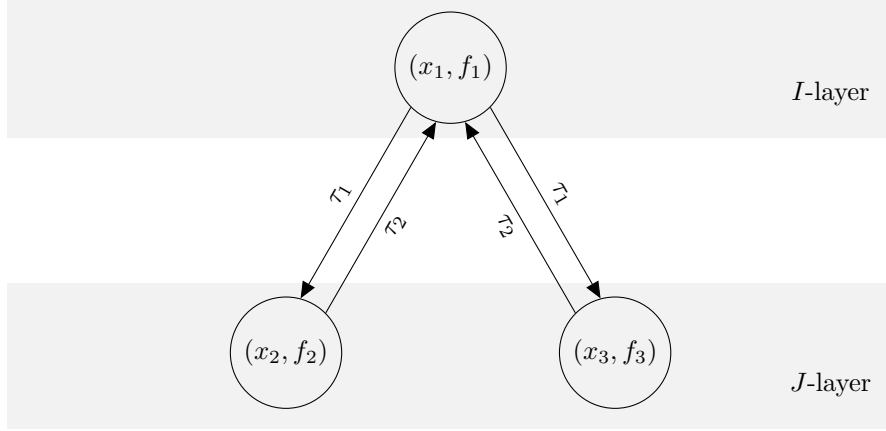


Figure 7: The graph of architecture for model (95).

state $(u_1, u_2, u_3) = (0, 0, 0)$ has a double zero eigenvalue at

$$c_{21} = c_{21}^0 = \frac{\mu_2^2 (\mu_1 (\mu_3 \tau + 1) + \mu_3)}{c_{12} (\mu_2 - \mu_3) f_1'(0) f_2'(0)},$$

$$c_{31} = c_{31}^0 = \frac{\mu_3^2 (\mu_1 (\mu_2 \tau + 1) + \mu_2)}{c_{13} (\mu_3 - \mu_2) f_1'(0) f_3'(0)}.$$

Lemma 11. Correction to [15, Lemma 3]. Let $(c_{21}, c_{31}) = (c_{21}^0, c_{31}^0)$,

$$\omega_0 = \frac{\sqrt{-\mu_1^2 - \mu_2^2 - \mu_3^2 + \sqrt{\zeta_0}}}{\sqrt{2}} \quad (97)$$

and $0 < \tau < \tau_0$, where τ_0 is the minimum positive solution to the nonlinear equation

$$\tan(\tau \omega_0) = \frac{b_0 \zeta_1 - a_0 \zeta_2}{a_0 \zeta_1 + b_0 \zeta_2}, \quad (98)$$

with

$$a_0 = -\mu_1 \mu_2 \mu_3,$$

$$b_0 = -\omega_0 (\mu_2 \mu_3 + \mu_1 (\mu_2 + \mu_3 + \mu_2 \mu_3 \tau)),$$

$$\zeta_0 = \mu_1^4 + (\mu_2^2 + \mu_3^2)^2 + 8\mu_1 \mu_2 \mu_3 (\mu_2 + \mu_3 + \mu_2 \mu_3 \tau) +$$

$$2\mu_1^2 (\mu_3^2 + 4\mu_2 \mu_3 (1 + \mu_3 \tau) + \mu_2^2 (1 + 2\mu_3 \tau (2 + \mu_3 \tau))),$$

$$\zeta_1 = \mu_1 \mu_2 \mu_3 - (\mu_1 + \mu_2 + \mu_3) \omega_0^2,$$

$$\zeta_2 = \mu_2 \mu_3 \omega_0 + \mu_1 (\mu_2 + \mu_3) \omega_0 - \omega_0^3.$$

Then the center manifold near the Bogdanov–Takens point is locally attractive.

For the numerical verification we consider, as in the simulations in [15, Example 1], the system (96) with the activation functions

$$f_1(x) = \tanh(x) + 0.1x^2, \quad f_2(x) = f_3(x) = \tanh(x),$$

and parameter values

$$\mu_1 = 0.1, \mu_2 = 0.3, \mu_3 = 0.2, c_{12} = c_{13} = 1, \tau = 5.$$

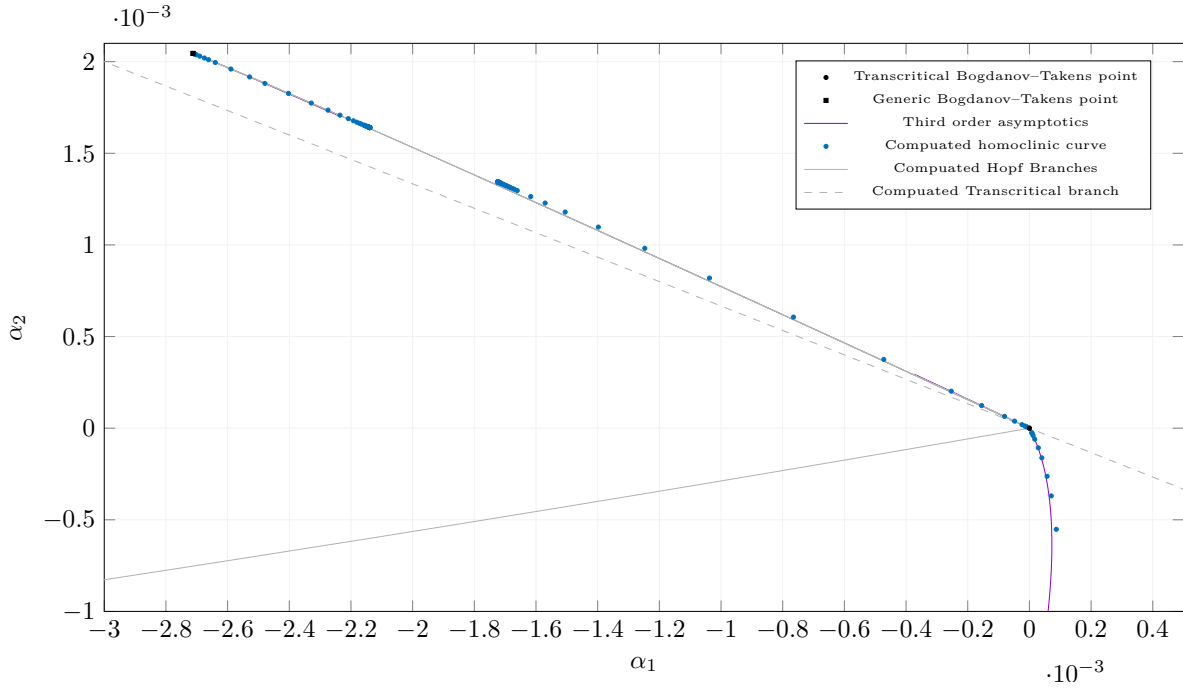


Figure 8: Bifurcation diagram near the transcritical Bogdanov–Takens bifurcation and a generic Bogdanov–Takens in (96) comparing computed codimension one using DDE-BifTool with the asymptotics obtained in this paper.

Then, from Lemma 10, we obtain two critical values

$$(c_{21}^0, c_{31}^0) = (0.36, -0.22),$$

at which there is a transcritical Bogdanov–Takens point. Furthermore, since $\tau < \tau_0 \approx 5.4320$ the center manifold is attractive. In fact, we will show in the Supplement that the center manifold is attractive for $0 < \tau < 13.2309348879375$. We write the system (96) as

$$\begin{cases} \dot{u}_1(t) &= -\mu_1 u_1(t) + (c_{21}^0 + \alpha_1) f_1(u_2(t - \tau)) + (c_{31}^0 + \alpha_2) f_1(u_3(t - \tau)), \\ \dot{u}_2(t) &= -\mu_2 u_2(t) + c_{12} f_2(u_1(t)), \\ \dot{u}_3(t) &= -\mu_3 u_3(t) + c_{13} f_3(u_1(t)), \end{cases} \quad (99)$$

where (α_1, α_2) are the new parameter values such that at $(\alpha_1, \alpha_2) = (0, 0)$ we have a Bogdanov–Takens bifurcation. The critical normal form coefficients

$$(a, b) \approx (0.0012, -0.0135),$$

indicate stable cycles. In Figure 8, we have plotted the local unfolding of the transcritical Bogdanov–Takens bifurcation using our implementation in DDE-BifTool to start the continuation of the transcritical, Hopf, and homoclinic codimension one bifurcation curves. Furthermore, using the ability to detect codimension two bifurcation points while continuing Hopf points, we discovered another Bogdanov–Takens point. From the transversality conditions, we see the secondary Bogdanov–Takens point is of the generic case. Thus, we can start continuation of the homoclinic orbits emanating from this point as well. We see that the numerically continued homoclinic curves in the upper half plane only exists in a

very small parameter region. Without our predictor, this homoclinic curve would be extremely difficult to locate. Lastly, in [Figure 4](#) the first and third-order homoclinic asymptotics are compared. Here we again see expected improvements of using the third-order homoclinic asymptotics. We refer to the [Supplement](#) to see the beautiful homoclinic orbits along the homoclinic curve in the lower half plane, and for an overall more detailed treatment of this example. In fact, we will show that the transcritical Bogdanov–Takens and generic Bogdanov–Takens points are connected, not only by a Hopf curve, but also through a homoclinic curve.

6 Concluding remarks

We have provided explicit formulas needed to initialize the codimension one equilibrium and homoclinic bifurcation curves emanating from the generic and transcritical codimension two Bogdanov–Takens bifurcation points in classical DDEs. Applications to four different models from the literature are given, confirming the correctness of the derivation of the time-reparametrization parameter-dependent center manifold transformation and the codimension one asymptotics.

By extending the normalization technique to include the time-reparametrization we are allowed to use orbital normal forms, instead of only smooth normal forms. One benefit of this approach is the reusability of the codimension one curves emanating from the universal unfolding of the Bogdanov–Takens codimension two bifurcation. Indeed, by a simple transformation [\(82\)](#), we obtain the homoclinic asymptotics for the transcritical Bogdanov–Takens bifurcation.

In this paper, we have restricted to the class of classical DDEs, and for the applications to the class of discrete DDEs. However, the proof in [\[2\]](#) of the existence of a smooth parameter-dependent center manifold is given in the general context of perturbation theory for dual semigroups (sun-star calculus). Therefore, the applicability of this result extends beyond classical DDEs. For example, in [\[36\]](#) and [\[14\]](#) the technique was used to calculate the critical normal form coefficients for Hopf and Hopf–Hopf bifurcations occurring in neural field models with propagation delays. For these models, sun-reflexivity is lost, which is typical for delay equations in abstract spaces or with infinite delay. However, it is often possible to overcome this functional analytic complication, so dual perturbation theory can still be employed successfully [\[11, 12, 23, 36\]](#). It follows that the derived coefficients in [Section 4](#) are valid in these settings as well.

Similarly, in [\[34\]](#) it is demonstrated that formally the normalization method still works for state-dependent delay differential equations. However, to employ our formulas in this situation, one first needs to implement the continuation of homoclinic orbits for state-dependent DDEs. Of course, the asymptotics are still useful to see where the homoclinic orbit should be located. Furthermore, the asymptotics can be used to numerically approximate the homoclinic solutions by periodic orbits with a large period.

Returning to the setting of classical DDEs, the most obvious next challenge is to derive normal forms for bifurcations of periodic orbits by generalizing [\[9, 10, 29\]](#). The resulting formulas can then be implemented in `DDE-BifTool` to facilitate numerical bifurcation analysis of periodic orbits in supported types of classical DDEs.

SUPPLEMENTARY MATERIALS FOR: Bifurcation analysis of Bogdanov-Takens bifurcations in delay differential equations

M.M. Bosschaert* Yu.A. Kuznetsov†

October 7, 2022

In this supplement, we will provide a full walk-through of the examples given in [Section 5](#) with the open source bifurcation software package `DDE-BifTool`¹ [35]. Additionally, the Julia code, used for the numerical simulation, with the package `DifferentialEquations.jl`² [30] is shown. This allows other researchers to replicate the findings in the main text fully. The given code can easily be modified to study other DDE models undergoing generic or transcritical Bogdanov-Takens bifurcations. While studying these models, some new results were obtained.

The code in this supplement has also been included into the `DDE-BifTool` package on the sourceforge repository and can be executed without the need to copy and paste. In this supplement, we mainly focus on the initialization and continuation of the various codimension one equilibrium and homoclinic bifurcation curves emanating from the Bogdanov–Takens points and on numerical simulation near the bifurcation points. The online tutorials, as well as the manual and its references, provide a comprehensive overview of `DDE-BifTool`'s capabilities and functionality.

Note that reading this supplement may feel, at times, somewhat repetitive. We see this as a positive sign. Indeed, our predictors need little to none adjustment before starting continuation of the codimension one curves emanating from the generic and transcritical Bogdanov–Takens bifurcation.

To follow the examples below, we recommend using the `DDE-BifTool` package supplied with the article. Also, note that the `MATLAB` code has been tested on `MATLAB 2020b` and `GNU Octave 6.4.0` using `GNU Octave` symbolic package version 2.9.0. Different results may occur on other versions of `MATLAB` or `GNU Octave`.

S1 Generic Bogdanov–Takens bifurcation in a predator-prey system with double Allee effect

In [25] the following predator-prey model with double Allee effect and delay is considered

$$\begin{cases} \dot{x}(t) = \frac{rx}{x+n_0} \left(1 - \frac{1}{K}\right) (x - m_0) - \frac{cxy}{x + \varrho y}, \\ \dot{y}(t) = -dy + \frac{c_1 x(t-\tau)y}{x(t-\tau) + \varrho y(t-\tau)}. \end{cases} \quad (\text{S1})$$

*Department of Mathematics, Hasselt University, Diepenbeek Campus, Agoralaan Gebouw D, 3590 Diepenbeek, Belgium (maikel.bosschaert@uhasselt.be).

†Department of Mathematics, Utrecht University, Budapestlaan 6, 3508 TA Utrecht, The Netherlands and Department of Applied Mathematics, University of Twente, Zilverling Building, 7500AE Enschede, The Netherlands (I.A.Kouznetsov@uu.nl).

¹<http://ddebiftool.sourceforge.net/>

²<https://github.com/SciML/DifferentialEquations.jl>

Here, the time delay $\tau \geq 0$ is introduced due to the fact that the reproduction of predator after consuming the prey is not instantaneous, but is mediated by some time lag required for gestation. The variables and parameters occurring in (S1) have the following meaning:

- $x, y: \mathbb{R} \rightarrow \mathbb{R}$ denote the prey and predator population densities, respectively.
- r denotes the maximum prey population growth in absence of the Allee effect.
- K is the carrying capacity of the environment.
- m_0 is the Allee threshold.
- n_0 is the auxiliary parameter in order to quantify the strength of the Allee effect.
- c denotes the capturing rate of the predator.
- ϱ is the half-capturing saturation constant.
- c_1 is the conversion rate of prey into predators biomass.
- d is the per capita predator mortality rate.

Following [25] let $(x, y, t) = \left(K\bar{x}, \frac{K}{\varrho}\bar{y}, \frac{t}{\tau}\right)$, and immediately dropping the bars again for readability, then (S1) becomes

$$\begin{cases} \dot{x}(t) = x \left(\frac{(1-x)(x-\gamma)}{x+\vartheta} - \frac{\alpha y}{x+y} \right), \\ \dot{y}(t) = \delta y \left(-1 + \frac{mx(t-\tau)}{x(t-\tau) + y(t-\tau)} \right), \end{cases} \quad (\text{S2})$$

where $\vartheta = \frac{n_0}{K}$, $\alpha = \frac{c}{r\varrho}$, $\gamma = \frac{m_0}{K}$, $\delta = \frac{d}{\tau}$ and $m = \frac{c_1}{d}$.

Thus, $(x, y, \vartheta, \delta) = (x_0, y_0, \vartheta_0, \delta_0)$, with $\delta_0 = \frac{\alpha}{m}$, we have a double zero eigenvalue, provided that $\det \Delta''(0) \neq 0$. To confirm their analytical findings in [25] numerically, the parameters $\gamma = 0.15$, $\alpha = 0.9$ and $m = 1.50298303$ are fixed and (ϑ, δ) are taken as unfolding parameters. For these parameters, we indeed have that $\det \Delta''(0) \neq 0$.

Remark 12. The MATLAB files for this demonstration can be found in the directory `demos/tutorial/VII/neural_network_model` relative to the main directory of the DDE-BifTool package.

S1.1 Generate system files

Before we start to analyze the system with DDE-BifTool, we first create a *system file*. This file contains the definition of the system (S2), the standard derivatives needed for calculation of the eigenvalues and eigenvectors, the continuation of bifurcation points, cycles, and also the multilinear forms, see [2, Section 6], used for the calculation of the coefficients of the critical and parameter-dependent normal forms and center manifold transformation. Alternatively, one can only supply the system itself, see Listing S2. Then finite difference is used to approximate the derivatives. However, this is less efficient and less accurate, and therefore not recommended. A separate script `gen_sym_predator_preym.m` is used to create a system file. The most important parts of this script are listed and discussed below.

```

18 %% Add paths and load sym package if GNU Octave is used
19 clear
20 ddebiftoolpath='../..../..../';
21 addpath(strcat(ddebiftoolpath, 'ddebiftool'), ...
22        strcat(ddebiftoolpath, 'ddebiftool_extra_symbolic'));

```

```

23 if dde_isoctave()
24     pkg load symbolic
25 end
26 %% Create parameter names as strings and define fixed parameters
27 % The demo has the parameters |theta|, |delta| and |tau|
28 parnames={'theta','delta','tau'};
29 %% Create symbols for parameters, states and delays states
30 % The array |par| is the array of symbols in the same order as parnames.
31 % Due to the following two lines we may, for example, use either theta or
32 % par(1) to refer to the delay.
33 syms(parnames{:});          % create symbols for theta, delta and tau
34 par=cell2sym(parnames);    % now theta is par(1) etc
35 %% Define system using symbolic algebra
36 syms x xt y yt % create symbols for u1(t) u1(t-tau), u2(t), u2(t-tau)
37 m = 1.502983803;
38 alpha = 0.9;
39 gamma = 0.15;
40 dx_dt = x*((1-x)*(x-gamma))/(x+theta) - alpha*y/(x+y)
41 dy_dt = delta*y*(-1 + m*xt/(xt+yt))
42 model = [dx_dt;dy_dt];
43 vars = [x,xt;y,yt];
44 modelname = 'predator_prey';
45 %% Differentiate and generate code, exporting it to sym_FHN_mf (multi-linear forms)
46 dde_sym2funcs(model, vars, par, 'filename',strcat('sym_',modelname,'_mf'), ...
47     'directional_derivative',false);
48 %% Differentiate and generate code, exporting it to sym_FHN (directional
49     ↪ derivatives)
49 dde_sym2funcs(model, vars, par, 'filename',strcat('sym_',modelname), ...
50     'directional_derivative',true);

```

The variable `ddebiftoolpath` is directed to the DDE-BifTool main folder, which should have been extracted somewhere on the computer. Here, a path relative to the current working directory is used. Note that although we only use the parameters (θ, δ) as unfolding parameters, in the current version of DDE-BifTool, we also need to include the delay(s) in the list of parameters. After running the script, the function `dde_sym2funcs` creates two system files `sym_predator_prey_mf.m` and `sym_predator_prey.m`. The first file `sym_predator_prey_mf.m` implements the higher order derivatives as multilinear forms, as explained in [2, Section 6], and therefore will be the only file used. The second file `sym_predator_prey.m` uses directional derivatives to implement the higher order derivatives. The directional derivatives approach *formally* allows the use of state-dependent delays, see [34]. Although both approaches yield (up to rounding errors) identical normal form coefficients and center manifold transformations, multilinear forms are more efficient to compute.

S1.2 Loading the DDE-BifTool package

Now that a system file is created, we continue with DDE-BifTool to analyze (S2) numerically. The code in the following sections highlight the important parts of the file `predator_prey.m`. The package DDE-BifTool consists of a set of MATLAB routines. Thus, in order to start using DDE-BifTool, we only need to add DDE-BifTool (sub)directories to the search path. There are four subdirectories added to the search path:

ddebiftool Containing the core files of DDE-BifTool.

```

17 %% Clean workspace and add DDE-BifTool scripts to the MATLAB search path
18 clear;          % clear variables
19 close all;      % close figures
20 ddebiftoolpath='../..../..../';
21 addpath(strcat(ddebiftoolpath, 'ddebiftool'),...
22         strcat(ddebiftoolpath, 'ddebiftool_extra_psol'),...
23         strcat(ddebiftoolpath, 'ddebiftool_extra_nmfm'),...
24         strcat(ddebiftoolpath, 'ddebiftool_utilities'),...
25         '../');

```

Listing S1: Code to add DDE-BifTool scripts to the search path.

ddebiftool_extra_psol An extension for enabling continuation of periodic orbit bifurcations for delay-differential equations with constant or state-dependent delay.

ddebiftool_extra_nmfm An extension for normal form computation.

ddebiftool_utilities Containing various utilities.

S1.3 Set parameter names

The following code allows us to use `ind.theta` instead of remembering the index of the parameter β in the parameter array, and similarly for the other parameters.

```

27 %% Set parameter names
28 parnames={'theta', 'delta', 'tau'};
29 cind=[parnames; num2cell(1:length(parnames))];
30 ind=struct(cind{:});

```

In this way, fewer mistakes are likely to be made, and the code is easier to read.

S1.4 Initialization

Next, we set up the `funcs` structure, containing information about where the system and its derivatives are stored, a function pointing to which parameters are delays, and various other settings.

```

32 %% Set the funcs structure
33 % We load the precalculated multilinear forms. These have been generated
34 % with the file gen_sym_predator_preymf.m.
35 funcs=set_symfuncs(@sym_predator_preymf, 'sys_tau', @()ind.tau);

```

Alternatively, when no system files have been generated, one could initialize the system (S2) as in Listing S2.

Inspecting the output of the `funcs` handle gives.

```
>> funcs
```

```

1 %% Define funcs structure without symbolic derivatives
2 m = 1.502983803;
3 alpha = 0.9;
4 gamma = 0.15;
5 dx_dt = @(x,y,theta) x.*((1-x).*(x-gamma)./(x+theta) ...
6     - alpha.*y./(x+y))
7 dy_dt = @(y,xt,yt,delta) delta.*y.*(-1 + m.*xt./(xt+yt))
8 predator_prey_sys = @(xx,par) ...
9     [dx_dt(xx(1,1,:),xx(2,1,:),par(1,ind.theta,:)); ...
10     dy_dt(xx(2,1,:),xx(1,2,:),xx(2,2,:),par(1,ind.delta,:))];
11 %% Set funcs structure
12 funcs = set_funcs('sys_rhs', predator_prey_sys, ...
13     'sys_tau', @() ind.tau,...
14     'x_vectorized', true, 'p_vectorized', true);

```

Listing S2: Code to define the system without a system file.

```

funcs =

struct with fields:

    sys_rhs: @(x,p)dde_wrap_rhs(x,p,funcs.sys_rhs,funcs.x_vectorized,
        funcs.p_vectorized)
    sys_ntau: @()0
    sys_tau: @()ind.tau
    sys_cond: @dde_dummy_cond
    sys_deriv: @(x,p,nx,np,v)dde_gen_deriv(funcs.sys_dirderiv,x,p,nx,np,v,1)
    sys_dtau: []
    sys_mfderiv: {}
    sys_dirderiv: {@(x,p,dx,dp)dde_dirderiv(derivbase,x,p,dx,dp,
        order-ldirderiv, 'nf',size(x,1),'hjac',
        funcs.hjac(order)) [function_handle]}
    sys_dirdtau: []
    x_vectorized: 1
    p_vectorized: 1
    hjac: @(ord)eps^(1/(2+ord))
    sys_cond_reference: 0
    lhs_matrix: @(sz)lhs_matrix(sz,funcs.lhs_matrix)
    tp_del: 0
    sys_deriv_provided: 0
    sys_dirderiv_provided: 0

```

The output shows that no derivative file is supplied. In this case, the derivatives are calculated using finite-difference approximations with the function `dde_dirderiv`. Again, we do not recommend using the latter approach. However, it can be useful for debugging purposes.

S1.5 Set parameter range

Since we are only interested here in the local unfolding, we restrict the allowed parameter range for the unfolding parameters. In practice, one may have physical restrictions which must be satisfied. Additionally, we also limit the maximum allowed step size during continuation. By doing so, we obtain more refined data to compare against our predictors.

```
37 %% Set bifurcation parameter range and step size bounds
38 brpars={'max_bound', [ind.delta 0.7],...
39         'min_bound', [ind.delta 0.4],...
40         'max_step', [ind.theta 0.002; ind.delta 0.002]};
```

S1.6 Stability and coefficients of the generic Bogdanov–Takens point

We manually construct a steady-state at the Bogdanov–Takens point derived in [Section 5.1](#), see also [\[25\]](#).

```
42 %% Define constants
43 m = 1.502983803; alpha = 0.9; gamma = 0.15;
44
45 %% Define analytically derived Bogdanov-Takens point
46 % construct steady-state point
47 x0 = (m*gamma-m*alpha+m*alpha)/(2*m);
48 stst=dde_stst_create('x', [x0; (m-1)*x0]);
49 stst.parameter(ind.theta) = (m^2*gamma^2 - 2*m*(m*alpha + m - alpha)*gamma +
   ↪ (m*alpha - m - alpha)^2)/(4*m*alpha*(m-1));
50 stst.parameter(ind.delta) = alpha/m;
51 stst.parameter(ind.tau) = 0.01;
52 % Calculate stability
53 method=df_mthod(funcs, 'stst');
54 stst.stability=p_stabil(funcs, stst, method.stability);
55 stst.stability.l1
```

Inspecting the `stst.stability` structure yields

```
>> stst.stability.l1

ans =

    1.0e-06 *

    0.197590320692559
   -0.197590756777676

>>
```

The eigenvalues confirm that the point under consideration is indeed (an approximation to) a Bogdanov–Takens point. Next, we convert the steady-state point to a Bogdanov–Takens point and calculate the normal form coefficients with the function `nmfm_bt_orbital`, which implements the

coefficients derived in [Section 4.1](#). For this, we need to set the argument `free_pars` to the unfolding parameter (θ, δ) . These coefficients will be used to start the continuation of the codimension one branches emanating from the Bogdanov–Takens point.

```

57 %% Calculate normal form coefficients
58 free_pars=[ind.theta, ind.delta];
59 bt = p_tobt(funcs,stst);
60 bt = nmfm_bt_orbital(funcs, bt, 'free_pars', free_pars);

```

The coefficients for the normal form, the time-reparametrization, and the center manifold transformation coefficients are stored in the `bt.nmfm` structure. Additionally, also the approximation to the parameters and center manifold transformation is given, which is used for the predictors.

```

>> bt.nmfm

ans =

    struct with fields:

         a: -0.145177185481861
         b: -1.446000370122628
    theta1000: -0.200700969579673
    theta0001: 5.128950206684711
         K10: [2x1 double]
         K01: [2x1 double]
         K02: [2x1 double]
         K11: [2x1 double]
         K03: [2x1 double]
         phi0: [1x1 struct]
         phi1: [1x1 struct]
        h0010: [1x1 struct]
        h0001: [1x1 struct]
        h2000: [1x1 struct]
        h1100: [1x1 struct]
        h0200: [1x1 struct]
        h1010: [1x1 struct]
        h1001: [1x1 struct]
        h0110: [1x1 struct]
        h0101: [1x1 struct]
        h0002: [1x1 struct]
        h0011: [1x1 struct]
        h3000: [1x1 struct]
        h2100: [1x1 struct]
        h1101: [1x1 struct]
        h2001: [1x1 struct]
        h0003: [1x1 struct]
        h1002: [1x1 struct]
        h0102: [1x1 struct]
         K: @(beta1,beta2)K10*beta1+K01*beta2+1/2*K02*beta2.^2

```

```
+K11*beta1.*beta2+1/6*K03*beta2^3
H: [function_handle]
```

Since the sign of ab is positive, we expect to find unstable periodic orbits nearby the Bogdanov–Takens point.

S1.7 Comparing profiles of computed and predicted homoclinic orbits

To test the homoclinic asymptotics from [Section 4.1.9](#) we compare the first and third order asymptotics to the Newton corrected solution. For this, we use the function `C1branch_from_C2point`. This function returns a branch, which by default returns two initial corrected approximations in order to start continuation of the codimension one curve under consideration. By setting the argument `'predictor'` to `true` the approximations are left uncorrected. To make the comparison visually clear, we set the perturbation parameter $\epsilon = 0.3$ (`step = 0.3` in the code below). The code below produces [Figure S1](#). The difference between the two approximations is clearly noticeable. While the first order asymptotics is close to the Newton corrected solution, the third order asymptotic is indistinguishable at this scale from the Newton corrected solution.

```
62 %% Plot comparing profiles computed and predicted homoclinic orbits
63 figure(1); clf; hold on;
64 cm=colormap('lines');
65 tiledlayout(2,2)
66 ylabel = {'x$', 'y$'};
67 step = 0.3;
68 for order=[1,3]
69
70     ↪ [~,hcli_br_approx,suc]=C1branch_from_C2point(funcs,bt,free_pars, 'order',order,...
71         'codim2','BT','codim1','hcli','step',step,'predictor',true);
72
73     ↪ [~,hcli_br_correc,suc]=C1branch_from_C2point(funcs,bt,free_pars, 'order',order,...
74         'codim2','BT','codim1','hcli','step',step);
75     for j=1:2
76         ax = nexttile; hold on; title(sprintf('order %d',order))
77         ↪ plot(ax,hcli_br_approx.point(1).mesh,hcli_br_approx.point(1).profile(j,:), '*')
78             plot(ax,hcli_br_correc.point(1).mesh,hcli_br_correc.point(1).profile(j,:))
79             xlabel('$t$', 'Interpreter', 'LaTeX');
80             ylabel(string(ylabel(j)), 'Interpreter', 'LaTeX')
81     end
82 end
```

S1.8 Continuation of the emanating codimension one curves

To continue the three codimension one curves emanating from the generic Bogdanov–Takens point, we can simply use the function `C1branch_from_C2point`, as shown in the code below. To monitor the continuation process, the argument `plot` must be set to 1. The most important setting is the perturbation parameter (or multiple), `step` in the code below. If left out, default step sizes are defined. However, depending on the problem, no convergence may then be obtained.

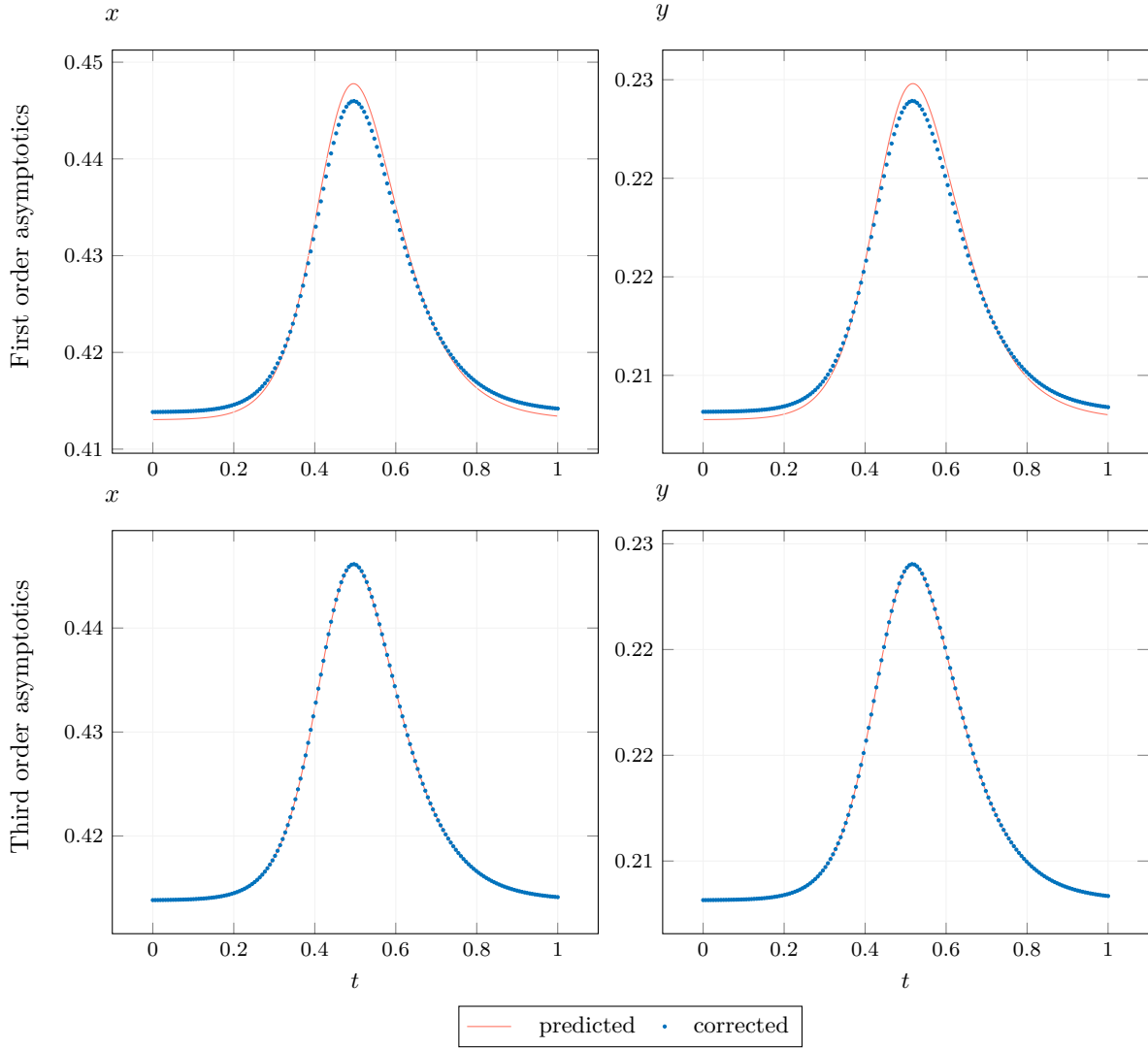


Figure S1: Comparison between the first and third-order asymptotics from Section 4.1.9 near the generic Bogdanov–Takens bifurcation in (S2) with the perturbation parameter set to $\epsilon = 0.3$.

```

82 %% Continue homoclinic solutions emanating from the BT point
83 [~,hcli_br,suc]=C1branch_from_C2point(funcs,bt,free_pars,...
84     'codim2','BT','codim1','hcli',brpars{:},'step',[0.1;0.11],'plot',0);
85 assert(all(suc(:)>0))
86 nop=300; hcli_br=br_contn(funcs,hcli_br,nop);assert(suc>0)
87
88 %% Continue Hopf curve
89 [~,hbr,suc]=C1branch_from_C2point(funcs,bt,free_pars,...
90     'codim2','BT','codim1','hopf',brpars{:},'step',1e-05,'plot',0);
91 assert(all(suc(:)>0))
92 nop=300; [hbr,suc]=br_contn(funcs,hbr,nop);assert(suc>0)

```

```

93
94 %% Continue fold curve emanating from Bogdanov-Takens point
95 [~,fold_br,suc]=C1branch_from_C2point(funcs,bt,free_pars,...
96     'codim2','BT','codim1','fold',brpars{:},'step',1e-03,'plot',0);
97 assert(all(suc(:)>0))
98 nop=300; [fold_br,suc]=br_contn(funcs,fold_br(1),nop);assert(suc>0)
99 fold_br = br_rvers(fold_br);
100 nop=300; [fold_br,suc]=br_contn(funcs,fold_br(1),nop);assert(suc>0)

```

S1.9 Predictors of the codimension one curves emanating from the Bogdanov–Takens point

Before we provide the bifurcation diagram in the next section, we first obtain the predictors for the codimension one curves. For this, we again use the function `C1branch_from_C2point`. We set the argument `predictor` to 1 and provide a range of perturbation parameters.

```

118 %% Predictors for homoclinic, Hopf, and fold curve
119 step = linspace(1e-4,0.6,50);
120 [~,hcli_br_pred,suc]=C1branch_from_C2point(funcs,bt,free_pars,'debug',0,...
121     'codim2','BT','codim1','hcli','step',step,'predictor',true);
122 step = linspace(0.0001,0.1,50);
123 [~,hbr_pred,suc]=C1branch_from_C2point(funcs,bt,free_pars,...
124     'codim2','BT','codim1','hopf','step',step,'predictor',true);
125 step = linspace(-0.05,0.05,40);
126 [~,fold_br_pred,suc]=C1branch_from_C2point(funcs,bt,free_pars,...
127     'codim2','BT','codim1','fold','step',step,'predictor',true);
128 hcli_br_pred_pm = [getpars(hcli_br_pred, ind.theta), getpars(hcli_br_pred,
    ↪ ind.delta)];
129 hbr_pm_pred = [getpars(hbr_pred,ind.theta); getpars(hbr_pred,ind.delta)];
130 fold_br_pm_pred = [getpars(fold_br_pred,ind.theta);
    ↪ getpars(fold_br_pred,ind.delta)];
131
132 %% Predictors from [Jiao2021]
133 mu1 = -linspace(1e-5,0.003,250);
134 mu2 = -1.386173725.*mu1 - 0.9901240893*sqrt(mu1.*(mu1 - 3.652165730));
135 hbr_pm_pred_2021 = bt.parameter(free_pars)' + [mu1; mu2];
136 mu2 = -1.386173725.*mu1 - 1.386173725*sqrt(mu1.*(mu1 - 3.652165730));
137 hcli_pm_pred_2021 = bt.parameter(free_pars)' + [mu1; mu2];

```

In the last part of the code above, we added the asymptotics obtained from [25].

S1.10 Bifurcation diagram

The code below produces a similar figure as [Figure S2](#) in MATLAB.

```

139 %% Plot the bifurcation curves with predictors
140 figure(3);clf;hold on
141 title(['Codimension 1 curves emanating from the generic', ...
142     'Bogdanov-Takens point with predictors']);

```

```

143 plot(hcli_br_pm(1,:),hcli_br_pm(2,:),'.','Color',cm(1,:), ...
144       'DisplayName','Homoclinic branches')
145 plot(hcli_br_pred_pm(:,1),hcli_br_pred_pm(:,2),'Color', cm(7,:), ...
146       'DisplayName','Third order homoclinic asymptotics')
147 plot(hcli_pm_pred_2021(1,:), hcli_pm_pred_2021(2,:), 'Color',cm(3,:), ...
148       'DisplayName','Asymptotics from Jiao2021');
149 plot(hbr_pm(1,:),hbr_pm(2,:),'o','Color',cm(1,:), ...
150       'DisplayName','Hopf branch')
151 plot(hbr_pm_pred(1,:),hbr_pm_pred(2,:), '--','Color',cm(7,:), ...
152       'DisplayName','Hopf asymptotics')
153 plot(hbr_pm_pred_2021(1,:),hbr_pm_pred_2021(2,:), '--','Color',cm(3,:), ...
154       'DisplayName','Hopf asymptotics from Jiao2021')
155 plot(fold_br_pm(1,:),fold_br_pm(2,:),'d','Color',cm(1,:), ...
156       'DisplayName','Fold branch')
157 plot(fold_br_pm_pred(1,:),fold_br_pm_pred(2,:),':','Color',cm(7,:), ...
158       'DisplayName','Fold asymptotics')
159 plot(bt.parameter(ind.theta),bt.parameter(ind.delta),'.k','MarkerSize', 18, ...
160       'DisplayName','generic Bogdanov-Takens point');
161 legend('Location','NorthWest')
162 xlabel('\theta','Interpreter','LaTeX');
163 ylabel('\delta','Interpreter','LaTeX');
164 axis([0.0978 0.1002 0.5086 0.6042])

```

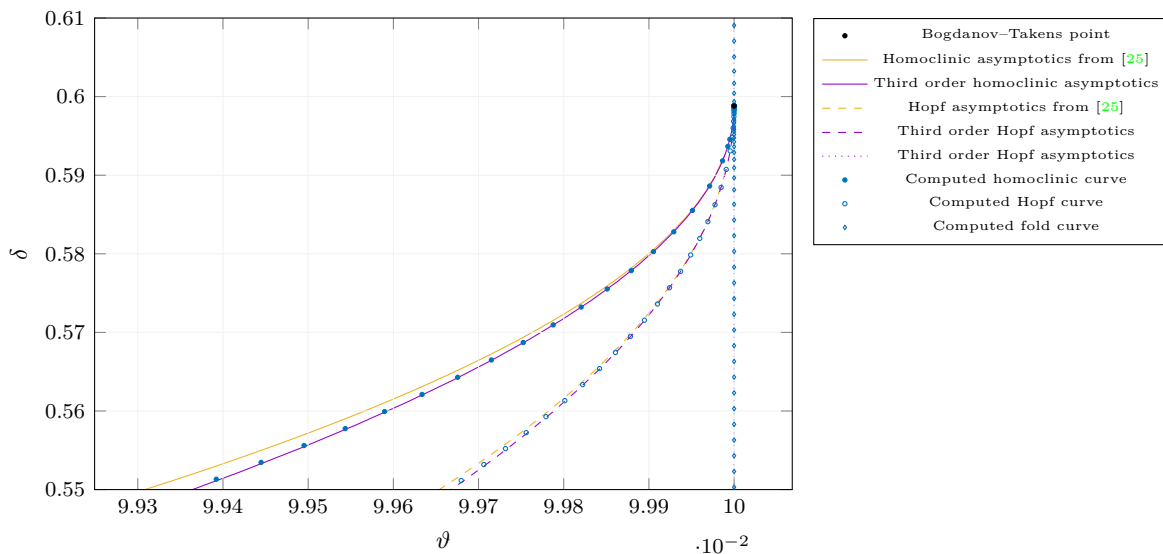


Figure S2: Bifurcation diagram near the analytically derived generic Bogdanov-Takens point in (S2) comparing computed codimension one curves using DDE-BifTool with the asymptotics obtained in this paper and in [25].

S1.11 Compare homoclinic solutions in phase-space

To get an impression of the third-order homoclinic asymptotics in phase-space, we compare the corrected and uncorrected homoclinic solutions with the perturbation parameter ranging from 0.1 to 0.3.

The code below results in [Figure S3](#). We see that the corrected and predicted homoclinic orbits are nearly identical.

```

166 %% Compare homoclinic solutions in phase-space
167 step = linspace(0.1,0.3,10);
168 [~,hcli_br_approx,suc]=C1branch_from_C2point(funcs,bt,free_pars,...
169     'codim2','BT','codim1','hcli','step',step,'predictor',true,'debug',0);
170 [~,hcli_br_correc,suc]=C1branch_from_C2point(funcs,bt,free_pars,...
171     'codim2','BT','codim1','hcli','step',step,'debug',0);
172 figure(4); clf; hold on
173 title('Compare homoclinic orbits in phase-space')
174 for i=1:length(hcli_br_approx.point)
175     profile = hcli_br_approx.point(i).profile;
176     plot(profile(1,:),profile(2,:), 'Color', cm(2,:))
177     profile_correc = hcli_br_correc.point(i).profile;
178     plot(profile_correc(1,:),profile_correc(2,:), '.', 'Color', cm(1,:))
179 end
180 legend({'Predicted homoclinic order', 'Corrected homoclinic orbir'})
181 xlabel('$x$', 'Interpreter', 'LaTeX');
182 ylabel('$y$', 'Interpreter', 'LaTeX');

```

The MATLAB console shows the following output.

```

hcli from BT: branch 1 of 1 correction of point 1, success=1
hcli from BT: branch 1 of 1 correction of point 2, success=1
hcli from BT: branch 1 of 1 correction of point 3, success=1
hcli from BT: branch 1 of 1 correction of point 4, success=1
hcli from BT: branch 1 of 1 correction of point 5, success=1
hcli from BT: branch 1 of 1 correction of point 6, success=1
hcli from BT: branch 1 of 1 correction of point 7, success=1
hcli from BT: branch 1 of 1 correction of point 8, success=1
hcli from BT: branch 1 of 1 correction of point 9, success=1
hcli from BT: branch 1 of 1 correction of point 10, success=1

```

That is, all predictions in this range are successfully corrected.

S1.12 Convergence plot

In [Figure S1](#) we compared the profiles of the first and third-order homoclinic asymptotics. Although the improvement of the third-order asymptotics is clearly visible, a better way to numerically compare the different orders is by creating a log-log convergence plot. Since we create convergence plots for all examples treated in this supplement, we created the function `convergence_plot`.

```

1 function relativeErrors = convergence_plot(funcs, bt, orders, amplitudes, varargin)
2
3     default = {'dir',0,'free_pars',[],'orders',3,'TTolerance',1e-5,'ntst',40, ...
4         'generic_unfolding',1,'debug',false};
5     [options,pass_on] = dde_set_options(default,varargin,'pass_on');
6

```

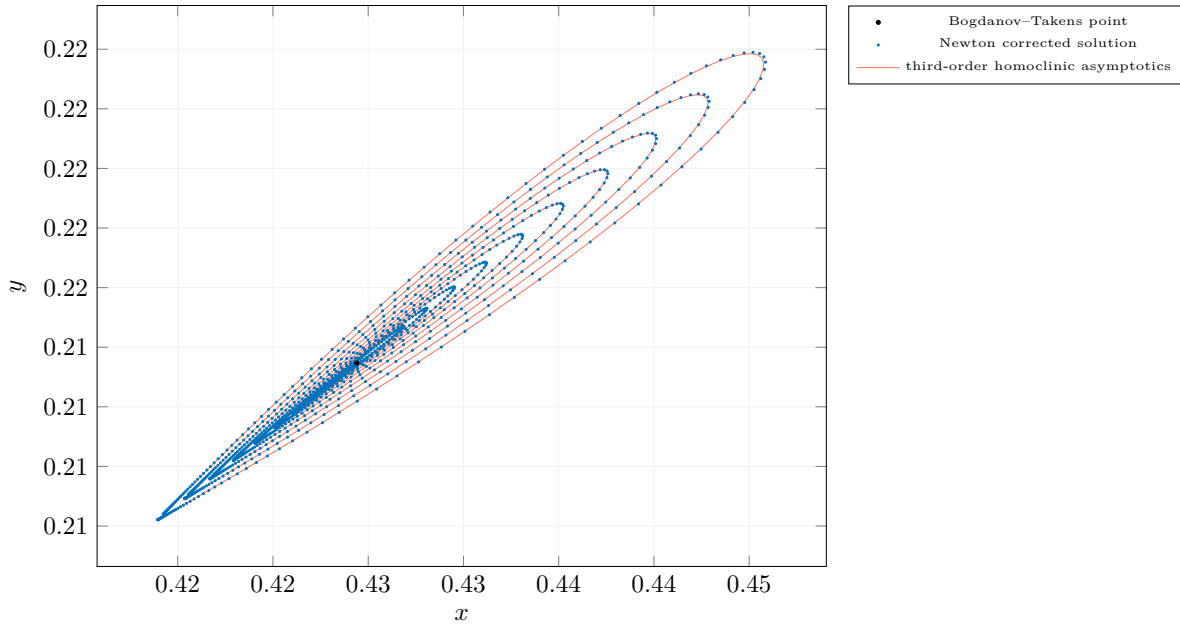


Figure S3: Plot comparing the third-order homoclinic asymptotics from Section 4.1.9 near the generic Bogdanov–Takens bifurcation in (S2) with the Newton correct homoclinic solutions in (x, y) phase-space.

```

7   mhcli=df_mthod(funcs,'hcli');
8   relativeErrors = {};
9   for i=orders
10      relativeErrors{i} = zeros(size(amplitudes));
11      options.order = i;
12      for j=1:length(amplitudes)
13         if options.generic_unfolding
14            options.amplitude = amplitudes(j);
15         else
16            options.amplitude = amplitudes(j)*[1,1];
17            options.TTolerance = options.TTolerance.*[1,1];
18         end
19         hcli = init_BT_Hom_orbital(funcs,bt,options);
20         if length(hcli) == 1
21            hcli_pred = hcli;
22         else
23            hcli_pred = hcli(2);
24         end
25         hcli_pred = hcli_pred{1};
26         if options.dir > 0
27            [hcli_corrected,s]=p_correc(funcs,hcli_pred, ...
28                                     options.free_pars(options.dir), [],mhcli.point);
29         else
30            secant=p_tangent(funcs,mhcli.point,hcli_pred,options.free_pars);
31            [hcli_corrected,s]=p_correc(funcs,hcli_pred, ...

```

```

32         options.free_pars,secant,mhcli.point);
33     end
34     if s
35         numerator = norm(hcli_corrected.profile-hcli_pred.profile,Inf);
36         denominator = norm(hcli_corrected.profile,Inf);
37         relativeErrors{i}(j) = numerator/denominator;
38     end
39 end
40 end
41
42 end

```

Listing S3: Auxiliary function for creating convergence plots.
Using this function, the code below yields [Figure S4](#).

```

184 %% Convergence plot
185 amplitudes = logspace(-4, -1, 20);
186 orders = [1:3];
187 relativeerrors = convergence_plot(funcs, bt, orders, amplitudes, 'free_pars', ...
188     free_pars, 'orders',orders,'ttolerance',1e-6,'ntst',82,'debug',false,'dir',1);
189 figure(5); clf; hold on
190 title('Convergence plot comparing first and third order homoclinic asymptotics')
191 plot(log10(amplitudes), log10(relativeerrors{1}(:)), '*-')
192 plot(log10(amplitudes), log10(relativeerrors{3}(:)), '*-')
193 legend({'first order', 'thrid order'})
194 xlabel('amplitude')
195 ylabel('relative error')

```

S1.13 Simulation with DifferentialEquations.jl

We finish this demonstration by simulating the dynamics near the generic Bogdanov–Takens point. In [Figure S5](#) we created the full local unfolding of the singularity. Note that, compared with [\[25\]](#), the simulation is done with the original delay differential equations ([S2](#)) and not with the ordinary differential equations of the reduced system on the center manifold. We are able to do this since the parameter-dependent center manifold is locally attractive. In order to integrate the system in the reverse direction, i.e., to obtain the orbits in the stable manifold of the equilibria, we multiplied the right-hand side of the system in ([S2](#)) by -1 . Note that, in general, this will not provide an accurate approximation at all. However, since the delay is relatively small, this approximation is accurate enough for our application. Also, note that the Bogdanov–Takens point still exists for the approximate system. Nonetheless, even without the backward solutions, the bifurcation diagram shows that the numerical analysis obtained in DDE-BifTool is correct.

Since the code for creating the local unfolding diagram is rather long, we show the code for reproducing the plot simulating the system near the homoclinic orbit. The code for creating the bifurcation diagram in [Figure S5](#) can be found in the GitHub repository.

S1.13.1 Loading necessary Julia packages

We start by loading the necessary packages. These are

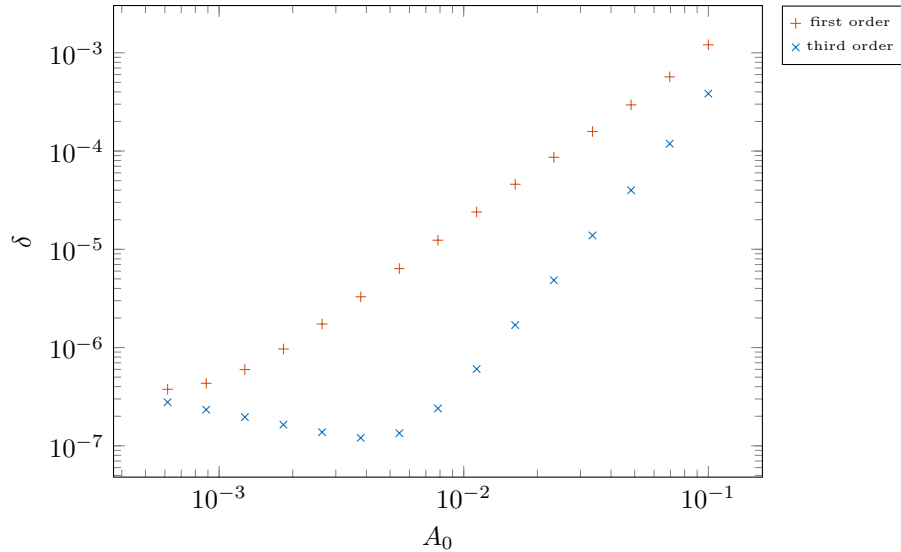


Figure S4: On the abscissa is the approximation to the amplitude A_0 and on the ordinate the relative error δ between the constructed solution `hcli_pred` to the defining system for the homoclinic orbit and the Newton corrected solution `hcli_corrected`.

- `DifferentialEquations.jl` A suite for numerically solving differential equations written in Julia.
- `GLMakie.jl` For high-level plotting on the GPU.
- `NonlinearEigenproblems.jl` A nonlinear eigenvalue problem determine a scalar λ and a vector v such that $M(\lambda)v = 0$. In our case, the matrix $M(\lambda)$ will be the characteristic matrix.
- `DDEBifTool.jl` We created this very minimalistic package to have some functionality for normal form calculations of DDEs in Julia. Here we use it to calculate the derivatives of the system necessary for `NonlinearEigenproblems.jl`.
- `DelimitedFiles.jl` Reading and writing of CSV files.
- `PGFPlotsX.jl` A Julia package for creating publication quality figures using the LaTeX library `PGFPlots` as the backend.

```

1 using DifferentialEquations
2 using GLMakie
3 using DDEBifTool
4 using NonlinearEigenproblems
5 using DelimitedFiles
6 using PGFPlotsX
7 using DataFrames
8 using Colors

```

S1.13.2 Define system

Next we define the system to be integrated, a system to approximate the reverse flow, and also an allocating version used for stability calculations.

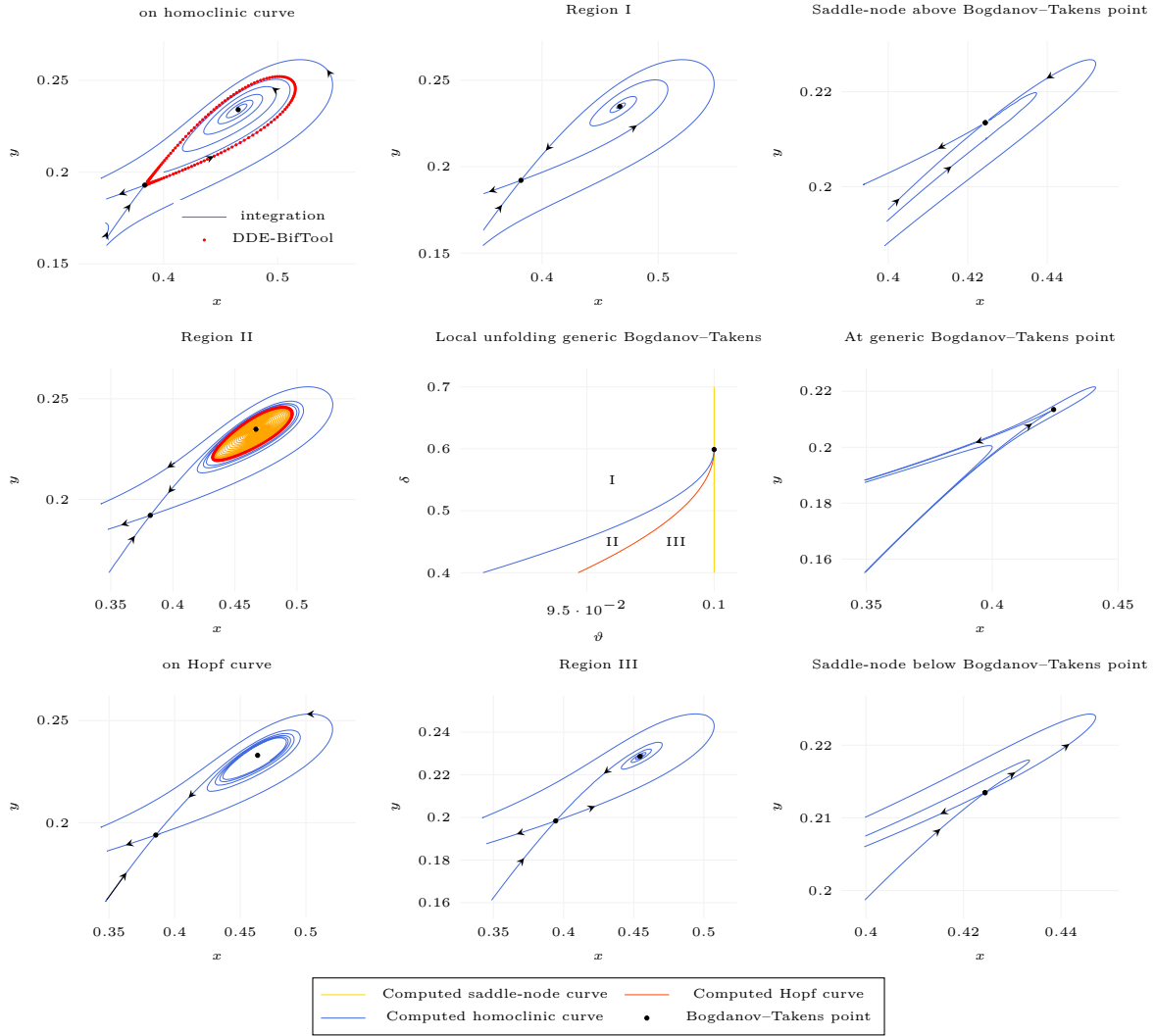


Figure S5: Bifurcation diagram near the derived generic Bogdanov-Takens point in (S3). In the center, we plotted the computed codimension one curves emanating from the Bogdanov-Takens point using DDE-BifTool with the third-order homoclinic asymptotics obtained in Section 4.1.9. The simulations surrounding the center plot have been performed in Julia.

```

10 # define constants
11 const m = 1.502983803
12 const α = 0.9
13 const γ = 0.15
14 const τ = 0.01
15
16 # define model
17 function predator_prey!(du,u,h,p,t)
18     θ, δ = p
19     x,y = u

```

```

20     xt, yt = h(p, t-τ)
21     du[1] = x*((1-x)*(x-γ)/(x+θ) - α*y/(x+y))
22     du[2] = δ*y*(-1 + m*xt/(xt+yt))
23 end
24
25 # approximate the reversed flow by multiplying
26 # the right-hand side by -1
27 function predator_prey_rev!(du,u,h,p,t)
28     predator_prey!(du,u,h,p,t)
29     du .= -du
30 end
31
32 # allocating version (used for calculating stability)
33 function predator_prey(xx, pars)
34     du = similar(xx[:,1])
35     h(p,t) = xx[:,2]
36     predator_prey!(du,xx[:,1],h,p,0)
37     du
38 end

```

S1.13.3 Functions for plotting arrows

We define a function to show in which direction the orbits flow, which is useful when plotting in phase-space. We also define a function to show the direction of the leading eigenvectors of the characteristic matrix.

```

40 # function to show the direction of the orbits
41 function draw_arrow_on_solution(ax,sol, pointnumber, direction; arrowsize=30)
42     x = [sol[1,pointnumber]]
43     y = [sol[2,pointnumber]]
44     u = [sol[1,direction(pointnumber,1)]-sol[1,pointnumber]]
45     v = [sol[2,direction(pointnumber,1)]-sol[2,pointnumber]]
46     arrows!(ax,x,y,u,v,arrowsize=arrowsize)
47     Dict(:x=>x[1], :y=>y[1], :u=>u[1], :v=>v[1])
48 end
49
50 # function for plotting arrows into the eigen direction of the saddle-node
51 function arrow(ax, point, V, δ, direction)
52     if direction > 0
53         x, y, u, v = [point; -δ*V]
54     else
55         endpoint = point + δ*V
56         lines!(ax,hcat([endpoint, point]...),color=:black)
57         x, y, u, v = [endpoint; -0.1δ*V]
58     end
59     arrows!(ax,[x],[y],[u],[v],arrowsize=30)
60
61     # return dictionary for PGFPlotsX
62     Dict(:x=>x, :y=>y, :u=>u, :v=>v)
63 end

```

```

64
65 function drawEigenDirections(ax, point, Vstable, Vunstable;
66     distance=1e-03)
67     arrow(ax, point.coords, Vunstable, distance, 1)
68     arrow(ax, point.coords, Vunstable, -distance, 1)
69     arrow(ax, point.coords, Vstable, distance, -1)
70     arrow(ax, point.coords, Vstable, -distance, -1)
71 end

```

Listing S4: Functions for plotting arrows.

S1.13.4 Define parameters, equilibria

We define parameters located on the continued homoclinic branch with DDE-BifTool. Then define the non-trivial equilibria points in (S2), which can be derived analytically.

```

73 ## Simulation at homoclinic curve
74  $\theta_0, \delta_0 = [0.09444852842823, 0.447783343351055]$ 
75  $\mathbf{p} = [\theta_0; \delta_0]$ 
76
77 # define equilibria analytically
78  $D(\theta) = (\alpha + m - \alpha*m + \gamma*m)^2 - 4*m*(\gamma*m + \alpha*(-1 + m)*\theta)$ 
79  $\mathbf{x}_0 = \theta \rightarrow [(\alpha + m - \alpha*m + \gamma*m - \sqrt{D(\theta)})/(2*m),$ 
80      $(\alpha + m - \alpha*m + \gamma*m + \sqrt{D(\theta)})/(2*m)]$ 

```

S1.13.5 Plot equilibria and homoclinic orbit

By plotting the homoclinic orbit obtained with DDE-BifTool, we can compare with the numerical simulations.

```

82 ## simulation from saddle-node
83 point = (coords = [ $\mathbf{x}_0(\theta_0)[1]; (m-1)*\mathbf{x}_0(\theta_0)[1]$ ], pars = [ $\theta_0, \delta_0$ ])
84
85 # plot equilibria
86 scatter(Point2f. ( $\mathbf{x}_0(\theta_0)$ ,  $(m-1)*\mathbf{x}_0(\theta_0)$ ), color=:black)
87
88 # plot homoclinic orbit from DDE-BifTool
89 csvdir = "/home/maikel/Documents/MyPapers/BTPaper/data/doubleAlleeEffect/"
90 homoclinic_orbit = readdlm(csvdir * "homoclinicorbit.csv")
91 scatter!(homoclinic_orbit, color=:orangered, label="Solution from DDE-BifTool")

```

S1.13.6 Eigenvectors

Next, we calculate and plot the leading eigenvectors of the characteristic matrix at the saddle-node bifurcation point.

```

93 # calculate stability
94  $\tau_s = [0.0 \ \tau]$ 

```

```

95 M = coefficient_matrices(predator_prey, point,  $\tau$ s)
96 dep=DEP([M[j](point.coords,point.pars) for j in 1:length( $\tau$ s)],vec( $\tau$ s))
97  $\lambda$ ,V=iar_chebyshev(dep,maxit=100,neigs=2)
98 V = real(V)
99 indx_unstable = findall( $\lambda \rightarrow$  real( $\lambda$ ) > 0,  $\lambda$ )
100 indx_stable = findall( $\lambda \rightarrow$  real( $\lambda$ ) < 0,  $\lambda$ )
101 Vunstable = vec(V[:,indx_unstable])
102 Vstable = vec(V[:,indx_stable])
103
104 # draw eigenvectors
105 drawEigenDirections(current_axis(), point, Vstable, Vunstable; distance=1e-03)

```

S1.13.7 Define callback

Since we are only interested in the flow near the equilibria points, we create a discrete callback to ensure the orbits do not become too large.

```

107 # create callback
108 condition(u,t,integrator) = u[1] < 0.35
109 affect!(integrator) = terminate!(integrator)
110 cb = DiscreteCallback(condition,affect!)

```

S1.13.8 Integrate the system

Now we define the problem to be integrated and choose the algorithm to be used. The first of the five numerical simulations below starts near the unstable eigendirection. We rotated the eigenvector slightly to follow the homoclinic orbit very close. The rotation value of α_0 was actually obtained by using the bisection method. However, we did not include this code here.

```

112 # define DDEProblem and choose integration algorithm
113 prob(h,p,tspan,direction) =
114     DDEProblem(direction > 0 ? predator_prey! : predator_prey_rev!,
115         h(p,0), h, tspan,p; constant_lags=[ $\tau$ ], callback=cb)
116 alg = MethodOfSteps(Tsit5())
117
118 # orbit startin in the unstable eigendirection crossing
119 # all points of the homoclinic orbit obtained in DDE-BifTool
120  $\epsilon$  = sign(Vunstable[1])*1e-03
121 R( $\alpha$ ) = [cos( $\alpha$ ) -sin( $\alpha$ );sin( $\alpha$ ) cos( $\alpha$ )]
122  $\alpha_0$  = 0.00032200554789652436
123 h(p,t) = point.coords +  $\epsilon$ *R( $\alpha_0$ )*Vunstable
124 tspan = (0.0, 310.0);
125 sol1 = solve(prob(h,p,tspan,1),alg,reltol=1e-12, abstol=1e-12)
126 lines!(sol1,color=:royalblue, label="Solution from integration")
127
128 # orbit converging to inner equilibria
129 h(p,t) = [0.4; 0.2]
130 sol2 = solve(prob(h,p,tspan,1),alg,reltol=1e-12, abstol=1e-12)
131 lines!(sol2,color=:royalblue1)

```



```

132
133 # orbit starting in the leading stable eigendirection
134 # and solved with the approximated system
135  $\epsilon = \text{sign}(\text{Vstable}[1]) * 1e-04$ 
136  $h(p,t) = \text{point.coords} - \epsilon * \text{Vstable}$ 
137 sol3 = solve(prob(h,p,tspan,-1),alg,reltol=1e-12,abstol=1e-12)
138 lines!(sol3,color=:royalblue, linestyle=:dash)
139
140 # the next two orbits show the flow around the stable eigendirection
141  $h(p,t) = [0.35; 0.16]$ 
142 sol4 = solve(prob(h,p,tspan,1),alg,reltol=1e-12,abstol=1e-12)
143 lines!(sol4,color=:royalblue)
144
145  $h(p,t) = [0.35; 0.166]$ 
146 sol5 = solve(prob(h,p,tspan,1),alg,reltol=1e-12,abstol=1e-12)
147 lines!(sol5,color=:royalblue)

```

S1.13.9 Finish the plot

Lastly, we add arrows to the obtained solutions using the function `draw_arrow_on_solution` defined above. Also, we add the legend and re-plot the equilibria, so that they appear on top.

```

149 # add arrows on solution
150 draw_arrow_on_solution(current_axis(), sol1, 120, +)
151 draw_arrow_on_solution(current_axis(), sol1, 600, +)
152 draw_arrow_on_solution(current_axis(), sol2, 370, +)
153 draw_arrow_on_solution(current_axis(), sol3, 150, -)
154 draw_arrow_on_solution(current_axis(), sol4, 150, +)
155 draw_arrow_on_solution(current_axis(), sol5, 24, +)
156
157 # add legend
158 axislegend(position = :lt)
159
160 # redraw equilibria
161 scatter!(Point2f.( $x_0(\theta_0)$ , (m-1)* $x_0(\theta_0)$ ), color=:black)

```

We should now obtain an interactive figure similar to the left figure in [Figure S6](#).

S2 Generic Bogdanov–Takens bifurcation in a neural network model

In this example, we will consider the model

$$\begin{cases} \mu \dot{u}_1(t) = -u_1(t) + q_{11}\alpha(u_1(t-T)) - q_{12}u_2(t-T) + e_1, \\ \mu \dot{u}_2(t) = -u_2(t) + q_{21}\alpha(u_1(t-T)) - q_{22}u_2(t-T) + e_2, \end{cases} \quad (\text{S3})$$

which describes the dynamics of a neural network consisting of excitatory and inhibitory neurons [19]. The variables and parameters occurring in (S3) have the following neurophysiological meaning:

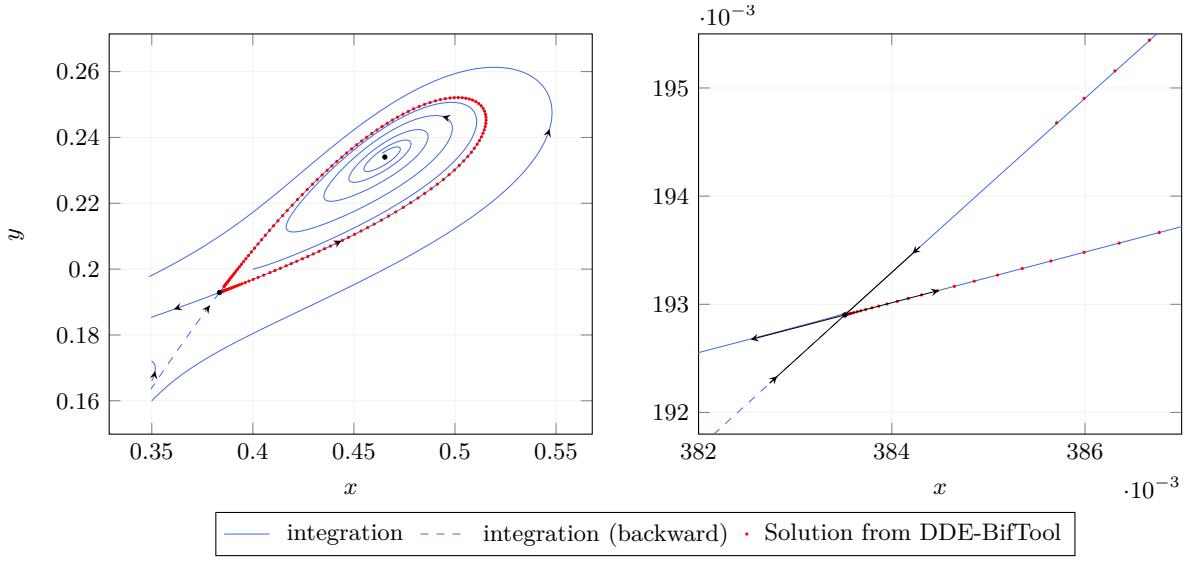


Figure S6: Integration of the delayed predator-prey model (S2) at parameter values $(\theta, \delta) = (0.094448552842823, 0.447783343351055)$ obtained from continuation of the homoclinic curve emanating from the Bogdanov–Takens point using DDE-BifTool. In the plot to the right a close-up near the saddle is given. Additionally, the leading eigenvectors of the characteristic matrix are shown.

- $u_1, u_2 : \mathbb{R} \rightarrow \mathbb{R}$ denote the total post-synaptic potential of the excitatory and inhibitory neurons, respectively.
- $\mu > 0$ is a time constant characterizing the dynamical properties of the cell membrane.
- $q_{ik} \geq 0$ represent the strength of the connection line from the k th neuron to the i th neuron.
- $\alpha : \mathbb{R} \rightarrow \mathbb{R}$ is the transfer function which describes the activity generation of the excitatory neuron as a function of its total potential u_1 . The function α is smooth, increasing and has a unique turning point at $u_1 = \theta$. The transfer function corresponding to the inhibitory neuron is assumed to be the identity.
- $T \geq 0$ is a time delay reflecting synaptic delay, axonal and dendritic propagation time.
- e_1 and e_2 are external stimuli acting on the excitatory and inhibitory neuron, respectively.

Following [19], we consider equation (S3) with

$$\alpha(u_1) = \frac{1}{1 + e^{-4u_1}} - \frac{1}{2}, \quad q_{11} = 2.6, \quad q_{21} = 1.0, \quad q_{22} = 0.0,$$

$$\mu = 1.0, \quad T = 1.0, \quad e_2 = 0.0,$$

and $Q := q_{12}$, $E := e_1$ as bifurcation parameters. Substituting into (S3) yields

$$\begin{cases} \dot{u}_1(t) = -u_1(t) + 2.6\alpha(u_1(t-1)) - Qu_2(t-1) + E, \\ \dot{u}_2(t) = -u_2(t) + \alpha(u_1(t-1)). \end{cases} \quad (\text{S4})$$

Notice that for any steady-state we have the symmetry

$$(u_1, u_2, E) \rightarrow (-u_1, -u_2, -E). \quad (\text{S5})$$

It is easy to explicitly derive that the system has a double eigenvalue zero for

$$\begin{cases} u_1(t) = \frac{1}{4} \log\left(\frac{8 - \sqrt{39}}{5}\right) \approx -0.2617, \\ u_2(t) = -\frac{1}{2} \sqrt{\frac{3}{13}} \approx -0.2402, \\ Q = \frac{13}{10}, \\ E = \frac{\sqrt{39} - 10 \operatorname{atanh} \sqrt{\frac{3}{13}}}{20} \approx 0.0505. \end{cases} \quad (\text{S6})$$

Remark 13. The MATLAB files for this demonstration can be found in the directory `demos/tutorial/VII/neural_network_model` relative to the main directory of the DDE-BifTool package. Here, we omit the code to generate the system file. We assume that the system file `sym_neural_network_mf.m` has been generated with the script `sym_neural_network.m`. Also, we assume that the DDE-BifTool package has been loaded as in [Listing S1](#). The code in [Sections S2.1](#) to [S2.11](#) highlights the important parts of the file `neural_network_model.m`.

S2.1 Set parameter names and funcs structure

As in the previous example, we set the parameter names and define the `funcs` structure.

```

28 %% Set parameter names
29 % This could also be loaded from mat file 'FHN_parnames.mat'.
30 parnames={'Q', 'E', 'tau'};
31 cind=[parnames; num2cell(1:length(parnames))];
32 ind=struct(cind{:});
33
34 %% Set the funcs structure
35 % We load the precalculated multilinear forms. These have been generated
36 % with the file gen_sym_neural_network.m.
37 funcs=set_symfuncs(@sym_neural_network_mf, 'sys_tau', @()ind.tau);
38 % Alternatively, uncomment the line below to use directional derivatives.
39 % funcs=set_symfuncs(@sym_FHN, 'sys_tau', @()ind.tau);

```

S2.2 Set parameter range

Since we are only interested here in the local unfolding, we restrict the allowed parameter range for the unfolding parameters. In practice, one may have physical restrictions which must be satisfied. Additionally, we also limit the maximum allowed step size during continuation. By doing so, we obtain more refined data to compare against our predictors.

```

41 %% Set bifurcation parameter range and step size bounds
42 brpars={'max_bound', [ind.Q 1.7], ...
43         'min_bound', [ind.Q 1.2; ind.E 0], ...
44         'max_step', [ind.Q 0.005; ind.E 0.005]};

```

S2.3 Stability and coefficients of the generic Bogdanov–Takens point

We manually construct a steady-state at the generic Bogdanov–Takens point.

```
46 %% Define analytically derived Bogdanov-Takens point
47 % construct steady-state point
48 Q0 = 13/10; E0 = (sqrt(39) - 10*atanh(sqrt(3/13)))/20; tau0 = 1;
49 stst=dde_stst_create('x',[1/4*log((8-sqrt(39))/5); -1/2*sqrt(3/13)]);
50 stst.parameter(ind.Q) = Q0;
51 stst.parameter(ind.E) = E0;
52 stst.parameter(ind.tau) = tau0;
53 % Calculate stability
54 method=df_mthod(funcs,'stst');
55 stst.stability=p_stabil(funcs,stst,method.stability);
56 stst.stability.l1
```

The MATLAB console shows the following output.

```
ans =

    1.0e-07 *

    0.548156278544666
   -0.548156314155979
```

The eigenvalues confirm that the point under consideration is indeed (an approximation to) a Bogdanov–Takens point. Furthermore, the remaining eigenvalues have negative real parts. Next, we calculate the normal form coefficients, the time-reparametrization, and the transformation to the center manifold with the function `nmfm_bt_orbital`, which implements the coefficients as derived in [Section 4.1](#). For this, we need to set the argument `free_pars` to the unfolding parameter (Q, E) . These coefficients will be used to start the continuation of the codimension one branches emanating from the Bogdanov–Takens point.

```
58 %% Calculate coefficients
59 free_pars=[ind.Q, ind.E];
60 bt = p_tobt(funcs,stst);
61 bt = nmfm_bt_orbital(funcs, bt,'free_pars', free_pars);
62 bt.nmfm
```

The MATLAB console shows the following output.

```
ans =

struct with fields:

    a: -0.190382124055415
    b: -0.951910620277072
theta1000: -0.546026508575597
```

```

theta0001: 1.4736111111111115
  K10: [2x1 double]
  K01: [2x1 double]
  K02: [2x1 double]
  K11: [2x1 double]
  K03: [2x1 double]
  phi0: [1x1 struct]
  phi1: [1x1 struct]
  h0010: [1x1 struct]
  h0001: [1x1 struct]
  h2000: [1x1 struct]
  h1100: [1x1 struct]
  h0200: [1x1 struct]
  h1010: [1x1 struct]
  h1001: [1x1 struct]
  h0110: [1x1 struct]
  h0101: [1x1 struct]
  h0002: [1x1 struct]
  h0011: [1x1 struct]
  h3000: [1x1 struct]
  h2100: [1x1 struct]
  h1101: [1x1 struct]
  h2001: [1x1 struct]
  h0003: [1x1 struct]
  h1002: [1x1 struct]
  h0102: [1x1 struct]
  K: @(beta1,beta2)K10*beta1+K01*beta2+1/2*K02*beta2.^2
      +K11*beta1.*beta2+1/6*K03*beta2^3
  H: [function_handle]

```

Since the sign of ab is positive, we expect to find unstable periodic orbits nearby the Bogdanov–Takens point.

S2.4 Comparing profiles of computed and predicted homoclinic orbits

To test the homoclinic asymptotics from [Section 4.1.9](#) we compare the first and third order asymptotics to the Newton corrected solution. For this, we use the function `C1branch_from_C2point`. This function returns a branch, which by default returns two initial corrected approximations in order to start continuation of the codimension one curve under consideration. By setting the argument `'predictor'` to `true` the approximations are left uncorrected. To make the comparison visually clear, we set the perturbation parameter $\epsilon = 0.25$ (`step = 0.25` in the code below). The code below produces [Figure S7](#). The difference between the two approximations is clearly noticeable. While the first order asymptotics is close to the Newton corrected solution, the third order asymptotics is indistinguishable at this scale from the Newton corrected solution.

```

64 %% Plot comparing profiles computed and predicted homoclinic orbits
65 figure(1); clf; hold on;
66 cm=colormap('lines');
67 tiledlayout(2,2)
68 ylabel = {'x$', 'y$'};

```

```

69 step = 0.2;
70 for order=[1,3]
71     ↪ [~,hcli_br_approx,suc]=C1branch_from_C2point(funcs,bt,free_pars,'order',order,...
72         'codim2','BT','codim1','hcli','step',step,'predictor',true,'debug',0);
73
74     ↪ [~,hcli_br_correc,suc]=C1branch_from_C2point(funcs,bt,free_pars,'order',order,...
75         'codim2','BT','codim1','hcli','step',step,'debug',0);
76     for j=1:2
77         ax = nexttile; hold on; title(sprintf('order %d',order))
78     ↪ plot(ax,hcli_br_approx.point(1).mesh,hcli_br_approx.point(1).profile(j,:),'*')
79         plot(ax,hcli_br_correc.point(1).mesh,hcli_br_correc.point(1).profile(j,:))
80         xlabel('$t$', 'Interpreter', 'LaTeX');
81         ylabel(string(ylabls(j)), 'Interpreter', 'LaTeX')
82     end
83 end

```

S2.5 Continuation of the codimension one curves emanating

To continue the three codimension one curves emanating from the generic Bogdanov–Takens point, we can simply use the function `C1branch_from_C2point`, as shown in the code below. To monitor the continuation process, the argument `plot` must be set to 1. The most important setting is the perturbation parameter (or multiple), `step` in the code below. If left out, default step sizes are defined. However, depending on the problem, no convergence may then be obtained.

```

84 %% Continue homoclinic solutions emanating from the BT point
85 [~,hcli_br,suc]=C1branch_from_C2point(funcs,bt,free_pars,...
86     'codim2','BT','codim1','hcli',brpars{:},'plot',0,'step',0.1);
87 assert(all(suc(:)>0))
88 nop=300; [hcli_br,suc]=br_contn(funcs,hcli_br,nop);assert(suc>0)
89
90 %% Continue Hopf curve
91 [~,hbr,suc]=C1branch_from_C2point(funcs,bt,free_pars,...
92     'codim2','BT','codim1','hopf',brpars{:},'step',1e-05,'plot',0);
93 assert(all(suc(:)>0))
94 nop=300; [hbr,suc]=br_contn(funcs,hbr,nop);assert(suc>0)
95
96 %% Continue fold curve emanating from Bogdanov-Takens point
97 [~,fold_br,suc]=C1branch_from_C2point(funcs,bt,free_pars,...
98     'codim2','BT','codim1','fold',brpars{:},'step',1e-03,'plot',0);
99 assert(all(suc(:)>0))
100 nop=300; [fold_br,suc]=br_contn(funcs,fold_br(1),nop);assert(suc>0)
101 fold_br = br_rvers(fold_br);
102 nop=300; [fold_br,suc]=br_contn(funcs,fold_br(1),nop);assert(suc>0)

```

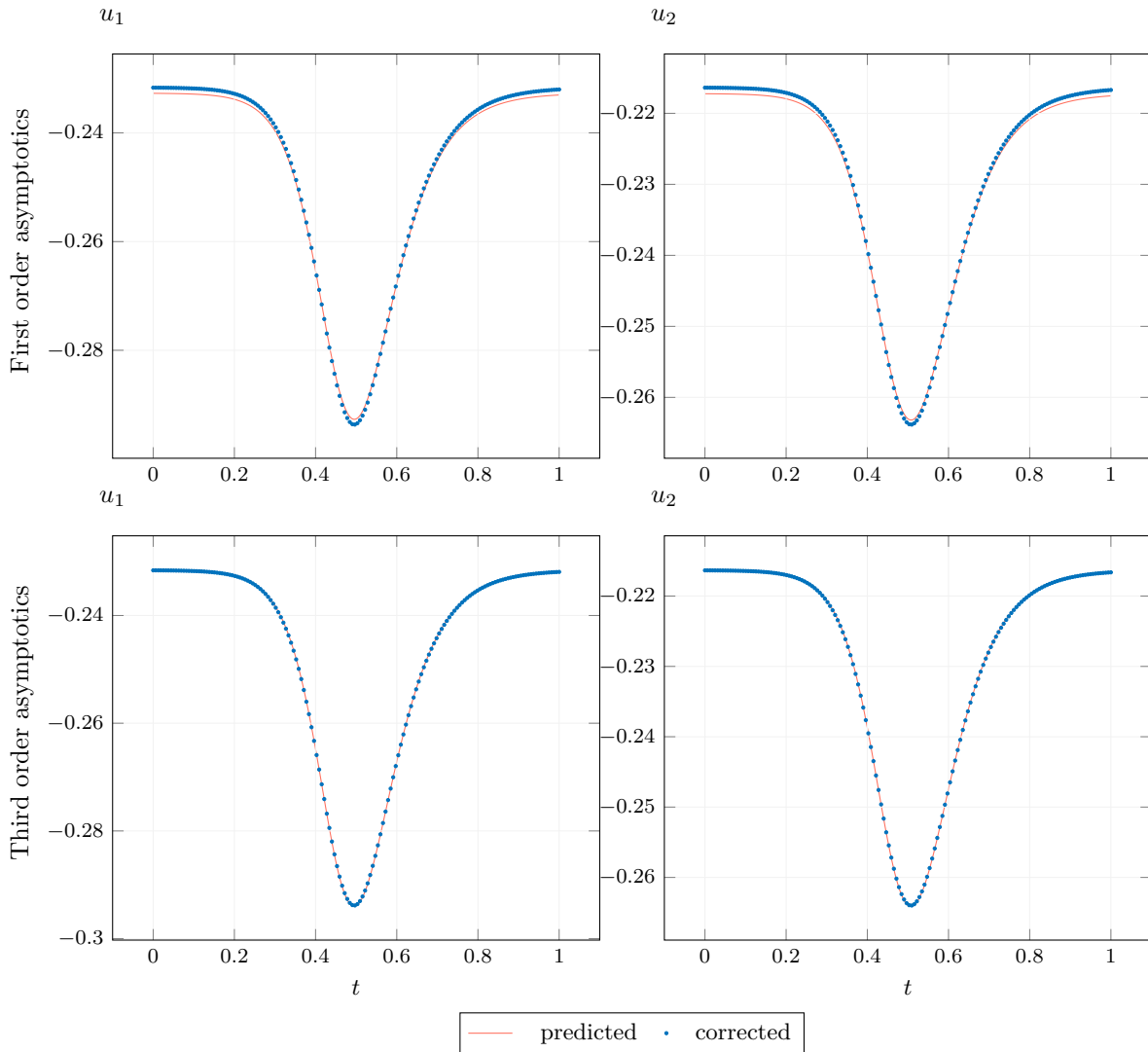


Figure S7: Comparison between the first and third-order asymptotics from Section 4.1.9 near the generic Bogdanov–Takens bifurcation in (S3) with the perturbation parameter set to $\epsilon = 0.25$.

S2.6 Predictors of the codimension one curves emanating from the Bogdanov–Takens point

Before we provide the bifurcation diagram in the next section, we first obtain the predictors for the codimension one curves. For this, we again use the function `C1branch_from_C2point`. We set the argument `predictor` to 1 and provide a range of perturbation parameters.

```

121 %% Predictors for homoclinic, Hopf, and transcritical curves
122 step = linspace(1e-4,0.6,50);
123 [~,hcli_br_pred,suc]=C1branch_from_C2point(funcs,bt,free_pars,'debug',0,...
124     'codim2','BT','codim1','hcli','step',step,'predictor',true);
125 step = linspace(0.0001,0.2,50);

```

```

126 [~,hbr_pred,suc]=C1branch_from_C2point(funcs,bt,free_pars,...
127     'codim2','BT','codim1','hopf','step',step,'predictor',true);
128 step = linspace(-0.1,0.3,40);
129 [~,fold_br_pred,suc]=C1branch_from_C2point(funcs,bt,free_pars,...
130     'codim2','BT','codim1','fold','step',step,'predictor',true);
131 hcli_br_pred_pm = [getpars(hcli_br_pred, ind.Q), getpars(hcli_br_pred, ind.E)];
132 hbr_pm_pred = [getpars(hbr_pred, ind.Q); getpars(hbr_pred, ind.E)];
133 fold_br_pm_pred = [getpars(fold_br_pred, ind.Q); getpars(fold_br_pred, ind.E)];

```

In the last part of the code above, we added the asymptotics obtained from [25].

S2.7 Bifurcation diagram

The code below produces (a figure similar to) [Figure S8](#).

```

135 %% Plot the bifurcation curves with predictors
136 figure(3);clf;hold on
137 title(['Codimension 1 curves emanating from the generic ', ...
138     'Bogdanov-Takens point with predictors']);
139 plot(hcli_br_pm(1,:),hcli_br_pm(2:,:),'.','Color',cm(1,:), ...
140     'DisplayName','Homoclinic branches')
141 plot(hcli_br_pred_pm(:,1),hcli_br_pred_pm(:,2),'Color', cm(7,:), ...
142     'DisplayName','Third order homoclinic asymptotics')
143 plot(hbr_pm(1,:),hbr_pm(2:,:),'o','Color',cm(1,:), ...
144     'DisplayName','Hopf branch')
145 plot(hbr_pm_pred(1,:),hbr_pm_pred(2:),'--','Color',cm(7,:), ...
146     'DisplayName','Hopf asymptotics')
147 plot(fold_br_pm(1,:),fold_br_pm(2:),'d','Color',cm(1,:), ...
148     'DisplayName','Fold branch')
149 plot(fold_br_pm_pred(1,:),fold_br_pm_pred(2:),':', 'Color',cm(7,:), ...
150     'DisplayName','Fold asymptotics')
151 plot(bt.parameter(ind.Q),bt.parameter(ind.E),'.k', 'MarkerSize', 18, ...
152     'DisplayName','generic Bogdanov-Takens point');
153 xlabel('$Q$', 'Interpreter', 'LaTeX')
154 ylabel('$E$', 'Interpreter', 'LaTeX')
155 axis([1.2928 1.4323 0.0209 0.0522])
156 legend

```

S2.8 Compare homoclinic solutions in phase-space

To obtain an impression of the third-order homoclinic asymptotics in phase-space, we compare the corrected and uncorrected homoclinic solutions with the perturbation parameter ranging from 0.1 to 0.3. The code below results in [Figure S9](#). We see that the corrected and predicted homoclinic orbits are nearly identical.

```

158 %% Compare predicted and corrected orbits in phase-space
159 step = linspace(0.1,0.3,10);
160 [~,hcli_br_approx,suc]=C1branch_from_C2point(funcs,bt,free_pars,'order',order,...

```

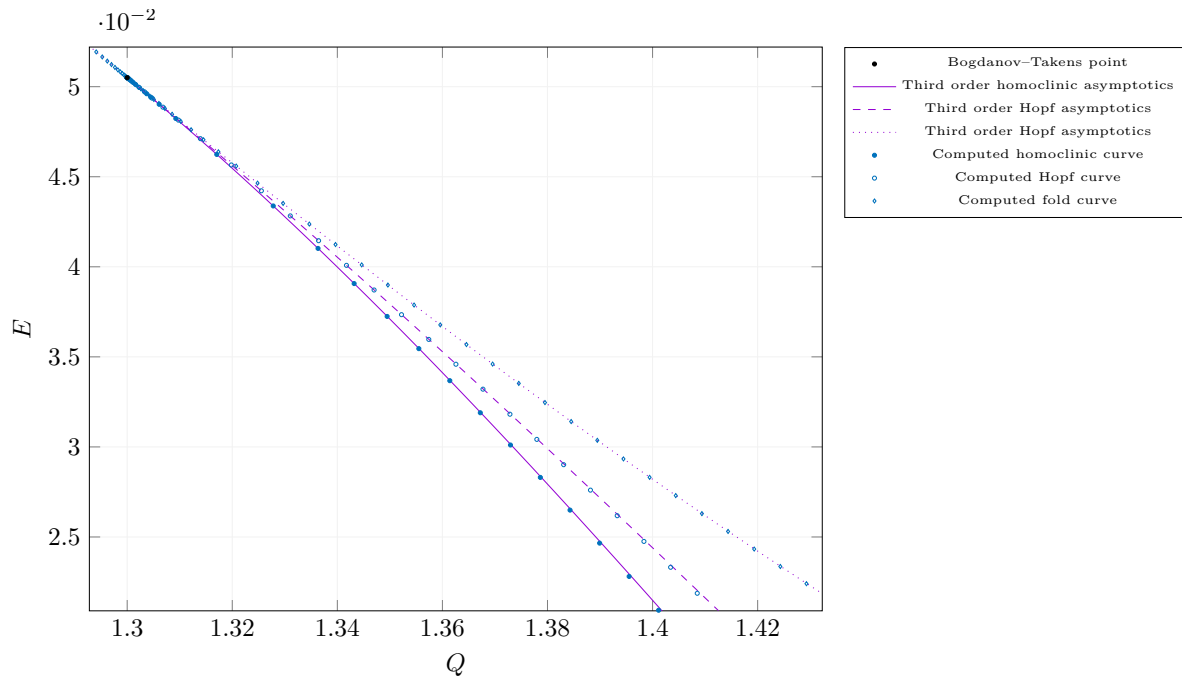



Figure S8: Bifurcation diagram near the derived generic Bogdanov-Takens point in (S3) comparing computed codimension one curves using DDE-BifTool with the third-order homoclinic parameter asymptotics obtained in Section 4.1.9.

```

161     'codim2','BT','codim1','hcli','step',step,'predictor',true,'debug',0);
162 [~,hcli_br_correc,suc]=C1branch_from_C2point(funcs,bt,free_pars,'order',order,...
163     'codim2','BT','codim1','hcli','step',step,'debug',0);
164 figure(4); clf; hold on
165 title('Continued homoclinic orbits in phase-space')
166 for i=1:length(hcli_br_approx.point)
167     profile = hcli_br_approx.point(i).profile;
168     plot(profile(1,:),profile(2,:), 'Color', cm(2,:))
169     profile = hcli_br_correc.point(i).profile;
170     plot(profile(1,:),profile(2,:), '.', 'Color', cm(1,:))
171 end
172 legend({'Predicted homoclinic order', 'Corrected homoclinic orbir'})
173 xlabel('$u_1$', 'Interpreter', 'LaTeX');
174 ylabel('$u_2$', 'Interpreter', 'LaTeX');

```

S2.9 Convergence plot

Using the function from Section S1.12, we create a log-log convergence plot comparing the convergence order of the first and third order homoclinic asymptotics from Section 4.1.9. The code below yields Figure S10.

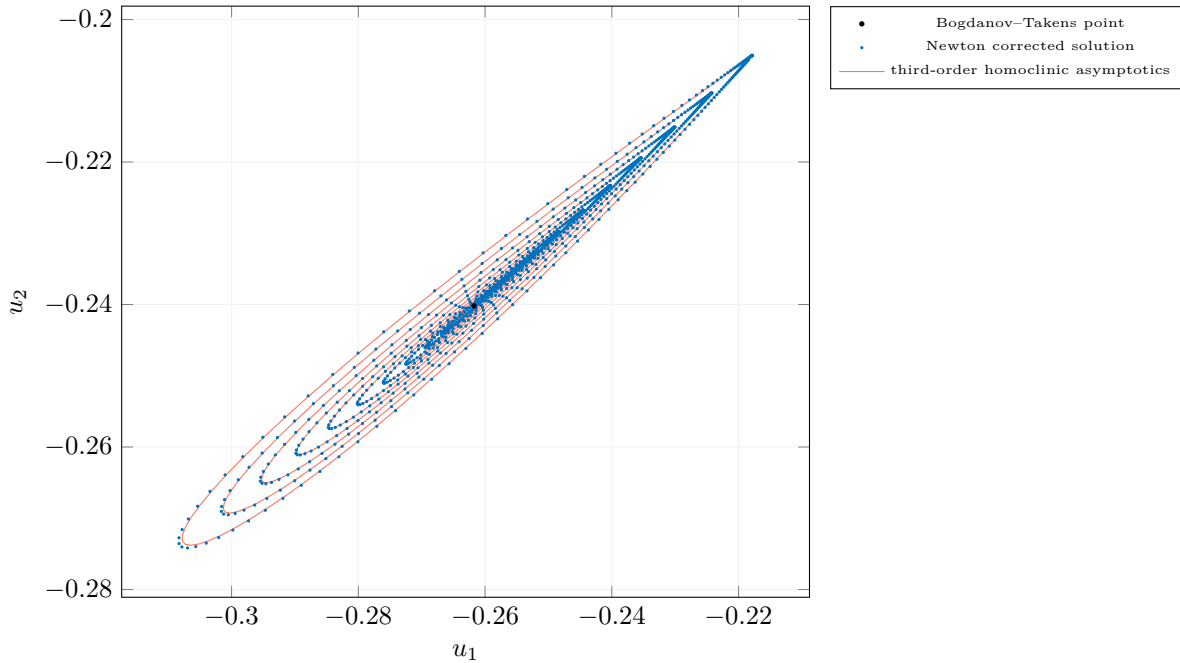


Figure S9: Plot comparing the third-order homoclinic asymptotics from Section 4.1.9 near the generic Bogdanov–Takens bifurcation in (S3) with the Newton correct homoclinic solutions in (u_1, u_2) phase-space.

```

176 %% Convergence plot
177 amplitudes = logspace(-2.6, -1, 20);
178 orders = [1:3];
179 relativeerrors = convergence_plot(funcs, bt, orders, amplitudes, 'free_pars', ...
180     free_pars, 'orders', orders, 'Tolerance', 1e-4, 'ntst', 82, 'debug', false, 'dir', 1);
181 figure(5); clf; hold on
182 title('Convergence plot comparing first and third order homoclinic asymptotics')
183 plot(log10(amplitudes), log10(relativeerrors{1}(:)), '*-')
184 plot(log10(amplitudes), log10(relativeerrors{3}(:)), '*-')
185 legend({'first order', 'thrid order'})
186 xlabel('amplitude')
187 ylabel('relative error')

```

S2.10 Continuation of the codimension one curves emanating from the second Bogdanov–Takens point

For completeness, we also continue the codimension one curves emanating from the second Bogdanov–Takens point, which exists due to the symmetry (S5). Of course, we could just use the symmetry instead of computing the curves numerically. However, we use it as an additional verification of our derived asymptotics. The code below defines the second Bogdanov–Takens point, calculates the stability, and continues the Hopf and homoclinic bifurcation curves.

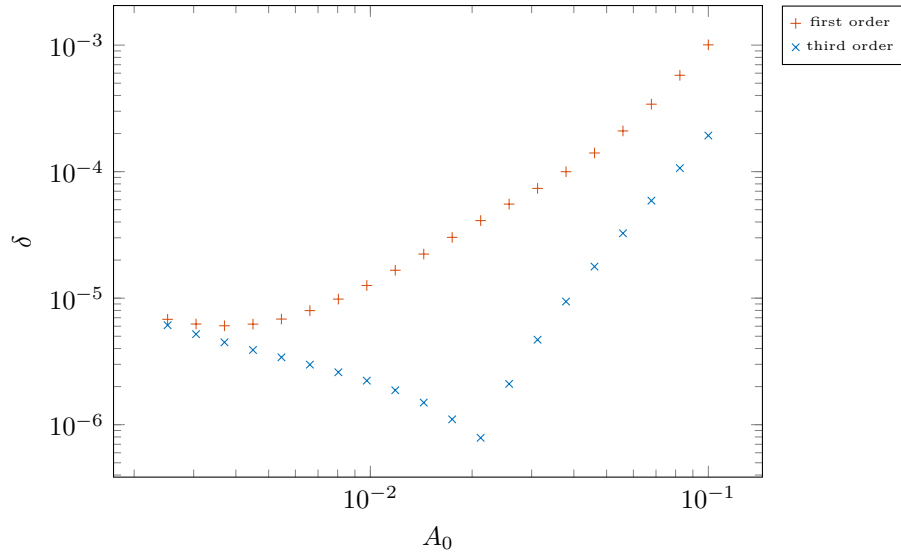


Figure S10: On the abscissa is the approximation to the amplitude A_0 and on the ordinate the relative error δ between the constructed solution `hcli_pred` to the defining system for the homoclinic orbit and the Newton corrected solution `hcli_corrected`.

```

189 %% Define second analytically derived Bogdanov-Takens point
190 % construct steady-state point
191 stst=dde_stst_create('x',-[1/4*log((8-sqrt(39))/5); -1/2*sqrt(3/13)]);
192 stst.parameter(ind.Q) = Q0;
193 stst.parameter(ind.E) = -E0;
194 stst.parameter(ind.tau) = tau0;
195 % Calculate stability
196 method=df_mthod(funcs,'stst');
197 stst.stability=p_stabil(funcs,stst,method.stability);
198 stst.stability.l1
199
200 %% Calculate coefficients
201 free_pars=[ind.Q, ind.E];
202 bt2 = p_tobt(funcs,stst);
203 bt2 = nmfm_bt_orbital(funcs, bt2,'free_pars', free_pars);
204 bt2.nmfm
205
206 %% Continue homoclinic solutions emanating from the BT point
207 [~,hcli_br2,suc]=C1branch_from_C2point(funcs,bt2,free_pars,...
208     'codim2','BT','codim1','hcli',brpars{:},'plot',0,'step',0.1);
209 assert(all(suc(:)>0))
210 nop=300; hcli_br2=br_contn(funcs,hcli_br2,nop);assert(suc>0)
211
212 %% Continue Hopf curve
213 [~,hbr2,suc]=C1branch_from_C2point(funcs,bt2,free_pars,...
214     'codim2','BT','codim1','hopf',brpars{:},'step',1e-05,'plot',0);
215 assert(all(suc(:)>0))

```

```
216 nop=300; [hbr2,suc]=br_contn(funcs,hbr2,nop);assert(suc>0)
```

S2.11 Bifurcation diagram with two Bogdanov–Takens points

Now that we continued the Hopf and homoclinic bifurcation curves emanating from the second Bogdanov–Takens point, we can reconstruct the bifurcation diagram given in [19, Figure 7]. The code below results into a similar figure as [Figure S11](#) in MATLAB.

```
218 %% Plot the bifurcation curves
219 figure(6);clf;hold on
220 title(['Codimension 1 curves emanating from the ', ...
221        'transcritical Bogdanov-Takens point']);
222 getpars=@(br,ind) arrayfun(@(p)p.parameter(ind),br.point);
223 hcli_br_pm = [getpars(hcli_br,ind.Q), getpars(hcli_br,ind.E)]';
224 hcli_br2_pm = [getpars(hcli_br2,ind.Q), getpars(hcli_br2,ind.E)]';
225 hbr_pm = [getpars(hbr,ind.Q); getpars(hbr,ind.E)];
226 hbr2_pm = [getpars(hbr2,ind.Q); getpars(hbr2,ind.E)];
227 fold_br_pm = [getpars(fold_br,ind.Q); getpars(fold_br,ind.E)];
228 plot(hcli_br_pm(1,:),hcli_br_pm(2:,:), 'Color',cm(1,:), ...
229      'DisplayName', 'Homoclinic branches')
230 plot(hcli_br2_pm(1,:),hcli_br2_pm(2:,:), 'Color',cm(1,:), ...
231      'HandleVisibility', 'Off')
232 plot(hbr_pm(1,:),hbr_pm(2:,:), 'Color',cm(2,:), ...
233      'DisplayName', 'Hopf branches')
234 plot(hbr2_pm(1,:),hbr2_pm(2:,:), 'Color',cm(2,:), ...
235      'HandleVisibility', 'Off')
236 plot(fold_br_pm(1,:),fold_br_pm(2:,:), 'Color',cm(3,:), ...
237      'DisplayName', 'Transcritical branch')
238 plot(bt.parameter(ind.Q),bt.parameter(ind.E), '.k', ...
239      'MarkerSize', 18, ...
240      'DisplayName', 'generic Bogdanov-Takens point');
241 plot(bt2.parameter(ind.Q),bt2.parameter(ind.E), '.k', ...
242      'MarkerSize', 18, 'HandleVisibility', 'Off');
243 xlabel('$Q$', 'Interpreter', 'LaTeX')
244 ylabel('$E$', 'Interpreter', 'LaTeX')
245 legend
```

S2.12 Simulation with DifferentialEquations.jl

Here we will perform two simulations. The first simulation will be at the double homoclinic orbits, which will confirm the continuation of both homoclinic orbits and is also ascetically pleasing, see [Figure S12](#). The second simulation will be in the region where there should be unstable periodic orbits, see [Figure S13](#).

S2.12.1 Loading necessary Julia packages

We start by loading the necessary packages.

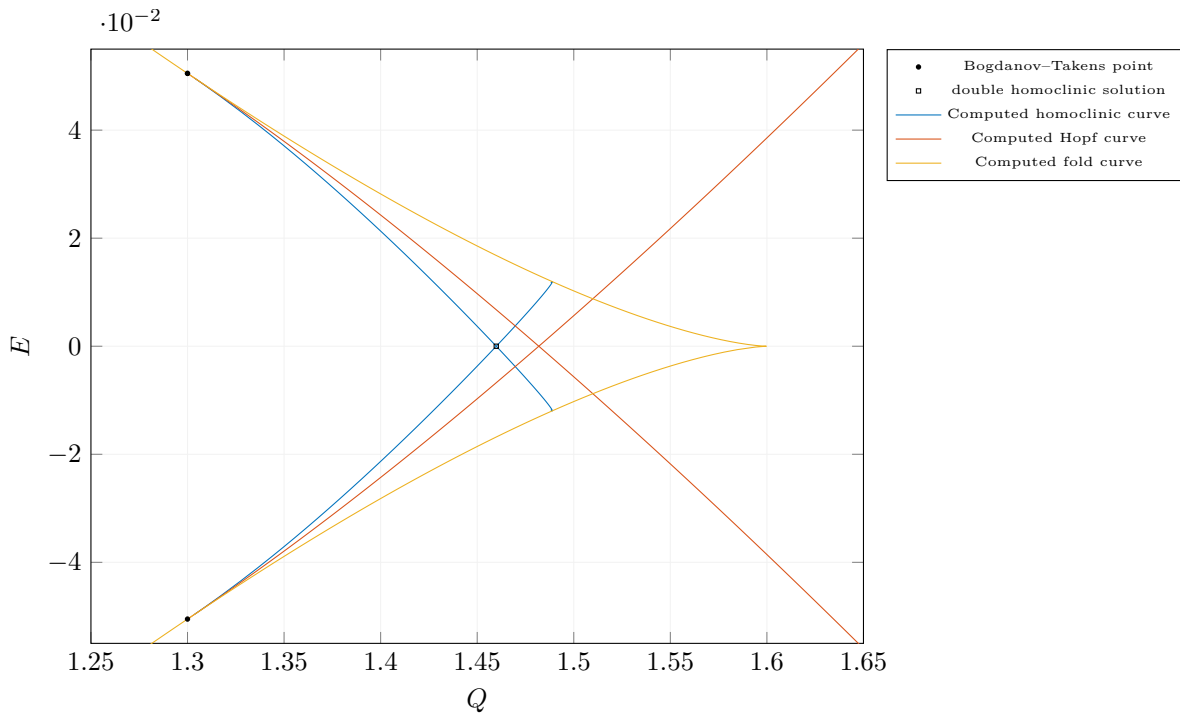


Figure S11: Reconstruction of the bifurcation diagram given in [19, Figure 7]. We could have used the symmetry (S5) instead of computing the additional curves numerically. However, it provides us an additional verification of our derived asymptotics.

```

1 using DifferentialEquations
2 using GLMakie
3 using DelimitedFiles
4 using IntervalArithmetic, IntervalRootFinding
5 using DDEBifTool
6 using NonlinearEigenproblems

```

Listing S5: Loading Julia packages for simulation in (S3).

In the previous demonstration we were able to derive the equilibria analytically. Here we will solve for the equilibria numerically with the packages `IntervalArithmetic.jl` [33] and `IntervalRootFinding.jl` [1].

S2.12.2 Define system

We define the system to be integrated, a system to approximate the reverse flow, and also an allocating version used for stability calculations.

```

8 # define constants
9 const τ = 1.0

```

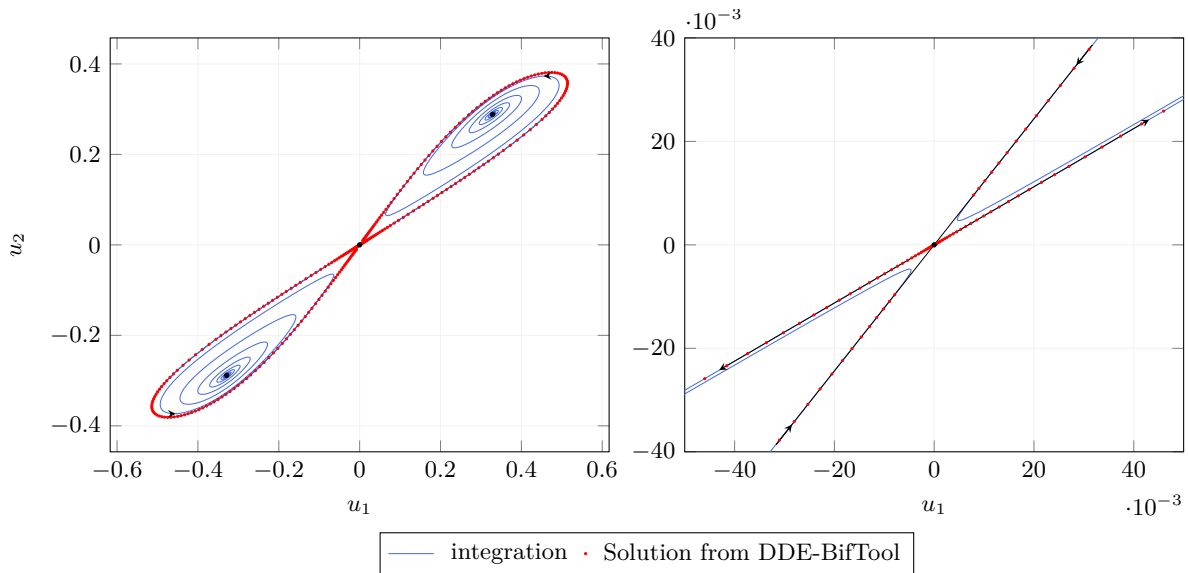


Figure S12: Comparing the computed double homoclinic orbit in (S3) with DDE-BifTool with the solutions obtained from numerical simulation with Julia. In the right plot is a close-up near the equilibrium at the origin. Also, the leading stable and unstable eigenvectors of the characteristic matrix are plotted. We see the numerical integrated solution intersects all the red points from the solution from DDE-BifTool.

```

10
11 # define model
12 @inline  $\alpha(u_1) = 1.0/(1.0+\exp(-4.0*u_1)) - 0.5$ 
13 function neural_network_model!(du,u,h,p,t)
14     Q, E = p
15     u1,u2 = u
16     u1t, u2t = h(p, t- $\tau$ )
17     du[1] = -u1 + 2.6* $\alpha(u_1t)$  - Q*u2t + E;
18     du[2] = -u2 +  $\alpha(u_1t)$ ;
19 end
20
21 # allocating version (used for calculating stability)
22 function neural_network_model(u, p)
23     du = similar(u[:,1])
24     h(p,t) = u[:,2]
25     neural_network_model!(du,u[:,1],h,p,0)
26     du
27 end

```

S2.12.3 Functions for plotting arrows

We define a function to show in which direction the orbits flow, which is useful when plotting in phase-space. We also define functions to show the direction of the leading eigenvectors of the characteristic matrix. The code is shown in Listing S4.

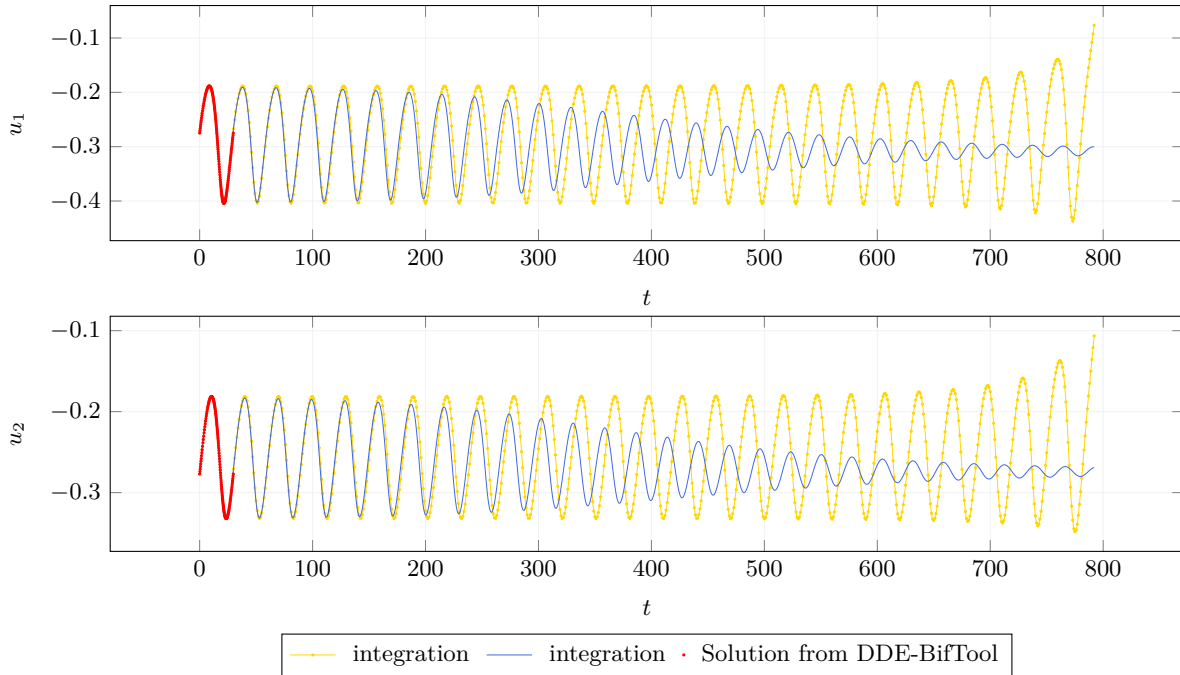


Figure S13: Comparing a computed periodic orbit in (S3) with DDE-BifTool at $(Q, E) = (1.476442865781454, 0.0)$ with the solution obtained from numerical simulation with Julia near the periodic orbit. The yellow dotted line has the constant history function $(u_1, u_2) = (-0.274863341578762, -0.27715979849863204)$ slightly below the periodic orbit. The blue line has the constant history function $(u_1, u_2) = (-0.274863341578762, -0.276969798498632)$, a point on the periodic orbit (red dots) located with DDE-BifTool.

S2.12.4 Create figure with several axes

We create a figure containing multiple axis in which we will plot the bifurcation diagram and the homoclinic and periodic orbits.

```

63 fig = Figure()
64 ax1 = Axis(fig[1:4,1], xlabel=L"u_1", ylabel=L"u_2",
65           title="Double Homoclinic orbit")
66 ax2 = Axis(fig[1:4,2], xlabel=L"Q", ylabel=L"E",
67           title="Bifucation diagram")
68 ax3 = Axis(fig[1,3], xlabel=L"t", ylabel = L"u_1",
69           title="Near periodic orbit")
70 ax4 = Axis(fig[2,3], xlabel=L"t", ylabel = L"u_2")
71 ax5 = Axis(fig[3,3], xlabel=L"t", ylabel=L"u_1",
72           title="Near periodic orbit (zoom in)")
73 ax6 = Axis(fig[4,3], xlabel=L"t", ylabel = L"u_2")

```

S2.12.5 Plot bifurcation diagram in the middle

Loading the continued bifurcation curves obtained with DDE-BifTool and plot these in the middle axis. This should give a similar bifurcation diagram as in Figure S11.

```

76 csvdir = "../data/neuralNetworkModel/"
77 fold_br = readdlm(csvdir * "foldbifurcationcurve.csv")
78 hopf_br = readdlm(csvdir * "hopfbifurcationcurve.csv")
79 hom_br = readdlm(csvdir * "homoclinicbifurcationcurve.csv")
80 hopf_br2 = readdlm(csvdir * "hopfbifurcationcurve2.csv")
81 hom_br2 = readdlm(csvdir * "homoclinicbifurcationcurve2.csv")
82 lines!(ax2, fold_br, label = "computed fold curve", color=:gold)
83 lines!(ax2, hopf_br, label = "computed Hopf curve", color=:orangered)
84 lines!(ax2, hom_br, label = "computed homoclinic curve", color=:royalblue)
85 lines!(ax2, hopf_br2, color=:orangered)
86 lines!(ax2, hom_br2, color=:royalblue)
87
88 # define Bogdanov-Takens point
89 u1 = 1/4*log((8-sqrt(39))/5)
90 u2 = -1/2*sqrt(3/13)
91 Q0 = 13/10
92 E0 = (sqrt(39) - 10*atanh(sqrt(3/13)))/20;
93 bt = (coords = [u1, u2], pars = [Q0, E0])
94 scatter!(ax2, Point2f(Q0, E0), label = "generic Bogdanov-Takens point", color=:black)
95 scatter!(ax2, Point2f(Q0, -E0), color=:black)
96
97 # add double homoclinic bifurcation point
98 scatter!(ax2, Point2f(1.459868437376255,0), label = "Double homoclinic orbit",
  ↪ color=:blue)
99
100 # add region labels
101 text!(ax2, "II", position = (1.4609, 3.304e-03), align = (:center,:center),
  ↪ textsize = 20)
102 axislegend(ax2, position = :ct)

```

S2.12.6 Simulation at the double homoclinic orbit

In the code below, we integrate at parameter values $(Q, E) = (1.459868437376222, 0)$, i.e., where we located the double homoclinic orbit. We start by locating the three equilibria points. Note that by the symmetry, we actually only need to solve for one of them. We calculate the stability of the equilibria and filter out the leading stable and unstable eigenvectors from the characteristic matrix of the saddle-node point. The rest of the code should be pretty straight forward, since it is very similar as in the simulation in the previous demonstration. After running this code, we should obtain a similar plot as in the left plot of [Figure S12](#).

```

105 Q0, E0 = 1.459868437376222,0
106 p = [Q0; E0]
107
108 # derive equilibria
109 y(u1) = -u1 + (2.6 - Q0)*alpha(u1) + E0
110 rts = roots(y,interval(-10,10), Newton, 1e-16)
111 u1 = sort(mid.(interval.(rts)))
112 u2 = alpha.(u1)
113

```



```

114 # calculate stability
115  $\tau_s = [0.0 \ \tau]$ 
116 point = [(coords = [u1[i]; u2[i]], pars = p) for i ∈ 1:length(u1)]
117 M = [coefficient_matrices(neural_network_model, point[i],  $\tau_s$ ) for i ∈ 1:length(u1)]
118 dep = [DEP([M[i][j](point[i].coords,point[i].pars) for j in 1:length( $\tau_s$ )],vec( $\tau_s$ ))
    ↪ for i ∈ 1:length(u1)]
119  $\lambda = \text{iar\_chebyshev}(\text{dep},\text{maxit}=100,\text{neigs}=2)$ 
120 saddle_indx = findall( $\lambda \rightarrow \text{abs}(\lambda[1]) < 1e-14, \text{imag}([\lambda[i][1] \text{ for } i \in 1:\text{length}(u_1)]])$ )
121 saddle = point[saddle_indx] []
122 V = real. ( $\lambda$ [saddle_indx] [] [2])
123 indx_unstable = findall( $\lambda \rightarrow \text{real}(\lambda) > 0, \lambda$ [saddle_indx] [] [1])
124 indx_stable = findall( $\lambda \rightarrow \text{real}(\lambda) < 0, \lambda$ [saddle_indx] [] [1])
125 Vunstable = vec(V[:,indx_unstable])
126 Vstable = vec(V[:,indx_stable])
127
128 # plot equilibria
129 scatter!(ax1,Point2f.([point[i].coords for i ∈ 1:length(u1)]),color=:black)
130
131 # plot homoclinic orbit from DDE-BifTool
132 homoclinic_orbit = readdlm(csvdir * "doubble_homoclinicorbit.csv")
133 scatter!(ax1, homoclinic_orbit, color=:orangered)
134
135 # create callback
136 condition(u,t,integrator) = !(abs(u[1]) < 0.55)
137 affect!(integrator) = terminate!(integrator)
138 cb = DiscreteCallback(condition,affect!)
139
140 # define DDEProblem and choose integration algorithm
141 prob(h,p,tspan) = DDEProblem(neural_network_model!, h(p,0),h,tspan,p;
    constant_lags=[ $\tau$ ], callback=cb)
142
143 alg = MethodOfSteps(Tsit5())
144
145 # integration from unstable direction
146  $\epsilon = \text{sign}(V\text{unstable}[1])*1e-04$ 
147  $R(\alpha) = [\cos(\alpha) \ -\sin(\alpha); \sin(\alpha) \ \cos(\alpha)]$ 
148  $\alpha_0 = 0.006$ 
149 h(p,t) = saddle.coords +  $\epsilon*R(\alpha_0)*V\text{unstable}$ 
150 tspan = (0.0, 350.0);
151 hom_sol1 = solve(prob(h,p,tspan),alg,reltol=1e-09,abstol=1e-09)
152 lines!(ax1,hom_sol1,color=:royalblue1)
153
154 h(p,t) = saddle.coords -  $\epsilon*R(\alpha_0)*V\text{unstable}$ 
155 hom_sol2 = solve(prob(h,p,tspan),alg,reltol=1e-09,abstol=1e-09)
156 lines!(ax1,hom_sol2,color=:royalblue1)
157
158 # add arrows
159 draw_arrow_on_solution(ax1, hom_sol1, 700, +)
160 draw_arrow_on_solution(ax1, hom_sol2, 700, +)
161
162 # redraw equilibria
163 scatter!(ax1,Point2f.([point[i].coords for i ∈ 1:length(u1)]),color=:black)

```

```

164
165 # draw leading eigenvectors from the characteristic matrix
166 drawEigenDirections(ax1, point[2], Vstable, Vunstable; distance=5e-02)

```

S2.12.7 Simulation near an unstable periodic orbit

To show by integration the existence of an unstable periodic orbit, we first located a periodic orbit in DDE-BifTool. This can be done by continuing a branch of periodic orbits emanating from a point on the continued Hopf curve. Then we load the profiles of the periodic orbits into Julia and start integration near the periodic orbits. After running the code below, we should obtain a similar plot as in [Figure S13](#).

```

169 Q0, E0 = [1.476442865781454, 0.0]
170 scatter!(ax2, Point2f(Q0,E0),color=:black)
171 p = [Q0; E0]
172
173 # plot periodic orbit computed with DDE-BifTool
174 periodic_orbit = readdlm(csvdir * "periodicorbit_20.csv")
175 scatter!(ax3, periodic_orbit[:,1:2], color=:orangered)
176 scatter!(ax4, periodic_orbit[:,[1,3]], color=:orangered)
177
178 # plot again for close up
179 scatter!(ax5, periodic_orbit[:,1:2], color=:orangered)
180 scatter!(ax6, periodic_orbit[:,[1,3]], color=:orangered)
181
182 # create callback
183 condition(u,t,integrator) = !(abs(u[1]) < 0.7)
184 affect!(integrator) = terminate!(integrator)
185 cb = DiscreteCallback(condition,affect!)
186
187 # integration from first point on the periodic solution
188 h(p,t) = periodic_orbit[1,2:3]
189 h(0,0)
190 tspan = (0.0, 792.0);
191 periodic_sol1 = solve(prob(h,p,tspan),alg,reltol=1e-08, abstol=1e-08)
192 lines!(ax3,periodic_sol1.t,periodic_sol1[1,:])
193 lines!(ax4,periodic_sol1.t,periodic_sol1[2,:])
194 lines!(ax5,periodic_sol1.t,periodic_sol1[1,:])
195 lines!(ax6,periodic_sol1.t,periodic_sol1[2,:])
196 xlims!(ax5, [0, 29.789440842376618]) # as vector
197 ylims!(ax5, [-0.42, -0.15]) # as vector
198 xlims!(ax6, [0, 29.789440842376618]) # as vector
199 ylims!(ax6, [-0.42, -0.15]) # as vector
200
201 # integration from a little below first point on the first periodic solution
202 h(p,t) = periodic_orbit[1,2:3] - [0; 1.90e-04]
203 tspan = (0.0, 792.0);
204 periodic_sol2 =
    ↪ solve(prob(h,p,tspan),MethodOfSteps(Tsit5()),reltol=1e-08, abstol=1e-08)
205 lines!(ax3,periodic_sol2.t,periodic_sol2[1,:])

```

```

206 lines!(ax4,periodic_sol2.t,periodic_sol2[2,:])
207 lines!(ax5,periodic_sol2.t,periodic_sol2[1,:])
208 lines!(ax6,periodic_sol2.t,periodic_sol2[2,:])

```

S3 Transcritical Bogdanov–Takens bifurcation in the Van der Pol oscillator with delay feedback

We consider the Van der Pol oscillator with delay feedback [24] given by

$$\ddot{x}(t) + \epsilon(x^2(t) - 1)\dot{x}(t) + x(t) = \epsilon g(x(t - \tau)) \quad (\text{S7})$$

where $\epsilon > 0$ is a parameter, $\tau > 0$ is a delay and $g : \mathbb{R} \rightarrow \mathbb{R}$ is a smooth function with $g(0) = 0$ and $g'(0) \neq 0$. We rewrite the Van der Pol equation (S7) as

$$\begin{cases} \dot{x}_1 = x_2, \\ \dot{x}_2 = \epsilon g(x_1(t - \tau)) - \epsilon(x_1^2 - 1)x_2 - x_1. \end{cases} \quad (\text{S8})$$

Rescaling time with $t \rightarrow \frac{t}{\tau}$ to normalize the delay yields

$$\begin{cases} \dot{x}_1 = \tau x_2, \\ \dot{x}_2 = \tau (\epsilon g(x_1(t - 1)) - \epsilon(x_1^2 - 1)x_2 - x_1). \end{cases} \quad (\text{S9})$$

This allows to treat τ as a bifurcation parameter.

Following [24], we consider (S7) with

$$g(x) = \frac{e^x - 1}{c_1 e^x + c_2},$$

where $c_1 = \frac{1}{4}$ and $c_2 = \frac{1}{2}$. Then the trivial equilibrium undergoes a transcritical Bogdanov–Takens bifurcation at parameter values $(\epsilon, \tau) = (0.75, 0.75)$, [24] and the supplement.

Remark 14. The MATLAB files for this demonstration can be found in the directory `demos/tutorial/VII/vdpo_bt_transcritical` relative to the main directory of the DDE-BifTool package. Here, we omit the code to generate a system file. The system file `sym_vdpo_mf.m` has been generated with the script `sym_vdpo_mf.m`. Also, we assume that the DDE-BifTool package has been loaded as in Listing S1. The code in Sections S3.1 to S3.9 highlights the important parts of the file `vanderPolOscillator.m`.

S3.1 Set parameter names and funcs structure

As in the previous example, we set the parameter names and define the `funcs` structure.

```

31 %% Set parameter names
32 parnames={'epsilon','tau','vartau'};
33 cind=[parnames;num2cell(1:length(parnames))];
34 ind=struct(cind{:});
35
36 %% Set the funcs structure
37 funcs=set_symfuncs(@sym_vdpo_mf,'sys_tau',@( )ind.vartau);

```

S3.2 Set parameter range

Since we are only interested here in the local unfolding, we restrict the allowed parameter range for the unfolding parameters. In practice, one may have physical restrictions which must be satisfied. Additionally, we also limit the maximum allowed step size during continuation. By doing so, we obtain more refined data to compare against our predictors.

```
39 %% Set bifurcation parameter range and step size bounds
40 brpars={'min_bound', [ind.epsilon 0.7122; ind.tau 0.7154],...
41         'max_bound', [ind.epsilon 0.7998; ind.tau 0.7905],...
42         'max_step', [ind.epsilon 0.0001; ind.tau 0.0001]};
```

S3.3 Stability and coefficients of the transcritical Bogdanov–Takens point

We manually construct a steady-state at the transcritical Bogdanov–Takens point and calculate its stability.

```
44 %% Define analytically derived Bogdanov-Takens point
45 % manually construct steady-state point
46 epsilon = 0.75; tau = 0.75;
47 stst=dde_stst_create('x',[0;0]);
48 stst.parameter(ind.epsilon) = epsilon;
49 stst.parameter(ind.tau) = tau;
50 stst.parameter(ind.vartau) = 1;
51
52 %% Compute stability
53 method=df_mthod(funcs,'stst');
54 stst.stability=p_stabil(funcs,stst,method.stability);
55 stst.stability.11
```

The MATLAB console shows the following output.

```
ans =
    1.0e-07 *
    0.6223
   -0.6223
```

The eigenvalues confirm that the point under consideration is indeed (an approximation to) a Bogdanov–Takens point. Furthermore, the remaining eigenvalues have negative real parts. Next, we calculate the normal form coefficients, the time-reparametrization, and the transformation to the center manifold with the function `nmfm_bt_orbital`, which implements the coefficients as derived in [Section 4.2](#). For this, we need to set the argument `free_pars` to the unfolding parameter (Q, E) . These coefficients will be used to start the continuation of the codimension one branches emanating from the Bogdanov–Takens point. Also, since we are in the transcritical case, we set the argument `generic_unfolding` to `false`.

```

57 %% Calculate parameter-dependent normal form coefficients
58 free_pars=[ind.epsilon, ind.tau];
59 bt = p_tobt(funcs,stst);
60 bt = mmfm_bt_orbital(funcs, bt, 'free_pars', free_pars, 'generic_unfolding', false);

```

The MATLAB console shows the following output.

```

ans =

struct with fields:

    a: 0.1304
    b: -0.2949
theta1000: 0.0780
theta0010: -21.1293
theta0001: -0.3811
    phi0: [1x1 struct]
    phi1: [1x1 struct]
    h2000: [1x1 struct]
    h1100: [1x1 struct]
    h0200: [1x1 struct]
    h3000: [1x1 struct]
    h2100: [1x1 struct]
    K10: [2x1 double]
    K01: [2x1 double]
    K02: [2x1 double]
    K11: [2x1 double]
    K20: [2x1 double]
    h1010: [1x1 struct]
    h1001: [1x1 struct]
    h0110: [1x1 struct]
    h0101: [1x1 struct]
    h2010: [1x1 struct]
    h1110: [1x1 struct]
    h2001: [1x1 struct]
    h1101: [1x1 struct]
    h1002: [1x1 struct]
    h0102: [1x1 struct]
    h1020: [1x1 struct]
    h0120: [1x1 struct]
    h1011: [1x1 struct]
    h0111: [1x1 struct]
    K: @(beta1,beta2)K10*beta1+K01*beta2+1/2*K20*beta1^2
        +K11*beta1*beta2+1/2*K02*beta2^2
    H: [function_handle]

```

Since the sign of ab is negative, we expect to find stable periodic orbits nearby the Bogdanov–Takens point.

S3.4 Comparing profiles of computed and predicted homoclinic orbits

To test the homoclinic asymptotics from [Section 4.1.9](#) we compare the first and third order asymptotics to the Newton corrected solution. For this, we use the function `C1branch_from_C2point`. This function returns a branch, which by default returns two initial corrected approximations in order to start continuation of the codimension one curve under consideration. By setting the argument `'predictor'` to `true` the approximations are left uncorrected. To make the comparison visually clear, we set the perturbation parameter $\epsilon = 0.1$ (`step = 0.1` in the code below). The code below produces [Figure S14](#). The difference between the two approximations is clearly noticeable. While the first order asymptotics is close to the Newton corrected solution, the third order asymptotics is indistinguishable at this scale from the Newton corrected solution.

```
63 %% Plot comparing profiles computed and predicted homoclinic orbits
64 figure(1); clf; hold on;
65 cm=colormap('lines');
66 tiledlayout(2,4)
67 ylabel = {'x$', '$y$'};
68 step = 0.1;
69 for order=[1,3]
70     [~,hcli_br_approx,suc]=C1branch_from_C2point(funcs,bt,free_pars, ...
71         'debug',0,'codim2','BT','codim1','hcli','step',step,'plot',0, ...
72         'generic_unfolding',false,'predictor',true,'order',order);
73     [~,hcli_br_correc,suc]=C1branch_from_C2point(funcs,bt,free_pars, ...
74         'order',order,'codim2','BT','codim1','hcli','step',step, ...
75         'plot',0,'generic_unfolding',false,'debug',0);
76     for i=1:2
77         for j=1:2
78             ax = nexttile; hold on; title(sprintf('order %d',order))
79             plot(ax,hcli_br_approx(i).point(1).mesh, ...
80                 hcli_br_approx(i).point(1).profile(j,:), '*')
81             plot(ax,hcli_br_correc(i).point(1).mesh, ...
82                 hcli_br_correc(i).point(1).profile(j,:))
83             xlabel('$t$', 'Interpreter', 'LaTeX');
84             ylabel(string(ylabel(j)), 'Interpreter', 'LaTeX')
85         end
86     end
87 end
```

S3.5 Continuation of the codimension one curves emanating

To continue the three codimension one curves emanating from the generic Bogdanov–Takens point, we can simply use the function `C1branch_from_C2point`, as shown in the code below. To monitor the continuation process, the argument `plot` must be set to 1. The most important setting is the perturbation parameter (or multiple), `step` in the code below. If left out, default step sizes are defined. However, depending on the problem, no convergence may then be obtained.

```
89 %% Continue homoclinic curve emanating from Bogdanov-Takens point
90 [~,hcli_br,suc]=C1branch_from_C2point(funcs,bt,free_pars, ...
91     'codim2','BT','codim1','hcli',brpars{:},'step',0.02, ...
```

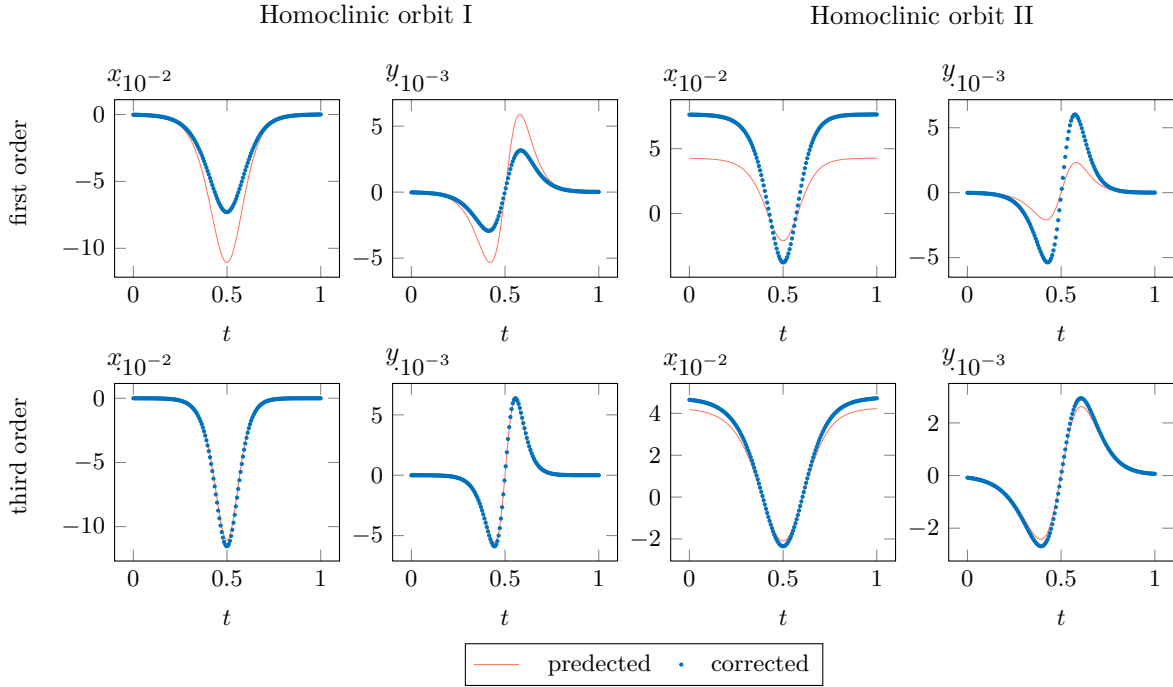


Figure S14: Comparison between the first and third-order homoclinic asymptotics from Section 4.2.3 near the transcritical Bogdanov–Takens bifurcation in (S9) with the perturbation parameter set to $\epsilon = 0.1$.

```

92     'plot',0,'generic_unfolding',false);
93 assert(all(suc(:)>0))
94 nop=300; [hcli_br(1),suc]=br_contn(funcs,hcli_br(1),nop);assert(suc>0)
95 nop=300; [hcli_br(2),suc]=br_contn(funcs,hcli_br(2),nop);assert(suc>0)
96
97 %% Continue Hopf curve emanating from Bogdanov-Takens point
98 [~,hbr,suc]=C1branch_from_C2point(funcs,bt,free_pars, ...
99     'codim2','BT','codim1','hopf',brpars{:},'step',1e-05, ...
100     'plot',0,'generic_unfolding',false);
101 assert(all(suc(:)>0))
102 nop=300; [hbr(1),suc]=br_contn(funcs,hbr(1),nop); assert(suc>0)
103 nop=300; [hbr(2),suc]=br_contn(funcs,hbr(2),nop); assert(suc>0)
104 [hbr(2),suc]=br_contn(funcs,hbr(2),nop); assert(suc>0)
105
106 %% Continue transcritical curve emanating from Bogdanov-Takens point
107 [~,tc_br,suc]=C1branch_from_C2point(funcs,bt,free_pars,'dir',2, ...
108     'codim2','BT','codim1','fold',brpars{:},'step',-1e-4, ...
109     'plot',0,'generic_unfolding',false);
110 assert(all(suc(:)>0))
111 nop=300; [tc_br,suc]=br_contn(funcs,tc_br(1),nop);assert(suc>0)
112 tc_br = br_rvers(tc_br);
113 nop=300; [tc_br,suc]=br_contn(funcs,tc_br(1),nop);assert(suc>0)

```

S3.6 Predictors of the codimension one curves emanating from the Bogdanov–Takens point

Before we provide the bifurcation diagram in the next section, we first obtain the predictors for the codimension one curves. For this, we again use the function `C1branch_from_C2point`. We set the argument `predictor` to 1 and provide a range of perturbation parameters.

```
135 % Predictors for homoclinic, Hopf, and transcritical curves
136 step = [linspace(1e-4,0.1,20);linspace(1e-4,0.1,20)];
137 [~,hcli_br_pred,suc]=C1branch_from_C2point(funcs,bt,free_pars,'debug',0, ...
138     'codim2','BT','codim1','hcli','step',step,'generic_unfolding',false, ...
139     'predictor',true);
140 step = [linspace(0.0001,0.1,20);linspace(0.0001,0.1,20)];
141 [~,hbr_pred,suc]=C1branch_from_C2point(funcs,bt,free_pars, ...
142     'codim2','BT','codim1','hopf','step',step,'generic_unfolding',false, ...
143     'predictor',true);
144 step = linspace(-0.04,0.04,40);
145 [~,tc_br_pred,suc]=C1branch_from_C2point(funcs,bt,free_pars, ...
146     'codim2','BT','codim1','fold','step',step,'generic_unfolding',false, ...
147     'predictor',true);
148 hcli_br1_pm_pred = [getpars(hcli_br_pred(1), ind.epsilon), ...
149     getpars(hcli_br_pred(1), ind.tau)];
150 hcli_br2_pm_pred = [getpars(hcli_br_pred(2), ind.epsilon), ...
151     getpars(hcli_br_pred(2), ind.tau)];
152 hbr1_pm_pred = [getpars(hbr_pred(1),ind.epsilon); getpars(hbr_pred(1),ind.tau)];
153 hbr2_pm_pred = [getpars(hbr_pred(2),ind.epsilon); getpars(hbr_pred(2),ind.tau)];
154 tc_br_pm_pred = [getpars(tc_br_pred,ind.epsilon); getpars(tc_br_pred,ind.tau)];
```

S3.7 Bifurcation diagram

The code below produces (a figure similar to) [Figure S2](#).

```
156 %% Plot the bifurcation curves with predictors
157 figure(3);clf;hold on
158 title(['Codimension 1 curves emanating from the transcritical', ...
159     'Bogdanov-Takens point with predictors']);
160 plot(hcli_br1_pm(1,:),hcli_br1_pm(2,:),'.','Color',cm(1,:), ...
161     'DisplayName','Homoclinic branches')
162 plot(hcli_br2_pm(1,:),hcli_br2_pm(2,:),'.','Color',cm(1,:), ...
163     'HandleVisibility','off')
164 plot(hbr1_pm(1,:),hbr1_pm(2,:),'o','Color',cm(2,:), 'DisplayName','Hopf branches')
165 plot(hbr2_pm(1,:),hbr2_pm(2,:),'o','Color',cm(2,:), 'HandleVisibility','off')
166 plot(tc_br_pm(1,:),tc_br_pm(2,:),'d','Color',cm(3,:), ...
167     'DisplayName','Transcritical branch')
168 plot(hcli_br1_pm_pred(:,1),hcli_br1_pm_pred(:,2),'Color', cm(7,:), ...
169     'DisplayName','Third order homoclinic asymptotics')
170 plot(hcli_br2_pm_pred(:,1),hcli_br2_pm_pred(:,2),'Color', cm(7,:), ...
171     'HandleVisibility','off')
172 plot(hbr1_pm_pred(1,:),hbr1_pm_pred(2,:), '--','Color',cm(7,:), ...
```



```

173     'DisplayName','Hopf asymptotics')
174 plot(hbr2_pm_pred(1,:),hbr2_pm_pred(2,:), '--','Color',cm(7,:), ...
175     'HandleVisibility','off')
176 plot(tc_br_pm_pred(1,:),tc_br_pm_pred(2,:), ':','Color',cm(7,:), ...
177     'DisplayName','Transcritical asymptotics')
178 plot(bt.parameter(ind.epsilon),bt.parameter(ind.tau),'.k','MarkerSize',18, ...
179     'DisplayName','generic Bogdanov-Takens point');
180 legend
181 xlabel('\epsilon','Interpreter','LaTeX');
182 ylabel('\tau','Interpreter','LaTeX');

```

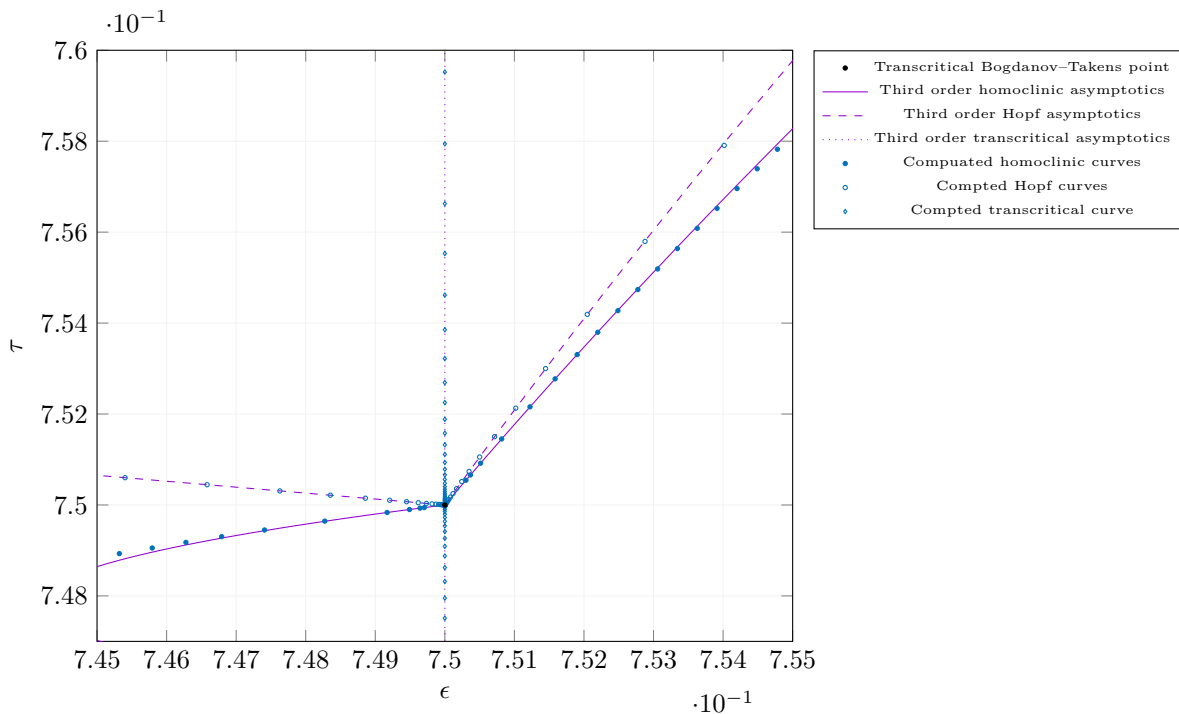


Figure S15: Bifurcation diagram near the derived transcritical Bogdanov-Takens point in (S9) comparing computed codimension one curves using DDE-BifTool with the third-order homoclinic parameter asymptotics obtained in Section 4.2.3.

S3.8 Compare homoclinic solutions in phase-space

To obtain an impression of the third-order homoclinic asymptotics in phase-space, we compare the corrected and uncorrected homoclinic solutions with the perturbation parameter ranging from 0.01 to 0.03. The code below produces (a figure similar to) Figure S16. We see that the corrected and predicted homoclinic orbits are nearly identical.

```

203 %% Compare homoclinic solutions in phase-space
204 step = linspace(0.01,0.03,10);

```

```

205 [~,hcli_br_approx,suc]=C1branch_from_C2point(funcs,bt,free_pars,...
206     'codim2','BT','codim1','hcli','step',step,'predictor',true,'debug',0, ...
207     'generic_unfolding', false);
208 [~,hcli_br_correc,suc]=C1branch_from_C2point(funcs,bt,free_pars,...
209     'codim2','BT','codim1','hcli','step',step,'debug',0, ...
210     'generic_unfolding', false);
211 figure(5); clf; hold on
212 title('Compare homoclinic orbits in phase-space')
213 for i=1:length(hcli_br_approx(1).point)
214     for j=1:2
215         point = hcli_br_approx(j).point(i);
216         profile = point.profile;
217         plot3(point.parameter(ind.epsilon)*ones(size(profile(1,:))), ...
218             profile(1,:),profile(2,:), 'Color',cm(2,:))
219         point_correc = hcli_br_correc(j).point(i);
220         profile_correc = point_correc.profile;
221         plot3(point_correc.parameter(ind.epsilon)*ones(size(profile(1,:))), ...
222             profile_correc(1,:),profile_correc(2,:), '.', 'Color',cm(1,:))
223     end
224 end
225 xlabel('\epsilon','Interpreter','LaTeX')
226 ylabel('x_1','Interpreter','LaTeX')
227 zlabel('x_2','Interpreter','LaTeX')
228 grid on
229 view(-46,7)
230 legend({'Predicted homoclinic order', 'Corrected homoclinic orbir'})

```

S3.9 Convergence plot

Using the function from [Section S1.12](#), we create a log-log convergence plot comparing the convergence order of the first and third order homoclinic asymptotics from [Section 4.2.3](#). The code below yields [Figure S17](#).

```

232 %% Convergence plot
233 amplitudes = logspace(-3.4, -1, 20);
234 orders = [1:3];
235 relativeErrors = convergence_plot(funcs, bt, orders, amplitudes, 'free_pars',
    ↪ free_pars,...
236     'orders',orders,'Tolerance',9e-6,'generic_unfolding',0,'debug',false);
237 figure(6); clf; hold on
238 title('Convergence plot comparing first and third order homoclinic asymptotics')
239 plot(log10(amplitudes), log10(relativeErrors{1}(:)), '*-')
240 plot(log10(amplitudes), log10(relativeErrors{3}(:)), '*-')
241 legend({'first order', 'thrid order'})
242 xlabel('amplitude')
243 ylabel('relative error')

```

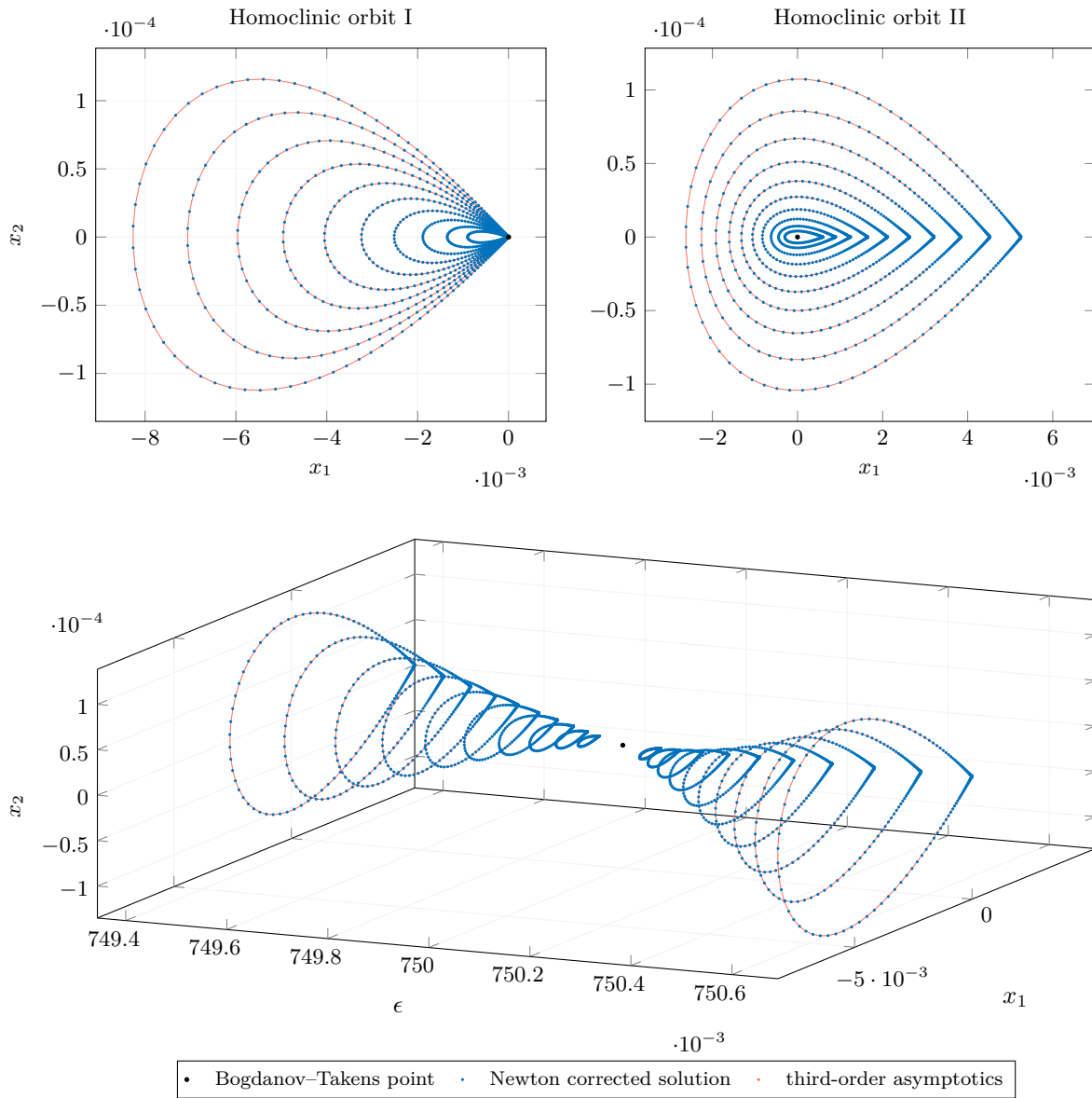


Figure S16: Plot comparing the third-order homoclinic asymptotics from Section 4.2.3 near the transcritical Bogdanov–Takens in (S9) with the Newton correct homoclinic solutions phase-space with the perturbation parameter ϵ ranging from 0.01 to 0.03.

S3.10 Simulation with DifferentialEquations.jl

Here we will perform four simulations. The first two simulations will be at two homoclinic orbits located on the two homoclinic curves emanating from the transcritical Bogdanov–Takens point continued with DDE-BifTool, see Figure S18. The second two simulations will be in the regions where there should be stable periodic orbits, see Figure S19.

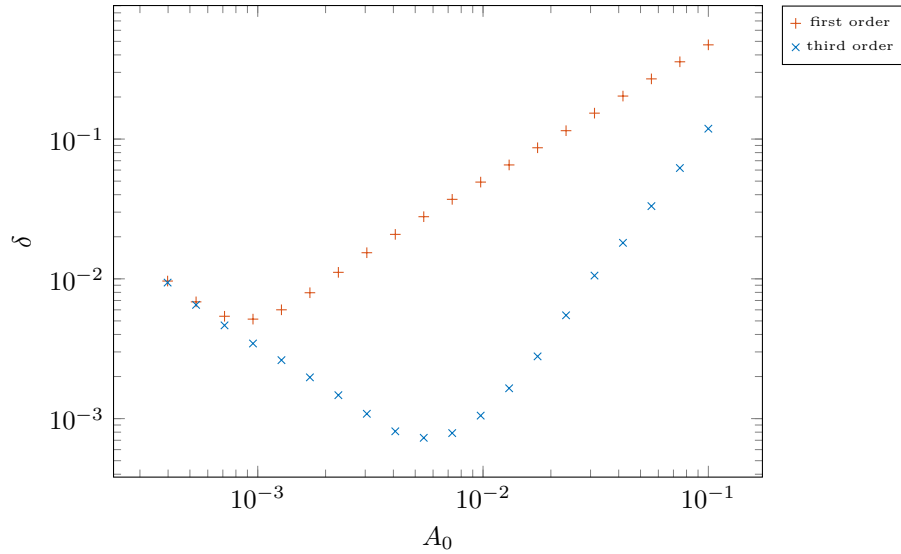


Figure S17: On the abscissa is the approximation to the amplitude A_0 and on the ordinate the relative error δ between the constructed solution `hcli_pred` to the defining system for the homoclinic orbit and the Newton corrected solution `hcli_corrected`.

S3.10.1 Loading necessary Julia packages

Since we do not have analytical expressions for the equilibria, we load the same Julia packages as in the previous demonstration, see [Listing S5](#).

S3.10.2 Define system

We define the system to be integrated and also an allocating version used for stability calculations.

```

8 # define constants
9 const tau = 1.0
10 const c1 = 0.25
11 const c2 = 0.5
12 const T = 1.0
13 @inline g(x) = (exp(x) - 1)/(c1*exp(x) + c2);
14
15 # define model
16 function vanderPolOscillator!(dx,x,h,p,t)
17     epsilon, tau = p
18     x1,x2 = x
19     x1t, x2t = h(p, t-T)
20     dx[1] = tau*x2
21     dx[2] = tau*(epsilon*g(x1t) - epsilon*(x1^2 - 1)*x2 - x1)
22 end
23
24 # allocating version (used for calculating stability)
25 function vanderPolOscillator(x, p)
26     dx = similar(x[:,1])

```

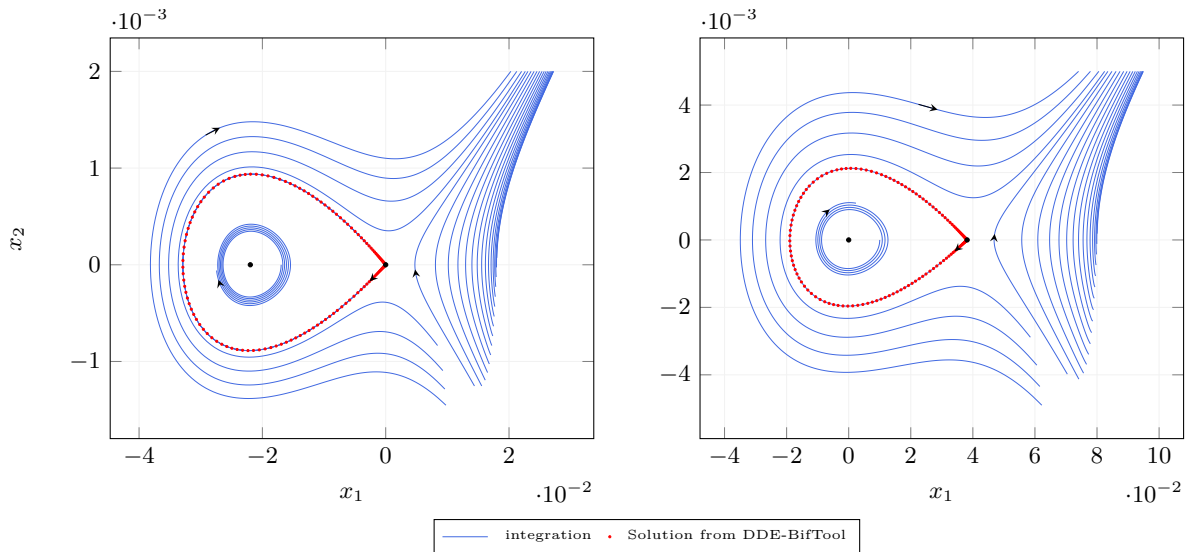


Figure S18: Comparing the computed homoclinic orbits in (S9) with DDE-BifTool with the solutions obtained from numerical simulation with Julia. We see the numerical integrated solution going through all the red points from the solution from DDE-BifTool.

```

27 h(p,t) = x[:,2]
28 vanderPolOscillator!(dx,x[:,1],h,p,0)
29 dx
30 end

```

S3.10.3 Functions for plotting arrows

We define a function to show in which direction the orbits flow, which is useful when plotting in phase space. We also define functions to show the direction of the leading eigenvectors of the characteristic matrix. The code is shown in Listing S4.

S3.10.4 Function for creating streamlines plot

To obtain an impression of the flow near transcritical Bogdanov–Takens point, we create a streamlines function. This is particularly useful for seeing the flow around the stable manifold of the saddle-node.

```

65 # function for creating streamlines plot
66 function streamlines(Tend, abscissa, ordinate, p, alg)
67     tspan = (0.0, Tend);
68     sols = []
69     for x ∈ abscissa
70         for y ∈ ordinate
71             h(p,t) = [x;y]
72             sol = solve(prob(h,p,tspan),alg,reltol=1e-06, abstol=1e-06)
73             push!(sols,sol)
74         end
75     end

```

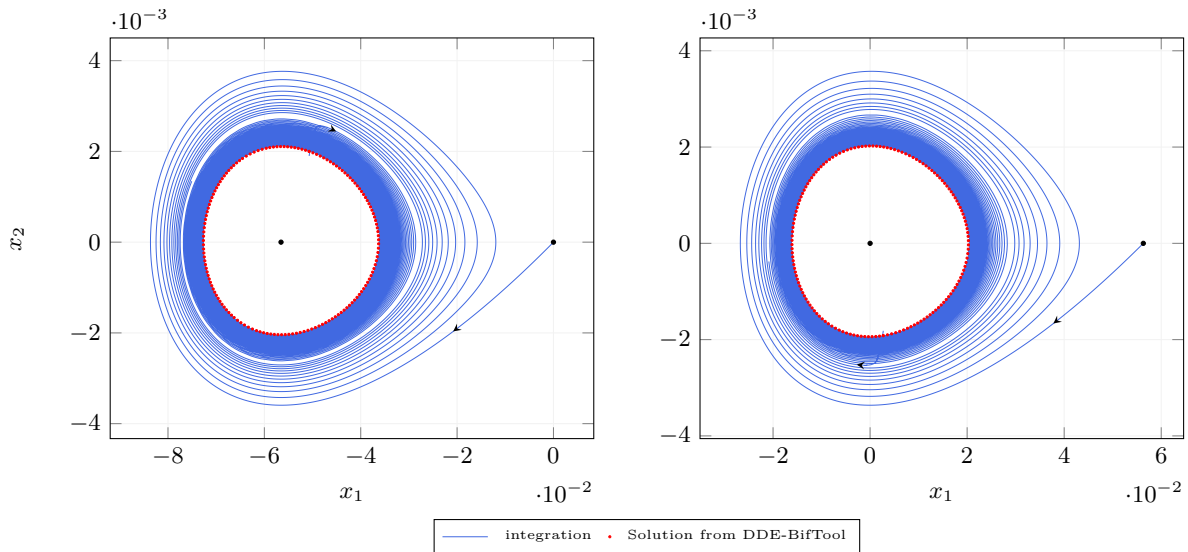


Figure S19: Comparing the computed periodic orbits in (S9) with DDE-BifTool with the solutions obtained from numerical simulation with Julia. We see the numerical integrated solution going through all the red points from the solution from DDE-BifTool.

```
76     sols
77 end
```

S3.10.5 Create figure with several axes

We create a figure containing multiple axis in which we will plot the two homoclinic and two periodic orbits.

```
79 # create figure
80 fig = Figure()
81 ax1 = Axis(fig[1,1], xlabel=L"x_1", ylabel=L"x_2", title="Homoclinic orbit I")
82 ax2 = Axis(fig[1,2], xlabel=L"x_1", ylabel=L"x_2", title="Homoclinic orbit II")
83 ax3 = Axis(fig[2,1], xlabel=L"x_1", ylabel=L"x_2", title="Periodic orbit I")
84 ax4 = Axis(fig[2,2], xlabel=L"x_1", ylabel=L"x_2", title="Periodic orbit II")
```

S3.10.6 Define parameters, equilibria

We define parameters located on the continued homoclinic branch with DDE-BifTool. Then calculate the equilibria points in (S9) near the transcritical Bogdanov–Takens point.

```
86 ## Simulation homoclinic orbit I
87  $\epsilon_0, \tau_0 = 0.752774810893411, 0.754736729675371$ 
88  $\mathbf{p} = [\epsilon_0; \tau_0]$ 
89
90 # derive equilibria numerically
91  $\mathbf{y}(\epsilon, \mathbf{x}_1) = \epsilon * \mathbf{g}(\mathbf{x}_1) - \mathbf{x}_1$ 
```

```

92 rts = roots(x1 -> y(epsilon_0, x1), interval(-1,1), Newton, 1e-16)
93 x1 = sort(mid.(interval.(rts)))

```

S3.10.7 Plot equilibria and homoclinic orbit

By plotting the homoclinic orbit obtained with DDE-BifTool located at parameter values

$$(\epsilon_0, \tau_0) = (0.752774810893411, 0.754736729675371),$$

we can compare with the numerical simulations.

```

95 # plot equilibria
96 scatter!(ax1, Point2f.([point[i].coords for i in 1:length(x1)]), color=:black)
97
98 # plot homoclinic orbit from DDE-BifTool
99 csvdir = "/home/maikel/Documents/MyPapers/BTPaper/data/vanderPolOscillator/"
100 homoclinicorbitI = readdlm(csvdir * "homoclinicorbitI.csv")
101 scatter!(ax1, homoclinicorbitI, color=:orangered)

```

S3.10.8 Leading eigenvectors

Next, we calculate and plot the leading eigenvectors of the characteristic matrix at the saddle-node bifurcation point.

```

103 # calculate stability
104 ts = [0.0 T]
105 point = [(coords = [x1[i]; 0], pars = [epsilon_0, tau_0]) for i in 1:length(x1)]
106 M = [coefficient_matrices(vanderPolOscillator, point[i], ts)
107      for i in 1:length(x1)]
108 dep = [DEP([M[i][j](point[i].coords, point[i].pars)
109            for j in 1:length(ts)], vec(ts)) for i in 1:length(x1)]
110 lambda = iar_chebyshev.(dep, maxit=100, neigs=2)
111 saddle_indx = findall(lambda -> abs(lambda[1]) < 1e-14, imag([lambda[i][1] for i in 1:length(x1)]))
112 saddle = point[saddle_indx]
113 V = real.(lambda[saddle_indx][2])
114 indx_unstable = findall(lambda -> real(lambda) > 0, lambda[saddle_indx][1])
115 indx_stable = findall(lambda -> real(lambda) < 0, lambda[saddle_indx][1])
116 Vunstable = vec(V[:, indx_unstable])
117 Vstable = vec(V[:, indx_stable])

```

S3.10.9 Define callback

Since we are only interested in the flow near the equilibria points, we create a discrete callback to ensure the orbits do not become too large.

```

122 # create continuous callback
123 condition(u, t, integrator) = u[2] - 0.002
124 affect!(integrator) = terminate!(integrator)
125 cb = ContinuousCallback(condition, affect!)

```

S3.10.10 Integrate the system at homoclinic orbits I

Now we define the problem to be integrated and choose the algorithm to be used. Then we integrate the system for a range of initial history functions using the function `streamlines`. Next, we integrate the system near the inner equilibrium, i.e., the equilibrium inside the homoclinic orbit. This equilibria should be an unstable spiral. By using the unstable eigenvector of the characteristic matrix, we obtain a solution going through the homoclinic solution obtained with DDE-BifTool.

```
127 # define DDEProblem and choose integration algorithm
128 prob(h,p,tspan) = DDEProblem(vanderPolOscillator!, h(p,0),h,tspan,p;
129                               constant_lags=[T], callback=cb)
130 alg = MethodOfSteps(Tsit5())
131
132 # create stream lines plot
133 solsI = streamlines(1000.0, 0.018, range(-0.0015,0.0,20), p, alg);
134 for sol ∈ solsI
135     Tend = sol.t[end]
136     lines!(ax1,sol(range(Tend-95*Tend/100,Tend,100)),color=:royalblue1)
137     # lines!(ax1,sol,color=:royalblue1)
138 end
139
140 # integrate near inner equilibria
141 h(p,t) = point[1].coords + [0.005; 0]
142 tspan = (0.0, 650.0);
143 homI_sol1 = solve(prob(h,p,tspan),alg,reltol=1e-06,abstol=1e-09)
144 lines!(ax1,homI_sol1,color=:royalblue1)
145
146 # integrate from the unstable eigenvector
147 ε = sign(Vunstable[1])*1e-04
148 R(α) = [cos(α) -sin(α);sin(α) cos(α)]
149 α0 = -0.030
150 h(p,t) = saddle.coords - ε*R(α0)*Vunstable
151 homI_sol2 = solve(prob(h,p,tspan),alg,reltol=1e-09,abstol=1e-09)
152 lines!(ax1,homI_sol2,color=:royalblue1)
```

S3.10.11 Add arrows on solutions

Lastly, we add arrows to the obtained solutions using the function `draw_arrow_on_solution` defined above.

```
154 # add arrows
155 draw_arrow_on_solution(ax1, homI_sol1, 540, +)
156 draw_arrow_on_solution(ax1, homI_sol2, 70, +)
157 draw_arrow_on_solution(ax1, solsI[1], 50, +)
158 draw_arrow_on_solution(ax1, solsI[5], 30, +)
```

We should now obtain an interactive figure similar to the left figure in [Figure S18](#).

S3.10.12 Simulation near stable periodic orbit I

The code for numerical simulation near the second homoclinic orbit, see the right plot in [Figure S18](#), is almost identical to the code above for the first homoclinic orbit and is therefore not included here.

To show by integration the existence of an stable periodic orbit, we first located a periodic orbit in DDE-BifTool. This can be done by continuing a branch of periodic orbits emanating from a point on the continued Hopf curves. Then we load the profiles of the periodic orbits into Julia. We perform two simulations. For the first simulation, we integrate with a constant history function equal to a point inside the periodic orbit. The second starts from the unstable eigenvector of the characteristic matrix calculated above.

```
230 ## Simulation periodic orbit I
231  $\epsilon_0, \tau_0 = 0.757267474481081, 0.762991619845455$ 
232  $p = [\epsilon_0; \tau_0]$ 
233
234 # derive equilibria
235  $rts = roots(x_1 \rightarrow y(\epsilon_0, x_1), interval(-1,1), Newton, 1e-16)$ 
236  $x_1 = sort(mid.(interval.(rts)))$ 
237
238 # calculate stability
239  $\tau_s = [0.0 T]$ 
240  $point = [(coords = [x_1[i]; 0], pars = [\epsilon_0, \tau_0]) \text{ for } i \in 1:length(x_1)]$ 
241  $M = [coefficient\_matrices(vanderPolOscillator, point[i], \tau_s) \text{ for } i \in 1:length(x_1)]$ 
242  $dep = [DEP([M[i][j](point[i].coords, point[i].pars) \text{ for } j \in 1:length(\tau_s)], vec(\tau_s))$ 
243  $\hookrightarrow \text{ for } i \in 1:length(x_1)]$ 
244  $\lambda = iar\_chebyshev.(dep, maxit=100, neigs=2)$ 
245  $saddle\_indx = findall(\lambda \rightarrow abs(\lambda[1]) < 1e-14, imag([\lambda[i][1] \text{ for } i \in 1:length(x_1)]))$ 
246  $V = real.(\lambda[saddle\_indx][2])$ 
247  $indx\_unstable = findall(\lambda \rightarrow real(\lambda) > 0, \lambda[saddle\_indx][1])$ 
248  $indx\_stable = findall(\lambda \rightarrow real(\lambda) < 0, \lambda[saddle\_indx][1])$ 
249  $Vunstable = vec(V[:, indx\_unstable])$ 
250  $Vstable = vec(V[:, indx\_stable])$ 
251
252 # plot equilibria
253  $scatter!(ax3, Point2f.([point[i].coords \text{ for } i \in 1:length(x_1)]), color=:black)$ 
254
255 # plot homoclinic orbit from DDE-BifTool
256  $periodicorbitI = readdlm(csvdir * "periodicorbitI.csv")$ 
257  $scatter!(ax3, periodicorbitI[:, [2,3]], color=:orangered)$ 
258
259 # create continous callback
260  $condition(u, t, integrator) = true$ 
261  $affect!(integrator) = terminate!(integrator)$ 
262  $cb = ContinuousCallback(condition, affect!)$ 
263
264 # integrate from inside periodic orbit I
265  $h(p, t) = periodicorbitI[1, [2,3]] - [0.0; 0.0001]$ 
266  $tspan = (0.0, 15050.0);$ 
267  $periodicI\_sol1 = solve(prob(h, p, tspan), alg, reltol=1e-06, abstol=1e-06)$ 
268  $lines!(ax3, periodicI\_sol1(range(0.0, tspan[2], 60000)), color=:royalblue1)$ 
```

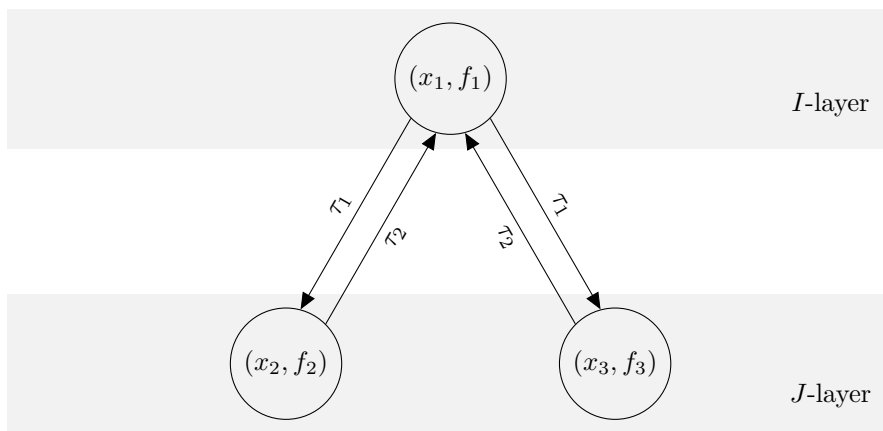


Figure S20: The graph of architecture for model (S10)

```

269
270 # integrate from unstable eigendirection of the saddle-node
271 tspan = (0.0, 1000.0);
272  $\epsilon$  = sign(Vunstable[1])*1e-04
273 h(p,t) = saddle.coords -  $\epsilon$ *Vunstable
274 periodicI_sol2 = solve(prob(h,p,tspan),alg,reltol=1e-09,abstol=1e-09)
275 lines!(ax3,periodicI_sol2,color=:royalblue1)
276
277 # add arrows
278 draw_arrow_on_solution(ax3, periodicI_sol1, 10, +)
279 draw_arrow_on_solution(ax3, periodicI_sol2, 100, +)

```

After running the above code, we should obtain a similar plot as in [Figure S19](#).

Remark 15. By the intersection of the orbits in the first simulation, we see that, although the system on the center manifold is equivalent to an ODE, the system we integrate is still a DDE.

S4 Transcritical Bogdanov–Takens bifurcation in a tri-neuron BAM neural network model

We consider a three-component system of a tri-neuron bidirectional associative memory (BAM) neural network model with multiple delays [15]. The architecture of this BAM model is illustrated in [Figure S20](#).

In this model, there is only one neuron with the activation function f_1 on the I -layer and there are two neurons with respective activation functions f_2 and f_3 on the J -layer. We assume that the time delay from the I -layer to the J -layer is τ_1 , while the time delay from the J -layer to the I -layer is τ_2 . Then the network can be described by the following delay differential equation:

$$\begin{cases} \dot{x}_1(t) = -\mu_1 x_1(t) + c_{21} f_1(x_2(t - \tau_2)) + c_{31} f_1(x_3(t - \tau_2)), \\ \dot{x}_2(t) = -\mu_2 x_2(t) + c_{12} f_2(x_1(t - \tau_1)), \\ \dot{x}_3(t) = -\mu_3 x_3(t) + c_{13} f_3(x_1(t - \tau_1)), \end{cases} \quad (\text{S10})$$

where:

- $x_i(t)$ ($i = 1, 2, 3$) denote the state of the neuron at time t ;
- μ_i ($i = 1, 2, 3$) describe the attenuation rate of internal neurons processing on the I -layer and the J -layer and $\mu_i > 0$;
- the real constants c_{i1} and c_{1i} ($2, 3$) denote the neurons in two layers: the I -layer and the J -layer.

Letting $u_1(t) = x_1(t - \tau_1)$, $u_2(t) = x_2(t)$, $u_3(t) = x_3(t)$ and $\tau = \tau_1 + \tau_2$, then system (S10) is equivalent to the following system:

$$\begin{cases} \dot{u}_1(t) = -\mu_1 u_1(t) + c_{21} f_1(u_2(t - \tau)) + c_{31} f_1(u_3(t - \tau)), \\ \dot{u}_2(t) = -\mu_2 u_2(t) + c_{12} f_2(u_1(t)), \\ \dot{u}_3(t) = -\mu_3 u_3(t) + c_{13} f_3(u_1(t)). \end{cases} \quad (\text{S11})$$

Lemma 16. *Assume that $f_i(0) = 0$ ($i = 1, 2, 3$), $f'_i(0) \neq 0$ ($i = 1, 2, 3$) and $\mu_2 \neq \mu_3$, then the steady-state $(u_1, u_2, u_3) = (0, 0, 0)$ has a double zero eigenvalue at*

$$\begin{aligned} c_{21} &= c_{21}^0 = \frac{\mu_2^2 (\mu_1 (\mu_3 \tau + 1) + \mu_3)}{c_{12} (\mu_2 - \mu_3) f'_1(0) f'_2(0)}, \\ c_{31} &= c_{31}^0 = \frac{\mu_3^2 (\mu_1 (\mu_2 \tau + 1) + \mu_2)}{c_{13} (\mu_3 - \mu_2) f'_1(0) f'_3(0)}. \end{aligned}$$

Proof. The characteristic matrix of (S11) is given by

$$\Delta(\lambda) = \begin{pmatrix} \lambda + \mu_1 & -e^{-\lambda\tau} c_{21} f'_1(0) & -e^{-\lambda\tau} c_{31} f'_1(0) \\ -c_{12} f'_2(0) & \lambda + \mu_2 & 0 \\ -c_{13} f'_3(0) & 0 & \lambda + \mu_3 \end{pmatrix}.$$

Thus, the characteristic equation becomes

$$\begin{aligned} \det \Delta(\lambda) &= \lambda^3 + (\mu_1 + \mu_2 + \mu_3) \lambda^2 + (-c_{12} c_{21} f'_1(0) f'_2(0) e^{-\lambda\tau} \\ &\quad - c_{13} c_{31} f'_1(0) f'_3(0) e^{-\lambda\tau} + \mu_1 \mu_2 + \mu_3 \mu_2 + \mu_1 \mu_3) \lambda \\ &\quad + \mu_1 \mu_2 \mu_3 - e^{-\lambda\tau} (c_{12} c_{21} \mu_3 f'_2(0) + c_{13} c_{31} \mu_2 f'_3(0)) f'_1(0) = 0. \end{aligned} \quad (\text{S12})$$

Clearly, $\lambda = 0$ is a root if and only if

$$\mu_1 \mu_2 \mu_3 = (c_{12} c_{21} \mu_3 f'_2(0) + c_{13} c_{31} \mu_2 f'_3(0)) f'_1(0).$$

Taking the derivative of (S12) with respect to λ gives

$$\begin{aligned} \frac{d}{d\lambda} \det \Delta(\lambda) &= 3\lambda^2 + 2(\mu_1 + \mu_2 + \mu_3) \lambda + (-c_{12} c_{21} f'_1(0) f'_2(0) e^{-\lambda\tau} \\ &\quad - c_{13} c_{31} f'_1(0) f'_3(0) e^{-\lambda\tau} + \mu_1 \mu_2 + \mu_3 \mu_2 + \mu_1 \mu_3) \\ &\quad + \tau (c_{12} c_{21} f'_2(0) e^{-\lambda\tau} + c_{13} c_{31} f'_3(0) e^{-\lambda\tau}) f'_1(0) \lambda \\ &\quad + \tau e^{-\lambda\tau} (c_{12} c_{21} \mu_3 f'_2(0) + c_{13} c_{31} \mu_2 f'_3(0)) f'_1(0) = 0. \end{aligned} \quad (\text{S13})$$

Therefore, we have

$$\det \Delta'(0) = (-c_{12} c_{21} f'_1(0) f'_2(0) - c_{13} c_{31} f'_1(0) f'_3(0) + \mu_1 \mu_2 + \mu_3 \mu_2 + \mu_1 \mu_3) = 0.$$

For any $\tau > 0$, it is easy to see that $\det \Delta(\lambda) = \det \Delta'(\lambda) = 0$, if and only if the following conditions are satisfied

$$\begin{cases} ((1 - \tau \mu_3) c_{12} c_{21} f'_2(0) + (1 - \tau \mu_2) c_{13} c_{31} f'_3(0)) f'_1(0) = \mu_1 \mu_2 + \mu_3 \mu_2 + \mu_1 \mu_3, \\ (c_{12} c_{21} \mu_3 f'_2(0) + c_{13} c_{31} \mu_2 f'_3(0)) f'_1(0) = \mu_1 \mu_2 \mu_3. \end{cases} \quad (\text{S14})$$

By solving (S14) for (c_{21}, c_{31}) we get $(c_{21}, c_{31}) = (c_{21}^0, c_{31}^0)$. Taking the derivative of (S13) yields

$$\begin{aligned} \frac{d^2}{d\lambda^2} \det \Delta(\lambda) &= 6\lambda + 2(\mu_1 + \mu_2 + \mu_3) + \tau f_1'(0)(c_{12}c_{21}f_2'(0)e^{-\lambda\tau} + c_{13}c_{31}f_3'(0)e^{-\lambda\tau}) \\ &\quad + \tau(c_{12}c_{21}f_2'(0)e^{-\lambda\tau} + c_{13}c_{31}f_3'(0)e^{-\lambda\tau})f_1'(0) \\ &\quad - \tau^2(c_{12}c_{21}f_2'(0)e^{-\lambda\tau} + c_{13}c_{31}f_3'(0)e^{-\lambda\tau})f_1'(0)\lambda \\ &\quad - \tau^2e^{-\lambda\tau}(c_{12}c_{21}\mu_3f_2'(0) + c_{13}c_{31}\mu_2f_3'(0))f_1'(0) = 0. \end{aligned} \quad (\text{S15})$$

Then we can obtain

$$\begin{aligned} \frac{d^2}{d\lambda^2} \det \Delta(0)|_{(c_{21}, c_{31})=(c_{21}^0, c_{31}^0)} &= 2(\mu_1 + \mu_2 + \mu_3) + 2\tau f_1'(0)(c_{12}c_{21}^0f_2'(0) + c_{13}c_{31}^0f_3'(0)) \\ &\quad - \tau^2 f_1'(0)(c_{12}c_{21}^0\mu_3f_2'(0) + c_{13}c_{31}^0\mu_2f_3'(0)) \\ &= 2(\mu_1 + \mu_2 + \mu_3) + \tau \left(\frac{\mu_2^2(\mu_1(\mu_3\tau + 1) + \mu_3)}{(\mu_2 - \mu_3)} + \frac{\mu_3^2(\mu_1(\mu_2\tau + 1) + \mu_2)}{(\mu_3 - \mu_2)} \right) \\ &\quad - \tau^2 \left(\frac{\mu_2^2(\mu_1(\mu_3\tau + 1) + \mu_3)}{(\mu_2 - \mu_3)}\mu_3 + \frac{\mu_3^2(\mu_1(\mu_2\tau + 1) + \mu_2)}{(\mu_3 - \mu_2)}\mu_2 \right) \\ &= 2(\mu_1 + \mu_2 + \mu_3) + 2\tau(\mu_1\mu_2 + \mu_1\mu_3 + \mu_2\mu_3) + \tau^2\mu_1\mu_2\mu_3. \end{aligned}$$

Since $\tau > 0$ and $\mu_i > 0 (i = 1, 2, 3)$ the second derivative of the characteristic equations at $(\lambda, c_{21}, c_{31}) = (0, c_{21}^0, c_{31}^0)$ does not vanish, and we obtain a double zero eigenvalue. \square

Lemma 17. Correction to [15, Lemma 3] Let $(c_{21}, c_{31}) = (c_{21}^0, c_{31}^0)$,

$$\omega_0 = \frac{\sqrt{-\mu_1^2 - \mu_2^2 - \mu_3^2} + \sqrt{\zeta_0}}{\sqrt{2}} \quad (\text{S16})$$

and $0 < \tau < \tau_0$, where τ_0 is the minimum positive solution to the nonlinear equation

$$\tan(\tau\omega_0) = \frac{b_0\zeta_1 - a_0\zeta_2}{a_0\zeta_1 + b_0\zeta_2}, \quad (\text{S17})$$

with

$$\begin{aligned} a_0 &= -\mu_1\mu_2\mu_3, \\ b_0 &= -\omega_0(\mu_2\mu_3 + \mu_1(\mu_2 + \mu_3 + \mu_2\mu_3\tau)), \\ \zeta_0 &= \mu_1^4 + (\mu_2^2 + \mu_3^2)^2 + 8\mu_1\mu_2\mu_3(\mu_2 + \mu_3 + \mu_2\mu_3\tau) + \\ &\quad 2\mu_1^2(\mu_3^2 + 4\mu_2\mu_3(1 + \mu_3\tau) + \mu_2^2(1 + 2\mu_3\tau(2 + \mu_3\tau))), \\ \zeta_1 &= \mu_1\mu_2\mu_3 - (\mu_1 + \mu_2 + \mu_3)\omega_0^2, \\ \zeta_2 &= \mu_2\mu_3\omega_0 + \mu_1(\mu_2 + \mu_3)\omega_0 - \omega_0^3. \end{aligned}$$

Then all roots of the characteristic equation (S12), except the double zero roots, have negative real parts.

Proof. Consider that there are eigenvalues $\lambda \neq 0$ on the imaginary axis for (c_{21}^0, c_{31}^0) . Substituting $\lambda = i\omega, (\omega > 0)$ and (c_{21}^0, c_{31}^0) into (S12), and rearranging terms according to its real and imaginary part yields

$$- \begin{pmatrix} \zeta_1 \\ \zeta_2 \end{pmatrix} = \begin{pmatrix} a_0 & b_0 \\ b_0 & -a_0 \end{pmatrix} \begin{pmatrix} \cos \tau\omega \\ \sin \tau\omega \end{pmatrix}. \quad (\text{S18})$$

By squaring and adding the above equations, it follows that

$$\zeta_1^2 + \zeta_2^2 = a_0^2 + b_0^2. \quad (\text{S19})$$

Solving the equation for positive $\omega > 0$ yields (S16).

Next, from (S18), we obtain (S17). First, notice that $\tau \mapsto \omega_0\tau$ is a strictly increasing function since it is the product of two strictly increasing positive functions. It follows that $\tau \mapsto \tan \omega_0\tau$ is periodic in τ with range \mathbb{R} . The next observation is that the denominator in the right-hand side of (S17) has a unique positive root $\tau = \tau_1$, at which that numerator does not vanish. In fact, it can be checked that the numerator does never vanish. Lastly, taking the limit of the right-hand side of (S17) of τ to infinity is 0, i.e.

$$\lim_{\tau \rightarrow \infty} \frac{-b_0\zeta_1 + a_0\zeta_2}{a_0\zeta_1 + b_0\zeta_2} = 0.$$

By the continuity of the right-hand side, it follows that (S17) has countable many solutions in τ . Let τ_0 be the minimum positive solution. Since for $\tau = 0$ all solutions to the characteristic equation, except of the double zero eigenvalue at the origin, have negative real parts. We conclude by [31, Corollary 2.3] that all eigenvalues, except for the double zero eigenvalues, are located in the left half plane for $0 < \tau < \tau_0$. \square

Remark 18. Note that, although $(\omega, \tau) = (\omega_0, \tau_0)$, solves (S17) and (S19), this not necessary means it solves the original equations (S18). Thus, the center manifold may still be stable for values $\tau > \tau_0$. We will demonstrate this in the example below.

For the numerical verification we consider, as in the simulations in [15, Example 1], the system (S11) with the activation functions

$$f_1(x) = \tanh(x) + 0.1x^2, \quad f_2(x) = f_3(x) = \tanh(x), \quad (\text{S20})$$

and parameter values

$$\mu_1 = 0.1, \mu_2 = 0.3, \mu_3 = 0.2, c_{12} = c_{13} = 1, \tau = 5. \quad (\text{S21})$$

Then, from Lemma 16, we obtain two critical values

$$(c_{21}^0, c_{31}^0) = (0.36, -0.22),$$

at which there is a transcritical Bogdanov–Takens point. Furthermore, since $\tau < \tau_0 \approx 5.4320$ the center manifold is locally attractive. In fact, we will show below that the center manifold is locally attractive for $0 < \tau < 13.2309348879375$.

Remark 19. The MATLAB files for this demonstration can be found in the directory `demos/tutorial/VII/BAM_neural_network_model` relative to the main directory of the package DDE-BifTool. Here, we omit the code to generate a system file. The system file `sym_BAMnn_mf.m` has been generated with the script `sym_BAMnn.m`. Also, we assume that the DDE-BifTool package has been loaded as in Listing S1. The code in Sections S4.1 to S4.17 highlights the important parts of the file `BAMnn.m`.

S4.1 Set parameter names and funcs structure

As in the previous example, we set the parameter names and define the `funcs` structure.

```

27 %% Set parameter names
28 parnames={'alpha1', 'alpha2', 'tau'};
29 cind=[parnames; num2cell(1:length(parnames))];
30 ind=struct(cind{:});

```

```

31
32 %% Set the funcs structure
33 funcs=set_symfuncs(@sym_BAMnn_mf, 'sys_tau', @()ind.tau);

```

S4.2 Set parameter range

Since we are only interested here in the local unfolding, we restrict the allowed parameter range for the unfolding parameters. In practice, one may have physical restrictions which must be satisfied. Additionally, we also limit the maximum allowed step size during continuation. By doing so, we obtain more refined data to compare against our predictors.

```

35 %% Set bifurcation parameter range and step size bounds
36 brpars={'max_bound', [ind.alpha1 0.5],...
37         'min_bound', [ind.alpha1 -0.35],...
38         'max_step', [ind.alpha1 0.01; ind.alpha2 0.01]};

```

S4.3 Stability and coefficients of the transcritical Bogdanov–Takens point

We manually construct a steady-state at the transcritical Bogdanov–Takens point and calculate its stability.

```

40 %% Define analytically derived Bogdanov-Takens point
41 % construct steady-state point
42 stst=dde_stst_create('x', zeros(3,1));
43 stst.parameter(ind.alpha1) = 0;
44 stst.parameter(ind.alpha2) = 0;
45 stst.parameter(ind.tau) = 5;
46 % Calculate stability
47 method=df_mthod(funcs, 'stst');
48 stst.stability=p_stabil(funcs, stst, method.stability);
49 stst.stability.l1

```

The MATLAB console shows the following output.

```

ans =

-0.0000 + 0.0000i
-0.0000 - 0.0000i
-0.2246 + 0.6600i
-0.2246 - 0.6600i
-0.6371 + 1.8063i
-0.6371 - 1.8063i
-0.8483 + 3.0681i
-0.8483 - 3.0681i
-0.9849 + 4.3336i
-0.9849 - 4.3336i

```

The eigenvalues confirm that the point under consideration is indeed (an approximation to) a Bogdanov–Takens point. Furthermore, the remaining eigenvalues have negative real parts. Next, we calculate the normal form coefficients, the time-reparametrization, and the transformation to the center manifold with the function `nmfm_bt_orbital`, which implements the coefficients as derived in [Section 4.2](#). For this, we need to set the argument `free_pars` to the unfolding parameter (α_1, α_2) . These coefficients will be used to start the continuation of the codimension one branches emanating from the Bogdanov–Takens point. Also, since we are in the transcritical case, we set the argument `generic_unfolding` to `false`.

```

51 %% Calculate parameter-dependent normal form coefficients
52 free_pars=[ind.alpha1, ind.alpha2];
53 bt = p_tobt(funcs,stst);
54 bt = nmfm_bt_orbital(funcs, bt,'free_pars', free_pars, 'generic_unfolding', false);
55 bt.nmfm

```

The MATLAB console shows the following output.

```

ans =

struct with fields:

    a: 0.0012
    b: -0.0135
theta1000: -2.5813
theta0010: 3.1322e+03
theta0001: -190.0753
    phi0: [1x1 struct]
    phi1: [1x1 struct]
    h2000: [1x1 struct]
    h1100: [1x1 struct]
    h0200: [1x1 struct]
    h3000: [1x1 struct]
    h2100: [1x1 struct]
    K10: [2x1 double]
    K01: [2x1 double]
    K02: [2x1 double]
    K11: [2x1 double]
    K20: [2x1 double]
    h1010: [1x1 struct]
    h1001: [1x1 struct]
    h0110: [1x1 struct]
    h0101: [1x1 struct]
    h2010: [1x1 struct]
    h1110: [1x1 struct]
    h2001: [1x1 struct]
    h1101: [1x1 struct]
    h1002: [1x1 struct]
    h0102: [1x1 struct]
    h1020: [1x1 struct]
    h0120: [1x1 struct]

```

```

h1011: [1x1 struct]
h0111: [1x1 struct]
K: @(beta1,beta2)K10*beta1+K01*beta2+1/2*K20*beta1^2
      +K11*beta1*beta2+1/2*K02*beta2^2
H: [function_handle]

```

Since the sign of ab is negative, we expect to find stable periodic orbits nearby the Bogdanov–Takens point.

S4.4 Comparing profiles of computed and predicted homoclinic orbits

To test the homoclinic asymptotics from [Section 4.1.9](#) we compare the first and third order asymptotics to the Newton corrected solution. For this, we use the function `C1branch_from_C2point`. This function returns a branch, which by default returns two initial corrected approximations in order to start continuation of the codimension one curve under consideration. By setting the argument `'predictor'` to `true` the approximations are left uncorrected. To make the comparison visually clear, we set the perturbation parameter $\epsilon = 0.02$ (`step = 0.02` in the code below). The code below produces [Figures S21](#) and [S22](#). The difference between the two approximations is clearly noticeable. While the first order asymptotics is close to the Newton corrected solution, the third order asymptotics is indistinguishable at this scale from the Newton corrected solution.

```

57 %% Plot comparing profiles computed and predicted homoclinic orbits
58 figure(1); clf; hold on;
59 cm=colormap('lines');
60 tiledlayout(2,6)
61 ylabel = {'u1','u2','u3'};
62 step = 0.02;
63 for order=[1,3]
64     [~,hcli_br_approx,suc]=C1branch_from_C2point(funcs,bt,free_pars, ...
65         'debug',0,'codim2','BT','codim1','hcli','step',step,'plot',0, ...
66         'generic_unfolding',false,'predictor',true,'order',order);
67     [~,hcli_br_correc,suc]=C1branch_from_C2point(funcs,bt,free_pars, ...
68         'order',order,'codim2','BT','codim1','hcli','step',step, ...
69         'plot',0,'generic_unfolding',false,'debug',0);
70     for i=1:2
71         for j=1:3
72             ax = nexttile; hold on; title(sprintf('order %d',order))
73             plot(ax,hcli_br_approx(i).point(1).mesh, ...
74                 hcli_br_approx(i).point(1).profile(j,:), '*')
75             plot(ax,hcli_br_correc(i).point(1).mesh, ...
76                 hcli_br_correc(i).point(1).profile(j,:))
77             xlabel('$t$', 'Interpreter', 'LaTeX');
78             ylabel(string(ylabel(j)), 'Interpreter', 'LaTeX')
79         end
80     end
81 end

```

Homoclinic orbit I

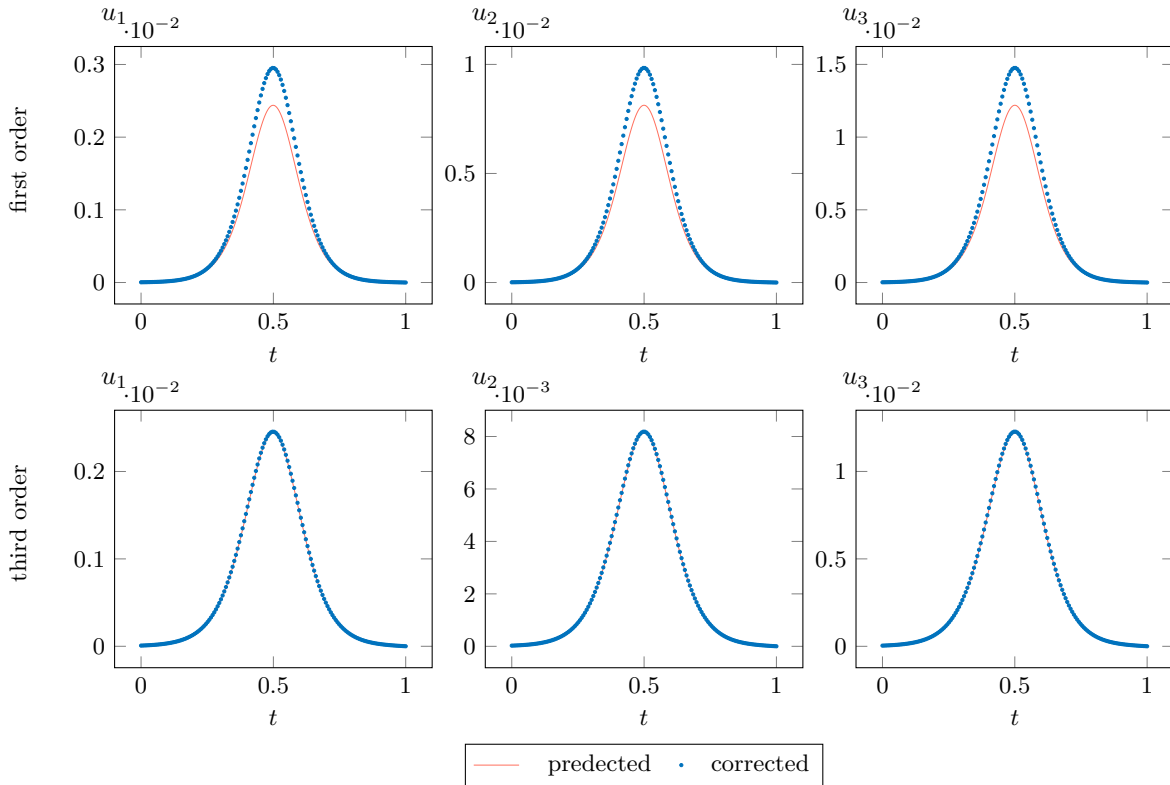


Figure S21: Comparison between the first and third-order homoclinic asymptotics from [Section 4.2.3](#) near the transcritical Bogdanov–Takens bifurcation in [\(S10\)](#) with the perturbation parameter set to $\epsilon = 0.02$.

S4.5 Continuation of the codimension one curves emanating

To continue the three codimension one curves emanating from the generic Bogdanov–Takens point, we can simply use the function `C1branch_from_C2point`, as shown in the code below. To monitor the continuation process, the argument `plot` must be set to 1. The most important setting is the perturbation parameter (or multiple), `step` in the code below. If left out, default step sizes are defined. However, depending on the problem, no convergence may then be obtained.

```

83 % Continue homoclinic curves emanating from Bogdanov-Takens point
84 [~,hcli_br,suc]=C1branch_from_C2point(funcs,bt,free_pars,...
85     'codim2','BT','codim1','hcli',brpars{:},'step',[0.003;0.012], ...
86     'plot',0,'generic_unfolding',false); assert(all(suc(:)>0))
87 hcli_br(1)=br_contn(funcs,hcli_br(1),80);
88 hcli_br(2)=br_contn(funcs,hcli_br(2),80);
89
90 % Continue Hopf curves emanating from Bogdanov-Takens point
91 [~,hbr,suc]=C1branch_from_C2point(funcs,bt,free_pars,...
92     'codim2','BT','codim1','hopf',brpars{:},'step',1e-04, ...
93     'plot',0,'generic_unfolding',false); assert(all(suc(:)>0))

```

Homoclinic orbit II

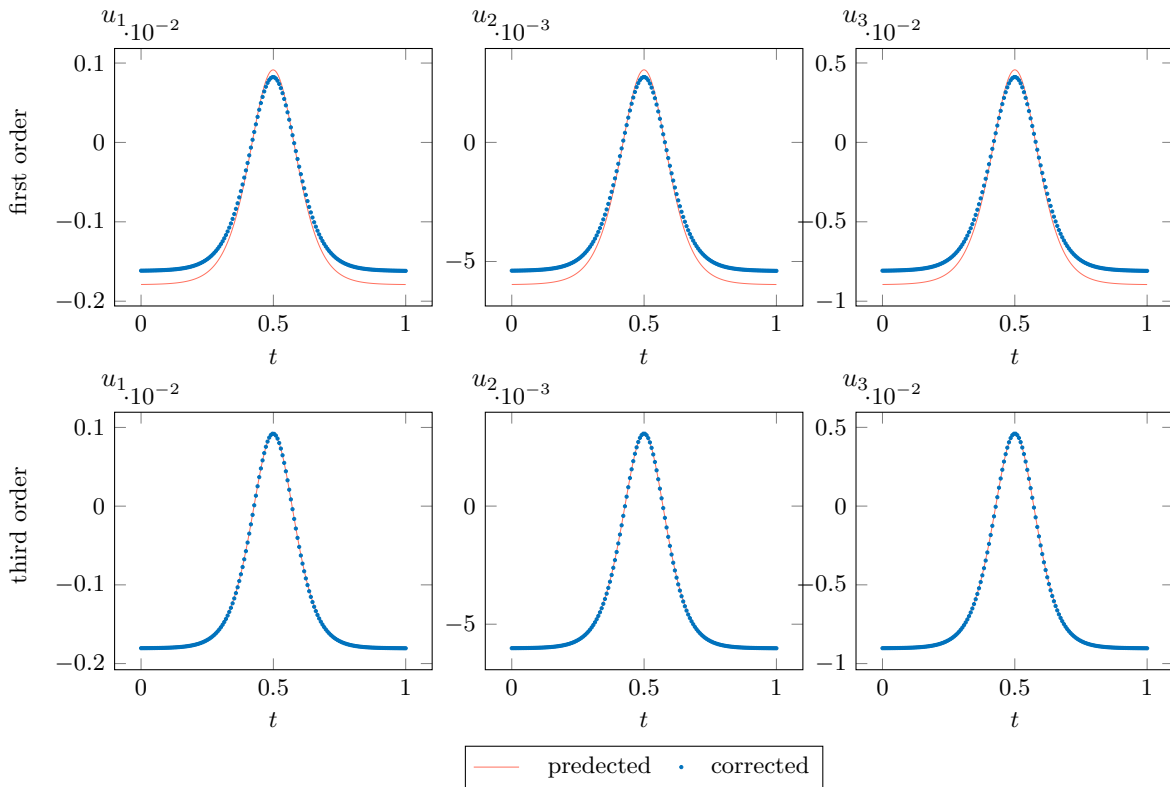


Figure S22: Comparison between the first and third-order homoclinic asymptotics from [Section 4.2.3](#) near the transcritical Bogdanov–Takens bifurcation in [\(S10\)](#) with the perturbation parameter set to $\epsilon = 0.02$.

```

94 nop=300; [hbr(1),suc]=br_contn(funcs,hbr(1),nop);assert(suc>0)
95 nop=80; [hbr(2),suc]=br_contn(funcs,hbr(2),nop);assert(suc>0)
96
97 % Continue transcritical curve emanating from Bogdanov-Takens point
98 [~,tc_br,suc]=C1branch_from_C2point(funcs,bt,free_pars,...
99     'codim2','BT','codim1','fold',brpars{:},'step',1e-03, ...
100    'plot',0,'generic_unfolding',false); assert(all(suc(:)>0))
101 nop=50; [tc_br,suc]=br_contn(funcs,tc_br(1),nop);assert(suc>0)
102 tc_br = br_rvers(tc_br);
103 nop=50; [tc_br,suc]=br_contn(funcs,tc_br(1),nop);assert(suc>0)

```

S4.6 Predictors of the codimension one curves emanating from the Bogdanov–Takens point

Before we provide the bifurcation diagram in the next section, we first obtain the predictors for the codimension one curves. For this, we again use the function `C1branch_from_C2point`. We set the argument `predictor` to 1 and provide a range of perturbation parameters.

```

127 %% Predictors for homoclinic, Hopf, and transcritical curves
128 step = [linspace(1e-4,0.02,20);linspace(1e-4,0.07,20)]
129 [~,hcli_br_pred,suc]=C1branch_from_C2point(funcs,bt,free_pars,'debug',0,...
130     'codim2','BT','codim1','hcli','step',step, ...
131     'generic_unfolding',false,'predictor',true);
132 step = [linspace(0.0001,0.014,20);linspace(0.0001,0.006,20)];
133 [~,hbr_pred,suc]=C1branch_from_C2point(funcs,bt,free_pars,...
134     'codim2','BT','codim1','hopf','step',step, ...
135     'generic_unfolding',false,'predictor',true);
136 step = linspace(-0.001,0.001,40);
137 [~,tc_br_pred,suc]=C1branch_from_C2point(funcs,bt,free_pars,...
138     'codim2','BT','codim1','fold','step',step, ...
139     'generic_unfolding',false,'predictor',true);
140 hcli_br1_pm_pred = [getpars(hcli_br_pred(1), ind.alpha1), ...
141     getpars(hcli_br_pred(1), ind.alpha2)];
142 hcli_br2_pm_pred = [getpars(hcli_br_pred(2), ind.alpha1), ...
143     getpars(hcli_br_pred(2), ind.alpha2)];
144 hbr1_pm_pred = [getpars(hbr_pred(1),ind.alpha1); getpars(hbr_pred(1),ind.alpha2)];
145 hbr2_pm_pred = [getpars(hbr_pred(2),ind.alpha1); getpars(hbr_pred(2),ind.alpha2)];
146 tc_br_pm_pred = [getpars(tc_br_pred,ind.alpha1); getpars(tc_br_pred,ind.alpha2)];

```

S4.7 Bifurcation diagram

The code below produces (a figure similar to) [Figure S23](#).

```

148 %% Plot the bifurcation curves with predictors
149 figure(3);clf;hold on
150 title(['Codimension 1 curves emanating from the transcritical ', ...
151     'Bogdanov-Takens point with predictors']);
152 plot(hcli_br1_pm(1,:),hcli_br1_pm(2,:),'.','Color',cm(1,:), ...
153     'DisplayName','Homoclinic branches')
154 plot(hcli_br2_pm(1,:),hcli_br2_pm(2,:),'.','Color',cm(1,:), ...
155     'HandleVisibility','off')
156 plot(hbr1_pm(1,:),hbr1_pm(2,:),'o','Color',cm(1:), 'DisplayName','Hopf branches')
157 plot(hbr2_pm(1,:),hbr2_pm(2,:),'o','Color',cm(1:), 'HandleVisibility','off')
158 plot(tc_br_pm(1,:),tc_br_pm(2,:),'d','Color',cm(1:), ...
159     'DisplayName','Transcritical branch')
160 plot(hcli_br1_pm_pred(:,1),hcli_br1_pm_pred(:,2),'Color', cm(7:), ...
161     'DisplayName','Third order homoclinic asymptotics')
162 plot(hcli_br2_pm_pred(:,1),hcli_br2_pm_pred(:,2),'Color', cm(7:), ...
163     'HandleVisibility','off')
164 plot(hbr1_pm_pred(1,:),hbr1_pm_pred(2,:), '--','Color',cm(7:), ...
165     'DisplayName','Hopf asymptotics')
166 plot(hbr2_pm_pred(1,:),hbr2_pm_pred(2,:), '--','Color',cm(7:), ...
167     'HandleVisibility','off')
168 plot(tc_br_pm_pred(1,:),tc_br_pm_pred(2,:), ':','Color',cm(7:), ...
169     'DisplayName','Transcritical asymptotics')
170 plot(bt.parameter(ind.alpha1),bt.parameter(ind.alpha2),'.k', ...
171     'MarkerSize', 18, 'DisplayName','generic Bogdanov-Takens point');

```

```

172 legend
173 xlabel('\alpha_1','Interpreter','LaTeX');
174 ylabel('\alpha_2','Interpreter','LaTeX');
175 axis(1.0e-03*[-0.3696 0.0714 -0.2838 0.2934])

```

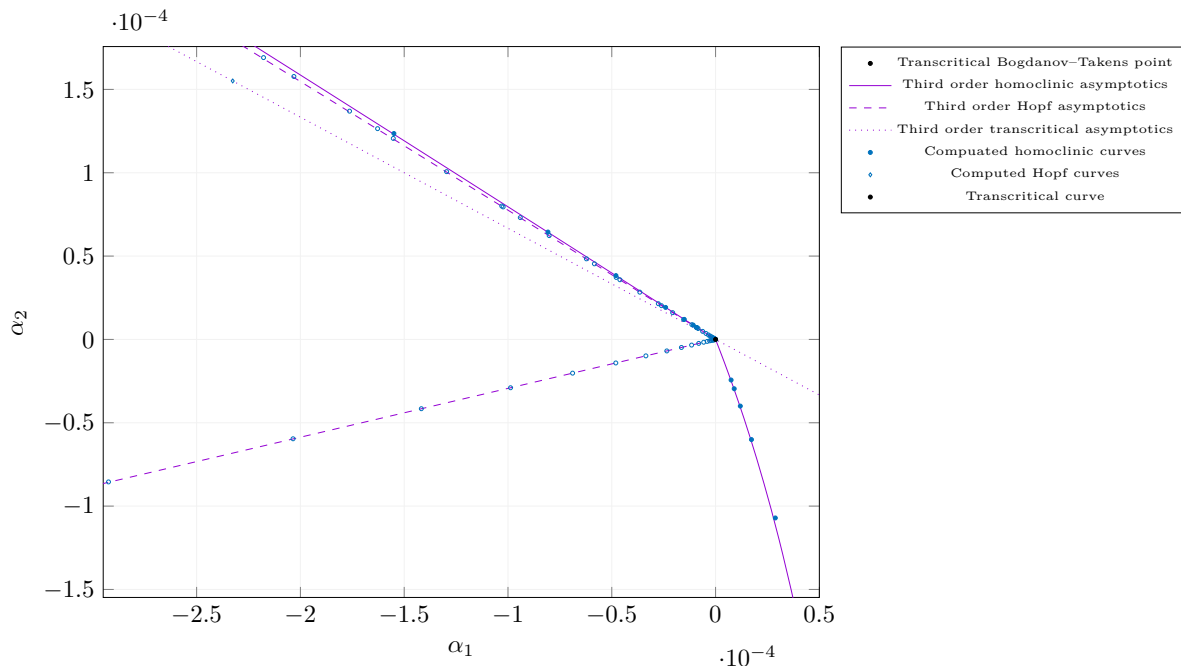


Figure S23: Bifurcation diagram near the analytically derived transcritical Bogdanov–Takens point in (S10) comparing the computed codimension one curves emanating from the Bogdanov–Takens point using DDE-BifTool with the third-order homoclinic parameter asymptotics obtained in Section 4.2.3.

S4.8 Detect bifurcations on the second Hopf branch

We can use the DDE-BifTool function `LocateSpecialPoints` to locate bifurcation points on the second Hopf branch.

```

177 %% Detect bifurcations on Hopf branch II
178 [hbr2_wbifs,hopftests,bifindx,~]=LocateSpecialPoints(funcs,hbr(2));

```

Inspecting the MATLAB output gives.

```

HopfCodimension2: calculate stability if not yet present
HopfCodimension2: calculate L1 coefficients
HopfCodimension2: (provisional) 2 gen. Hopf 2 Takens-Bogdanov detected.
br_insert: detected 1 of 4: genh. Normalform:
    L2: 5.7933e+03
    L1: 1.0106e-09

```

```
br_insert: detected 2 of 4: BT. Normalform:
```

```
  a2: -5.8499e-04
```

```
  b2: -0.0031
```

```
br_insert: detected 3 of 4: genh. Normalform:
```

```
  L2: -5.7933e+03
```

```
  L1: -2.1214e-09
```

```
br_insert: detected 4 of 4: BT. Normalform:
```

```
  a2: -0.0012
```

```
  b2: 0.0135
```

Thus, there are two Bogdanov–Takens points detected. By inspection of the normal form coefficients a and b (a2 and b2 in the output above) with the coefficients of the transcritical Bogdanov–Takens point, we see that one is (very likely) already known. Indeed, while continuing the second Hopf curve from the transcritical Bogdanov–Takens point, we encounter another Bogdanov–Takens point, at which the Hopf curve turns around, and continues in the reverse direction, back to the transcritical Bogdanov–Takens point. Similarly, we also deduce that there is only one generalized Hopf point detected on the Hopf curve. Inspecting the parameters indeed confirm our claim.

Since the newly detected Bogdanov–Takens point is on the Hopf curve on which the equilibrium changes position under variation of the parameters, we extract the Bogdanov–Takens point and computed the coefficients of the generic case.

```
179 bt2 = hbr2_wbifs.point(bifindx(2));
180 bt2 = p_tobt(funcs, bt2);
181 bt2 = nmfm_bt_orbital(funcs, bt2, 'free_pars', free_pars);
```

S4.9 Plot Bogdanov-Takens test function along the Hopf curve

Before we continue the homoclinic branch emanating from the generic Bogdanov–Takens point, we first plot the test function for the Bogdanov–Takens point, i.e. we plot the imaginary part for the critical eigenvalues along the second Hopf curve. The code below produces (a figure similar to) [Figure S24](#).

```
185 %% Plot Bogdanov-Takens test function along Hopf curve
186 figure(4);clf;hold on
187 title('Bogdanov--Takens testfunction along Hopf bifurcation curve')
188 plot3(getpars(hbr2_wbifs, ind.alpha1), getpars(hbr2_wbifs, ind.alpha2), hopftests.bt)
189 plot3(bt.parameter(ind.alpha1), bt.parameter(ind.alpha2), ...
190       hopftests.bt(bifindx(4)), '*k')
191 plot3(bt2.parameter(ind.alpha1), bt2.parameter(ind.alpha2), ...
192       hopftests.bt(bifindx(2)), '*k')
193 xlabel('\alpha_1$', 'Interpreter', 'LaTeX');
194 ylabel('\alpha_2$', 'Interpreter', 'LaTeX');
195 zlabel('\omega')
196 grid on
197 view(-47, 29)
```

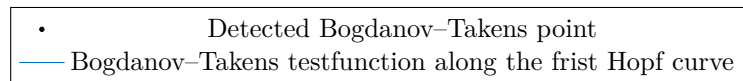
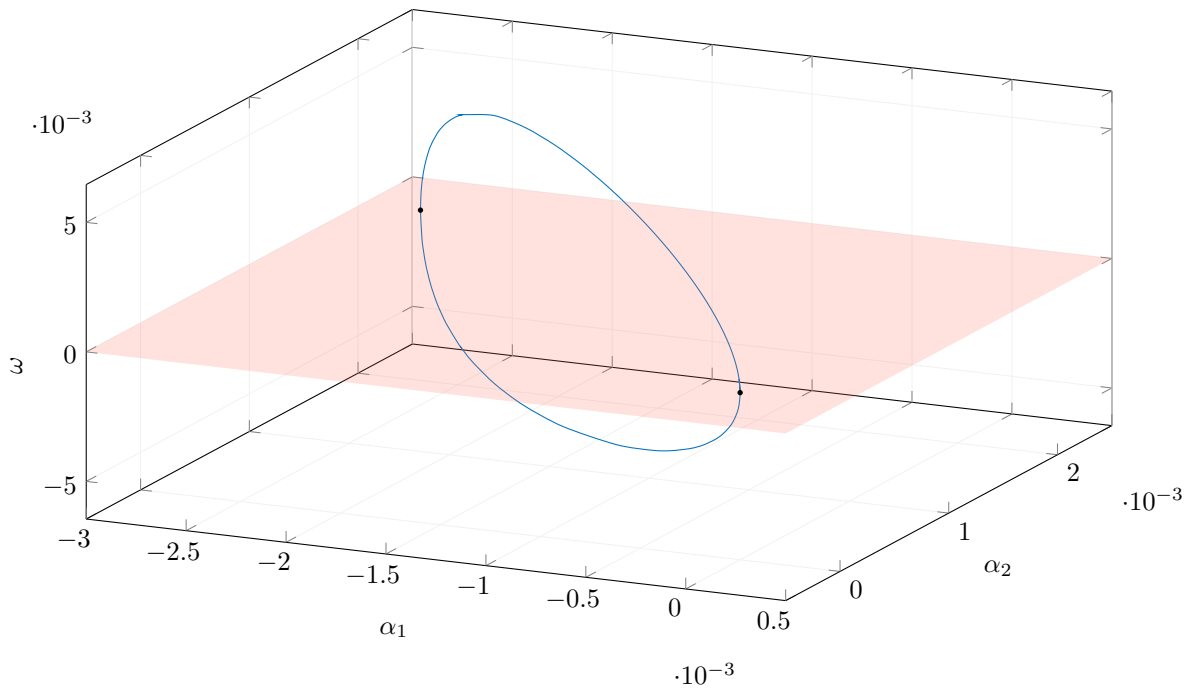


Figure S24: Plot of the Bogdanov–Takens test function along the second Hopf curve. We see that surface $\omega = 0$ is intersected transversally two times while continuing the Hopf curve.

S4.10 Continue third homoclinic curve

The code below continues the homoclinic solution emanating from the generic Bogdanov–Takens detected on the second Hopf branch. The last line extracts the parameters used for plotting.

```

199 % Continue homoclinic solutions emanating from the detected BT point
200 [~,hcli_br(3),suc]=C1branch_from_C2point(funcs,bt2,free_pars,...
201     'codim2','BT','codim1','hcli',brpars{:},'step',0.002,'plot',0);
202 assert(all(suc(:)>0))
203 hcli_br(3) = br_contn(funcs,hcli_br(3),300);
204 hcli_br3_pm = [getpars(hcli_br(3),ind.alpha1), getpars(hcli_br(3),ind.alpha2)]';
205

```

S4.11 Bifurcation plot

We are now in the position to recreate the bifurcation plot as shown in the main text. There, we left out the predictors for the codimension one equilibria bifurcation curves and changed the color of the computed codimension one equilibria curves to gray. In this way, focus will be on the homoclinic

curves. The code below produces (a figure similar to) [Figure S25](#).

```

213 %% Plot the bifurcation curves with predictors
214 figure(5);clf;hold on
215 title(['Codimension 1 curves emanating from the generic ', ...
216       'and transcritical Bogdanov-Takens point with predictors']);
217 plot(hcli_br1_pm(1,:),hcli_br1_pm(2:),'.','Color',cm(1,:), ...
218       'DisplayName','Homoclinic branches', 'MarkerSize', 20)
219 plot(hcli_br2_pm(1,:),hcli_br2_pm(2:),'.','Color',cm(1,:), ...
220       'HandleVisibility','off', 'MarkerSize', 20)
221 plot(hcli_br3_pm(1,:),hcli_br3_pm(2:),'.','Color',cm(1,:), ...
222       'HandleVisibility','off', 'MarkerSize', 20)
223 plot(hbr1_pm(1,:),hbr1_pm(2:),'Color','#ccc', ...
224       'DisplayName','Hopf branches')
225 plot(hbr2_pm(1,:),hbr2_pm(2:),'Color','#ccc','HandleVisibility','off')
226 plot(tc_br_pm(1,:),tc_br_pm(2:),'--','Color','#ccc', ...
227       'DisplayName','Transcritical branch')
228 plot(hcli_br1_pm_pred(:,1),hcli_br1_pm_pred(:,2),'Color', cm(7,:), ...
229       'DisplayName','Third order homoclinic asymptotics')
230 plot(hcli_br2_pm_pred(:,1),hcli_br2_pm_pred(:,2),'Color', cm(7,:), ...
231       'HandleVisibility','off')
232 plot(hcli_br3_pm_pred(:,1),hcli_br3_pm_pred(:,2),'Color', cm(7,:), ...
233       'HandleVisibility','off')
234 plot(bt.parameter(ind.alpha1),bt.parameter(ind.alpha2),'ok', ...
235       'DisplayName','Transcritical Bogdanov-Takens point', ...
236       'MarkerFaceColor',[0 0 0], 'MarkerSize', 09);
237 plot(bt2.parameter(ind.alpha1),bt2.parameter(ind.alpha2),'sk', ...
238       'DisplayName','generic Bogdanov-Takens point', 'MarkerFaceColor', ...
239       [0 0 0], 'MarkerSize', 10);
240 legend
241 xlabel('$\alpha_1$', 'Interpreter', 'LaTeX');
242 ylabel('$\alpha_2$', 'Interpreter', 'LaTeX');
243 axis([-0.0030, 0.0005, -0.0010, 0.0021])

```

S4.12 Large view bifurcation plot without predictors

Although the first and third homoclinic bifurcation curves exist only in a very small parameter region, the second is continued in a relatively large parameter range. The code below produces (a figure similar to) [Figure S26](#).

```

245 %% Plot larger bifurcation diagram without predictors
246 figure(6);clf;hold on
247 tiledlayout(1,2)
248 hold on;
249 title(['Codimension 1 curves emanating from the generic ', ...
250       'and transcritical Bogdanov-Takens point with predictors']);
251 plot(hcli_br1_pm(1,:),hcli_br1_pm(2:),'Color',cm(1,:), ...
252       'DisplayName','Homoclinic branches')
253 plot(hcli_br2_pm(1,:),hcli_br2_pm(2:),'Color',cm(1:),'HandleVisibility','off')

```

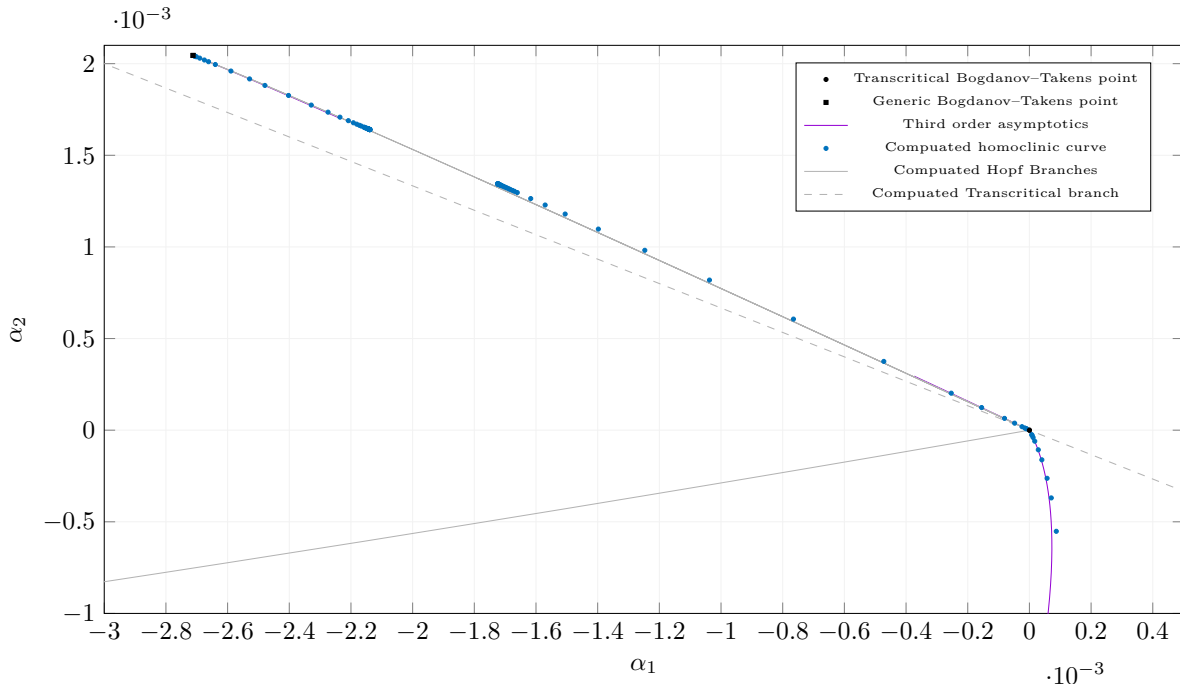


Figure S25: Bifurcation diagram near the transcritical and generic Bogdanov–Takens bifurcation points in (S11) comparing computed codimension one curves using DDE-BifTool with the asymptotics obtained in the main text.

```

254 plot(hcli_br3_pm(1,:),hcli_br3_pm(2,:), 'Color', cm(1,:), 'HandleVisibility', 'off')
255 plot(hbr1_pm(1,:),hbr1_pm(2,:), 'Color', cm(2,:), 'DisplayName', 'Hopf branches')
256 plot(hbr2_pm(1,:),hbr2_pm(2,:), 'Color', cm(2,:), 'HandleVisibility', 'off')
257 plot(tc_br_pm(1,:),tc_br_pm(2,:), 'Color', cm(3,:), ...
258       'DisplayName', 'Transcritical branch')
259 plot(bt.parameter(ind.alpha1),bt.parameter(ind.alpha2), 'ok', ...
260       'DisplayName', 'Transcritical Bogdanov-Takens point', ...
261       'MarkerFaceColor', [0 0 0], 'MarkerSize', 09);
262 plot(bt2.parameter(ind.alpha1),bt2.parameter(ind.alpha2), 'sk', ...
263       'DisplayName', 'generic Bogdanov-Takens point', ...
264       'MarkerFaceColor', [0 0 0], 'MarkerSize', 10);
265 legend
266 xlabel('\alpha_1$', 'Interpreter', 'LaTeX');
267 ylabel('\alpha_2$', 'Interpreter', 'LaTeX');

```

S4.13 Homoclinic orbits in phase-space

To obtain an expression of the continued homoclinic orbits, we plot the solutions on the various homoclinic branches in phase-space. The code below produces (a figure similar to) Figure S27. In the top left plot, the homoclinic orbits connected to the origin are shown. However, we see that this does not provide much insight. One way to visualize homoclinic solutions is by inspection the profiles of the solutions. This will be done in the next section. Another way to reveal the homoclinic solutions

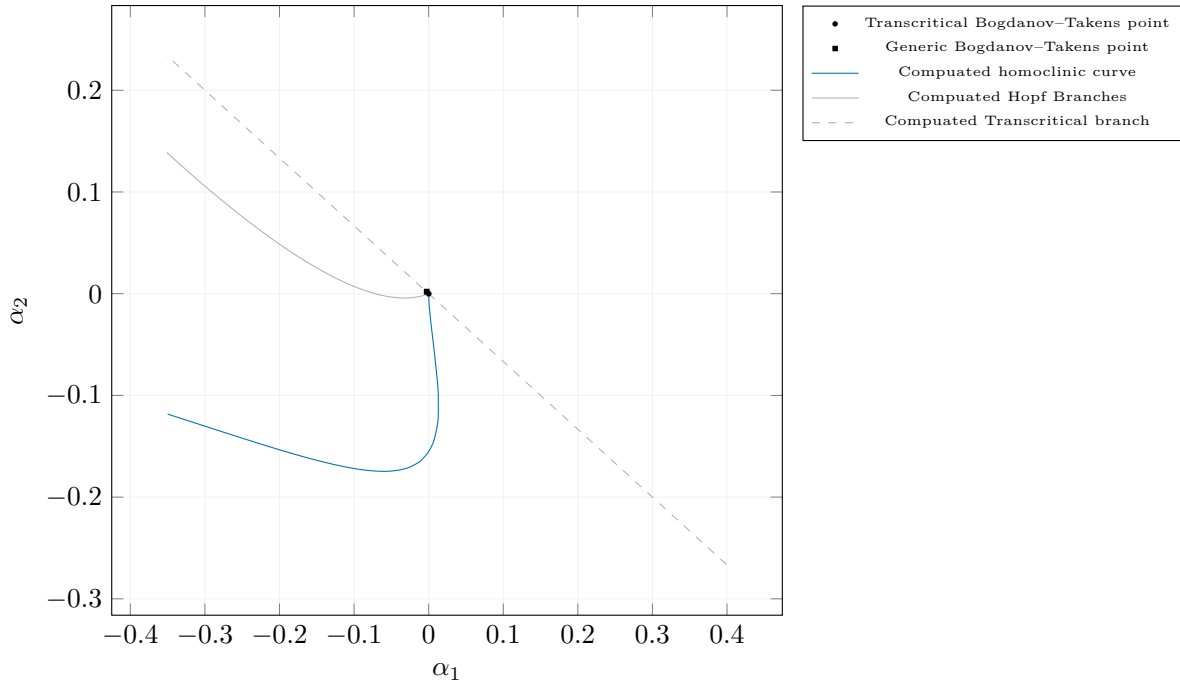


Figure S26: Bifurcation diagram near the transcritical and a generic Bogdanov–Takens bifurcation points in (S11) showing the fully continued homoclinic branch connected to the non-trivial equilibrium emanating from the transcritical Bogdanov–Takens point.

connected to the origin is by rotating the coordinates (u_1, u_2) . The result is seen in the top right plot in Figure S27. In the bottom left plot the solutions on the second homoclinic branch emanating from the transcritical Bogdanov–Takens point are shown. Lastly, we plotted the rotated homoclinic orbits emanating from the generic Bogdanov–Takens point in the bottom right plot of Figure S28.

```

269 %% Plot continued homoclinic orbits I
270 figure(7); clf
271 title('Continued homoclinic orbits in phase-space');
272 tiledlayout(1,5)
273 nexttile; hold on;
274 for i=1:length(hcli_br(1).point)
275     profile = hcli_br(1).point(i).profile;
276     plot3(profile(1,:),profile(2,:),profile(3,:), 'Color',cm(1,:))
277 end
278 grid on
279 view(-12,12)
280 xlabel('$u_1$', 'Interpreter', 'LaTeX')
281 ylabel('$u_2$', 'Interpreter', 'LaTeX')
282 zlabel('$u_3$', 'Interpreter', 'LaTeX')
283
284 %% Plot continued homoclinic orbits I (rotated)
285 nexttile; hold on;

```

```

286 R = @(alpha) [cos(alpha) -sin(alpha); sin(alpha) cos(alpha)]
287 for i=1:length(hcli_br(1).point)
288     profile = hcli_br(1).point(i).profile;
289     profileRotated = R(0.29)*profile([1,2],:);
290     plot3(profileRotated(1,:),profileRotated(2,:),profile(3,:), 'Color',cm(1,:))
291 end
292 grid on
293 view(-12,12)
294 xlabel('$u_1$', 'Interpreter', 'LaTeX')
295 ylabel('$u_2$', 'Interpreter', 'LaTeX')
296 zlabel('$u_3$', 'Interpreter', 'LaTeX')
297
298 %% Plot continued homoclinic orbits II
299 nexttile; hold on;
300 for i=1:length(hcli_br(2).point)
301     profile = hcli_br(2).point(i).profile;
302     plot3(profile(1,:),profile(2,:),profile(3,:), 'Color',cm(1,:))
303 end
304 profile = hcli_br(2).point(end).profile;
305 plot3(profile(1,:),profile(2,:),profile(3,:), 'Color',cm(2,:))
306 grid on
307 view(-12,12)
308 xlabel('$u_1$', 'Interpreter', 'LaTeX')
309 ylabel('$u_2$', 'Interpreter', 'LaTeX')
310 zlabel('$u_3$', 'Interpreter', 'LaTeX')
311
312 %% Plot continued homoclinic orbits III
313 nexttile; hold on;
314 for i=1:length(hcli_br(3).point)
315     profile = hcli_br(3).point(i).profile;
316     plot3(profile(1,:),profile(2,:),profile(3,:), 'Color',cm(1,:))
317 end
318 grid on
319 view(-12,12)
320 xlabel('$u_1$', 'Interpreter', 'LaTeX')
321 ylabel('$u_2$', 'Interpreter', 'LaTeX')
322 zlabel('$u_3$', 'Interpreter', 'LaTeX')
323
324 %% Plot continued homoclinic orbits III (rotated)
325 nexttile; hold on;
326 for i=1:length(hcli_br(3).point)
327     profile = hcli_br(3).point(i).profile;
328     profileRotated = R(0.29)*profile([1,2],:);
329     plot3(profileRotated(1,:),profileRotated(2,:),profile(3,:), 'Color',cm(1,:))
330 end
331 grid on
332 view(-12,12)
333 xlabel('$u_1$', 'Interpreter', 'LaTeX')
334 ylabel('$u_2$', 'Interpreter', 'LaTeX')
335 zlabel('$u_3$', 'Interpreter', 'LaTeX')

```

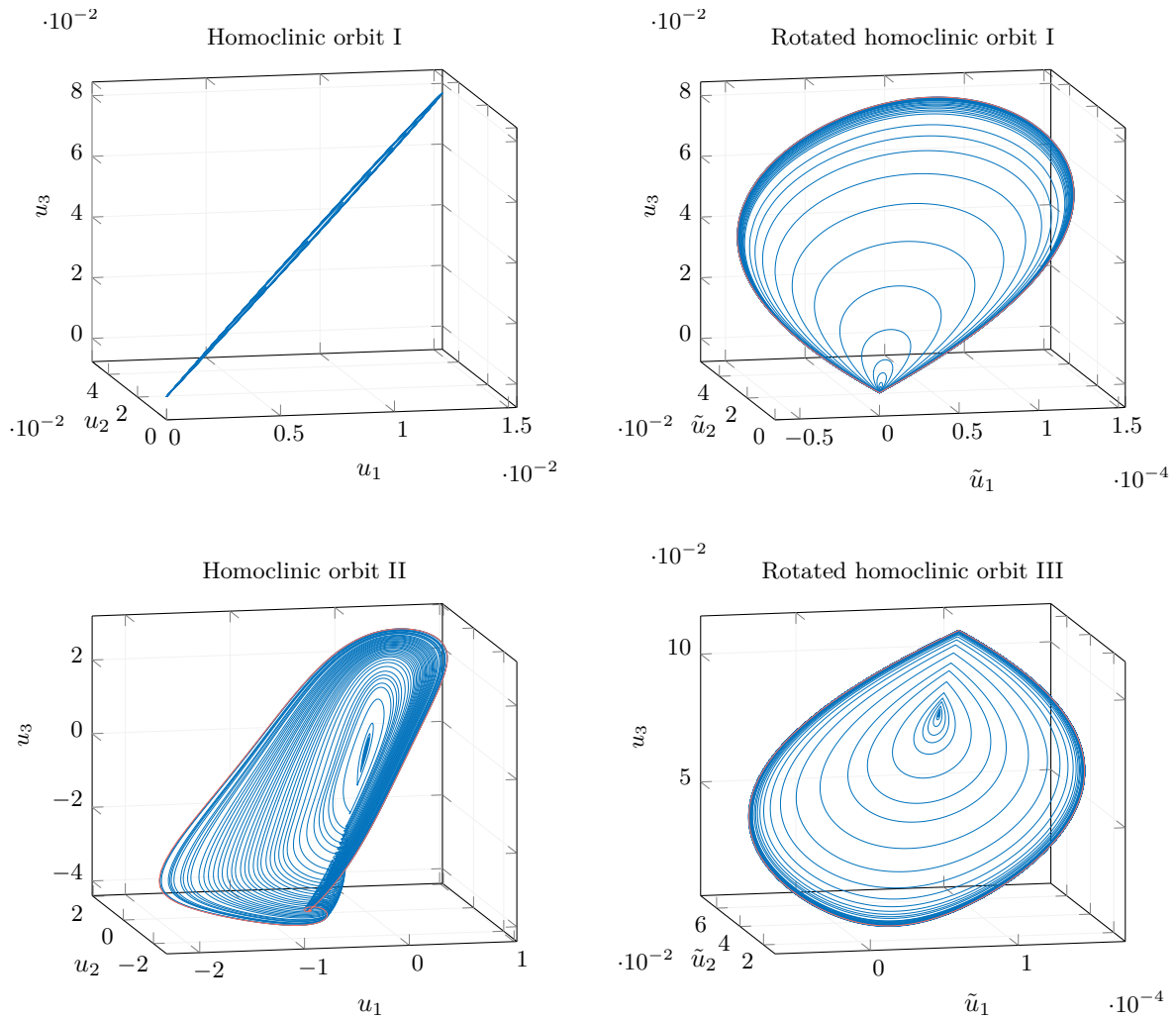


Figure S27: Plots of homoclinic solutions emanating from the generic and transcritical Bogdanov–Takens bifurcations in (S11). In the top left plot the homoclinic solutions emanating from the transcritical Bogdanov–Takens point with fixed saddle points are shown. In the top right plot, we rotated the (u_1, u_2) coordinates in order to make these homoclinic solutions visible. The bottom left plot shows the second branch of homoclinic solutions emanating from the transcritical Bogdanov–Takens point. Lastly, in the bottom right plot, the homoclinic solutions emanating from the generic Bogdanov–Takens point are shown. Here also the (u_1, u_2) coordinates are rotated.

S4.14 Compare homoclinic solutions in phase-space

Here, we compare the corrected and uncorrected profiles of the homoclinic solutions on the two homoclinic curves emanating from the transcritical Bogdanov–Takens point with the perturbation parameter ranging from 0.003 to 0.009. The code below produces (a figure similar to) Figure S28. We see that the corrected and predicted homoclinic orbits are nearly identical.

```

356 % Compare homoclinic solutions in phase-space
357 step = linspace(0.003,0.009,10);

```

```

358 [~,hcli_br_approx,suc]=C1branch_from_C2point(funcs,bt,free_pars,...
359     'codim2','BT','codim1','hcli','step',step,'predictor',true,'debug',0, ...
360     'generic_unfolding', false);
361 [~,hcli_br_correc,suc]=C1branch_from_C2point(funcs,bt,free_pars,...
362     'codim2','BT','codim1','hcli','step',step,'debug',0, ...
363     'generic_unfolding', false);
364 figure(9); clf; hold on
365 title('Compare homoclinic orbits in phase-space')
366 for i=1:length(hcli_br_approx(1).point)
367     for j=1:2
368         point = hcli_br_approx(j).point(i);
369         profile = point.profile;
370         mesh = point.mesh;
371         plot3(point.parameter(ind.alpha2)*ones(size(profile(1,:))), ...
372             mesh,profile(2,:), 'Color',cm(2,:))
373         point_correc = hcli_br_correc(j).point(i);
374         profile_correc = point_correc.profile;
375         mesh_correc = point_correc.mesh;
376         plot3(point_correc.parameter(ind.alpha2)*ones(size(profile(1,:))), ...
377             mesh,profile_correc(2,:), '.', 'Color',cm(1,:))
378     end
379 end
380 xlabel('\epsilon','Interpreter','LaTeX')
381 ylabel('\tilde t','Interpreter','LaTeX')
382 zlabel('u_1','Interpreter','LaTeX')
383 grid on
384 view(-46,7)
385 legend({'Predicted homoclinic order', 'Corrected homoclinic orbir'})

```

S4.15 Continue periodic solutions from Hopf branch to homoclinic branch

We continue a branch of periodic solutions emanating from point number 29 on the first Hopf branch emanating from the transcritical Bogdanov–Takens point. The periodic solution converges to a homoclinic orbit located on the second homoclinic branch emanating from transcritical Bogdanov–Takens point. We will use point number 28 on the periodic solution branch to compare against the simulation in Julia in [Section S4.18](#). The code below produces (a figure similar to) [Figure S29](#).

```

387 %% Continue periodic orbit from Hopf point on the first Hopf branch
388 psol_br1=SetupPsol(funcs,hbr(1),29,'contpar',ind.alpha1, ...
389     ⇨ 'degree',3,'intervals',50,brpars{1:4},'max_step',[0,inf],'plot',0,'radius',1e-03);
390 psol_br1=br_contn(funcs,psol_br1,40);
391 psol_br1_pm = [getpars(psol_br1,ind.alpha1); getpars(psol_br1,ind.alpha2)'];

```

```

398 %% Plot periodic branch
399 % we see that the periodoidic orbit converges to a homoclinic orbit
400 figure(10); clf; hold on;
401 title('Continued periodic orbits in phase-space');

```

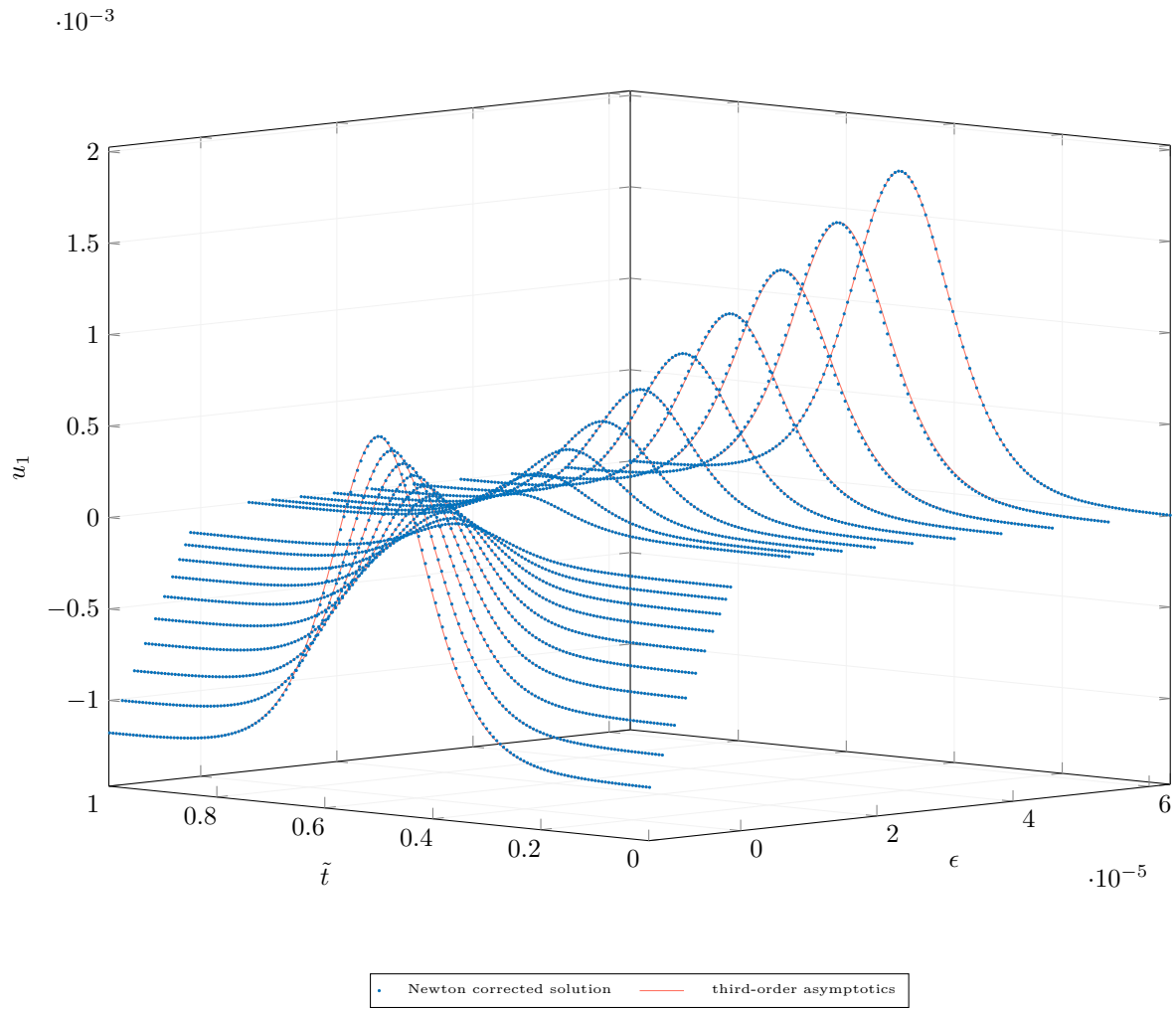


Figure S28: Plot comparing the third-order homoclinic asymptotics with the Newton correct homoclinic solutions in $(\epsilon, \tilde{t}, u_1)$ phase-space. Here \tilde{t} is the time t rescaled to the interval $[0, 1]$.

```

402 for i=1:length(psol_br1.point)
403     profile = psol_br1.point(i).profile;
404     profileRotated = R(0.29)*profile([1,2],:);
405     plot3(profileRotated(1,:),profileRotated(2,:),profile(3,:), 'Color',cm(1,:))
406 end
407 profile = psol_br1.point(end).profile;
408 profileRotated = R(0.29)*profile([1,2],:);
409 plot3(profileRotated(1,:),profileRotated(2,:),profile(3,:), '.', 'Color',cm(2,:))
410 grid on
411 view(-12,12)
412 xlabel('$u_1$', 'Interpreter', 'LaTeX')
413 ylabel('$u_2$', 'Interpreter', 'LaTeX')
414 zlabel('$u_3$', 'Interpreter', 'LaTeX')

```

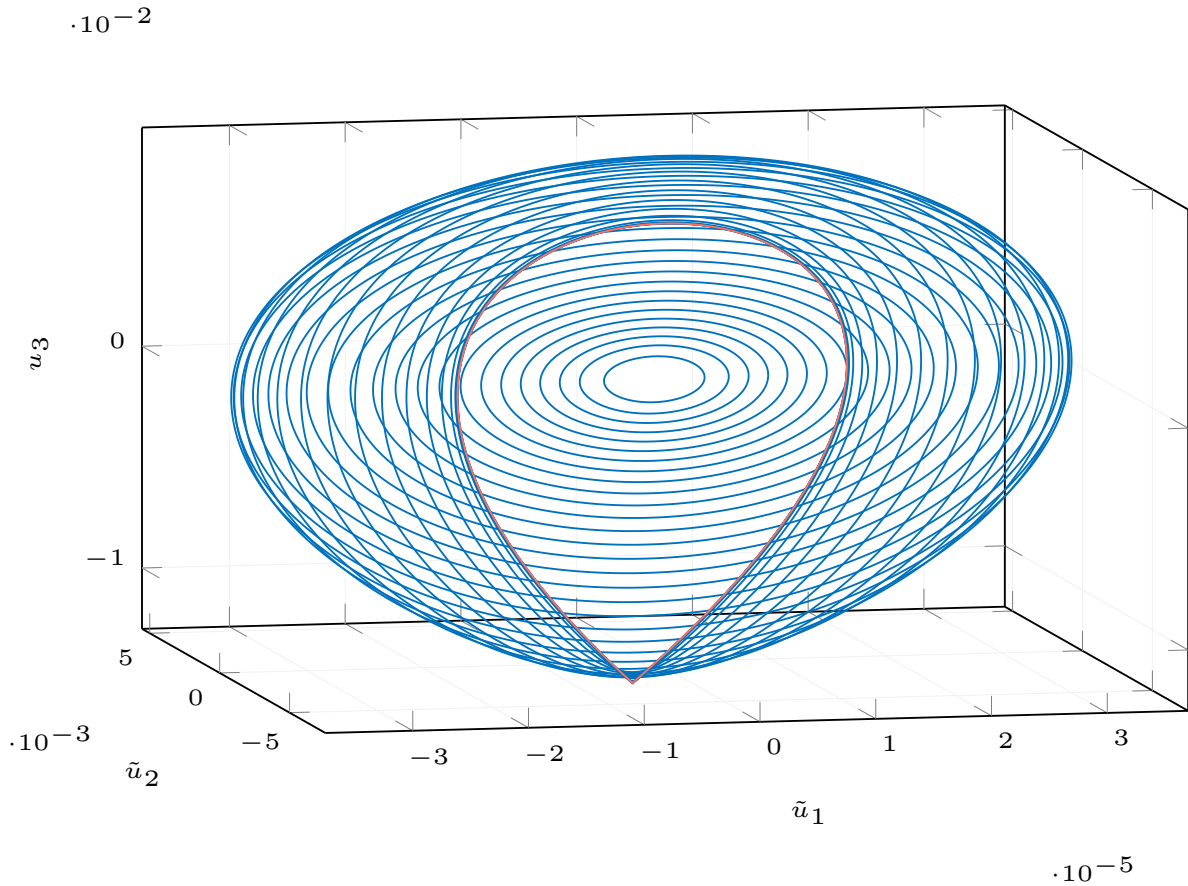


Figure S29: Branch of periodic solutions emanating from the last point on the first Hopf branch emanating from the transcritical Bogdanov–Takens point in (S11). The last point on the periodic solution branch is colored red, at which the periodic orbits have converged to a homoclinic orbit.

S4.16 Homoclinic branch connecting the two Bogdanov–Takens points

Here we will show that the transcritical and generic Bogdanov–Takens points are connected, not only by a Hopf curve, but also through a homoclinic curve. For this, we first continue the second Hopf branch emanating from the transcritical Bogdanov–Takens point again, but with a smaller step size.

```

416 %% Set bifurcation parameter range and step size bounds
417 brpars={'max_bound', [ind.alpha1 0.5],...
418         'min_bound', [ind.alpha1 -0.35],...
419         'max_step', [ind.alpha1 1e-5; ind.alpha2 1e-5]};
420
421 %% Continue Hopf curve emanating from Bogdanov-Takens point again
422 % but with smaller stepsize
423 [~,hbr_small_stepsize,suc]=C1branch_from_C2point(funcs,bt,free_pars,...
424         'codim2','BT','codim1','hopf',brpars{:},'step',1e-04, ...
425         'plot',0,'generic_unfolding',false); assert(all(suc(:)>0))
426 nop=285; [hbr_small_stepsize(2),suc]=br_contn(funcs,hbr_small_stepsize(2),nop);

```

```

427 assert(suc>0)
428 hbr_small_stepsize_pm = [getpars(hbr_small_stepsize(2),ind.alpha1);
429     getpars(hbr_small_stepsize(2),ind.alpha2)];

```

Next, we continue from (almost) each point on the new Hopf branch the emerging periodic solutions in the parameter α_2 .

```

436 %% Continue periodic orbits from every Hopf point on the second Hopf branch
437 % (takes a few minutes)
438 start_ind = 19;
439 end_ind = length(hbr_small_stepsize_pm)-5;
440 for i=start_ind:end_ind
441     psol_br(i-start_ind+1)=SetupPsol(funcs,hbr_small_stepsize(2),i,'contpar',...
442         ind.alpha2, ...
443         'degree',3,'intervals',50,brpars{1:4},'max_step',[0,inf],'plot',0, ...
444         'radius', 0.001);
445     psol_br(i-start_ind+1)=br_contn(funcs,psol_br(i-start_ind+1),50);
446 end

```

By plotting the last point on each of the periodic solutions branches in $(\alpha_1, \tilde{u}_1, \tilde{u}_2)$ -space, together with the homoclinic solutions on the first and third homoclinic branches continued above, it is indeed clear that the two homoclinic branches are connected through a single homoclinic curve, see [Figure S30](#). We also see how the transition is made from the homoclinic orbits with a fixed saddle point at the origin to the homoclinic orbits with a moving saddle. Clearly, DDE-BifTool has difficulties continuing the homoclinic orbits near the global homoclinic bifurcation point.

```

461 %% Plot homoclinic solutions in (\alpha_2, \tilde{u}_1, \tilde{u}_2) space
462 figure(12); clf; hold on
463 for i=1:end_ind-start_ind+1
464     profile = psol_br(i).point(end).profile;
465     profileRotated = R(0.29)*profile([1,2],:);
466     plot3(psol_br(i).point(end).parameter(ind.alpha1)*ones(size(profile(1,:))), ...
467         profileRotated(1,:),profileRotated(2,:), 'Color',cm(2,:))
468 end
469 for i=1:length(hcli_br(1).point)
470     profile = hcli_br(1).point(i).profile;
471     profileRotated = R(0.29)*profile([1,2],:);
472     plot3(hcli_br(1).point(i).parameter(ind.alpha1)*ones(size(profile(1,:))), ...
473         profileRotated(1,:),profileRotated(2,:), 'Color',cm(1,:))
474 end
475 for i=1:length(hcli_br(3).point)
476     profile = hcli_br(3).point(i).profile;
477     profileRotated = R(0.29)*profile([1,2],:);
478     plot3(hcli_br(3).point(i).parameter(ind.alpha1)*ones(size(profile(1,:))), ...
479         profileRotated(1,:),profileRotated(2,:), 'Color',cm(1,:))
480 end
481 grid on
482 view(-12,12)
483 xlabel('$\alpha_1$', 'Interpreter', 'LaTeX')

```

```

484 ylabel('\tilde{u}_1$', 'Interpreter', 'LaTeX')
485 zlabel('\tilde{u}_2$', 'Interpreter', 'LaTeX')
486 plot3(bt.parameter(ind.alpha1),bt.x(1),bt.x(2),'.k', ...
487       'MarkerSize', 18, 'DisplayName', 'transcritical Bogdanov-Takens point');
488 bt2rotated = R(0.29)*bt2.x([1,2])
489 plot3(bt2.parameter(ind.alpha1),bt2rotated(1),bt2rotated(2),'.k', ...
490       'MarkerSize', 18, 'DisplayName', 'Bogdanov-Takens point');

```

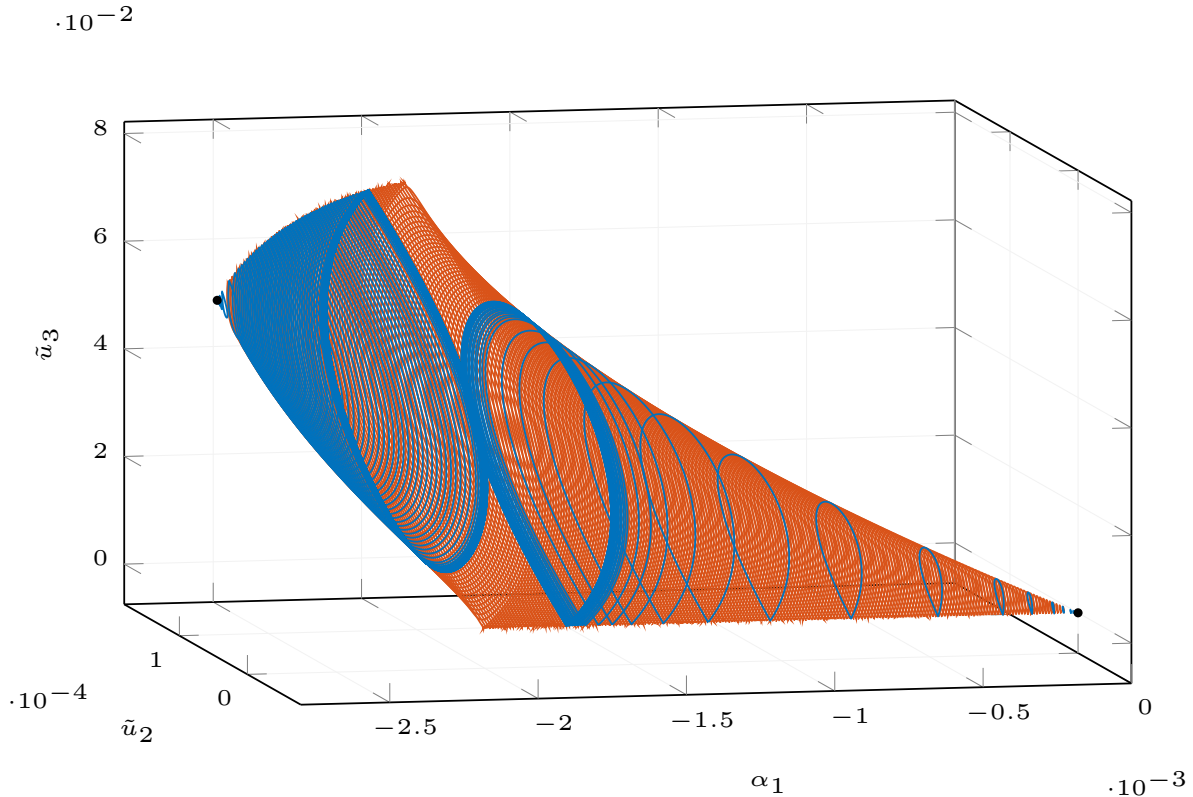


Figure S30: Branch of homoclinic solutions (orange) connecting the transcritical Bogdanov–Takens point (the right black dot) with the generic Bogdanov–Takens point (the left black dot) in (S11). The blue homoclinic curve emerging from the transcritical and generic Bogdanov–Takens points are the previously continued homoclinic branches.

To obtain an impression of the parameter curves connecting the transcritical and generic Bogdanov–Takens points, we rotated the curves through an angle of $\theta_2 = 0.646045233034992$. By doing so, the two Bogdanov–Takens points are aligned on the abscissa. In Figure S31, we plotted the first and third homoclinic branch, emanating from the transcritical Bogdanov–Takens and generic Bogdanov–Takens points respectively, the Hopf curve connecting the two Bogdanov–Takens points, and the newly obtained homoclinic bifurcation curve.

```

501 %% Plot rotated bifurcation homoclinic bifurcation curves
502 figure(13);clf;hold on

```



```

503 title(['Codimension 1 curves emanating from the generic ', ...
504        'and transcritical Bogdanov-Takens']);
505 theta2 = abs(atan(bt2.parameter(2)/bt2.parameter(1)))
506 hcli_br1_rotated_pm = R(theta2)*hcli_br1_pm;
507 hcli_br3_rotated_pm = R(theta2)*hcli_br3_pm;
508 hcli_bifurcation_br_rotated_pm = R(theta2)*hcli_bifurcation_br_pm';
509 hbr2_rotated_pm = R(theta2)*hbr2_pm(:,1:45);
510 bt_rotated_pm = R(theta2)*bt.parameter([ind.alpha1, ind.alpha2]);
511 bt2_rotated_pm = R(theta2)*bt2.parameter([ind.alpha1, ind.alpha2]);
512 plot(hcli_br1_rotated_pm(1,:),hcli_br1_rotated_pm(2,:), 'Color',cm(1,:), ...
513      'DisplayName','Homoclinic branches')
514 plot(hcli_br3_rotated_pm(1,:),hcli_br3_rotated_pm(2,:), 'Color',cm(1,:), ...
515      'HandleVisibility','off')
516 plot(hcli_bifurcation_br_rotated_pm(1,:),hcli_bifurcation_br_rotated_pm(2,:), ...
517      ':','Color',cm(4,:), ...
518      'DisplayName','Homoclinic bifurcation branch')
519 plot(hbr2_rotated_pm(1,:),hbr2_rotated_pm(2,:), 'Color',cm(2,:), ...
520      'DisplayName','Hopf branch')
521 plot(bt_rotated_pm(1),bt_rotated_pm(2),'ok', ...
522      'DisplayName','Transcritical Bogdanov-Takens point', ...
523      'MarkerFaceColor',[0 0 0], 'MarkerSize', 09);
524 plot(bt2_rotated_pm(1),bt2_rotated_pm(2),'dk', ...
525      'DisplayName','generic Bogdanov-Takens point', ...
526      'MarkerFaceColor',[0 0 0], 'MarkerSize', 10);
527 legend
528 xlabel('$\tilde{\alpha}_1$', 'Interpreter','LaTeX');
529 ylabel('$\tilde{\alpha}_2$', 'Interpreter','LaTeX');

```

S4.17 Convergence plot

Using the function from [Section S1.12](#), we create a log-log convergence plot comparing the convergence order of the first and third order homoclinic asymptotics from [Section 4.2.3](#). The code below yields [Figure S32](#).

```

531 %% Convergence plot
532 amplitudes = logspace(-3, -1.4, 20);
533 orders = [1:3];
534 relativeErrors = convergence_plot(funcs, bt, orders, amplitudes, 'free_pars',
535     ↪ free_pars,...
536     ↪ 'orders',orders,'TTolerance',1e-5,'ntst',82,'generic_unfolding',0,'debug',false);
537 figure(14); clf; hold on
538 plot(log10(amplitudes), log10(relativeErrors{1}(:)), '*-')
539 plot(log10(amplitudes), log10(relativeErrors{3}(:)), '*-')
540 legend({'first order', 'thrid order'})
541 xlabel('amplitude')
542 ylabel('relative error')

```

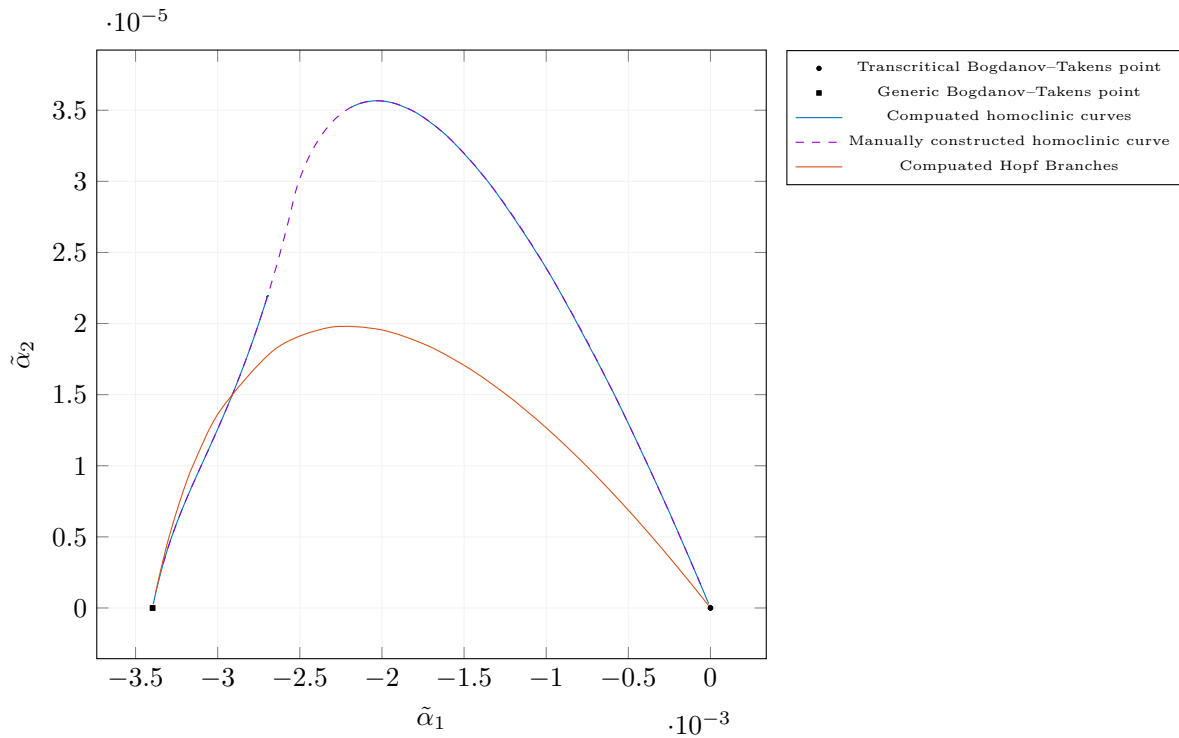


Figure S31: Bifurcation diagram near the transcritical and generic Bogdanov–Takens bifurcation points in (S11) showing the fully continued homoclinic branch connected to the non-trivial equilibrium emanating from the transcritical Bogdanov–Takens point.

S4.18 Simulation with DifferentialEquations.jl

Here we will perform four simulations. The first two simulations will be at two homoclinic orbits located on the two homoclinic curves emanating from the transcritical Bogdanov–Takens point continued with DDE-BifTool, see Figure S33. The second two simulations will be in the regions where there should be stable periodic orbits, see Figure S34.

S4.18.1 Loading necessary Julia packages

We start by loading the necessary Julia packages. Compared with the previous demonstrations, we also need to load the Julia package Symbolics.jl [21] to differentiate the activation functions f_1, f_2, f_3 .

```

1 using DifferentialEquations
2 using GLMakie
3 using DelimitedFiles
4 using DDEBifTool
5 using NonlinearEigenproblems
6 using Colors
7 using IntervalArithmetic, IntervalRootFinding
8 using LinearAlgebra
9 using Symbolics

```

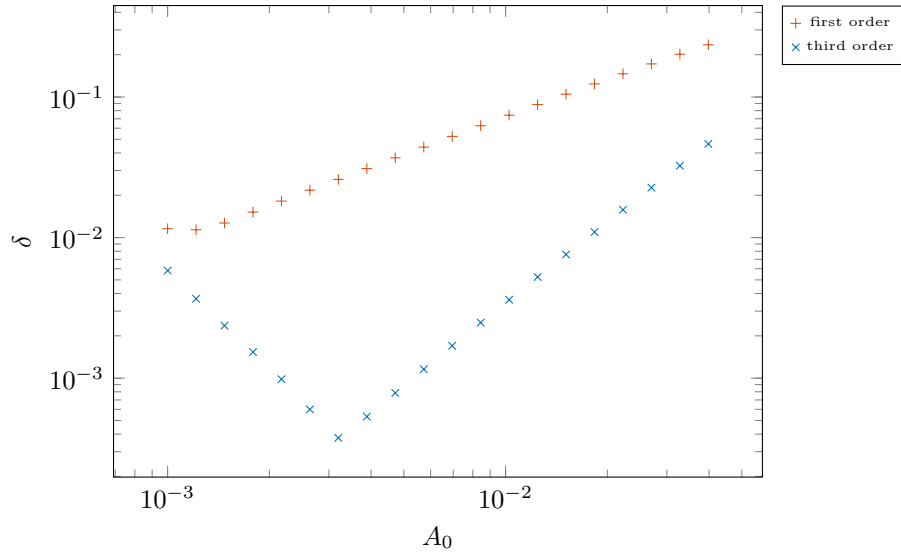


Figure S32: On the abscissa is the approximation to the amplitude A_0 and on the ordinate the relative error δ between the constructed solution `hcli_pred` to the defining system for the homoclinic orbit and the Newton corrected solution `hcli_corrected`.

S4.18.2 Define system

Next we define the system to be integrated, a system to approximate the reverse flow, and also an allocating version used for stability calculations. Note that we need the Julia `Symbolics.jl` to differentiate the activation functions.

```

11 # define constants
12 const  $\tau$  = 5.0
13 const  $\mu_1$  = 0.1
14 const  $\mu_2$  = 0.3
15 const  $\mu_3$  = 0.2
16 const  $c_{12}$  = 1.0
17 const  $c_{13}$  = 1.0
18
19 # define functions used in the model
20 @inline  $f_1(x)$  = tanh(x) + 0.1*x^2
21 @inline  $f_2(x)$  = tanh(x)
22  $f_3$  =  $f_2$ 
23
24 # define derivatives of functions used in the model
25 @variables x
26  $df_1$  = eval(build_function(Symbolics.derivative( $f_1(x)$ ), x),x)
27  $df_2$  = eval(build_function(Symbolics.derivative( $f_2(x)$ ), x),x)
28  $df_3$  =  $df_2$ 
29
30 const  $c_{21}^0$  =  $\mu_2^2 * (\mu_1 * (\mu_3 * \tau + 1.0) + \mu_3) / (c_{12} * (\mu_2 - \mu_3) * df_1(0) * df_2(0))$ 
31 const  $c_{31}^0$  =  $\mu_3^2 * (\mu_1 * (\mu_2 * \tau + 1.0) + \mu_2) / (c_{13} * (\mu_3 - \mu_2) * df_1(0) * df_3(0))$ 
32

```

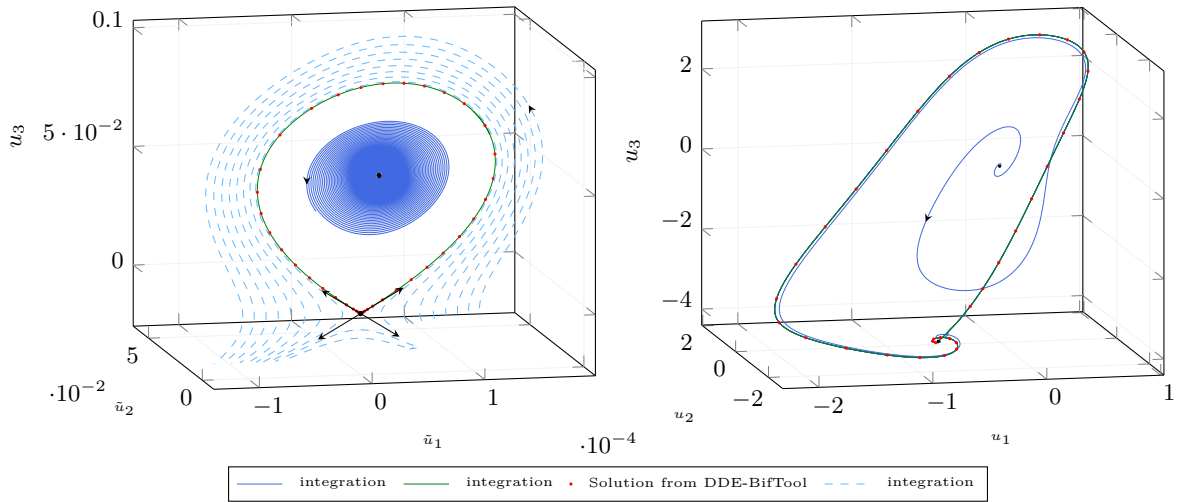


Figure S33: Comparing the computed homoclinic orbits in (S11) with DDE-BifTool with the solutions obtained from numerical simulation with Julia. We see the numerical integrated solution going through all the red points from the solution from DDE-BifTool.

```

33 # define model
34 function triNeuralBAMNetworkModel!(du,u,h,p,t)
35      $\alpha_1, \alpha_2 = p$ 
36      $u_1, u_2, u_3 = u$ 
37      $u_1t, u_2t, u_3t = h(p, t-\tau)$ 
38      $du[1] = -\mu_1*u_1 + (c_{21}^0 + \alpha_1)*f_1(u_2t) + (c_{31}^0 + \alpha_2)*f_1(u_3t);$ 
39      $du[2] = -\mu_2*u_2 + c_{12}*f_2(u_1);$ 
40      $du[3] = -\mu_3*u_3 + c_{13}*f_3(u_1);$ 
41 end
42
43 # allocating version (used for calculating stability)
44 function triNeuralBAMNetworkModel(u, p)
45     du = similar(u[:,1])
46     h(p,t) = u[:,2]
47     triNeuralBAMNetworkModel!(du,u[:,1],h,p,0)
48     du
49 end
50
51 # version used for calculating stability at the end of the script
52 function triNeuralBAMNetworkModel(u, p,  $\tau$ )
53      $\alpha_1, \alpha_2 = p$ 
54      $u_1, u_2, u_3 = u[:,1]$ 
55      $u_1t, u_2t, u_3t = u[:,2]$ 
56      $c_{21}^0 = \mu_2^2*(\mu_1*(\mu_3*\tau + 1.0) + \mu_3)/(c_{12}*(\mu_2 - \mu_3)*df_1(0)*df_2(0))$ 
57      $c_{31}^0 = \mu_3^2*(\mu_1*(\mu_2*\tau + 1.0) + \mu_2)/(c_{13}*(\mu_3 - \mu_2)*df_1(0)*df_3(0))$ 
58     du = similar(u[:,1])
59      $du[1] = -\mu_1*u_1 + (c_{21}^0 + \alpha_1)*f_1(u_2t) + (c_{31}^0 + \alpha_2)*f_1(u_3t);$ 
60      $du[2] = -\mu_2*u_2 + c_{12}*f_2(u_1);$ 
61      $du[3] = -\mu_3*u_3 + c_{13}*f_3(u_1);$ 

```

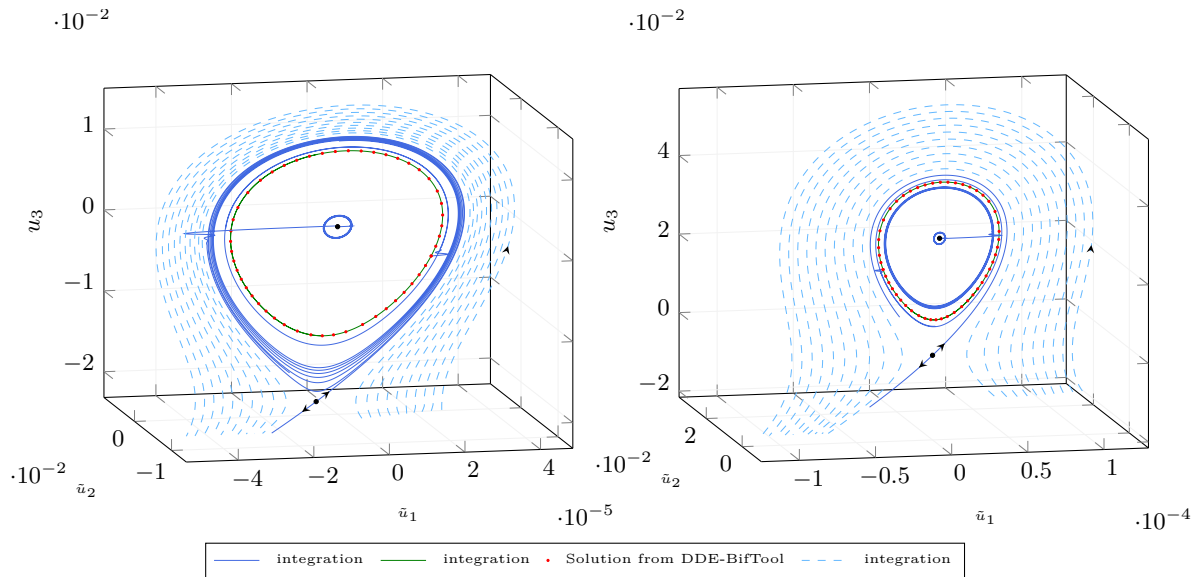


Figure S34: Comparing the computed periodic orbits in (S11) with DDE-BifTool with the solutions obtained from numerical simulation with Julia. We see the numerical integrated solution going through all the red points from the solution from DDE-BifTool.

```
62 du
63 end
```

S4.18.3 Function for creating streamlines plot

To obtain an impression of the flow near transcritical Bogdanov–Takens point, we create a streamlines function. This is particularly useful for seeing the flow around the stable manifold of the saddle-node.

```
65 # stream lines
66 function stream_lines(Tend, abscissa, ordinate, z, p, alg)
67     tspan = (0.0, Tend);
68     sols = []
69     for x ∈ abscissa
70         for y ∈ ordinate
71             h(p,t) = [x;y;z]
72             sol = solve(prob(h,p,tspan),alg,reltol=1e-09, abstol=1e-09)
73             push!(sols,sol)
74         end
75     end
76     sols
77 end
```

S4.18.4 Create figure with several axes

We create a figure containing multiple axis in which we will plot the homoclinic, periodic orbits, and the left and right-hand sides of (S17).

```

79 # create figure
80 fig = Figure()
81 set_theme!(theme_light())
82 labels = (xlabel=L"\tilde{u}_1", ylabel=L"\tilde{u}_2", zlabel=L"u_2")
83 ax1 = Axis3(fig[1,1], title="Homoclinic orbit I"; labels...)
84 ax2 = Axis3(fig[1,2], title="Homoclinic orbit II"; labels...)
85 ax3 = Axis3(fig[2,1], title="Periodic orbit I"; labels...)
86 ax4 = Axis3(fig[2,2], title="Periodic orbit II"; labels...)
87 ax5 = GLMakie.Axis(fig[3,1], title="Stabilitiy determining functions",
  ↪ xlabel=L"\tau")
88 ax6 = GLMakie.Axis(fig[3,2], title="Eigenvalues",
89                 xlabel=L"\Re(\lambda)", ylabel=L"\Im(\lambda)")

```

S4.18.5 Define parameters, equilibria

We define parameters located on the continued homoclinic branch with DDE-BifTool. Then calculate the equilibria points in (S10) near the transcritical Bogdanov–Takens point.

```

91 ## Simulation homoclinic orbit I
92  $\alpha_1, \alpha_2 = -0.001724521613831, 0.001344362436730$ 
93  $\mathbf{p} = [\alpha_1; \alpha_2]$ 
94
95 # derive equilibria
96  $\mathbf{rts} = \text{roots}(u_1 \rightarrow -\mu_1 * u_1 + (c_{21}^0 + \alpha_1) * f_1(c_{12} * f_2(u_1) / \mu_2) +$ 
97              $(c_{31}^0 + \alpha_2) * f_1(c_{13} * f_3(u_1) / \mu_3), \text{interval}(-0.01, 0.01))$ 
98  $u_1 = \text{sort}(\text{mid}(\text{interval}(\mathbf{rts})))$ 

```

S4.18.6 Plot equilibria and homoclinic orbit

By plotting the homoclinic orbit obtained with DDE-BifTool located at parameter values

$$(\alpha_1, \alpha_2) = (-0.001724521613831, 0.001344362436730),$$

we can compare with the numerical simulations. As in the analysis with DDE-BifTool, we rotate the coordinates of the solutions to visualize the solutions in phase-space.

```

100 # rotation matrix
101  $R(\alpha) = [\cos(\alpha) \ -\sin(\alpha) \ 0; \sin(\alpha) \ \cos(\alpha) \ 0; \ 0 \ 0 \ 1]$ 
102
103 # plot equilibria
104 scatter!(ax1, Point3f.([R(0.29)*p.coords for p ∈ point]), color=:black)
105
106 # plot homoclinic orbit from DDE-BifTool
107 csvdir = "/home/maikel/Documents/MyPapers/BTPaper"*
108         "/data/triNeuronBAMNeuralNetworkModel/"
109 homoclinicorbitI = readdlm(csvdir * "homoclinicorbitI_45.csv")
110 scatter!(ax1, R(0.29)*homoclinicorbitI[1:3:end,:]', color=:red)

```

S4.18.7 Leading eigenvectors

Next, we calculate and plot the leading eigenvectors of the characteristic matrix at the saddle-node bifurcation point.

```
112 # calculate stability
113  $\tau s = [0.0 \tau]$ 
114 point = [(coords = [ $u_1$ ,  $c_{12} * f_2(u_1) / \mu_2$ ,  $c_{13} * f_3(u_1) / \mu_3$ ], pars = p) for  $u_1 \in u_1$ ]
115 M = [coefficient_matrices(triNeuralBAMNetworkModel, point[i],  $\tau s$ )
116     for i in 1:length( $u_1$ )]
117 dep = [DEP([M[i][j](point[i].coords,point[i].pars) for j in 1:length( $\tau s$ )],
118         vec( $\tau s$ )) for i in 1:length( $u_1$ )]
119  $\lambda = \text{iar\_chebyshev}(\text{dep}, \text{maxit}=100, \text{neigs}=2)$ 
120 saddle_indx = findall( $\lambda \rightarrow \text{abs}(\lambda[1]) < 1e-14$ ,
121     imag([\lambda[i][1] for i in 1:length( $u_1$ )]))
122 saddle = point[saddle_indx]
123 V = real.(\lambda[saddle_indx][2])
124 indx_unstable = findall( $\lambda \rightarrow \text{real}(\lambda) > 0$ ,  $\lambda$ [saddle_indx][1])
125 indx_stable = findall( $\lambda \rightarrow \text{real}(\lambda) < 0$ ,  $\lambda$ [saddle_indx][1])
126 Vunstable = vec(V[:,indx_unstable])
127 Vstable = vec(V[:,indx_stable])
128
129 # draw leading eigenvectors of the characteristic matrix at the saddle-node
130 psHomIEigenvectors = repeat([Point3f(saddle.coords)],4)
131 nsHomIEigenvectors = [op.(0,1e-02Vec3f(R(0.29)*V)) for op in [+,-]
132     for V in [[Vunstable]; [Vstable]]]
133 arrows!(ax1, psHomIEigenvectors, nsHomIEigenvectors, linewidth = 0.000003,
134     arrowsize = Vec3f(1.0e-5,1.0e-3,1.0e-3),
135 )
```

S4.18.8 Define callback

Since we are only interested in the flow near the equilibria points, we create a continuous callback to ensure the orbits do not become too large.

```
137 # create continuous callback
138 condition(u,t,integrator) = u[3] + 0.015
139 affect!(integrator) = terminate!(integrator)
140 cb = ContinuousCallback(condition,affect!)
```

S4.18.9 Integrate the system at homoclinic orbits I

Now we define the problem to be integrated and choose the algorithm to be used. Then we integrate the system for a range of initial history functions using the function `streamlines`. Next, we integrate the system near the inner equilibrium, i.e., the equilibrium inside the homoclinic orbit. This equilibria should be an unstable spiral. We show the first and last part of the obtained solutions. We see that the last part of the integrated solutions completely overlap the homoclinic solution obtained with DDE-BifTool.

```

142 # define DDEProblem and choose integration algorithm
143 prob(h,p,tspan) = DDEProblem(triNeuralBAMNetworkModel!, h(p,0),h,tspan,p;
144                             constant_lags=[ $\tau$ ], callback=cb)
145 alg = MethodOfSteps(Tsit5())
146
147 # integrate over a range of history functions
148 homSolsI = stream_lines(3000.0, range(-0.00205,-0.0016,10),
149                             -0.010183777508431096, -0.014999999999999973, p, alg);
150 for sol ∈ homSolsI
151     Tend = sol.t[end]
152     lines!(ax1,R(0.29)*sol(range(Tend-94*Tend/100,Tend,100)),
153           color=:steelblue1, linestyle=:dash)
154 end
155
156 # integrate near inner equilibria
157 h(p,t) = [u1[2], c12*f2(u1[2])/μ2, c13*f3(u1[2])/μ3] + [0.0; 0.0; 0.00001]
158 tspan = (0.0, 200000.0);
159 homI_sol1 = solve(prob(h,p,tspan),alg,reltol=1e-06,abstol=1e-09)
160
161 # plot first part of the orbit, showing the solution spirals out
162 lines!(ax1,R(0.29)*homI_sol1(range(0,100000,10000)), color=:royalblue1)
163
164 # plot last part to show that it overlaps the homoclinic solution from DDE-BifTool
165 lines!(ax1,R(0.29)*homI_sol1(range(197400,200000,1000)),color=:green)

```

S4.18.10 Add arrows on solutions

Lastly, we add arrows to the obtained solutions and redraw the equilibria.

```

167 # add direction arrows
168 pointnumber = [180, 99900]
169 psHomI = Point3f.([R(0.29)*homSolsI[10][pointnumber[1]],
170                  R(0.29)*homI_sol1(pointnumber[2])])
171 nsHomI = Vec3f.([R(0.29)*homSolsI[10][pointnumber[1]+1],
172                 R(0.29)*homI_sol1(pointnumber[2]+1)] - psHomI)
173 arrows!(ax1, psHomI,nsHomI, linewidth = 0.000003,
174          arrowsize = Vec3f(1.0e-5,1.0e-3,1.0e-3), lengthscale = 1e-02)
175
176 # redraw equilibria
177 scatter!(ax1,Point3f.([R(0.29)*[u1, c12*f2(u1)/μ2, c13*f3(u1)/μ3] for u1 ∈ u1]),
178          color=:black)

```

We should now obtain an interactive figure similar to the left figure in [Figure S33](#).

S4.18.11 Simulation near stable periodic orbit I

The code for numerical simulation near the second homoclinic orbit, see the right plot in [Figure S33](#), is not included here.

To show by integration the existence of a stable periodic orbit, we first located a periodic orbit in DDE-BifTool. This can be done by continuing a branch of periodic orbits emanating from a point on the continued Hopf curves. Then we load the profiles of the periodic orbits into Julia. We perform two simulations. For the first we integrate with a constant history function equal to a point inside the periodic orbit. The second simulation starts from the unstable eigenvector of the characteristic matrix calculated above.

```

237 ## Simulation periodic orbit I
238  $\alpha_1, \alpha_2 = -4.211633510571706e-05, -8.548339944470298e-05$ 
239  $p = [\alpha_1; \alpha_2]$ 
240
241 # derive equilibria
242  $rts = roots(u_1 \rightarrow -\mu_1 * u_1 + (c_{21}^0 + \alpha_1) * f_1(c_{12} * f_2(u_1) / \mu_2) +$ 
243  $(c_{31}^0 + \alpha_2) * f_1(c_{13} * f_3(u_1) / \mu_3), interval(-0.01, 0.0))$ 
244  $u_1 = sort(mid.(interval.(rts)))$ 
245
246 # calculate stability
247  $\tau s = [0.0 \tau]$ 
248  $point = [(coords = [u_1, c_{12} * f_2(u_1) / \mu_2, c_{13} * f_3(u_1) / \mu_3], pars = p) \text{ for } u_1 \in u_1]$ 
249  $M = [coefficient\_matrices(triNeuralBAMNetworkModel, point[i], \tau s)$ 
250  $\text{ for } i \in 1:length(u_1)]$ 
251  $dep = [DEP([M[i][j](point[i].coords, point[i].pars)$ 
252  $\text{ for } j \text{ in } 1:length(\tau s)], vec(\tau s)) \text{ for } i \in 1:length(u_1)]$ 
253  $\lambda = iar\_chebyshev.(dep, maxit=100, neigs=2)$ 
254  $\lambda[1][1]$ 
255  $\lambda[2][1]$ 
256  $saddle\_indx = findall(\lambda \rightarrow abs(\lambda[1]) < 1e-14,$ 
257  $\text{ imag}([\lambda[i][1] \text{ for } i \in 1:length(u_1)]))$ 
258  $saddle = point[saddle\_indx][1]$ 
259  $V = real.(\lambda[saddle\_indx][1][2])$ 
260  $indx\_unstable = findall(\lambda \rightarrow real(\lambda) > 0, \lambda[saddle\_indx][1][1])$ 
261  $indx\_stable = findall(\lambda \rightarrow real(\lambda) < 0, \lambda[saddle\_indx][1][1])$ 
262  $Vunstable = vec(V[:, indx\_unstable])$ 
263  $Vstable = vec(V[:, indx\_stable])$ 
264
265 # plot equilibria
266  $scatter!(ax3, Point3f.([R(0.29) * point[i].coords \text{ for } i \in 1:length(u_1)]), color=:black)$ 
267
268 # plot homoclinic orbit from DDE-BifTool
269  $psolI = readdlm(csvdir * "psolI_28.csv")$ 
270  $scatter!(ax3, R(0.29) * psolI[1:3:end, :]', color=:orangered)$ 
271
272 # create continous callback
273  $condition(u, t, integrator) = u[3] + 0.02$ 
274  $affect!(integrator) = terminate!(integrator)$ 
275  $cb = ContinuousCallback(condition, affect!)$ 
276
277 # integrate from periodic orbit I
278  $h(p, t) = psolI[1, :]$ 
279  $tspan = (0.0, 800000.0);$ 

```

```

280 periodicI_sol1 = solve(prob(h,p,tspan),alg,reltol=1e-09,abstol=1e-09)
281 lines!(ax3,R(0.29)*periodicI_sol1(range(0.0,2000,1000)),color=:royalblue1)
282 lines!(ax3,R(0.29)*periodicI_sol1(range(tspan[2]-2000,tspan[2],1000)),color=:green)
283
284 # integrate from near inner equilibrium
285 h(p,t)=[0.0; 0.0; -0.00001]
286 tspan = (0.0, 400000.0);
287 periodicI_sol2 = solve(prob(h,p,tspan),alg,reltol=1e-09,abstol=1e-09)
288 lines!(ax3,R(0.29)*periodicI_sol2(range(0.0,10000,10000)),color=:royalblue1)
289
290 # integrate from near inner equilibrium
291 h(p,t)=[0.0; 0.0; 0.0001]
292 tspan = (0.0, 300000.0);
293 periodicI_sol3 = solve(prob(h,p,tspan),alg,reltol=1e-09,abstol=1e-09)
294 lines!(ax3,R(0.29)*periodicI_sol3(range(0.0,10000,10000)),color=:royalblue1)
295
296 # integrate from unstable eigendirection
297  $\epsilon$  = sign(Vunstable[1])*1e-04
298 h(p,t) = saddle.coords -  $\epsilon$ *Vunstable
299 periodicI_sol4 = solve(prob(h,p,tspan),alg,reltol=1e-09,abstol=1e-09)
300 lines!(ax3,R(0.29)*periodicI_sol4,color=:royalblue1)
301
302 # integrate from unstable eigendirection
303 tspan = (0.0, 40000.0);
304  $\epsilon$  = sign(Vunstable[1])*1e-04
305 h(p,t) = saddle.coords +  $\epsilon$ *Vunstable
306 periodicI_sol5 = solve(prob(h,p,tspan),alg,reltol=1e-09,abstol=1e-09)
307 lines!(ax3,R(0.29)*periodicI_sol5(range(0.0,2000,10000)),color=:royalblue1)
308
309 # integrate over a range of history functions
310 psolSolsI = stream_lines(30000.0, range(-0.00373,-0.0036,10),
311                             -0.013391304482590667,
312                             -0.01999999999999997 , p, alg);
313 for sol  $\in$  psolSolsI
314     Tend = sol.t[end]
315     lines!(ax3,R(0.29)*sol(range(Tend-98*Tend/100,Tend,100)),color=:steelblue1,
316             linestyle=:dash)
317 end
318
319 # add direction arrows
320 pointnumber = [100, 100, 120]
321 psPeriodicI = Point3f.([R(0.29)*periodicI_sol4[pointnumber[1]],
322                        R(0.29)*periodicI_sol5[pointnumber[2]],
323                        R(0.29)*psolSolsI[10][pointnumber[3]]])
324 nsPeriodicI = Vec3f.([R(0.29)*periodicI_sol4[pointnumber[1]+1],
325                       R(0.29)*periodicI_sol5[pointnumber[2]+1],
326                       R(0.29)*psolSolsI[10][pointnumber[3]+1]] - psPeriodicI)
327 arrows!(ax3, psPeriodicI, nsPeriodicI, linewidth = 0.0,
328          arrowsize = 0.5*Vec3f(5.0e-6,5.0e-4,5.0e-4))

```

After running the above code, we should obtain a similar plot as in [Figure S34](#).

S4.18.12 Stability of the center manifold

To confirm [Lemma 17](#) numerically, we consider again [\(S20\)](#) and [\(S21\)](#). The code below plots the left and right-hand sides of [\(S17\)](#). We see in [Figure S35](#) that there are two points of intersection.

```
421 ## Stability of the center manifold
422  $\omega_0(\tau) = 0.7071067811865476\sqrt{-0.14 + \sqrt{0.0484 + 0.00528\tau +$ 
423  $0.00014400000000000006\tau^2}}$ 
424  $\mathbf{a}_0 = -\mu_1\mu_2\mu_3$ 
425  $\mathbf{b}_0(\tau) = -\omega_0(\tau)(\mu_2\mu_3 + \mu_1(\mu_2 + \mu_3 + \mu_2\mu_3\tau))$ 
426  $\zeta_0(\tau) = \mu_1^4 + (\mu_2^2 + \mu_3^2)^2 + 8\mu_1\mu_2\mu_3(\mu_2 + \mu_3 + \mu_2\mu_3\tau) +$ 
427  $2\mu_1^2(\mu_3^2 + 4\mu_2\mu_3(1+\mu_3\tau) + \mu_2^2(1 + 2\mu_3\tau(2 + \mu_3\tau)))$ 
428  $\zeta_1(\tau) = \mu_1\mu_2\mu_3 - (\mu_1 + \mu_2 + \mu_3)\omega_0(\tau)^2$ 
429  $\zeta_2(\tau) = \mu_2\mu_3\omega_0(\tau) + \mu_1(\mu_2 + \mu_3)\omega_0(\tau) - \omega_0(\tau)^3$ 
430
431  $\tau\mathbf{s} = \text{range}(0.0, 20.0, 1000)$ 
432  $\text{lhs}(\tau) = \tan(\tau\omega_0(\tau))$ 
433  $\text{rhs}(\tau) = (\mathbf{b}_0(\tau)\zeta_1(\tau) - \mathbf{a}_0\zeta_2(\tau))/(\mathbf{a}_0\zeta_1(\tau) + \mathbf{b}_0(\tau)\zeta_2(\tau))$ 
434  $\text{empty!}(\text{ax5})$ 
435  $\text{scatter!}(\text{ax5}, \tau\mathbf{s}, \text{lhs}(\tau\mathbf{s}), \text{markersize}=2, \text{label}=\text{L}"\tan(\tau\omega_0(\tau))",$ 
436  $\text{scatter!}(\text{ax5}, \tau\mathbf{s}, \text{rhs}(\tau\mathbf{s}), \text{markersize}=2,$ 
437  $\text{label}=\text{L}"\frac{\mathbf{b}_0\zeta_1 - \mathbf{a}_0\zeta_2}{\mathbf{a}_0\zeta_1 + \mathbf{b}_0\zeta_2}"$ )
438  $\text{ylims!}(\text{ax5}, -40, 40)$ 
439  $\text{axislegend}(\text{ax5}, \text{position} = :lt)$ 
```

Using the function `roots` from the package `IntervalRootFinding.jl` we search for points of intersection.

```
441 # locate points of intersection
442  $\text{rts} = \text{roots}(\tau \rightarrow \text{lhs}(\tau) - \text{rhs}(\tau), \text{interval}(0.0, 20.0))$ 
443  $\text{rts\_unique} = \text{rts}[\text{isunique.}(\text{rts})]$ 
444  $\tau_0 = \text{sort}(\text{mid.}(\text{interval.}(\text{rts\_unique})))$ 
```

In the Julia output we obtain

```
7-element Vector{Root{Interval{Float64}}}:
 Root([13.2309, 13.231], :unique)
 Root([19.2374, 19.2375], :unique)
 Root([19.7337, 19.7338], :unknown)
 Root([6.00301, 6.00302], :unique)
 Root([8.33333, 8.33334], :unknown)
 Root([13.5353, 13.5354], :unknown)
 Root([5.75402, 5.75403], :unknown)
 Root([8.33333, 8.33334], :unknown)
```

Note that, since there are multiple discontinuities, there are many unknown solutions returned. We extract the unique solutions from the list of solutions and test if these provide solutions to the characteristic equation.

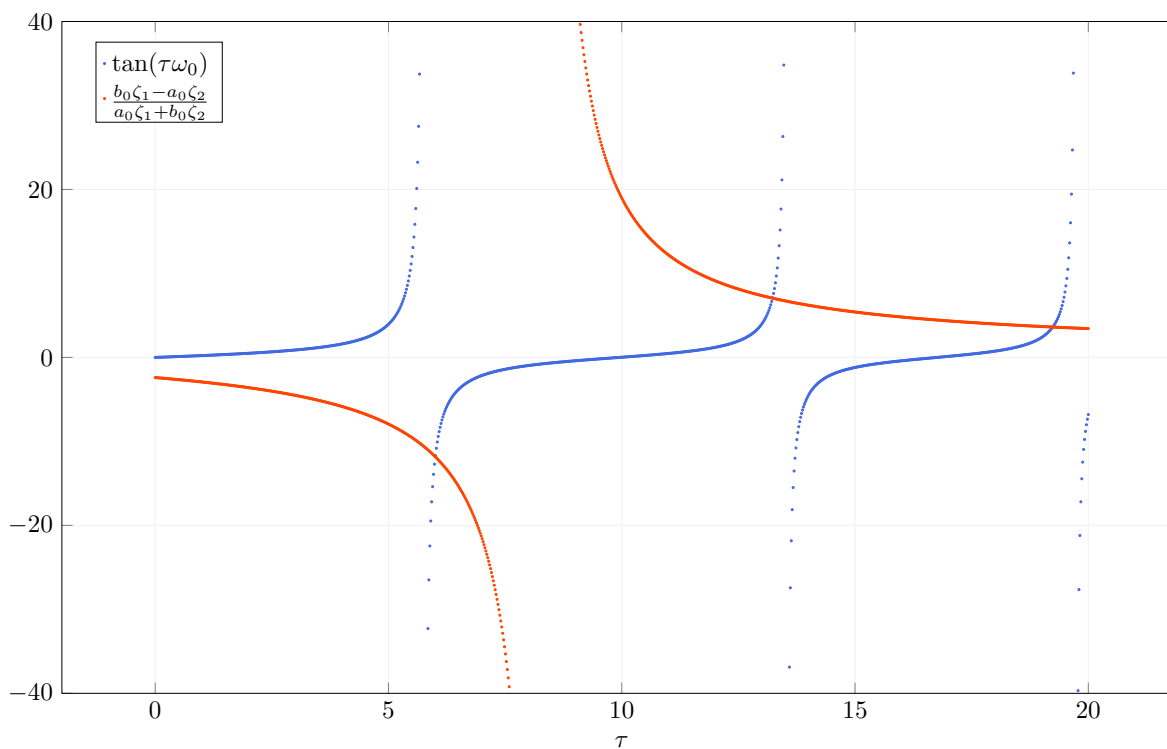


Figure S35: Plot of the left and right-hand sides of (S17). Points of intersection are candidates for the center manifold to lose its stability.

```

446 # characteristic equation
447 bt = (coords = zeros(3), pars = zeros(2))
448 Δ(λ,τ) = -λ*I + M[1](bt.coords,bt.pars) + M[2](bt.coords,bt.pars)*exp(-τ*λ)
449 for τ ∈ τ₀
450     M = coefficient_matrices((u,p) -> triNeuralBAMNetworkModel(u, p, τ),
451                             bt, zeros(2))
452     if ≈(det(Δ(ω₀(τ)im,τ)), 0.0 + 0.0im, atol=1e-12)
453         println("The centermanifold is attractive for 0 < τ < $τ.")
454         τ₀ = τ
455         break
456     end
457 end

```

In the Julia output we obtain

```
The centermanifold is locally attractive for 0 < τ < 13.230934887939895.
```

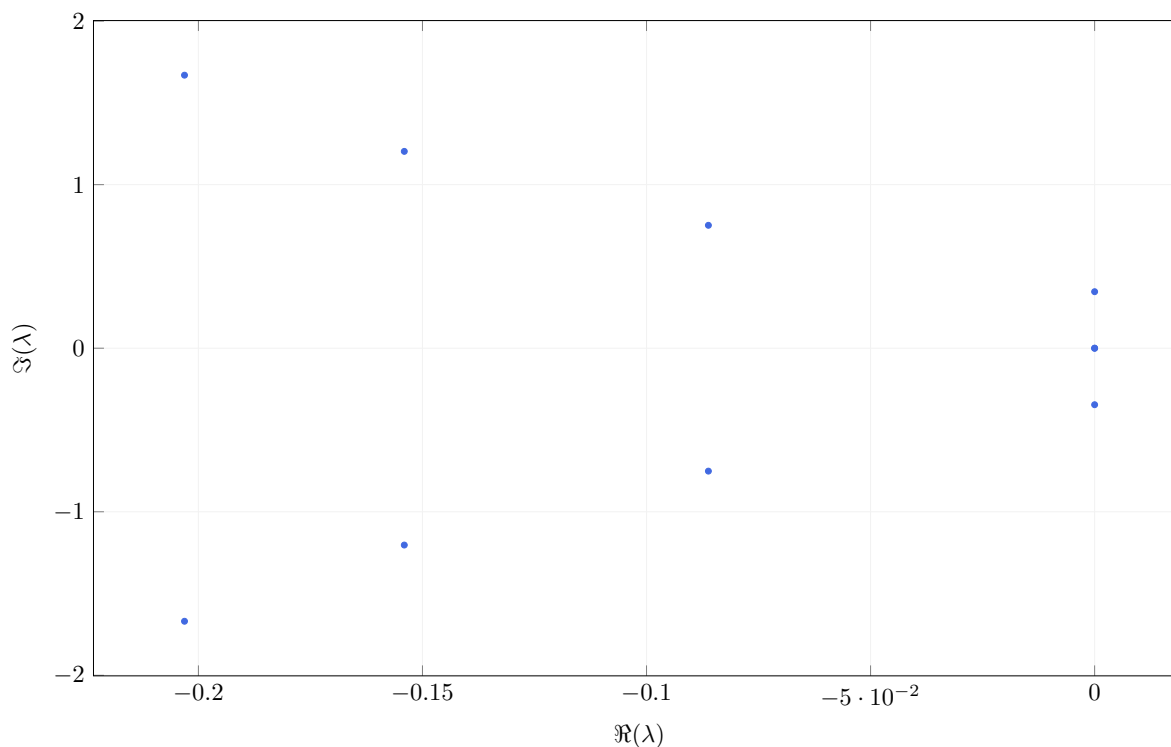


Figure S36: Plot of the leading eigenvalues at the analytically derived transcritical Bogdanov–Takens point with $\tau = 13.230934887939895$ and $\omega = \omega(\tau)$ from (S19). At this point there are four eigenvalues on the imaginary axis. For $\tau > 13.230934887939895$ the center manifold is locally unstable.

S4.18.13 Calculate and plot stability at Bogdanov–Takens point

We finish this demonstration by confirming the stability of the transcritical Bogdanov–Takens point at $\tau = 13.230934887939895$ obtained in the previous section. In Figure S36 we have plotted the eigenvalues. We indeed see that at $\tau = 13.230934887939895$ the center manifold loses stability. Lastly, we also verified in the code below that the eigenvalues with positive imaginary part on the imaginary axis is approximately equal to the expression for ω obtained in (S19).

```

459 # calculate and plot leading eigenvalues at Bogdanov--Takens point with  $\tau=\tau_0$ 
460  $\tau s = [0.0, \tau_0]$ 
461  $M = \text{coefficient\_matrices}((u,p) \rightarrow \text{triNeuralBAMNetworkModel}(u, p, \tau_0), \text{bt}, \tau s)$ 
462  $\text{dep} = \text{DEP}([M[j](\text{bt.coords}, \text{bt.pars}) \text{ for } j \text{ in } 1:\text{length}(\tau s)], \tau s)$ 
463  $\lambda = \text{iar\_chebyshev}(\text{dep}, \text{maxit}=200, \text{neigs}=10, \sigma=-.1)$ 
464  $\lambda[1]$ 
465  $\text{hopf\_indx} = \text{findall}(\lambda \rightarrow \text{abs}(\text{real}(\lambda)) < 1e-10 \ \&\& \ \text{imag}(\lambda) > 0.1, \lambda[1])$ 
466  $\text{imag}(\lambda[1][\text{hopf\_indx}])[1] \approx \omega_0(\tau_0)$ 
467  $\text{scatter}!(\text{ax6}, \text{real}(\lambda[1]), \text{imag}(\lambda[1]))$ 

```

References for main text and supplement

- [1] L. BENET AND D. P. SANDERS, *IntervalRootFinding.jl*. <https://github.com/JuliaIntervals/IntervalRootFinding.jl>, 2021.
- [2] M. M. BOSSCHAERT, S. G. JANSSENS, AND YU. A. KUZNETSOV, *Switching to nonhyperbolic cycles from codimension two bifurcations of equilibria of delay differential equations*, SIAM J. Appl. Dyn. Syst., 19 (2020), pp. 252–303, <https://doi.org/10.1137/19M1243993>.
- [3] M. M. BOSSCHAERT AND YU. A. KUZNETSOV, *Interplay between normal forms and center manifold reduction for homoclinic predictors near bogdanov-takens bifurcation*, 2021, <https://arxiv.org/abs/arXiv:2109.12570>.
- [4] H. W. BROER, F. DUMORTIER, S. J. VAN STRIEN, AND F. TAKENS, *Structures in dynamics*, vol. 2 of Studies in Mathematical Physics, North-Holland Publishing Co., Amsterdam, 1991. Finite-dimensional deterministic studies.
- [5] P. CLÉMENT, O. DIEKMANN, M. GYLLENBERG, H. J. A. M. HEIJMANS, AND H. R. THIEME, *Perturbation theory for dual semigroups. I. the sun-reflexive case*, Math. Ann., 277 (1987), pp. 709–725, <https://doi.org/10.1007/BF01457866>.
- [6] P. CLÉMENT, O. DIEKMANN, M. GYLLENBERG, H. J. A. M. HEIJMANS, AND H. R. THIEME, *Perturbation theory for dual semigroups. II. time-dependent perturbations in the sun-reflexive case*, Proc. Roy. Soc. Edinburgh Sect. A, 109 (1988), pp. 145–172, <https://doi.org/10.1017/S0308210500026731>.
- [7] P. CLÉMENT, O. DIEKMANN, M. GYLLENBERG, H. J. A. M. HEIJMANS, AND H. R. THIEME, *Perturbation theory for dual semigroups. III. nonlinear Lipschitz continuous perturbations in the sun-reflexive case*, in Volterra integrodifferential equations in Banach spaces and applications (Trento, 1987), vol. 190 of Pitman Res. Notes Math. Ser., Longman Sci. Tech., Harlow, 1989, pp. 67–89.
- [8] P. CLÉMENT, O. DIEKMANN, M. GYLLENBERG, H. J. A. M. HEIJMANS, AND H. R. THIEME, *Perturbation theory for dual semigroups. IV. the intertwining formula and the canonical pairing*, in Semigroup Theory and Applications (Trieste, 1987), vol. 116 of Lecture Notes in Pure and Appl. Math., Dekker, New York, 1989, pp. 95–116.
- [9] V. DE WITTE, F. DELLA ROSSA, W. GOVAERTS, AND YU. A. KUZNETSOV, *Numerical periodic normalization for codim 2 bifurcations of limit cycles: computational formulas, numerical implementation, and examples*, SIAM J. Appl. Dyn. Syst., 12 (2013), pp. 722–788, <https://doi.org/10.1137/120874904>.
- [10] V. DE WITTE, W. GOVAERTS, YU. A. KUZNETSOV, AND H. G. E. MEIJER, *Analysis of bifurcations of limit cycles with Lyapunov exponents and numerical normal forms*, Phys. D, 269 (2014), pp. 126–141, <https://doi.org/10.1016/j.physd.2013.12.002>.
- [11] O. DIEKMANN AND M. GYLLENBERG, *Abstract delay equations inspired by population dynamics*, in Functional Analysis and Evolution Equations, Birkhäuser, 2008, pp. 187–200, https://doi.org/10.1007/978-3-7643-7794-6_12.
- [12] O. DIEKMANN AND M. GYLLENBERG, *Equations with infinite delay: blending the abstract and the concrete*, J. Differential Equations, 252 (2012), pp. 819–851, <https://doi.org/10.1016/j.jde.2011.09.038>.

- [13] O. DIEKMANN, S. A. VAN GILS, S. M. VERDUYN LUNEL, AND H.-O. WALTHER, *Delay Equations: Functional-, Complex-, and Nonlinear Analysis*, Applied Mathematical Sciences, Springer, 1995, <https://doi.org/10.1007/978-1-4612-4206-2>.
- [14] K. DIJKSTRA, S. A. VAN GILS, S. G. JANSSENS, YU. A. KUZNETSOV, AND S. VISSER, *Pitchfork-Hopf bifurcations in 1D neural field models with transmission delays*, Phys. D, 297 (2015), pp. 88–101, <https://doi.org/10.1016/j.physd.2015.01.004>.
- [15] T. DONG AND X. LIAO, *Bogdanov-Takens bifurcation in a tri-neuron BAM neural network model with multiple delays*, Nonlinear Dynam., 71 (2013), pp. 583–595, <https://doi.org/10.1007/s11071-012-0683-9>.
- [16] K. ENGELBORGH, T. LUZYANINA, AND D. ROOSE, *Numerical bifurcation analysis of delay differential equations using DDE-BIFTOOL*, ACM Trans. Math. Software, 28 (2002), pp. 1–21, <https://doi.org/10.1145/513001.513002>.
- [17] T. FARIA AND L. T. MAGALHÃES, *Normal forms for retarded functional-differential equations and applications to Bogdanov-Takens singularity*, J. Differential Equations, 122 (1995), pp. 201–224, <https://doi.org/10.1006/jdeq.1995.1145>.
- [18] T. FARIA AND L. T. MAGALHÃES, *Normal forms for retarded functional differential equations with parameters and applications to Hopf bifurcation*, Journal of differential equations, 122 (1995), pp. 181–200, <https://doi.org/10.1006/jdeq.1995.1144>.
- [19] F. GIANNAKOPOULOS AND A. ZAPP, *Bifurcations in a planar system of differential delay equations modeling neural activity*, Physica D: Nonlinear Phenomena, 159 (2001), pp. 215–232.
- [20] W. J. F. GOVAERTS, *Numerical Methods for Bifurcations of Dynamical Equilibria*, Society for Industrial and Applied Mathematics, Philadelphia, PA, 2000, <https://doi.org/10.1137/1.9780898719543>.
- [21] S. GOWDA, Y. MA, A. CHELI, M. GWÓZDZ, V. B. SHAH, A. EDELMAN, AND C. RACKAUCKAS, *High-performance symbolic-numeric via multiple dispatch*, ACM Commun. Comput. Algebra, 55 (2022), p. 92–96, <https://doi.org/10.1145/3511528.3511535>, <https://doi.org/10.1145/3511528.3511535>.
- [22] S. G. JANSSENS, *On a Normalization Technique for Codimension Two Bifurcations of Equilibria of Delay Differential Equations*, master’s thesis, Utrecht University, The Netherlands, 2010, <https://dspace.library.uu.nl/handle/1874/312252>. Corrections and updates are available via <http://sebastianjanssens.nl/pdf/normalization.pdf>.
- [23] S. G. JANSSENS, *A class of abstract delay differential equations in the light of suns and stars*, Jan. 2019, <https://arxiv.org/abs/1901.11526>.
- [24] W. JIANG AND Y. YUAN, *Bogdanov-Takens singularity in van der Pol’s oscillator with delayed feedback*, Physica D: Nonlinear Phenomena, 227 (2007), pp. 149–161.
- [25] J. JIAO AND C. CHEN, *Bogdanov-Takens bifurcation analysis of a delayed predator-prey system with double allee effect*, Nonlinear Dynamics, 104 (2021), pp. 1697–1707, <https://doi.org/10.1007/s11071-021-06338-x>, <https://doi.org/10.1007/s11071-021-06338-x>.
- [26] H. B. KELLER, *Lectures on Numerical Methods in Bifurcation Problems*, vol. 79 of Tata Institute of Fundamental Research Lectures on Mathematics and Physics, Published for the Tata Institute of Fundamental Research, Bombay; by Springer-Verlag, Berlin, 1987. With notes by A. K. Nandakumaran and Mythily Ramaswamy.

- [27] YU. A. KUZNETSOV, *Numerical normalization techniques for all codim 2 bifurcations of equilibria in ODEs*, SIAM Journal on Numerical Analysis, 36 (1999), pp. 1104–1124, <https://doi.org/10.1137/S0036142998335005>.
- [28] YU. A. KUZNETSOV, *Practical computation of normal forms on center manifolds at degenerate Bogdanov–Takens bifurcations*, International Journal of Bifurcation and Chaos, 15 (2005), pp. 3535–3546.
- [29] YU. A. KUZNETSOV, W. GOVAERTS, E. J. DOEDEL, AND A. DHOOGHE, *Numerical periodic normalization for codim 1 bifurcations of limit cycles*, SIAM J. Numer. Anal., 43 (2005), pp. 1407–1435, <https://doi.org/10.1137/040611306>.
- [30] C. RACKAUCKAS AND Q. NIE, *Differentialequations.jl—a performant and feature-rich ecosystem for solving differential equations in julia*, Journal of Open Research Software, 5 (2017).
- [31] S. RUAN, *On the zeros of a third degree exponential polynomial with applications to a delayed model for the control of testosterone secretion*, Mathematical Medicine and Biology, 18 (2001), pp. 41–52, <https://doi.org/10.1093/imammb/18.1.41>, <https://doi.org/10.1093%2Fimammb%2F18.1.41>.
- [32] G. SAMAËY, K. ENGELBORGHs, AND D. ROOSE, *Numerical computation of connecting orbits in delay differential equations*, Numer. Algorithms, 30 (2002), pp. 335–352, <https://doi.org/10.1023/A:1020102317544>, <https://doi-org.proxy.library.uu.nl/10.1023/A:1020102317544>.
- [33] D. P. SANDERS, L. BENET, LUCAFERRANTI, KRISH AGARWAL, B. RICHARD, J. GRAWITTER, EESHAN GUPTA, M. FORETS, M. F. HERBST, YASHRAJGUPTA, E. HANSON, BRAAM VAN DYK, C. RACKAUCKAS, RUSHABH VASANI, S. MICLUȚA-CÂMPEANU, SHEEHAN OLVER, T. KOOLEN, C. WORMELL, FAVIO ANDRÉ VÁZQUEZ, G. DALLE, J. SARNOFF, J. TAGBOT, K. O’BYRANT, K. CARLSSON, M. PIIBELEHT, M. GIORDANO, , RENO, R. DEITS, T. HOLY, AND VENKATESHPRASAD, *Juliaintervals/intervalarithmetic.jl: v0.20.6*, 2022, <https://doi.org/10.5281/ZENODO.6569509>, <https://zenodo.org/record/6569509>.
- [34] J. SIEBER, *Local bifurcations in differential equations with state-dependent delay*, Chaos: An Interdisciplinary Journal of Nonlinear Science, 27 (2017), p. 114326, <https://doi.org/10.1063/1.5011747>, <https://arxiv.org/abs/1705.07550>.
- [35] J. SIEBER, K. ENGELBORGHs, T. LUZYANINA, G. SAMAËY, AND D. ROOSE, *DDE-BIFTOOL Manual - Bifurcation analysis of delay differential equations*, June 2014, <https://arxiv.org/abs/1406.7144>.
- [36] S. A. VAN GILS, S. G. JANSSENS, YU. A. KUZNETSOV, AND S. VISSER, *On local bifurcations in neural field models with transmission delays*, Journal of Mathematical Biology, 66 (2013), pp. 837–887, <https://doi.org/10.1007/s00285-012-0598-6>, <https://arxiv.org/abs/1209.2849>.